Light in the Universe :

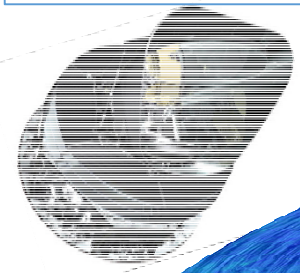

Telescopes, photometers, spectrometers and polarimeters for Cosmic Light - 2

Paolo de Bernardis

Dipartimento di Fisica, Sapienza Università di Roma

Winter College on Optics 2015 - Trieste, 9-20 February

Isotropy of the CMB ?

Several physical phenomena happening at recombination and before suggest that the CMB should be (slightly) anisotropic.

Horizons – Inflation – seeds of structures

Oscillations in the primeval fireball

Horizons

- At recombination (t=380000 years), only regions of the Universe closer than 380000 light years have had the possibility (enough time) to interact.
- That length, as seen from a distance of the order of c/H_o = 14 Glyrs, has an angular size of about 1 degree.

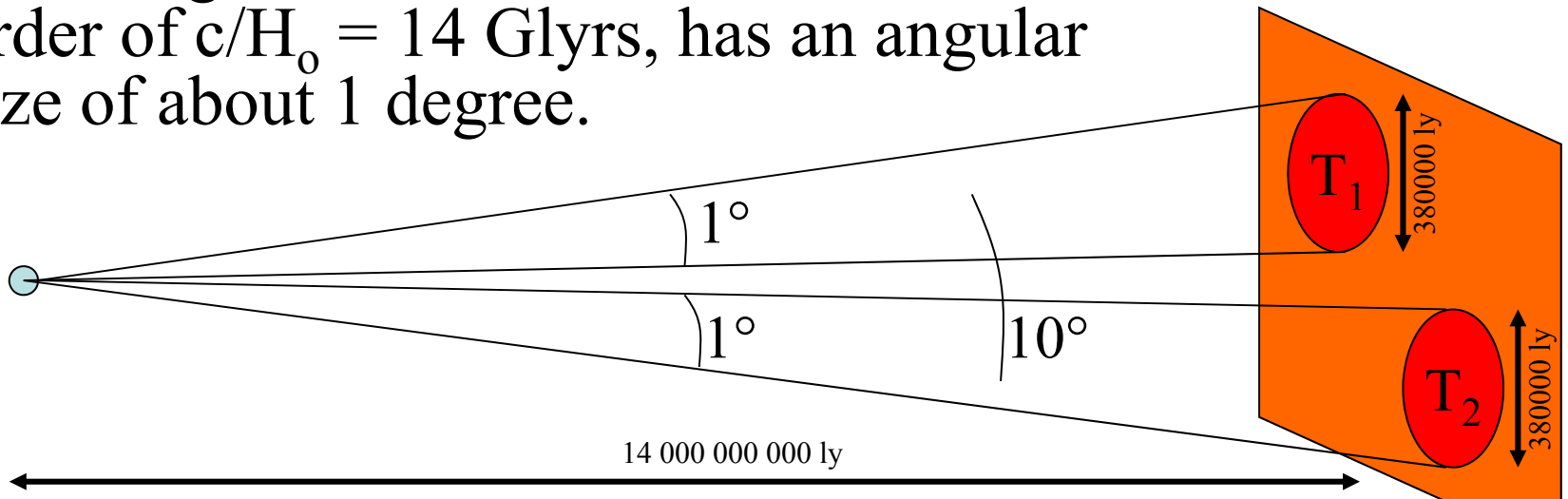

- They might be very different, since they could not interact during all the previous history of the Universe, from the Big Bang to recombination !
- However, measurements show that this is not the case.
- CMB anisotropy measurements.

Measuring anisotropy

- Anisotropy means that brightness is a function of the observed direction.
- Large brightness variations would be evident in a map.
- However, since its discovery, it was evident that the CMB is a very isotropic background.
- At a few mm of wavelength, the brightness of the sky is dominated by the CMB, and is isotropic to at least 1 part over 100.
- Only if we remove the average brightness and increase the contrast of the image, we start to see structures.
- But this requires special experimental configurations, removing a large background an enhancing small fluctuations.

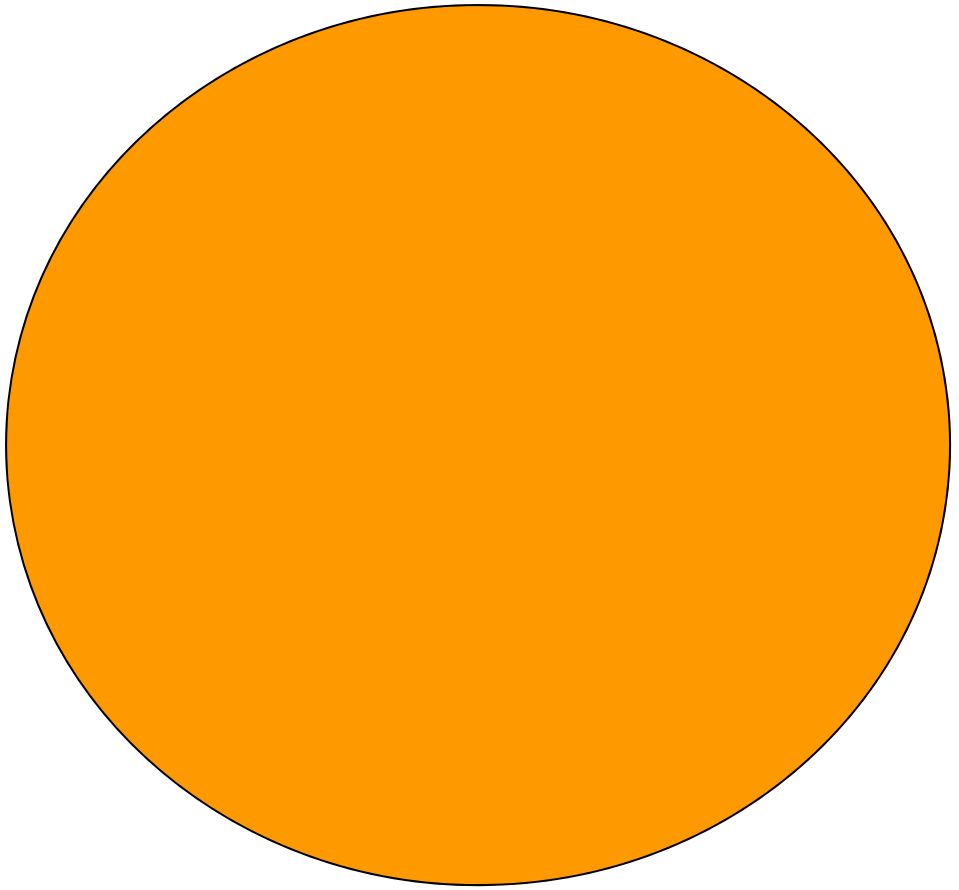

Measuring anisotropy

- A way to remove the common-mode signal is to alternate on the detector two contiguous regions of the sky, and measure the AC signal removing the DC signal electronically.
- A small AC signal synchronous to the modulation can be extracted from detector noise using a demodulation technique (a lock-in amplifier).

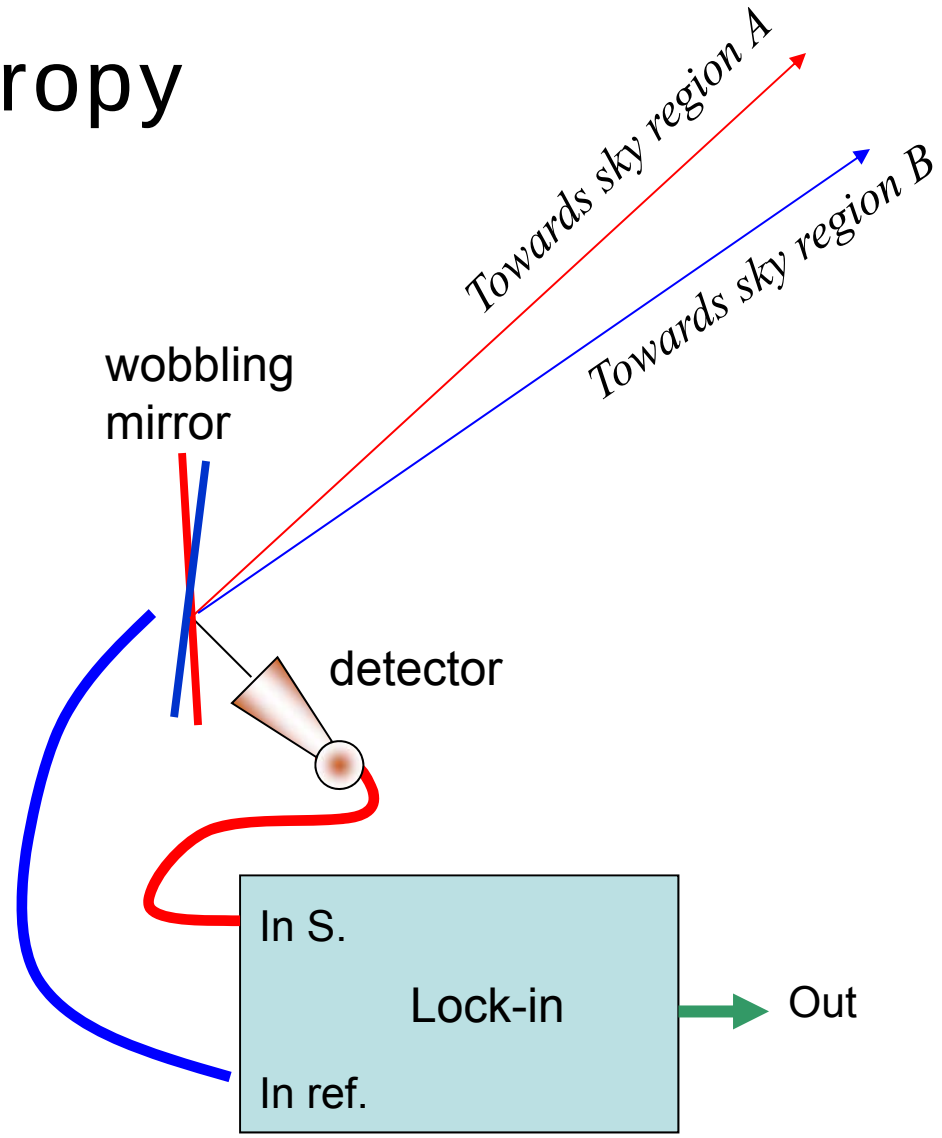

Lock-in

- Using a modulation/demodulation technique has 3 purposes:
- Remove the common mode signal (instrumental and atmospheric emission – to first order)
- Remove noise at frequencies different from the modulation frequency
- Produce a signal proportional to the Difference of Brightness between the two observed regions.

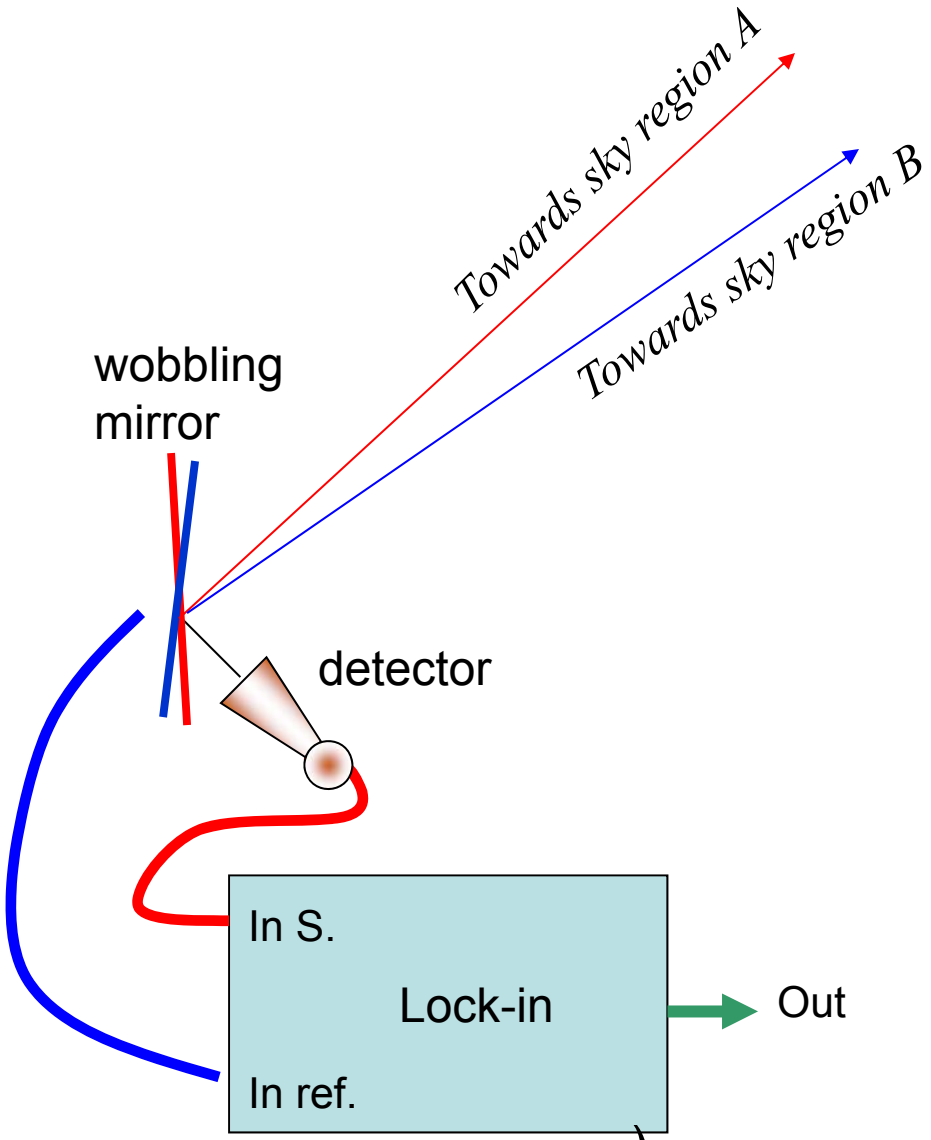

$$P_A = A\Omega ER\left(B_{instr} + (1-t_{atm})B_{atmosph} + t_{atm}B_s(A)\right)$$
$$P_B = A\Omega ER\left(B_{instr} + (1-t_{atm})B_{atmosph} + t_{atm}B_s(B)\right)$$
$$\Delta P = A\Omega ERt_{atm}\left\{B_s(A) - B_s(B)\right\}$$

Lock-in

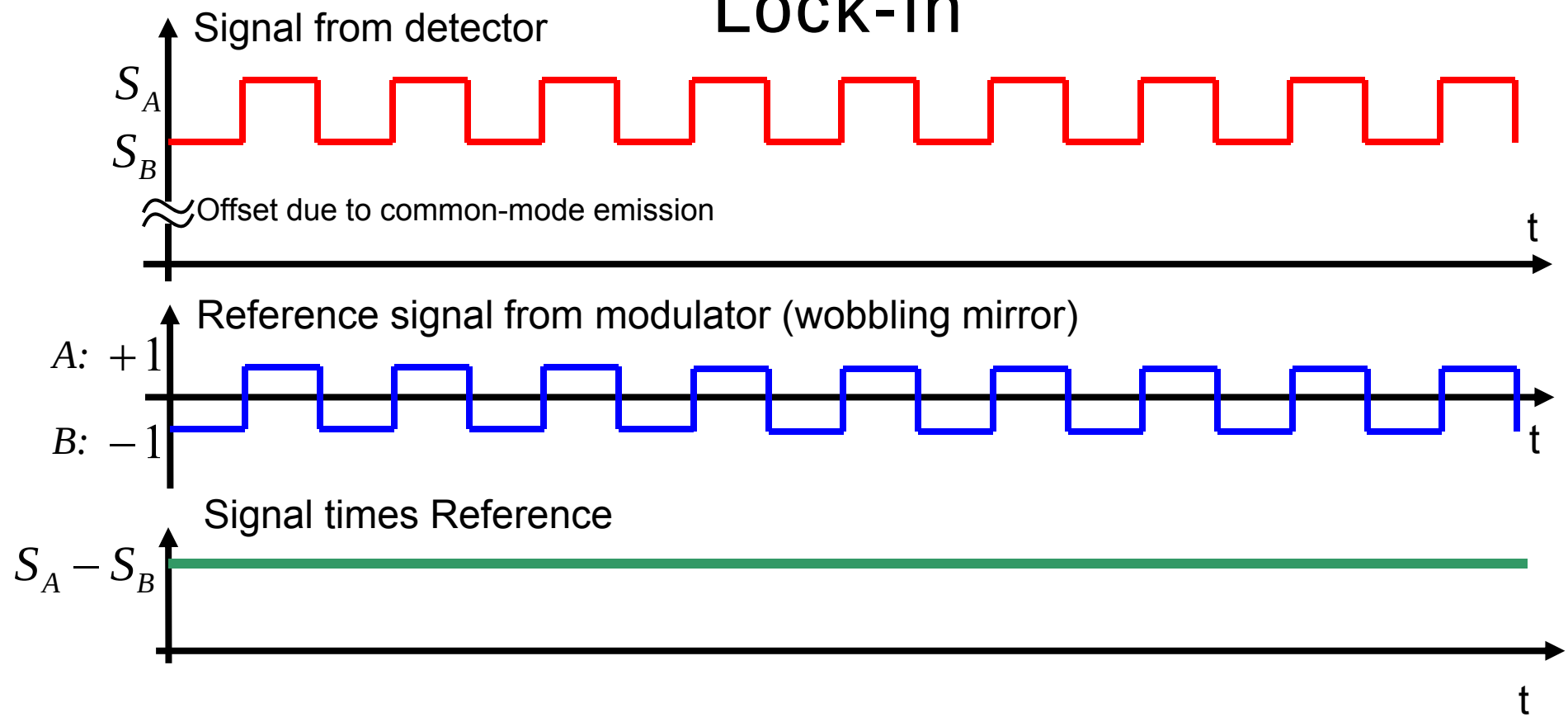

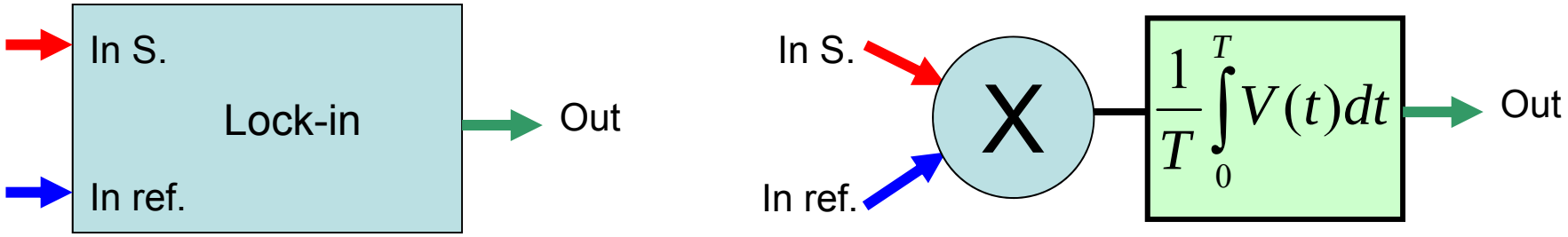

$$S_{out} = \langle S(t)R(t) \rangle = \tfrac{1}{2}\langle S_A \times 1 \rangle + \tfrac{1}{2}\langle S_B \times -1 \rangle = \tfrac{1}{2}[S_A - S_B]$$

Lock-in

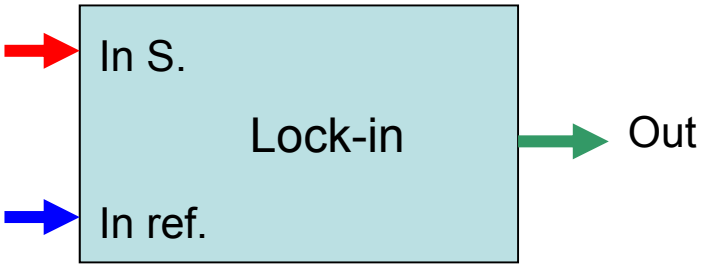

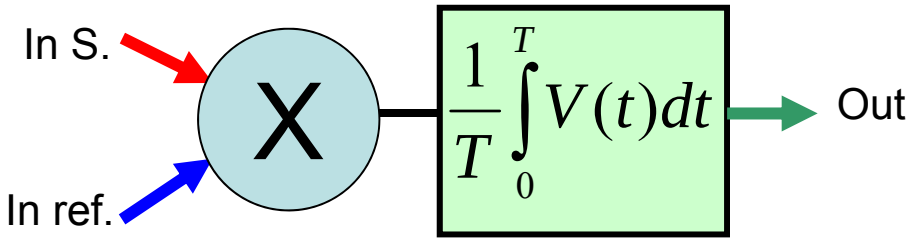

In presence of noise :

$$S_{out} = \langle [S(t) + n(t)] R(t) \rangle =$$

$$= \tfrac{1}{2}\langle S_A \times 1 \rangle + \tfrac{1}{2}\langle S_B \times -1 \rangle + \tfrac{1}{2}\langle n(t) \times 1 \rangle + \tfrac{1}{2}\langle n(t) \times -1 \rangle =$$

$$= \tfrac{1}{2}[S_A - S_B] + n'$$

n' is a zero-average noise: due to the lack of correlation between *n(t)* and *R(t)*, *n'* tends to 0 if the average period is long enough (many modulation cycles).
To quantify, we need to specify the noise better.

The combination multiplier + integrator is equivalent to a band-pass filter centered on the reference frequency.

- Let's consider for simplicity a sine-wave signal :

$$S(t) = V_s \cos(\omega_s t + \varphi_s)$$

- The signal from the sky will be at the same frequency of the reference, while the noise will have contributions at all frequencies.
- The reference also can be a sine-wave at the same frequency as the signal:

$$R(t) = \cos(\omega_R t + \varphi_R)$$

- At the output of the multiplier we get

$$V_p(t) = V_s \cos\left[(\omega_s + \omega_R)t + (\varphi_s + \varphi_R)\right] + V_s \cos\left[(\omega_s - \omega_R)t + (\varphi_s - \varphi_R)\right]$$

- If the low-pass filter has a cut-off frequency lower than $f_c = 1/T < 2\pi/\omega$, the sum frequency will be cut, while the difference frequency will pass with an amplitude

$$V_s \left| H\left| \omega_s - \omega_R \right| \right| \cos(\varphi_s - \varphi_R)$$

- Where H is the tranfer function of the low-pass filter.

$$V_{out} = V_S \left| H(|\omega_S - \omega_R|) \right|$$

The sky signal is exactly at the same frequency as the reference, with no phase delay, so it is transferred to the output as it is.

Noise contributes to all frequencies, but only those within the bandpass $\Delta\omega=2(2\pi f_c)=4\pi/T$ will contribute to the output signal.

In case of wide-band noise the improvement in S/N is very significant !

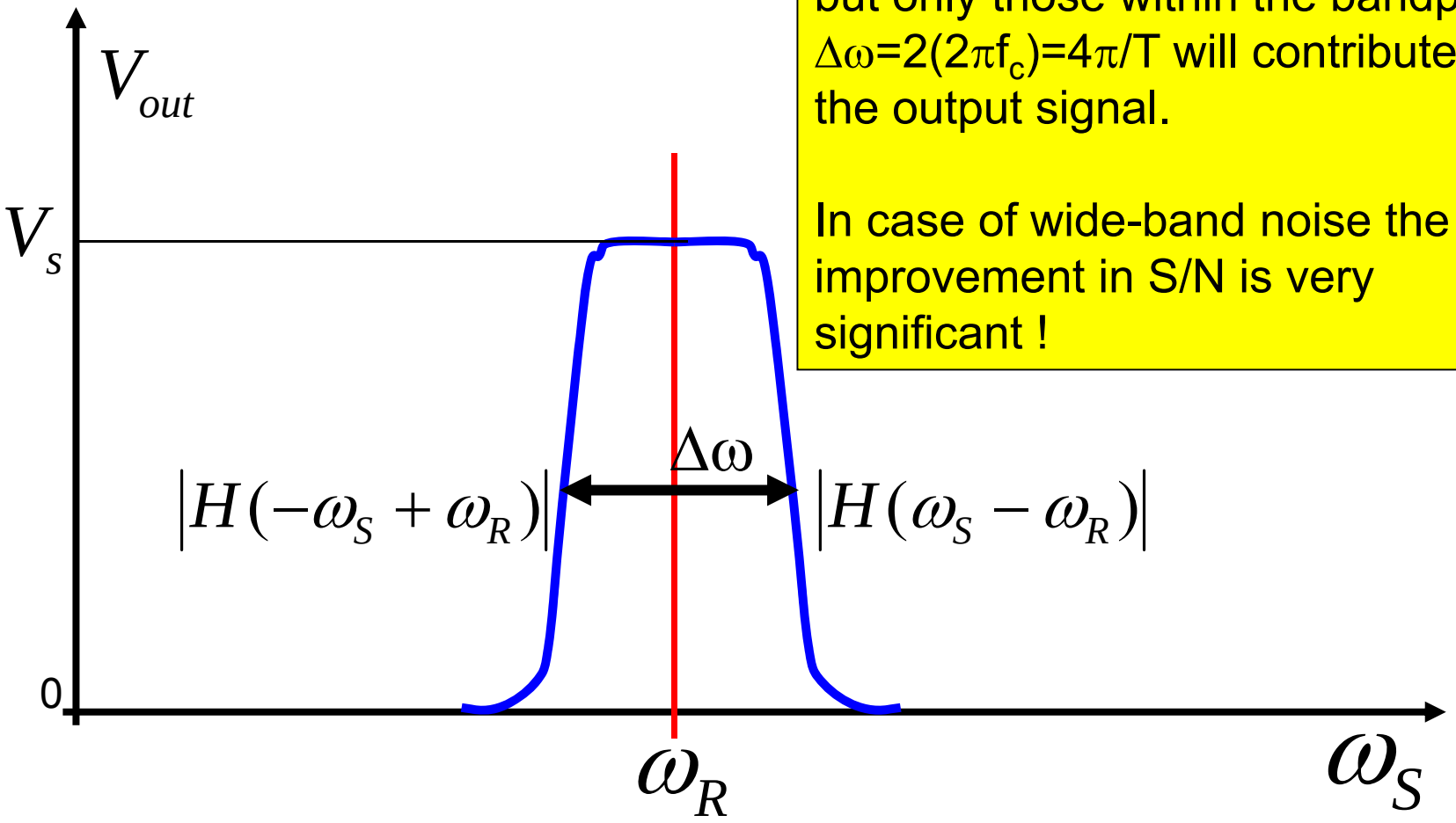

If w_V is the spectral density of the noise (in V^2/Hz) :

$$N_{in} = \sqrt{w_V \, f_{\max}} \quad ; \quad N_{out} = \sqrt{\frac{w_V}{2T}}$$

$$\frac{S / N_{out}}{S / N_{in}} = \sqrt{2Tf_{\max}}$$

Early measurements of CMB anisotropy

- Using the beam-switching technique described above, you can integrate for some time on one couple of directions, then change directions and integrate again, then change … until you get a statistical sample of the sky, consisting typically in a few tens to a few hundreds sky temperature differences ΔT_i .
- This is enough to estimate the rms fluctuation of the temperature (brightness) of the sky, extracting it from the noise.
- These experiments started immediately after the discovery of the CMB (Penzias and Wilson stated in the discovery paper of 1965 that it was isotropic to 10%)… and were very frustrating !
- For more than two decades a few groups of pioneers of the CMB improved their isotropometers, obtaining increasingly stringent upper limits for the anisotropy of the CMB, down to a level

$$\frac{\Delta T}{T} < 10^{-4}$$

at scales of the order of the horizon. So regions which have never been in causal contact before produce the same CMB brightness, with outstanding precision. How is this possible ? This is the **paradox of horizons.**

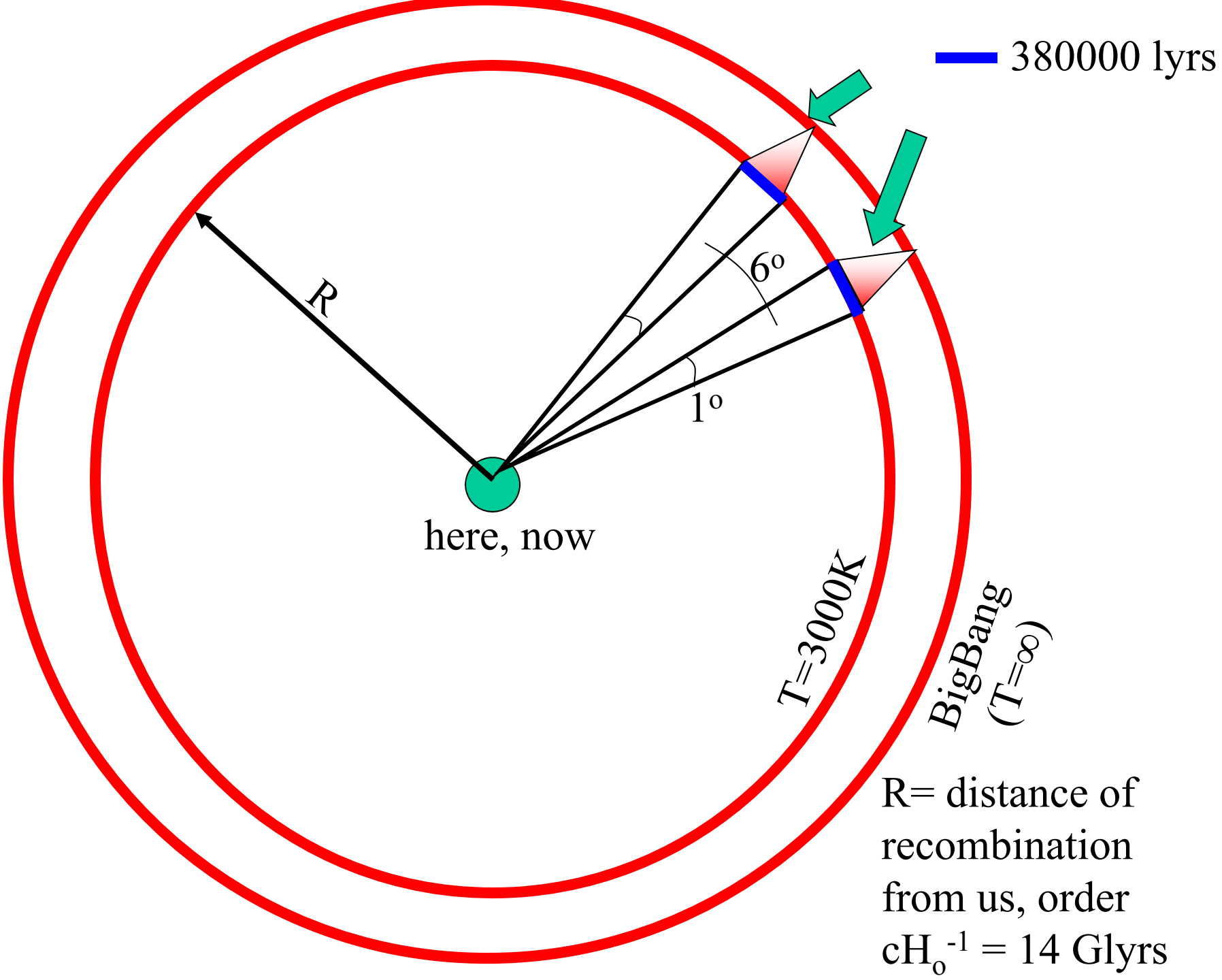

R= distance of recombination from us, order cH_o^{-1} = 14 Glyrs

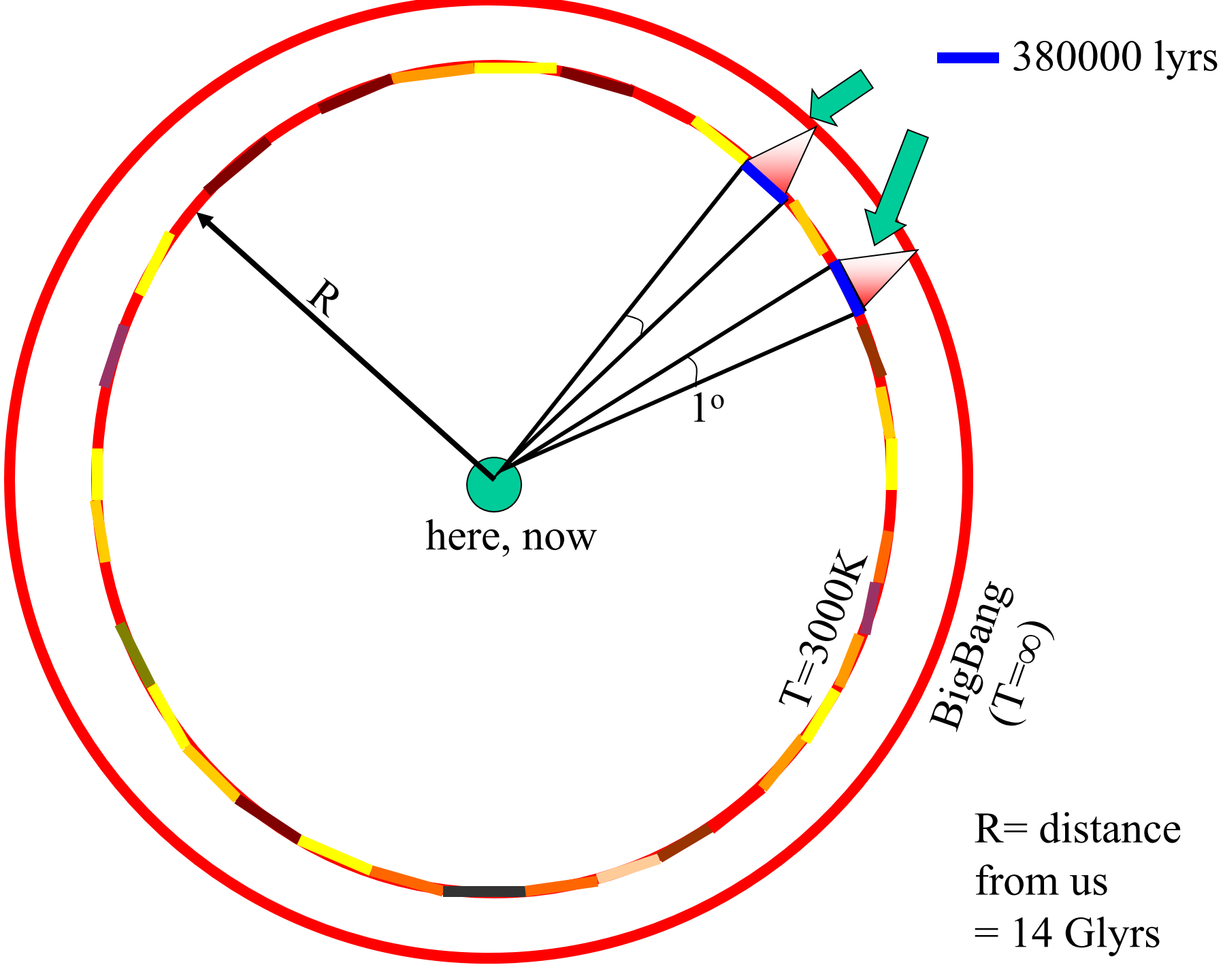
380000 lyrs
R
1°
here, now
T=3000K
BigBang
(T=∞)
R= distance
from us
= 14 Glyrs

1992 : COBE-DMR

- COBE-DMR was a set of 3 differential radiometers aboard of the COBE satellite.
- Each radiometer had two horn antennas and a switch to measure the difference in sky temperature (brightness) between two directions 60° apart.
- The angular resolution of the antennas was 7° FWHM.
- The satellite was spinning, so each differential radiometer scanned the sky, producing a large number of independent difference measurements, which were eventually converted into maps of the microwave sky at 31.5, 53, 90 GHz, with a resolution around 10°

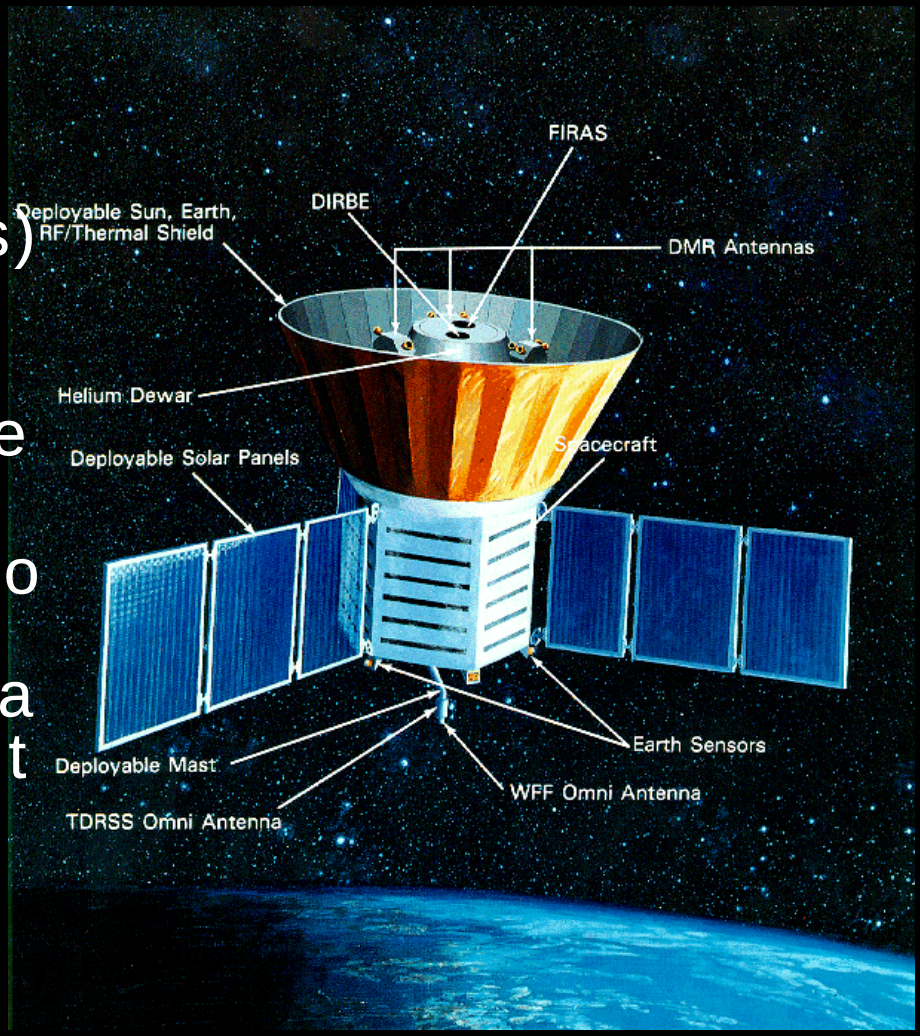

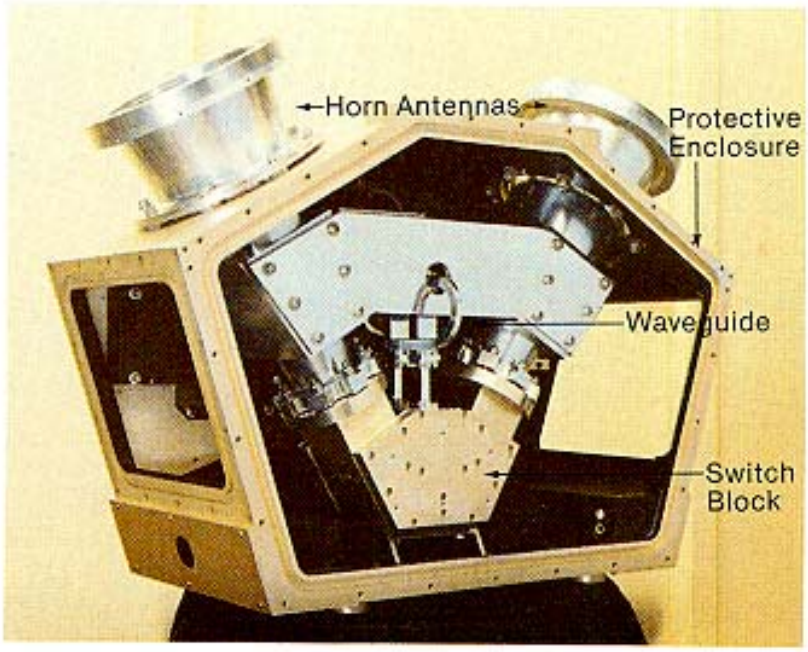

The 9.6 mm DMR receiver partially assembled. Corrugated cones are antennas.

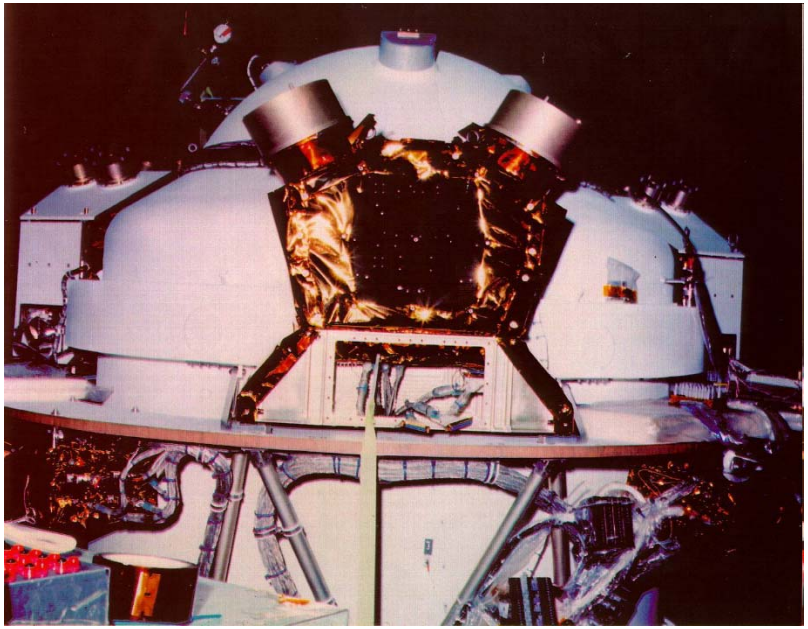

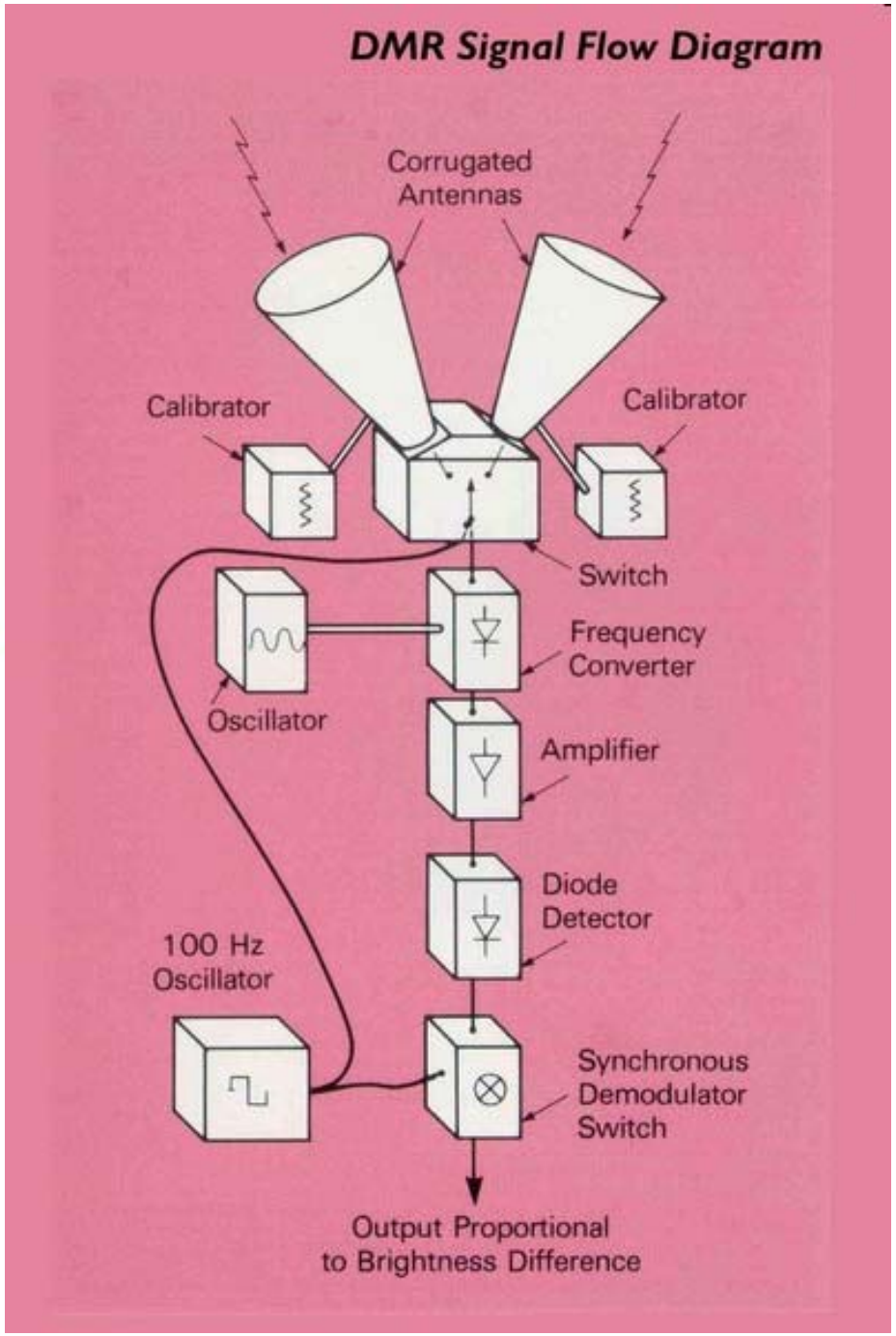

- COBE map of the whole sky :

Red : $\Delta T = + 3$ mK
Blue : $\Delta T = - 3$ mK

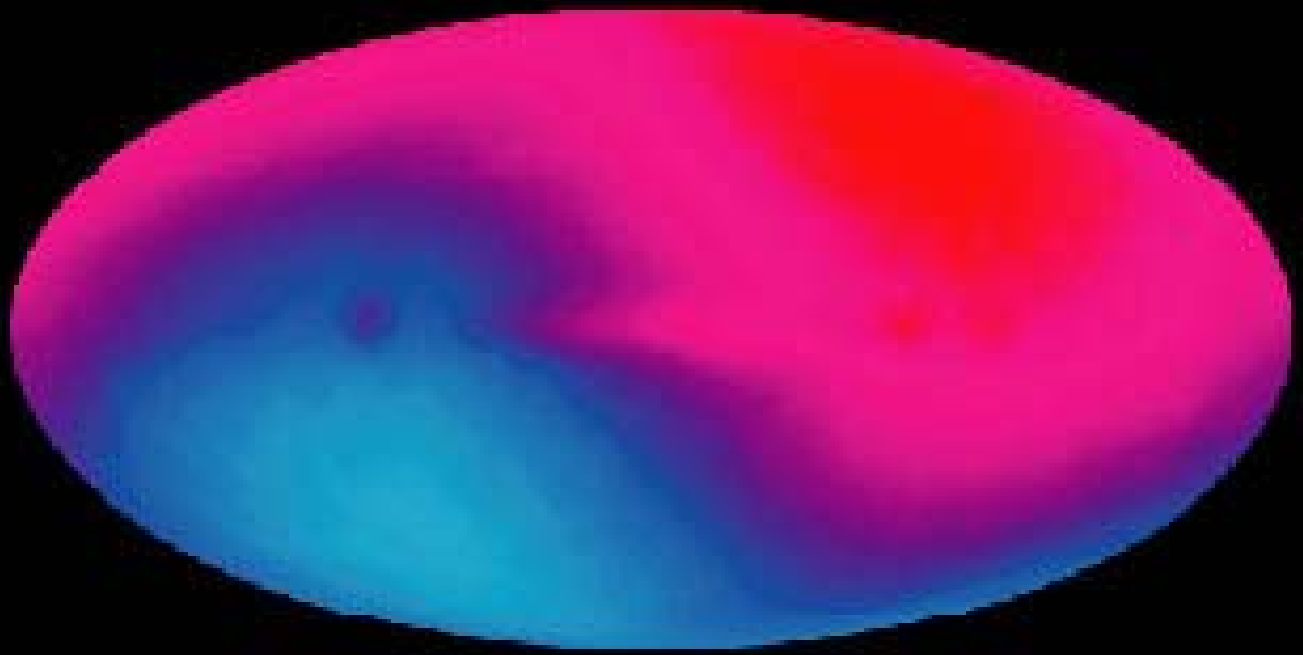

- COBE map of the whole sky

Red : $\Delta T = +3$ mK
Blue : $\Delta T = -3$ mK

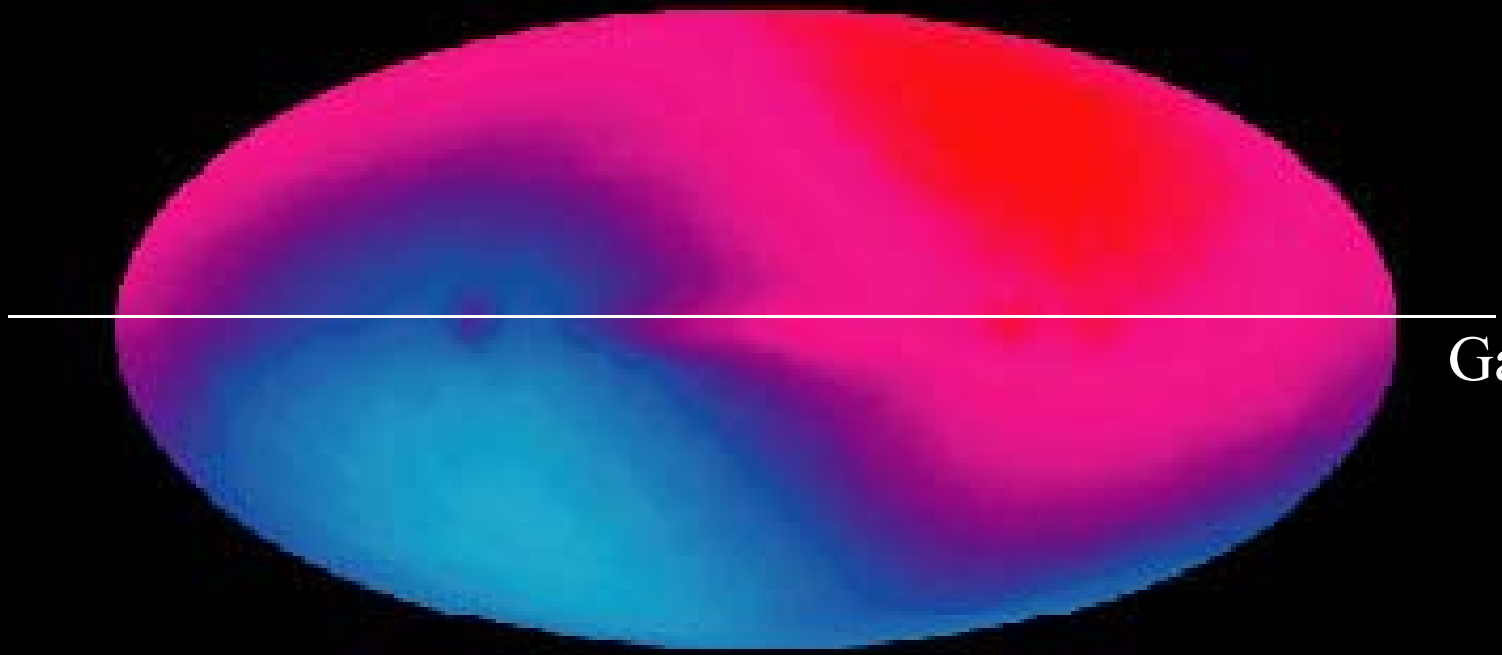

- COBE map of the whole sky

Red : $\Delta T = +3$ mK
Blue : $\Delta T = -3$ mK

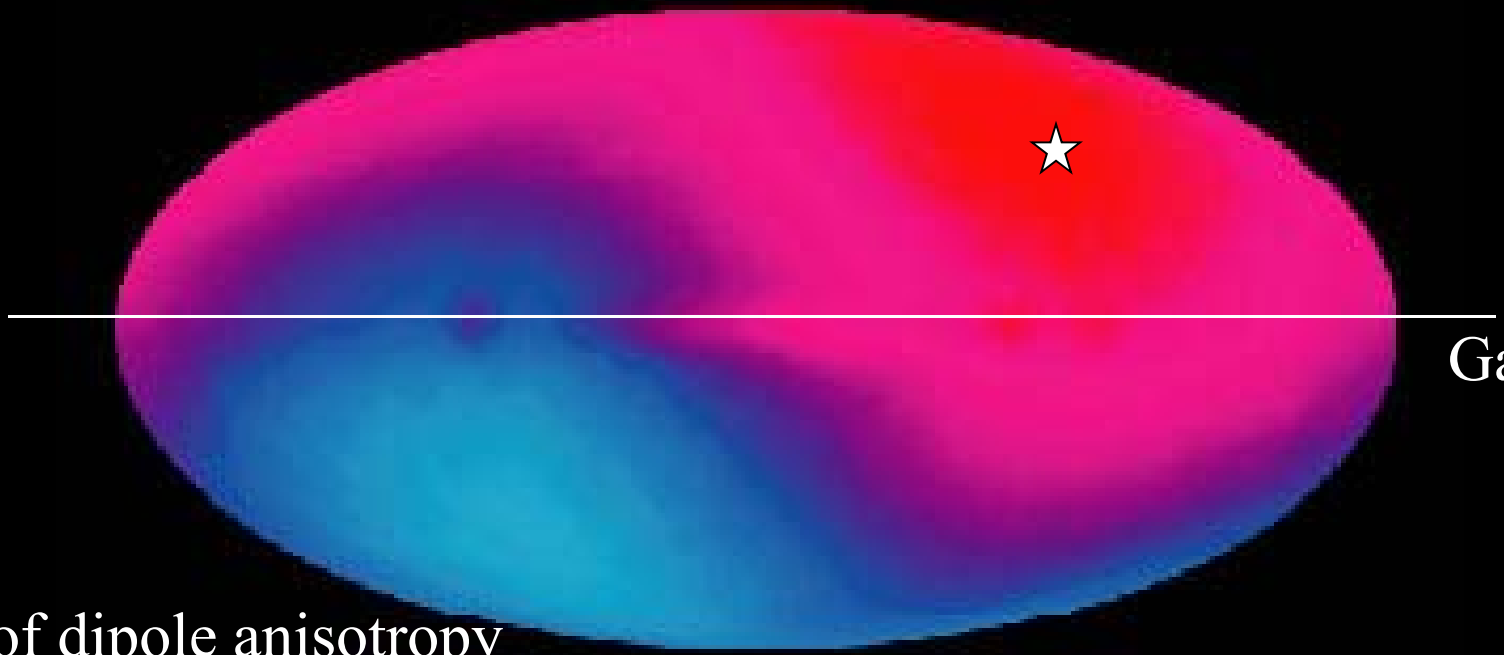

★ apex of dipole anisotropy (WMAP)
$l=(263.85\pm0.1)^o$
$b=(48.25\pm0.04)^o$
(close to the ecliptic…)

Amplitude of dipole anisotropy (WMAP)
$\Delta T=(3.346\pm0.017)$mK

Derivation of the CMB dipole

- We are moving with a velocity v with respect to the CMB Last Scattering Surface.
- The CMB is isotropic in the reference frame O' of the LSS, but is not isotropic in the restframe O of the observer, which is in motion.
- The distribution function f of particles with momentum $\mathbf{p}$ is a Lorentz invariant: In fact

$$f(\mathbf{p}) = \frac{dN}{dx^i dp^i}$$

where dN is a scalar, so is invariant, and the phase space volume $dx^i dp^i$ can also be shown to be a Lorentz invariant. So

$$f'(\mathbf{p}') = f(\mathbf{p})$$

Derivation of the CMB dipole

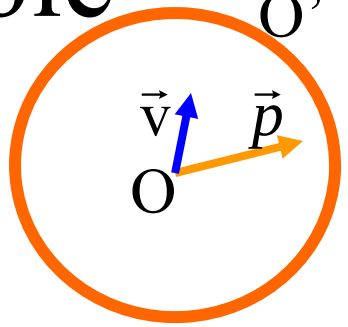

- The Lorentz transformation for the momentum **p** is

$$c\vec{p} = \frac{\sqrt{1 - v^2/c^2}}{1 - \vec{v} \times \vec{n}/c} c\vec{p}' \qquad \vec{n} = \vec{p}/p$$

- Applying this eq. to the Planck distribution function for photons we get

$$T = \frac{p}{p'} T' \quad \Rightarrow T = \frac{\sqrt{1 - v^2/c^2}}{1 - \vec{v} \times \vec{n}/c} T' = \frac{\sqrt{1 - \beta^2}}{1 - \beta \cos(\theta)} T'$$

- This formula was first derived by Mosengheil (1907), and rederived by Peebles and Wilkinson (1968), Heer and Kohl (1968), Forman (1970).
- For small β:

$$T(\theta) \cong T_o \left[1 + \beta \cos(\theta) + \frac{\beta^2}{2} \cos(2\theta) \right]$$

kinematic term

light aberration term

β

- The motion of the Earth with respect to the CMB is the combination of
  - The motion of the Earth around the Sun (well known)
  - The motion of the Sun in the Galaxy (well known)
  - The motion of the Galaxy in the Local Group (known)
  - The bulk motion of the Local Group (not well known) due to the gravitational acceleration generated by all other large masses present in the Universe
- The annual revolution of the Earth around the Sun is known extremely well (v ~ 30 km/s), and produces an **annual modulation in the CMB dipole**. This is the main signal used in COBE and WMAP for the Dipole calibration, since it is known from astrometric measurements, much better than the total motion of the earth.
- This effect produces a modulation of the order of βT_o, i.e. about 300μK, on a total dipole of the order of 3.5 mK.

CMB dipole signal

- The CMB temperature fluctuation corresponds to a CMB brightness fluctuation, which can be found by deriving the Planck formula with respect to T:

$$\Delta I = \frac{x e^x}{e^x - 1} B(T_{CMB}, \nu) \Delta T \quad ; \quad x = \frac{h\nu}{kT_{CMB}}$$

- This conversion from Temperature to Brightness is the same for the dipole and for any smaller scale temperature or polarization anisotropy. For this reason the Dipole spectrum is the same as the spectrum of CMB anisotropy. The maximum of this spectrum is at 271 GHz.

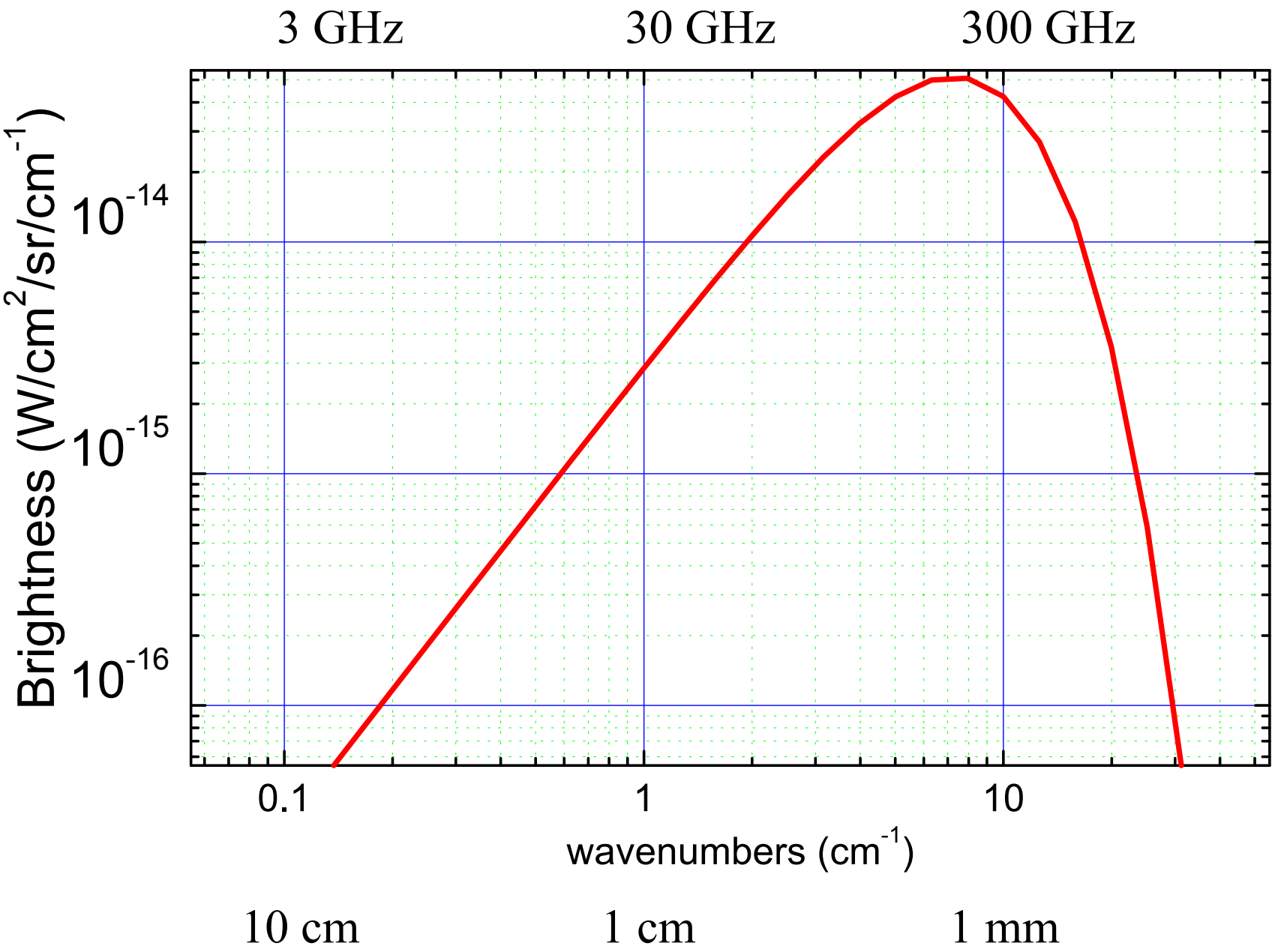
3 GHz
30 GHz
300 GHz
Brightness (W/cm^2/sr/cm^{-1})
10^{-14}
10^{-15}
10^{-16}
0.1
1
10
wavenumbers (cm^{-1})
10 cm
1 cm
1 mm

Large-Scale Anisotropy

- Removing the dipole component, COBE-DMR detects a small (10ppm rms) large-scale anisotropy of the CMB.
- This incredible smoothness *requires* an inflationary process, happening in the first split second after the Big Bang, and causally connecting regions which, at recombination, are separated more than the horizon.

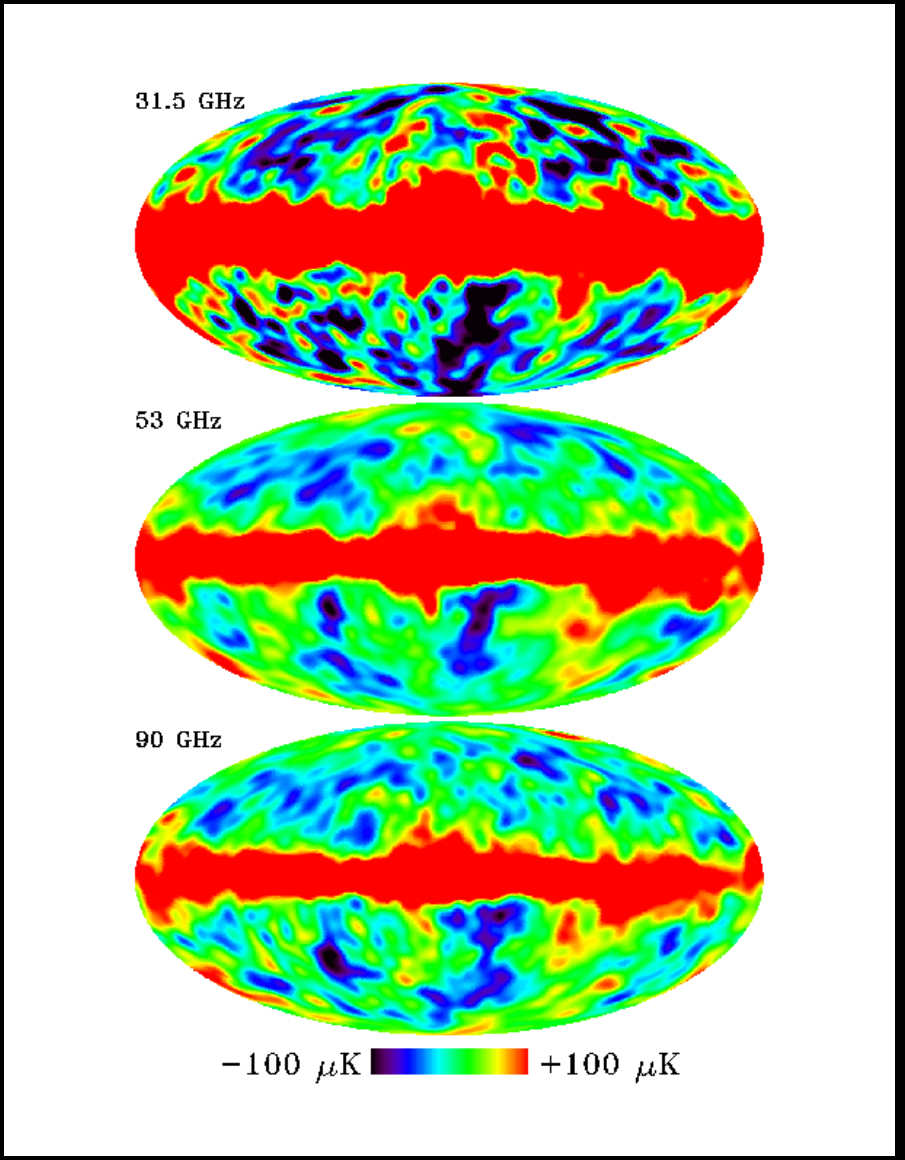

G. Smoot et al. 1992, Nobel Pize in 2006

Expansion vs Horizon

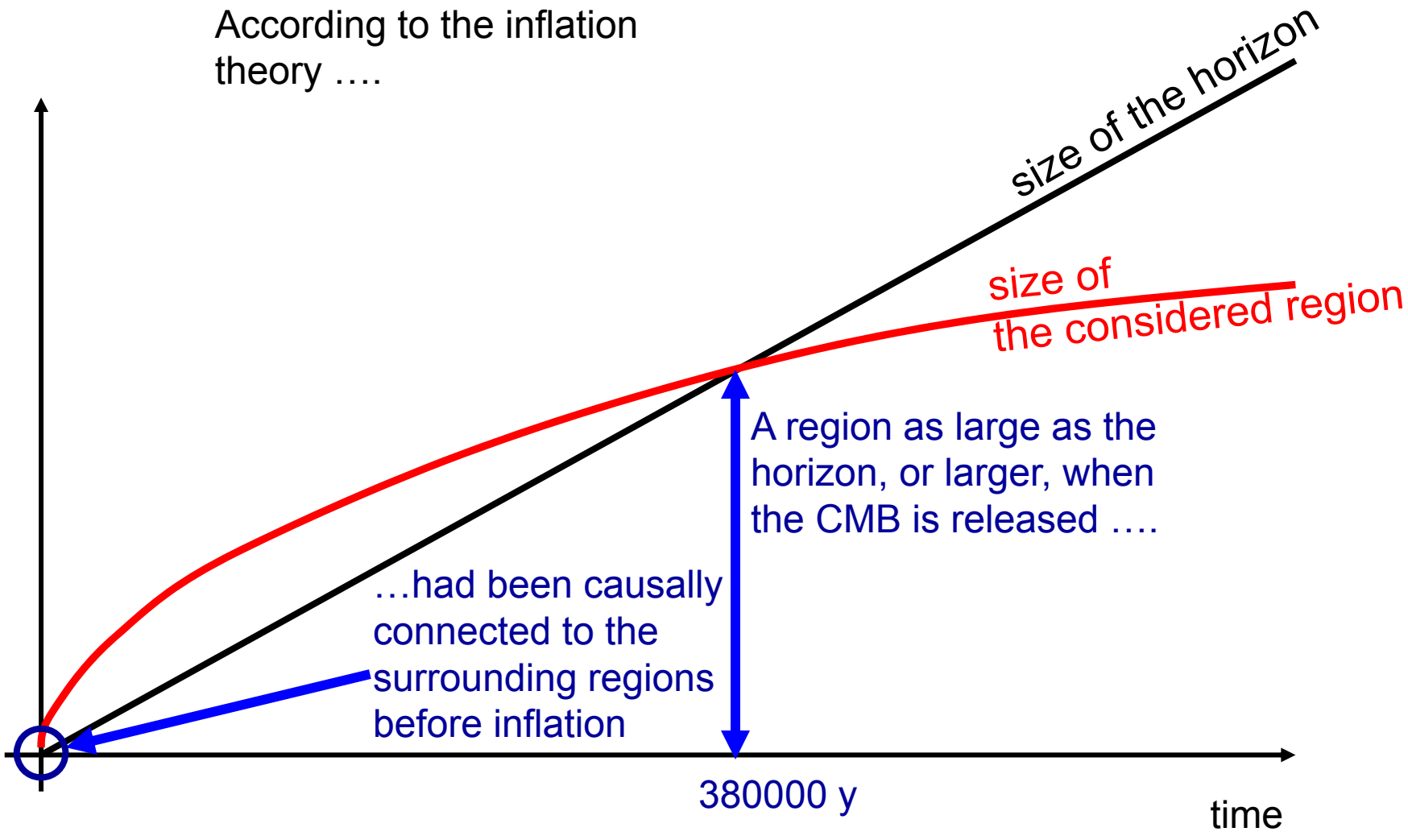

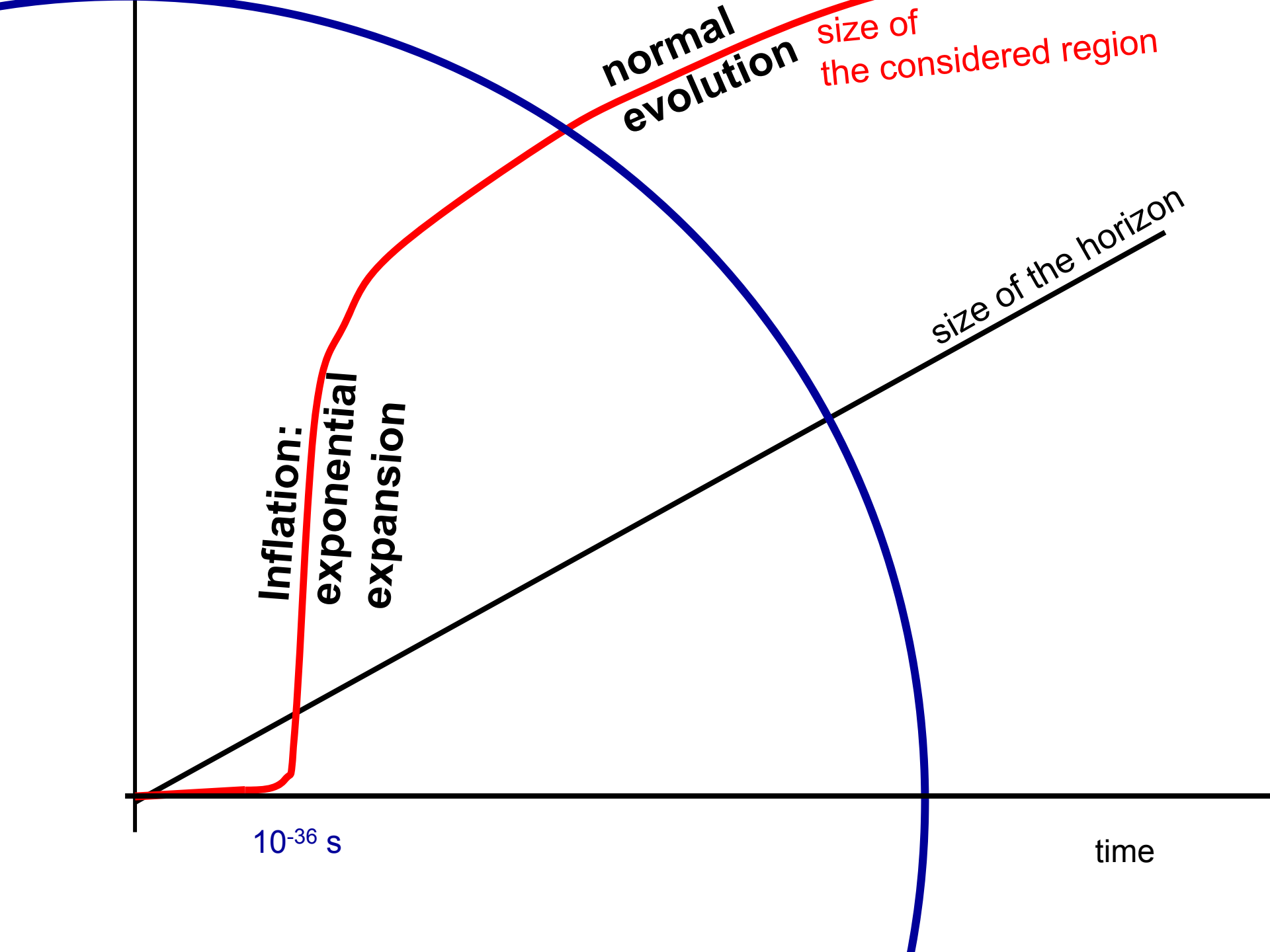
normal
evolution
size of
the considered region
size of the horizon
Inflation:
exponential
expansion
10-36 s
time

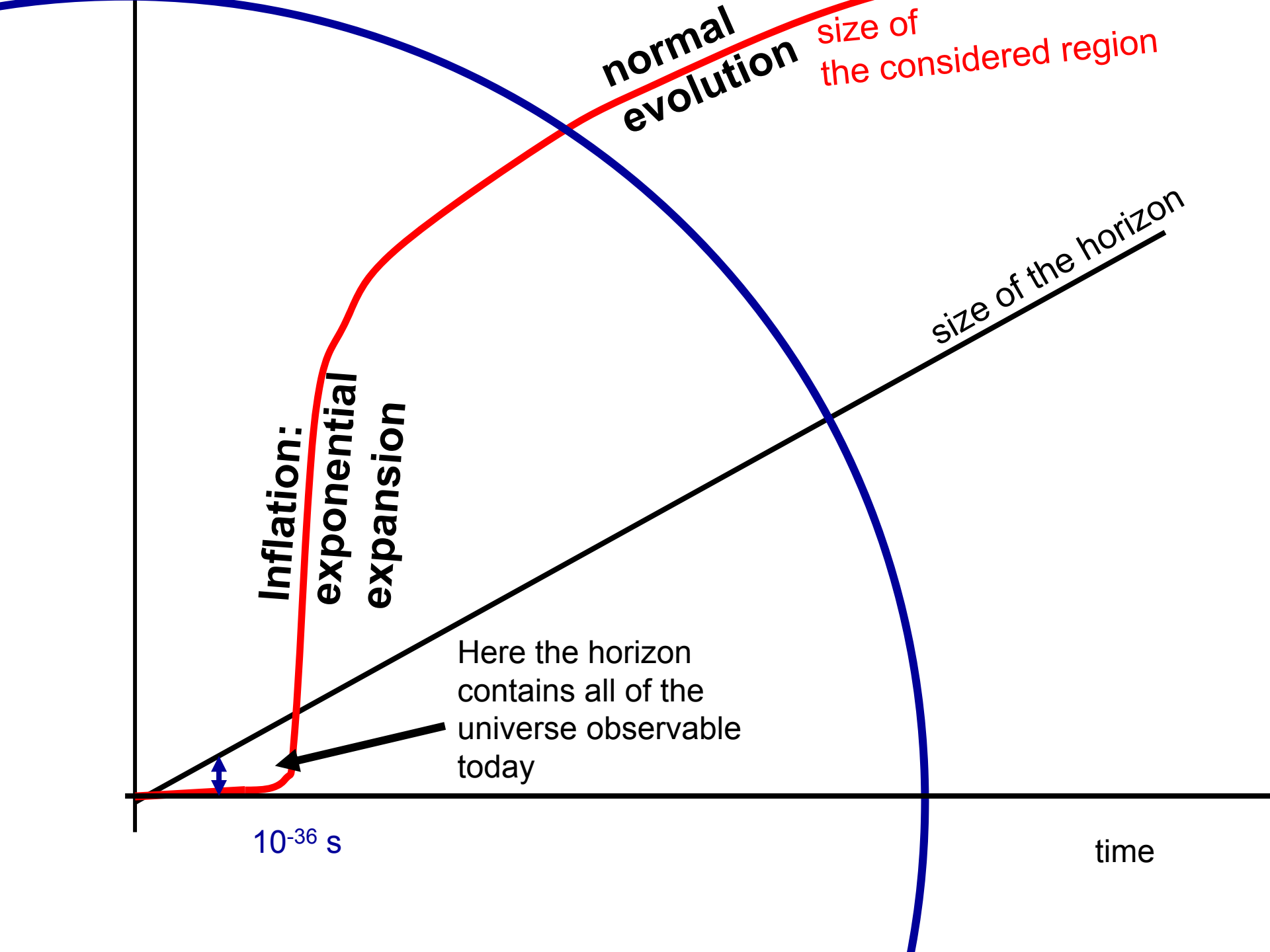
normal evolution
size of the considered region
size of the horizon
Inflation: exponential expansion
Here the horizon contains all of the universe observable today
10^{-36} s
time

Inflation

- Inflation is produced by a phase transition in the very early universe, resulting in a very short period of exponential expansion of space.
- It was introduced to solve the paradox of horizons, but also to solve other problems: the paradox of flatness, the paradox of magnetic monopoles, …
- .. and to provide a physical origin for the density fluctuations producing large-scale structures in the universe.
- As we will see later, inflation is a *predictive* theory, and most of its predictions have been *tested* quite deeply.
- But let's go back to CMB measurements.

The quest for sensitivity and angular resolution.

- Having solved the paradox of horizons, we still have a long time (basically all the 380000 years of the primeval fireball before recombination) in which horizon-sized regions evolve independently.
- We still expect to see the characteristic size of the horizon at recombination imprinted in the microwave sky, even if not dramatically as in the paradox of horizons.
- COBE-DMR was on-board of a small satellite, and did not have large telescopes, only feed-horns directly looking at the sky, limiting its resolution to 7° FWHM .
- This was not sufficient to measure degree-sized horizons..

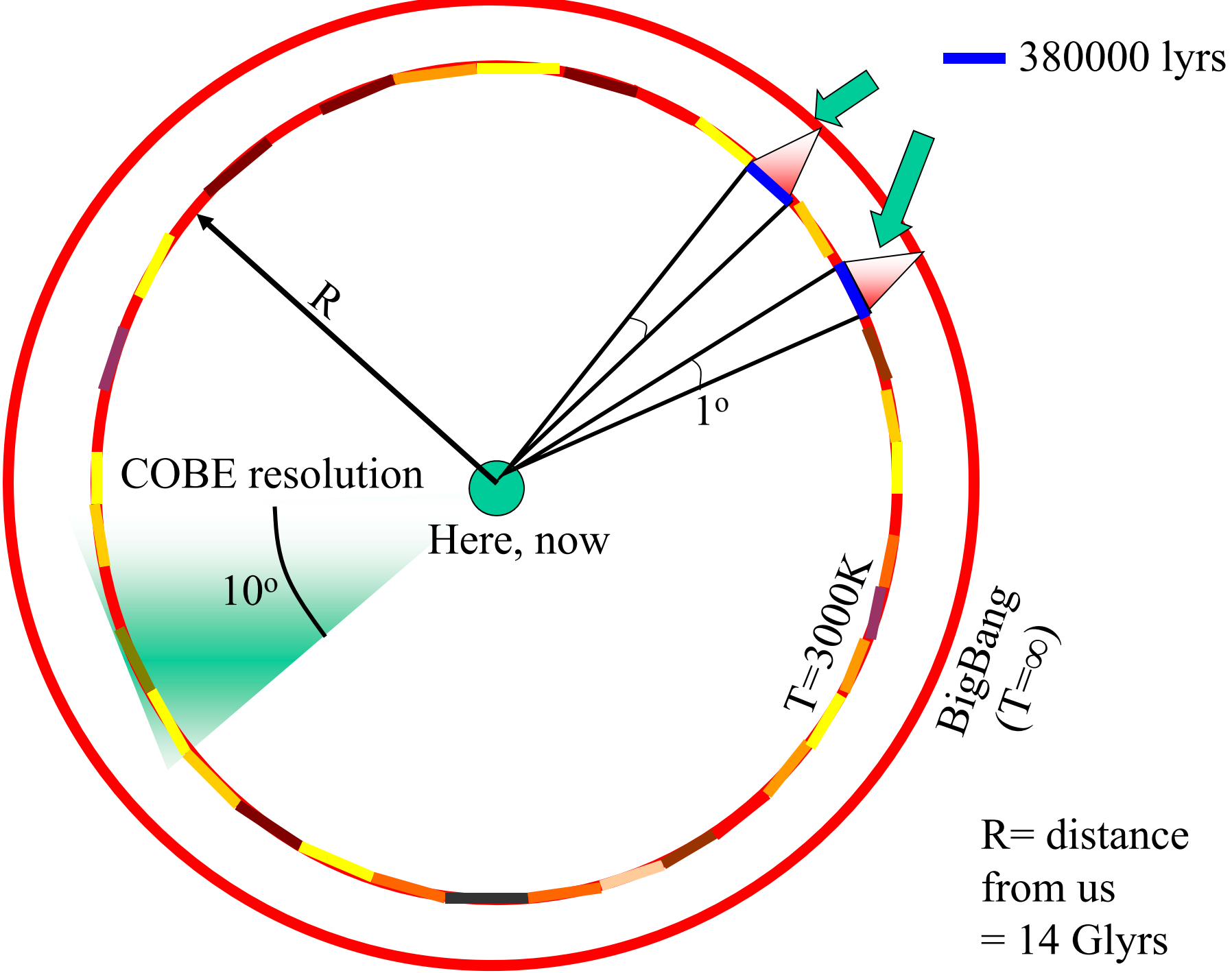
380000 lyrs
R
1°
COBE resolution
10°
Here, now
T=3000K
BigBang
(T=∞)
R= distance
from us
= 14 Glyrs

- The study of solar oscillations allows us to investigate the interior structure of the sun, well below the solar photosphere.

- The study of CMB anisotropy allows us to investigate the oscillations of the primeval plasma, and the universe well behind (well before) the cosmic photosphere (the recombination epoch)

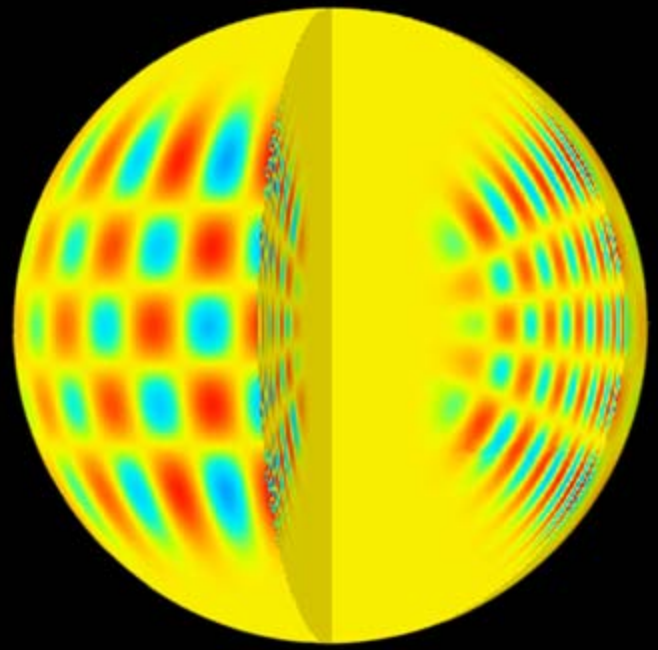

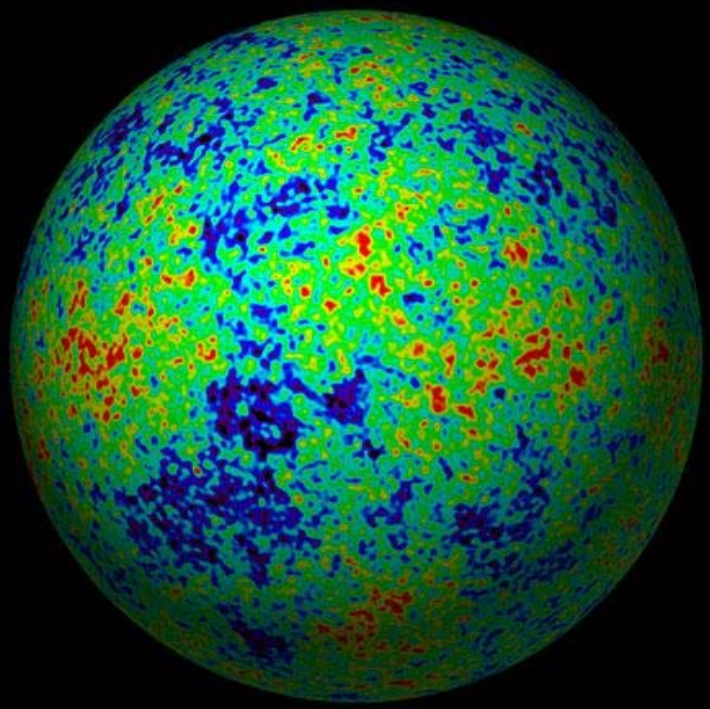

Density perturbations ($\Delta\rho/\rho$) were **oscillating** in the primeval plasma (as a result of the opposite effects of gravity and photon pressure).

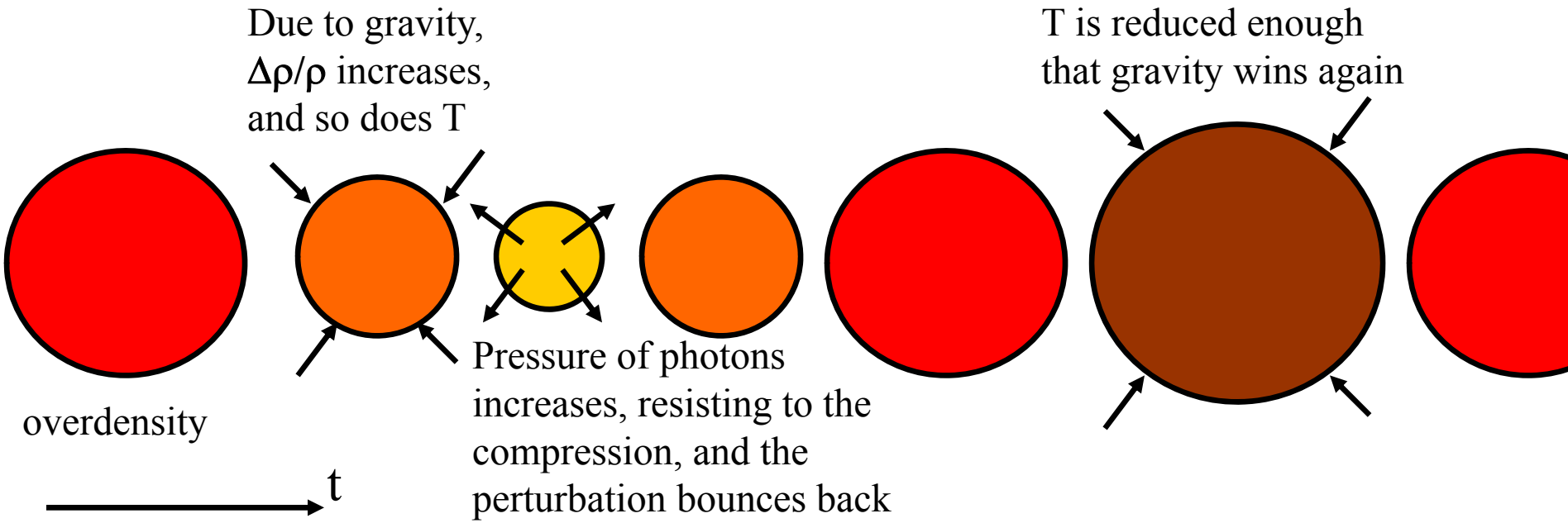

After recombination, density perturbation can **grow** and create the hierarchy of structures we see in the nearby Universe.

- The brightness (temperature) fluctuations are due to small density fluctuations present in the primeval fireball, and to their motions:

$$\frac{\Delta T}{T} = \frac{1}{4}\frac{\Delta \rho_\gamma}{\rho_\gamma} + \frac{1}{3}\frac{\Delta \varphi}{c^2} + \frac{\mathrm{v}}{c}$$

Photon Density fluctuations

Gravitational redshift

Scattering against moving e^-

- Overdensity : Gravitational redshift :

$$\frac{\delta T}{T} = -\frac{\delta\Phi}{c^2}$$

- Overdensity : time delay

$$\frac{\delta t}{t} = -\frac{\delta\Phi}{c^2}$$

- During the matter-dominated phase:

$$T \propto 1/a \quad ; \quad a \propto t^{2/3} \quad \rightarrow \quad \frac{\delta T}{T} = -\frac{\delta a}{a} = -\frac{2}{3}\frac{\delta t}{t} = \frac{2}{3}\frac{\delta\Phi}{c^2}$$

- So, in total $\frac{\delta T}{T} = -\frac{1}{3}\frac{\delta\Phi}{c^2}$ Sachs-Wolfe Effect (1967)

In the primeval plasma, photons/baryons density perturbations start to oscillate only when the sound horizon becomes larger than their linear size . Small wavelength perturbations oscillate faster than large ones.

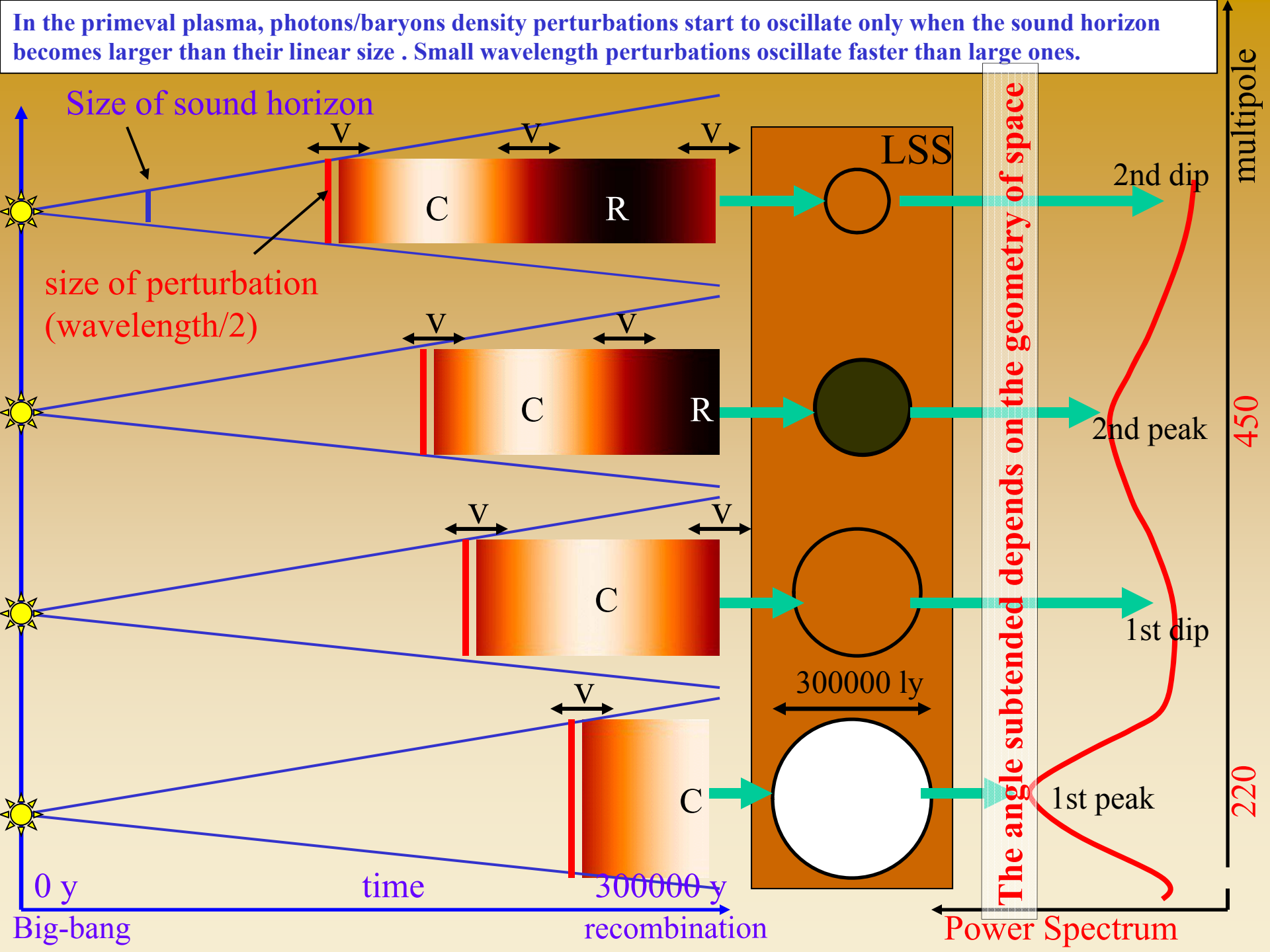

Paradigm of CMB anisotropies

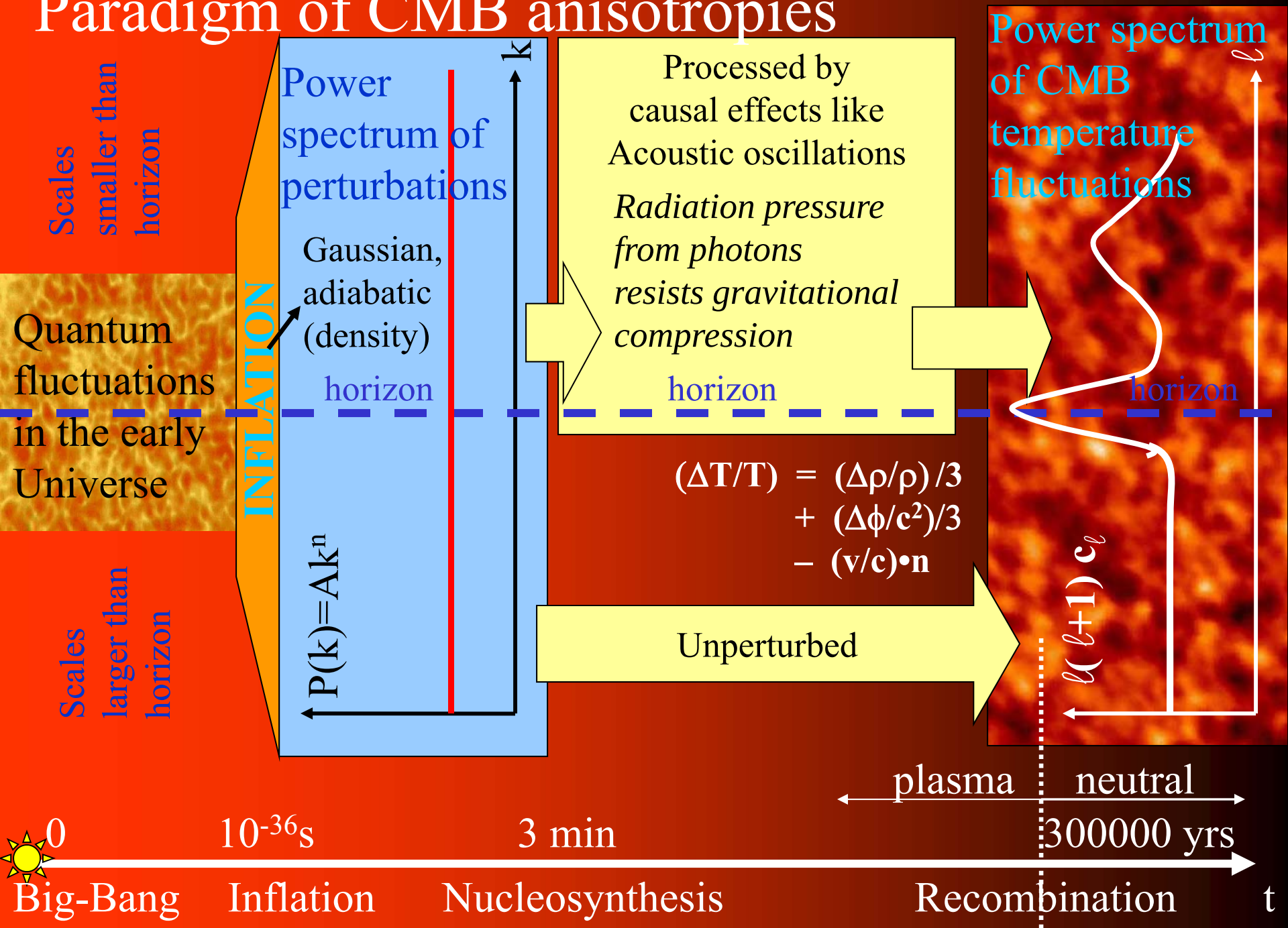

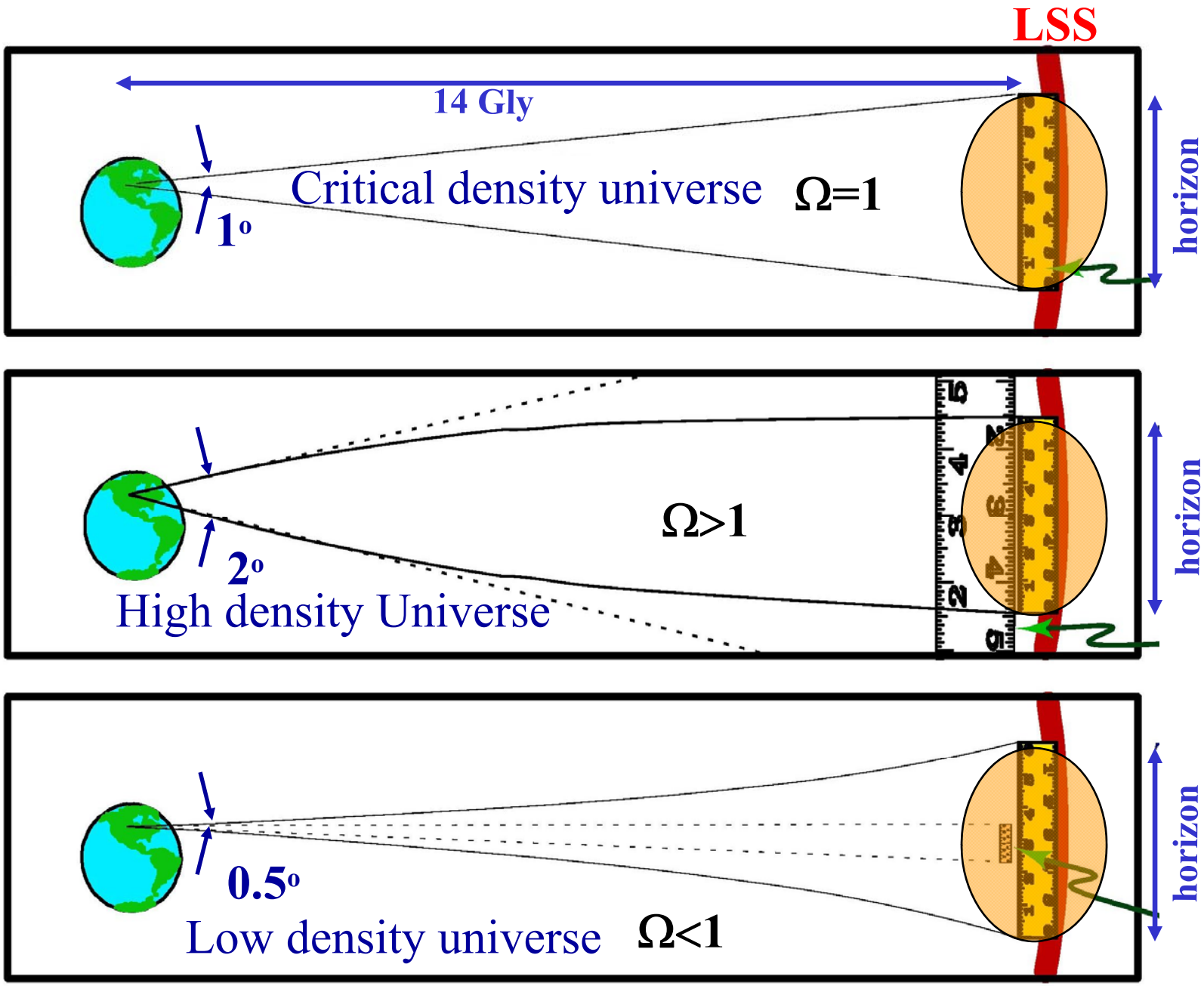
LSS
14 Gly
Critical density universe
Ω=1
1°
horizon
Ω>1
2°
High density Universe
horizon
0.5°
Low density universe
Ω<1
horizon

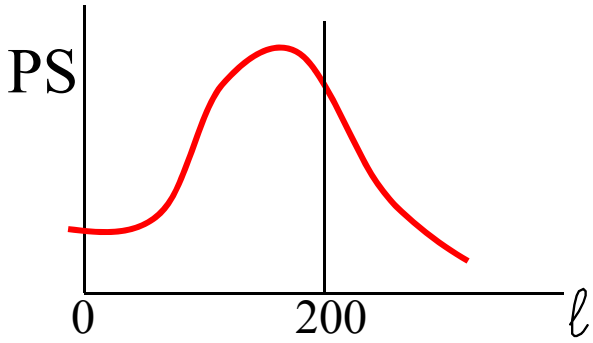

High density Universe

Ω>1

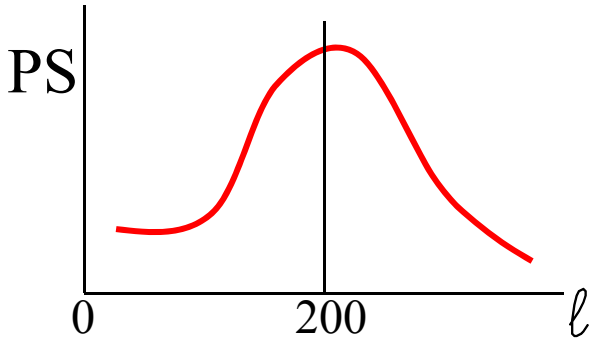

Critical density Universe

Ω=1

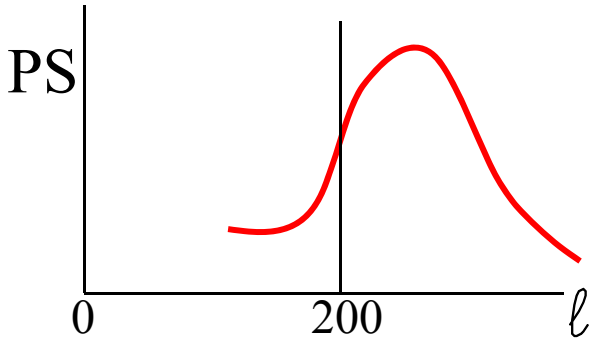

Low density Universe

Ω<1

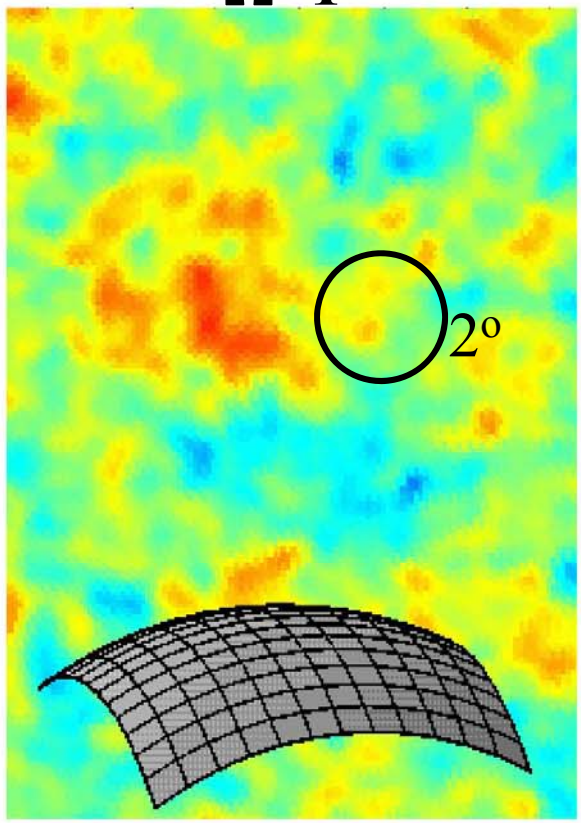

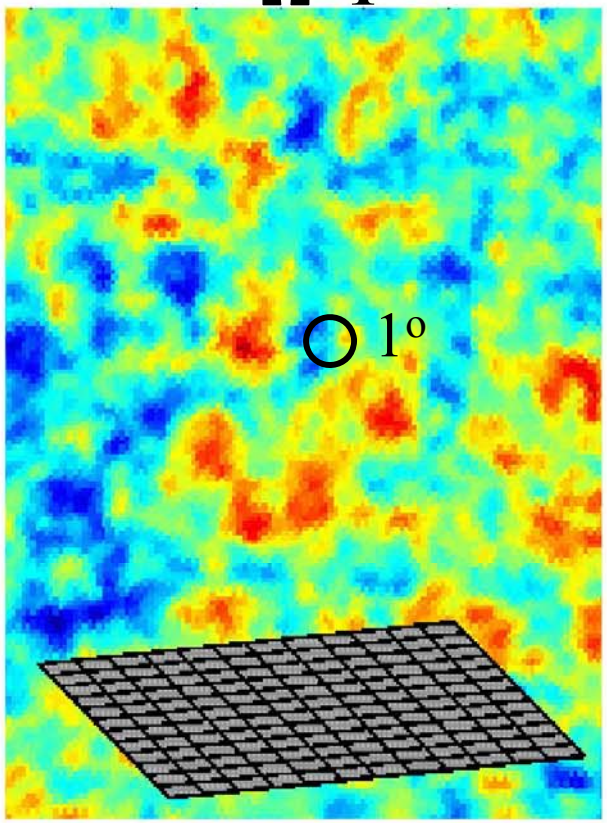

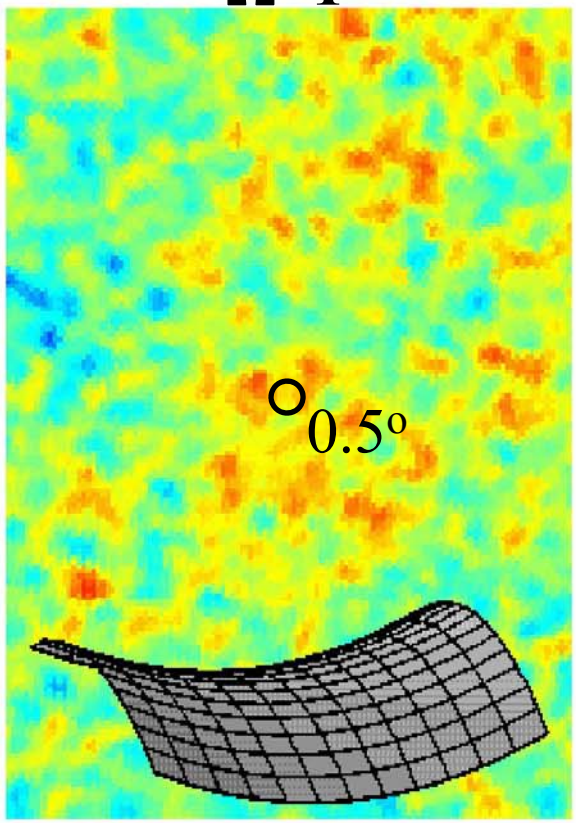

The quest for high angular resolution

- The **angular power spectrum** $\mathbf{c}_\ell$ of the anisotropy defines the contribution to the rms ΔT from the different multipoles:

$$\Delta T(\theta,\varphi) = \sum_{\ell,m} a_{\ell m} Y_\ell^m(\theta,\varphi)$$

$$c_\ell = \left\langle a_{\ell m}^2 \right\rangle$$

$$\left\langle \Delta T^2 \right\rangle = \frac{1}{4\pi} \sum_\ell (2\ell+1) c_\ell$$

- A real experiment will not be sensitive in the same way to all the multipoles of the CMB, because it has a finite angular resolution, i.e. the response to off-axis radiation RA(θ,ϕ) is not a delta.
- For example, if the angular response is a gaussian beam with s.d. σ, the corresponding multipoles transform is

$$w_\ell^{LP} = e^{-\ell(\ell+1)\sigma^2}$$

- The detected signal will be:

$$\left\langle \Delta T^2 \right\rangle_{meas} = \frac{1}{4\pi} \sum_\ell (2\ell+1) w_\ell c_\ell$$

$$\frac{\Delta T}{T} = \sum a_{\ell,m} Y_\ell^m(\theta, \phi)$$

$$c_\ell = \langle a_{\ell,m}^2 \rangle$$

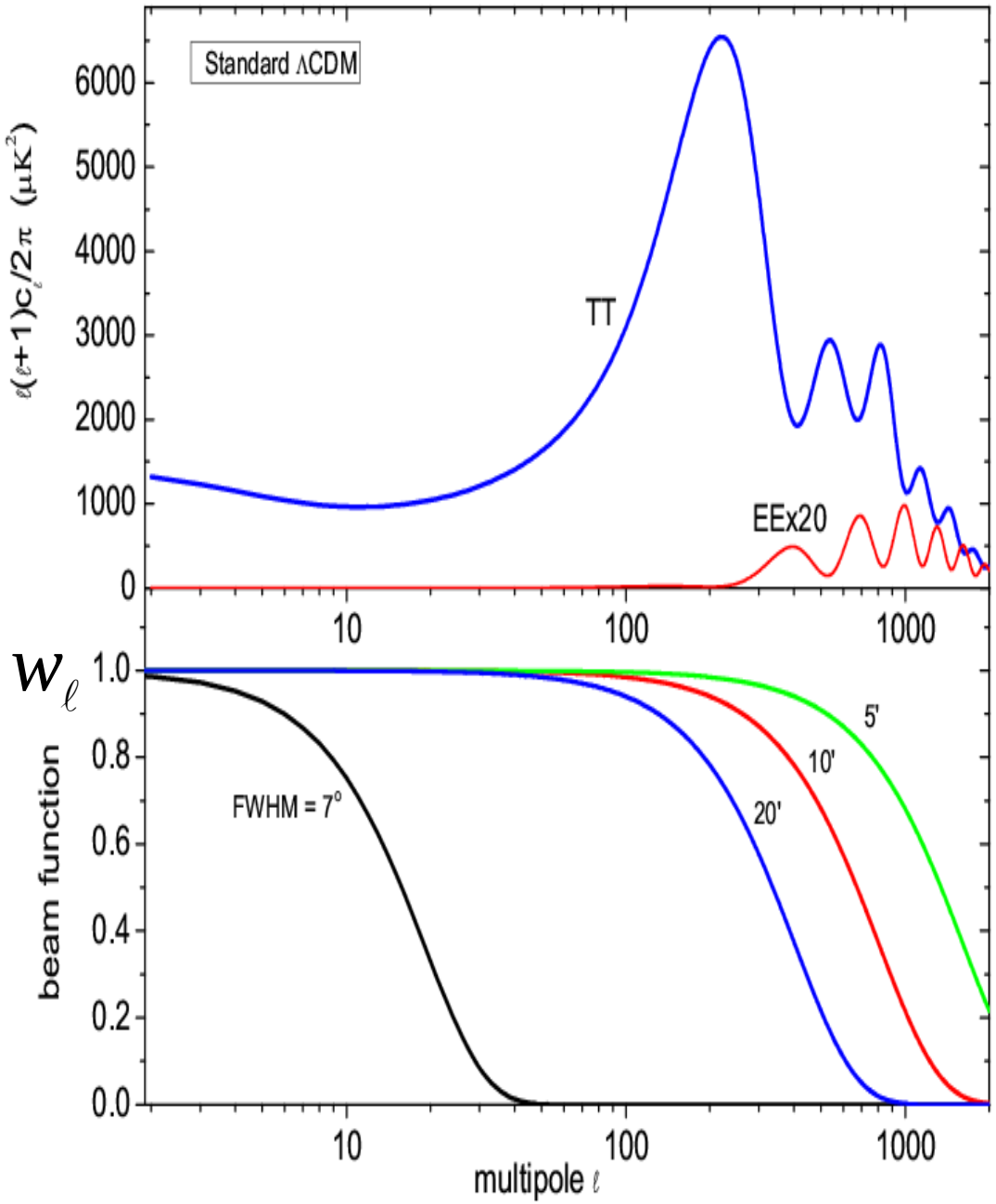

CAMB code

http://camb.info/

Telescopes for the CMB

- Large dimensions of the optical system collecting CMB radiation are required for two reasons :
  - To limit diffraction and detect small structures in the CMB sky
  - To limit far sidelobes and reject strong signals from the ground and other hot sources.

Importance of low sidelobes

- The power detected is the integral of the brightness times the solid angle, weighted with the angular response of the telescope:

Brightness from direction (θ,ϕ)

Telescope response in direction (θ,ϕ)

$$W = A\int_{4\pi} B(\theta,\varphi)RA(\theta,\varphi)d\Omega$$

- Typical telescope response $RA(\theta,\phi)$

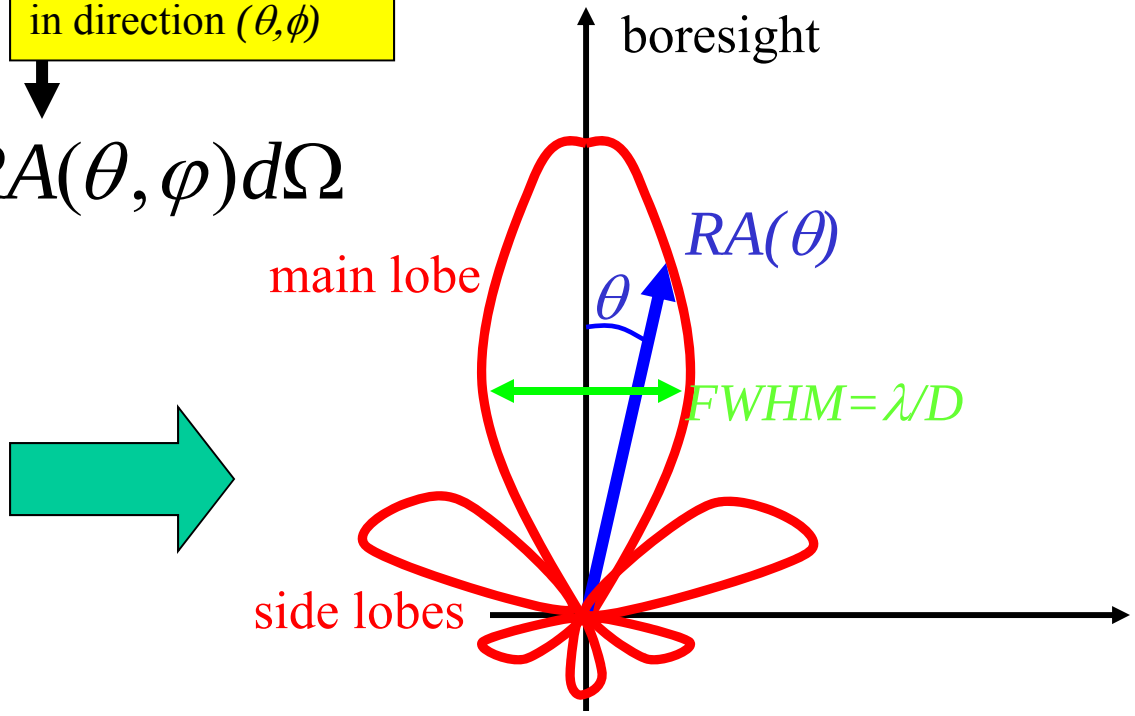

Importance of low sidelobes

- The power detected is the integral of the brightness times the solid angle, weighted with the angular response of the telescope:

Brightness from direction (θ,ϕ)

Telescope response in direction (θ,ϕ)

$$W = A\int_{4\pi} B(\theta,\varphi)RA(\theta,\varphi)d\Omega$$

- Typical telescope response $RA(\theta,\phi)$

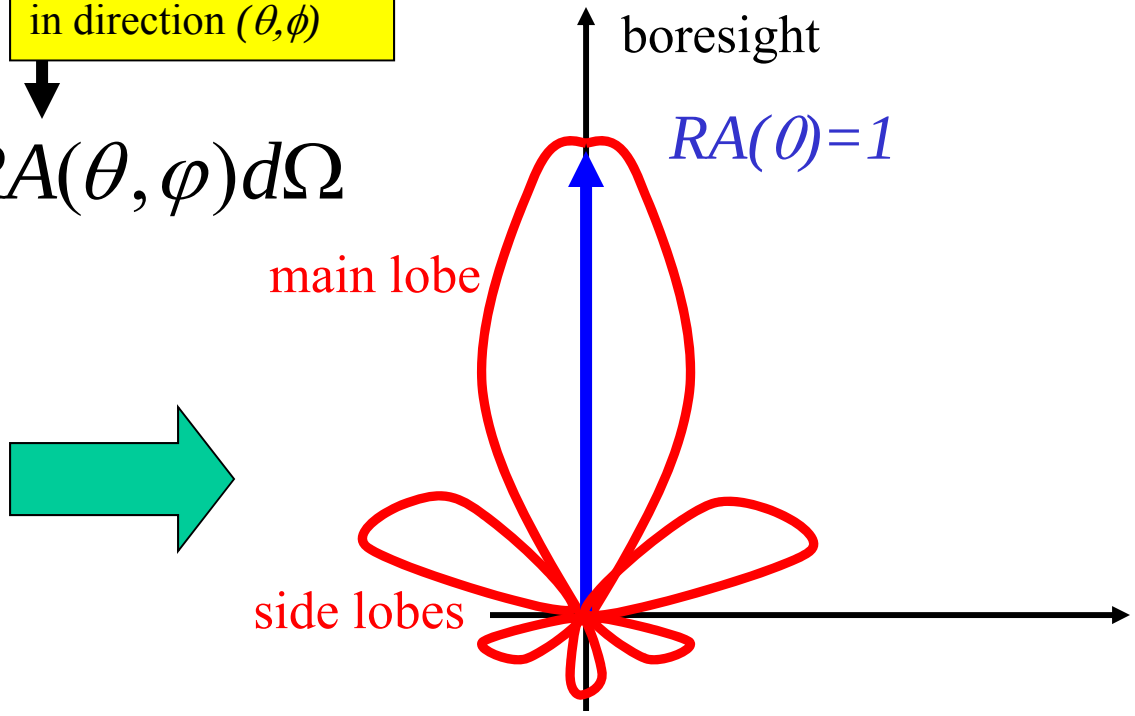

Importance of low sidelobes

- The power detected is the integral of the brightness times the solid angle, weighted with the angular response of the telescope:

Brightness from direction (θ,ϕ)

Telescope response in direction (θ,ϕ)

$$W = A\int_{4\pi} B(\theta,\varphi)RA(\theta,\varphi)d\Omega$$

- Typical telescope response $RA(\theta,\phi)$

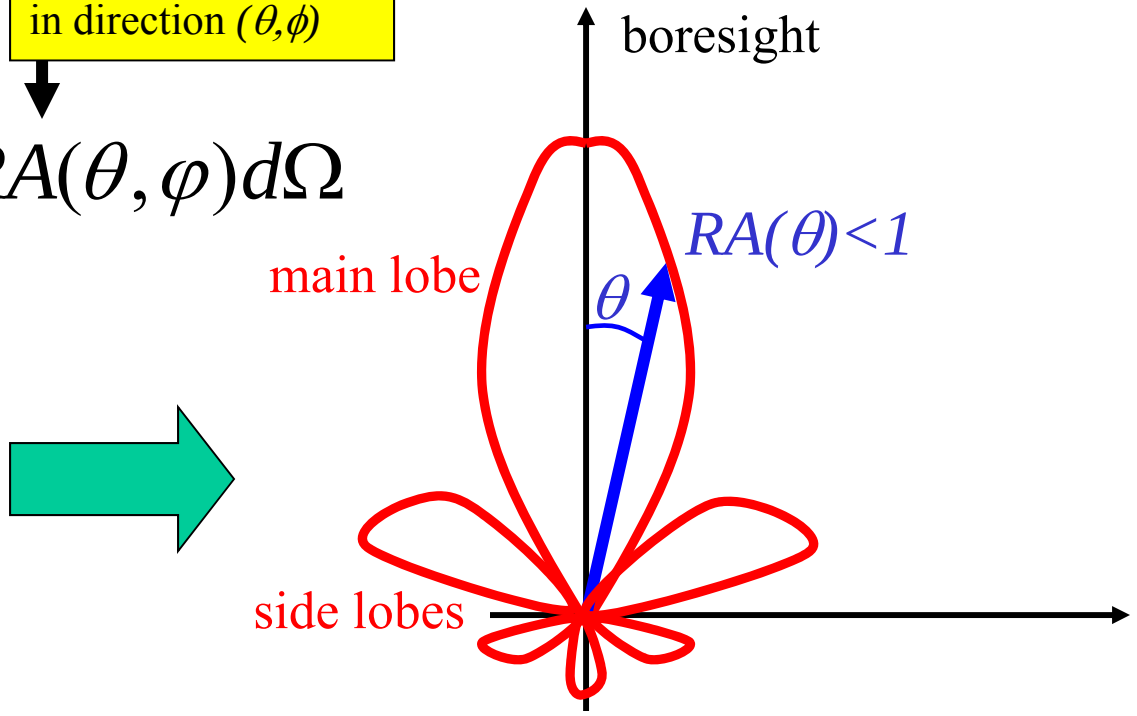

Importance of low sidelobes

- The power detected is the integral of the brightness times the solid angle, weighted with the angular response of the telescope:

Brightness from direction (θ,ϕ)

Telescope response in direction (θ,ϕ)

$$W = A\int_{4\pi} B(\theta,\varphi)RA(\theta,\varphi)d\Omega$$

- Typical telescope response $RA(\theta,\phi)$

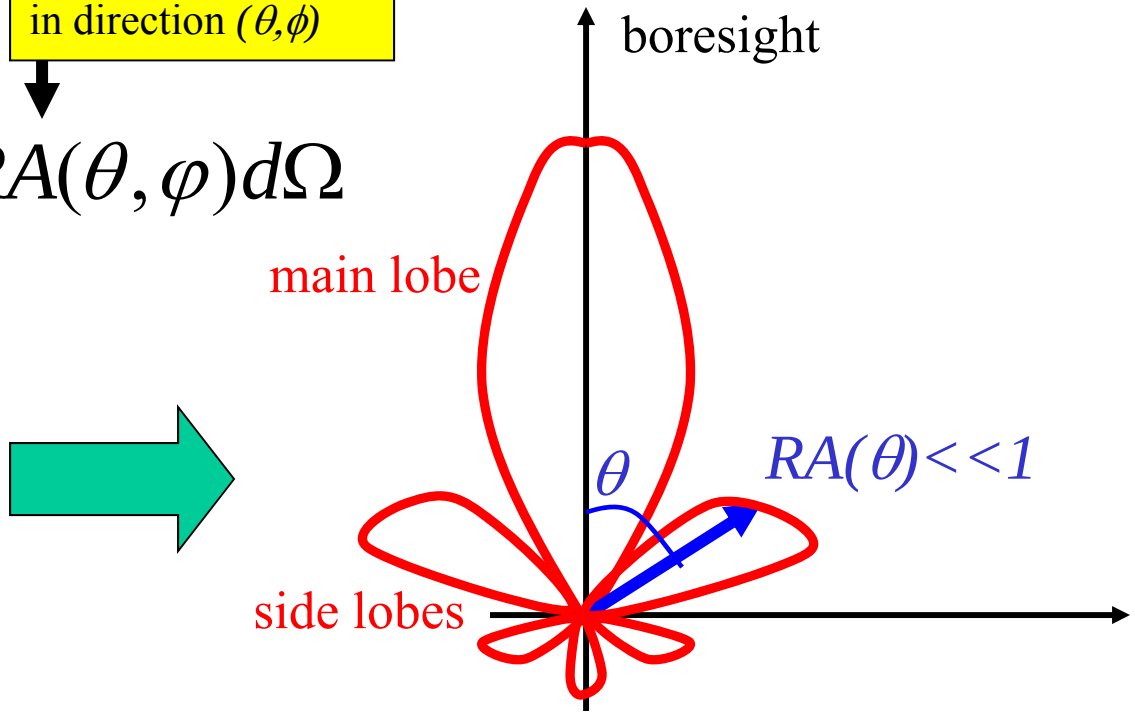

Importance of low sidelobes

- The power detected is the integral of the brightness times the solid angle, weighted with the angular response of the telescope:

Brightness from direction (θ,ϕ)

Telescope response in direction (θ,ϕ)

$$W = A\int_{4\pi} B(\theta,\varphi)RA(\theta,\varphi)d\Omega$$

- Typical telescope response $RA(\theta,\phi)$

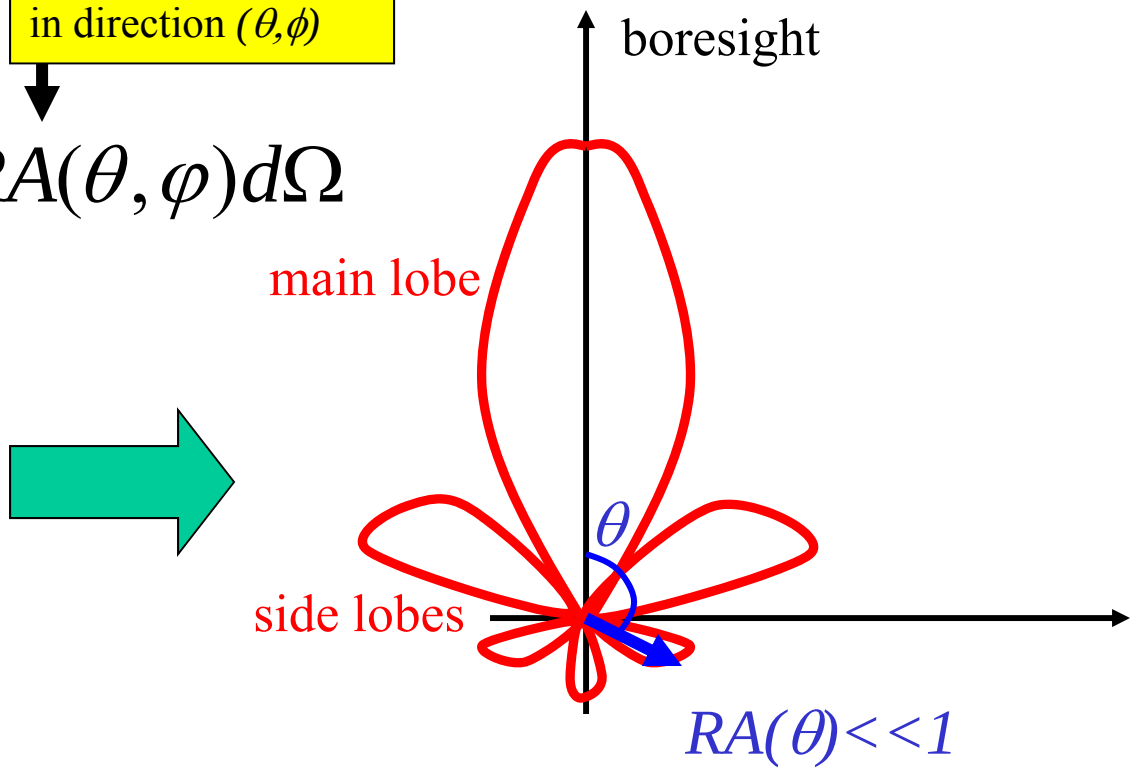

Importance of low sidelobes

- In the case of CMB observations, the detected brightness is the sum of the brightness from the sky (dominant for the solid angles directed towards the sky, in the main lobe) and the Brightness from the ground (dominant for the solid angles directed towards ground, in the sidelobes).

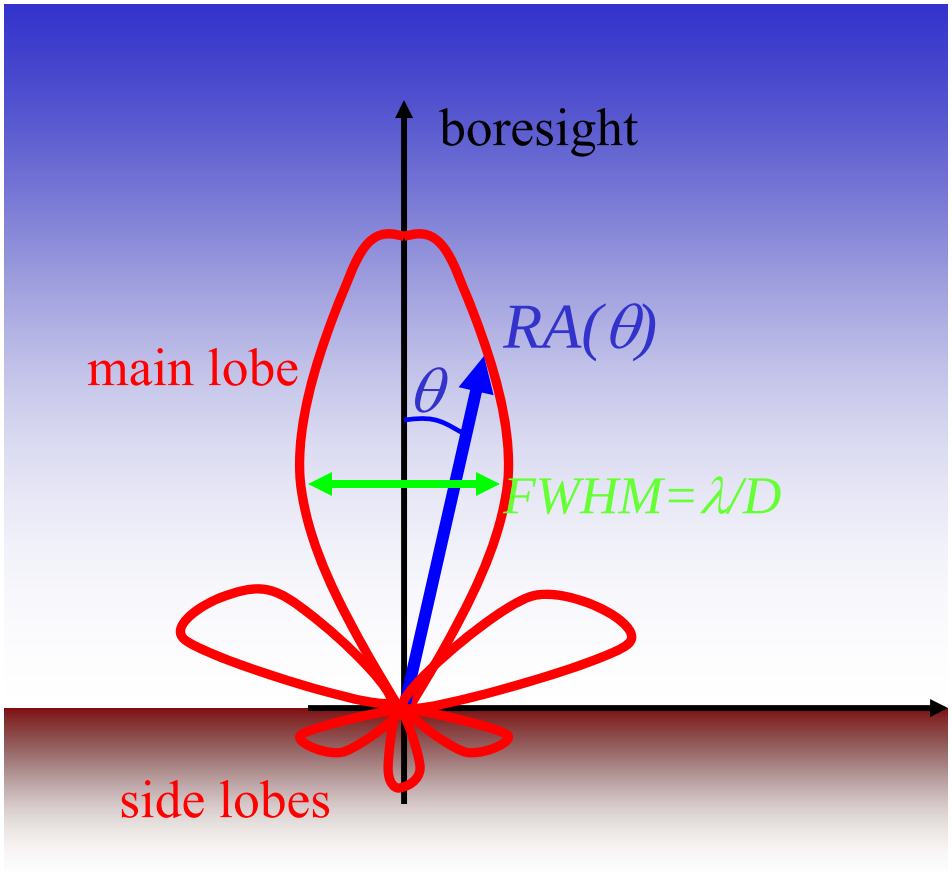

$$W = A\left[\int_{\substack{main\\lobe}} B_{sky}(\theta,\varphi)RA(\theta,\varphi)d\Omega + \int_{\substack{side\\lobes}} B_{Ground}(\theta,\varphi)RA(\theta,\varphi)d\Omega\right]$$

Importance of low sidelobes

$$W = A\left[\int_{\substack{main\\lobe}} B_{sky}(\theta,\varphi)RA(\theta,\varphi)d\Omega + \int_{\substack{side\\lobes}} B_{Ground}(\theta,\varphi)RA(\theta,\varphi)d\Omega\right]$$

signal of interest

disturbance signal

$$W \approx A\left[B_{sky}(\theta,\varphi)\left\langle RA_{\substack{main\\lobe}}(\theta,\varphi)\right\rangle \Omega_{\substack{main\\lobe}} + B_{Ground}(\theta,\varphi)\left\langle RA_{\substack{side\\lobes}}(\theta,\varphi)\right\rangle \Omega_{\substack{side\\lobes}}\right]$$

$\approx 3K$ $\quad \approx 1$ $\quad << 1\ srad$ $\quad \approx 300K$ $\quad \approx 2\pi\ srad$

signal of interest >> disturbance signal requires

$$\left\langle RA_{\substack{main\\lobe}}(\theta,\varphi)\right\rangle >>> \left\langle RA_{\substack{side\\lobes}}(\theta,\varphi)\right\rangle$$

signal of interest

disturbance signal

$$W \approx A\left[B_{sky}(\theta,\varphi)\left\langle RA_{\substack{main\\lobe}}(\theta,\varphi)\right\rangle \Omega_{\substack{main\\lobe}} + B_{Ground}(\theta,\varphi)\left\langle RA_{\substack{side\\lobes}}(\theta,\varphi)\right\rangle \Omega_{\substack{side\\lobes}}\right]$$

$\approx 3K$ $\quad \approx 1$ $\quad << 1\ srad$ $\quad \approx 300K$ $\quad \approx 2\pi\ srad$

$$\left\langle RA_{\substack{side\\lobes}}(\theta,\varphi)\right\rangle << \left\langle RA_{\substack{main\\lobe}}(\theta,\varphi)\right\rangle \left[\frac{\Omega_{\substack{main\\lobe}}}{\Omega_{\substack{side\\lobes}}}\right]\left[\frac{B_{sky}(\theta,\varphi)}{B_{Ground}(\theta,\varphi)}\right] \approx \frac{\Omega_{\substack{main\\lobe}}(srad)}{600}$$

FWHM	$\Omega_{mainlobe}$	$\langle RA_{sidelobes}\rangle$
10^o	2×10^{-2} srad	$<<4\times10^{-5}$
1^o	2×10^{-4} srad	$<<4\times10^{-7}$
10’	7×10^{-6} srad	$<<1\times10^{-8}$
1’	7×10^{-8} srad	$<<1\times10^{-10}$

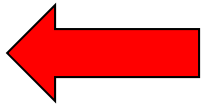

!!!

What is $RA(\theta,\phi)$?

- Fraunhofer diffraction from a circular aperture (radius *a*) (at large distances from shield)
- The incident wave is an infinite plane wave (wavevector k_{in} parallel to the z axis).
- The outgoing wave is not infinite, and for this very reason it will have components with wavevectors k in different directions. So it is not a plane wave.
- We want to find out which are the amplitudes of the different components of the outgoing wave.

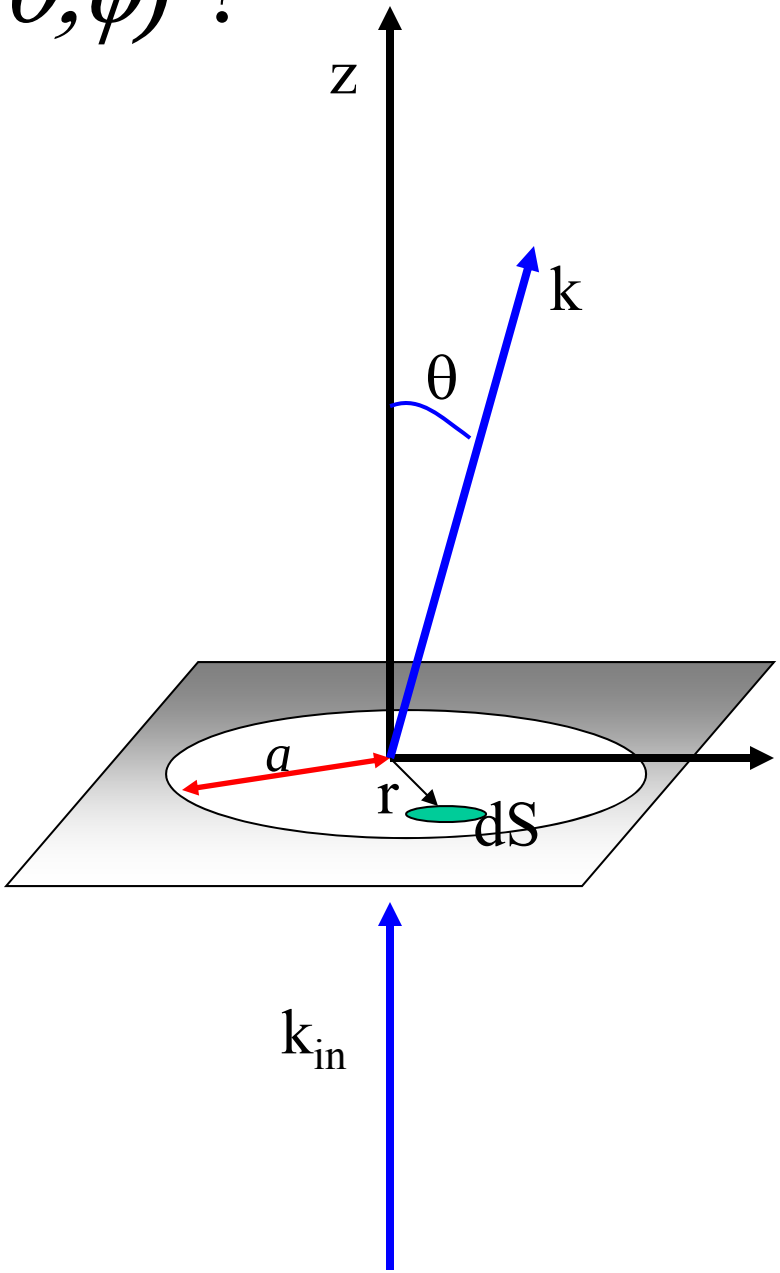

What is $RA(\theta,\phi)$?

- For small angles θ the vector $q=k-k_{in}$ is in the plane of the aperture and $q=k\theta$.
- The diffracted component with wavevector k is the sum of the contributions from all the elements dS of the aperture, each with its own phase:

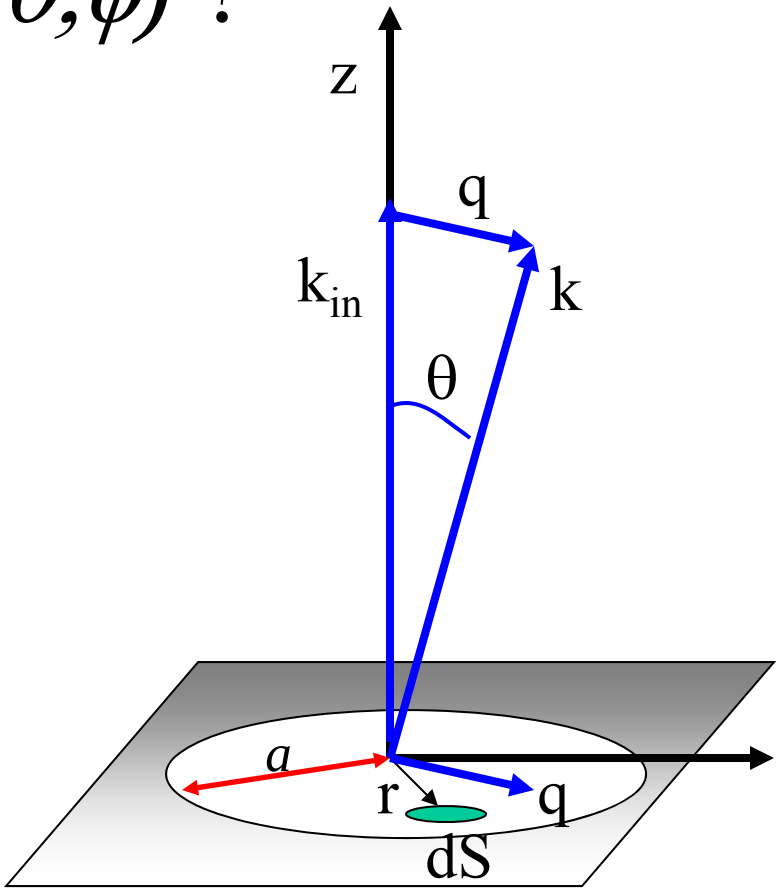

$$u_q = \iint_S u_o e^{-i\vec{q}\cdot\vec{r}}\, dS$$

Bessel functions

$$u_q = u_o \int_0^a \int_0^{2\pi} e^{-iqr\cos\varphi} r\, d\varphi\, dr = 2\pi u_o \int_0^a J_o(qr) r\, dr = u_o \frac{2J_1(aq)}{aq}$$

What is $RA(\theta,\phi)$?

- The intensity is the square of the field:

$$\frac{dI}{d\Omega} = I_o \left[\frac{2J_1(ak\theta)}{ak\theta} \right]^2$$

- Example: a 2m diameter mirror used at 1 cm and at 1 mm

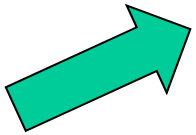

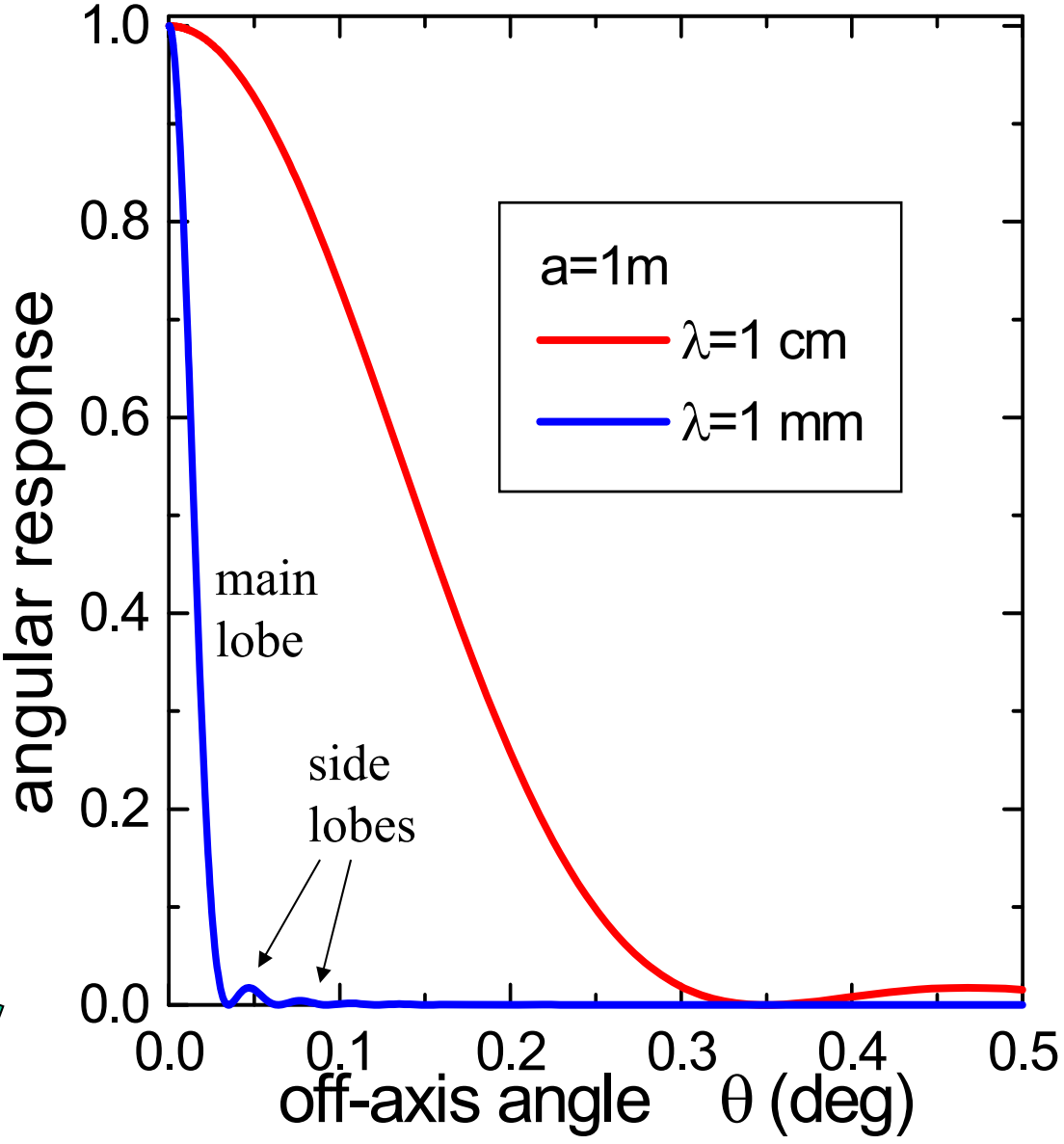

What is $RA(\theta,\phi)$?

- The intensity is the square of the field:

$$\frac{dI}{d\Omega} = I_o \left[\frac{2J_1(ak\theta)}{ak\theta} \right]^2$$

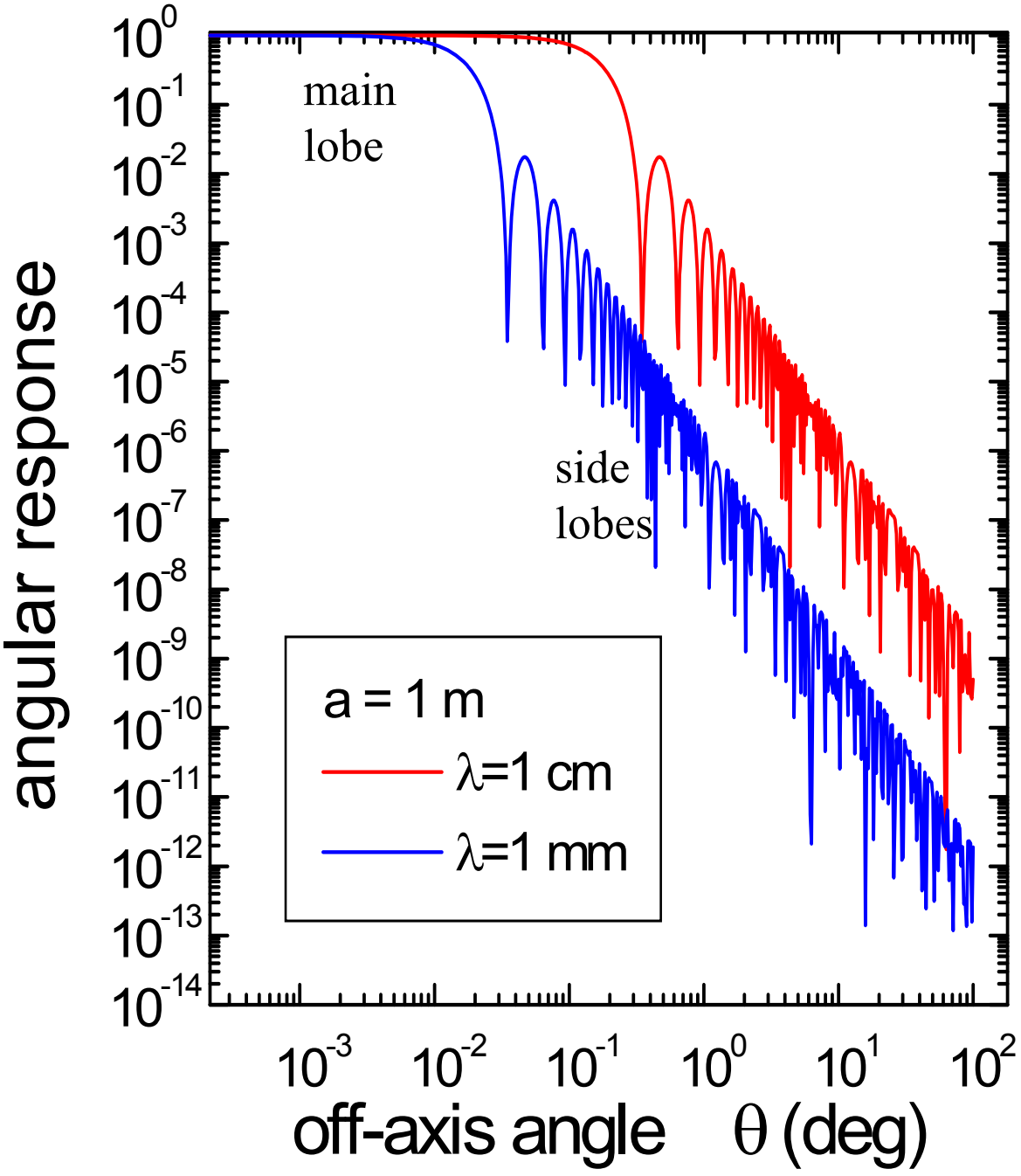

What is $RA(\theta,\phi)$?

- The intensity is the square of the field:

$$\frac{dI}{d\Omega} = I_o\left[\frac{2J_1(ak\theta)}{ak\theta}\right]^2$$

- The first zero is for

$$\theta_{10} = 1.22\frac{\lambda}{2a}$$

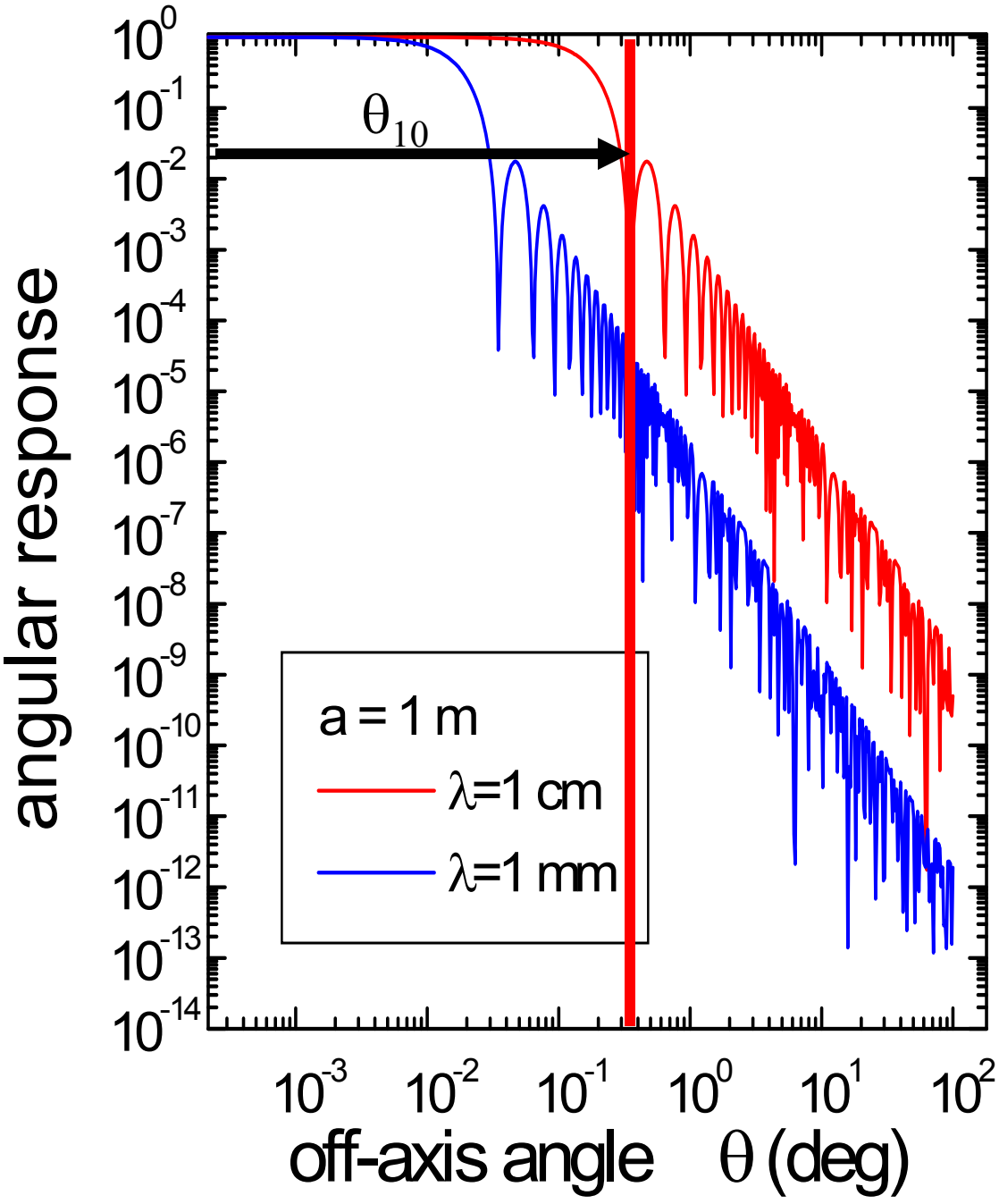

What is $RA(\theta,\phi)$?

- The intensity is the square of the field:

$$\frac{dI}{d\Omega} = I_o\left[\frac{2J_1(ak\theta)}{ak\theta}\right]^2$$

- The first zero is for

$$\theta_{10} = 1.22\frac{\lambda}{2a}$$

- The FWHM is similar

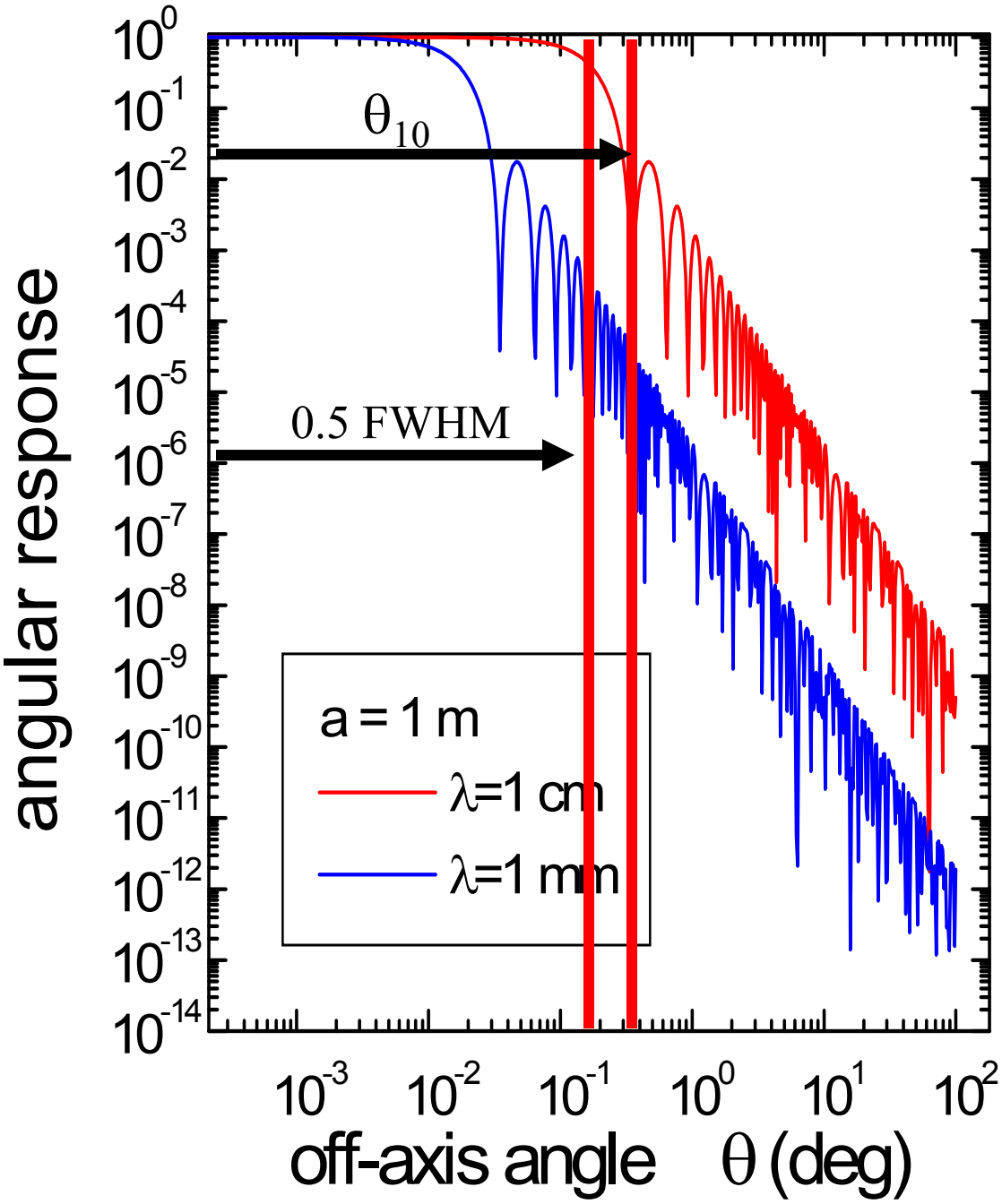

What is $RA(\theta,\phi)$?

- The intensity is the square of the field:

$$\frac{dI}{d\Omega} = I_o\left[\frac{2J_1(ak\theta)}{ak\theta}\right]^2$$

- The envelope of the off-axis response scales as θ^{-3} approximately starting from 0.5 at the FWHM

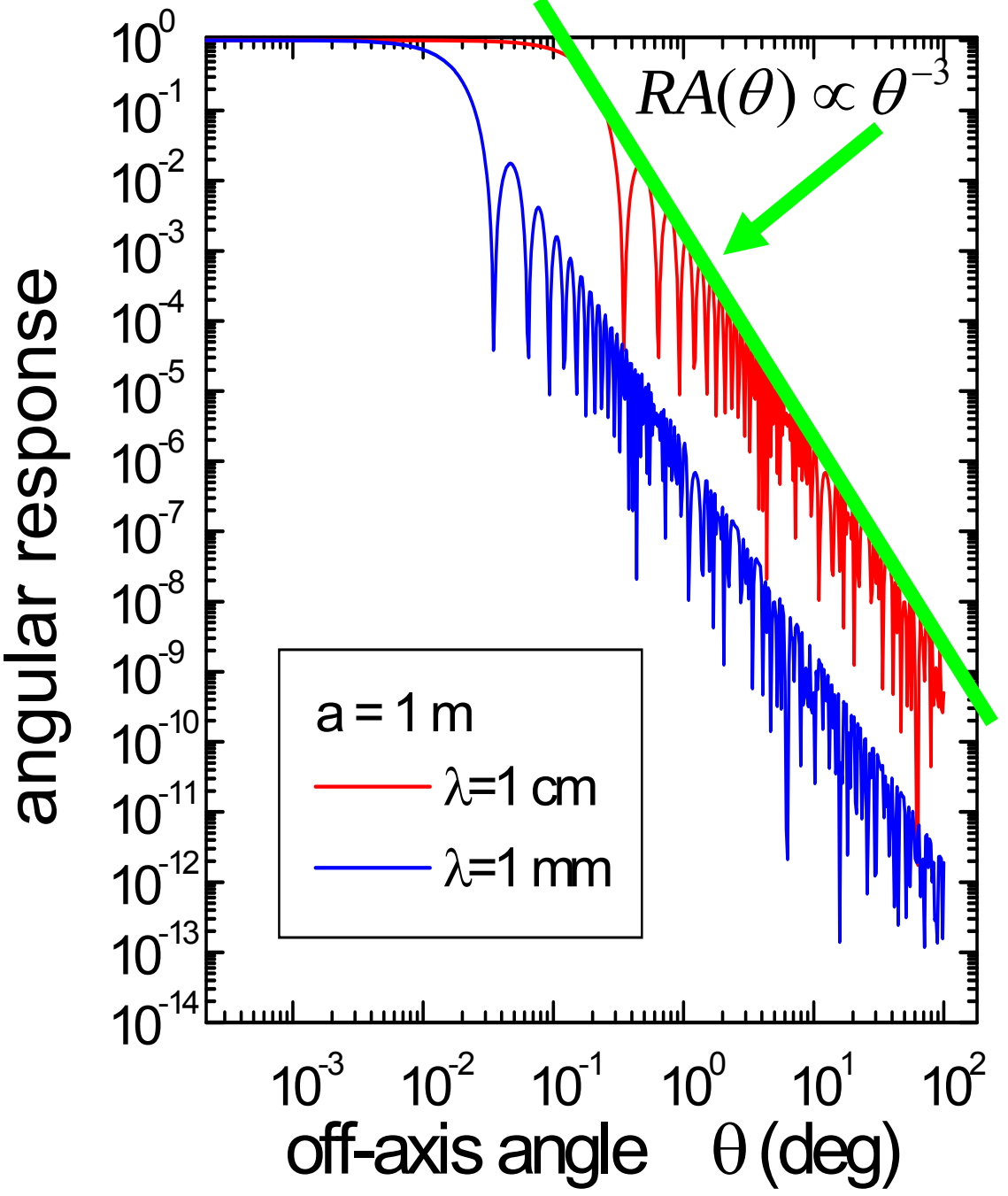

exercise

- For the angular response of a circular aperture, compare the power in the main lobe to the power in the sidelobes
- Hint:

$$\frac{P_{\substack{side\\lobes}}}{P_{\substack{main\\lobe}}} = \frac{2\pi A \int_{0.61\lambda/a}^{\pi} B_{\substack{side\\lobes}} \left[\frac{2J_1(ak\theta)}{ak\theta}\right]^2 \sin\theta d\theta}{2\pi A \int_{0}^{0.61\lambda/a} B_{\substack{main\\lobe}} \left[\frac{2J_1(ak\theta)}{ak\theta}\right]^2 \sin\theta d\theta}$$

- But use approximated formulas …

Low diffraction design

- Real world angular responses are worse than the one studied here.
- Sharp edges are in general important sources of diffraction, and must be avoided in low sidelobes design. Use smoothed edges.
- A trumpet has a slow transition to free space at the aperture to avoid diffraction of sound waves.
- The spider supporting the secondary mirror in a Cassegrain telescope is an important source of diffraction.
- Penzias and Wilson used an under-illuminated off-axis paraboloid, to get low sidelobes

10dB = a factor 10 in power

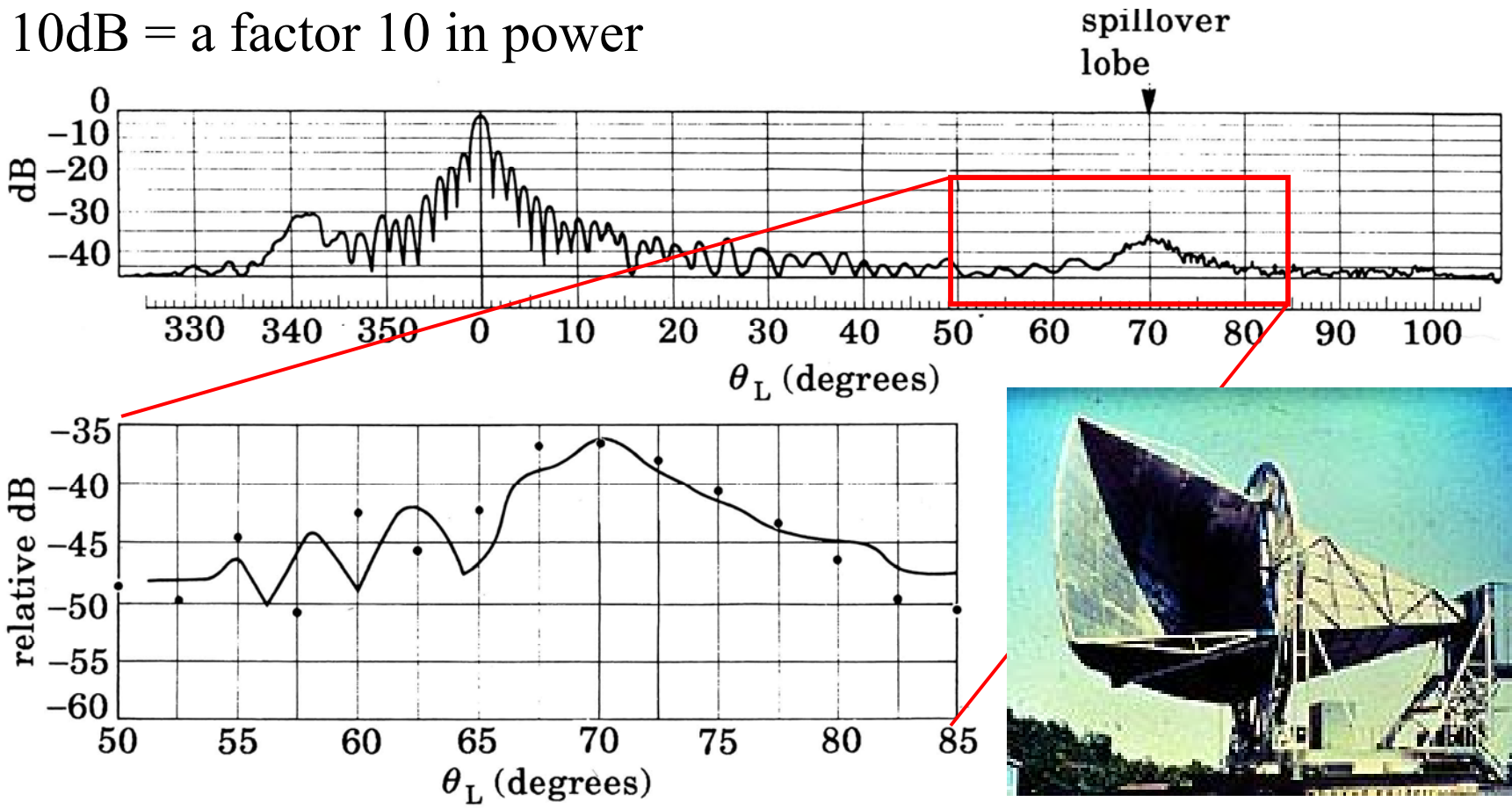

Fig. 12. – Upper panel: scheme of the horn-antenna. It is a part of a large paraboloid: lateral shields prevent spurious radiation entering in the system outside the nominal beam width. Isotropic level — 43 dB. Lower panel: angular response of the antenna, as measured by means of a transmitter located in front of the antenna at different angles. The spillover lobe is studied in detail in the lowest part of the graph. Earth's radiation entering via the spillover lobe determines the antenna temperature noise. —— Measured data, ● computed data. (Adapted by Crawford *et al.* [34].)

Other example of low sidelobes design: Planck

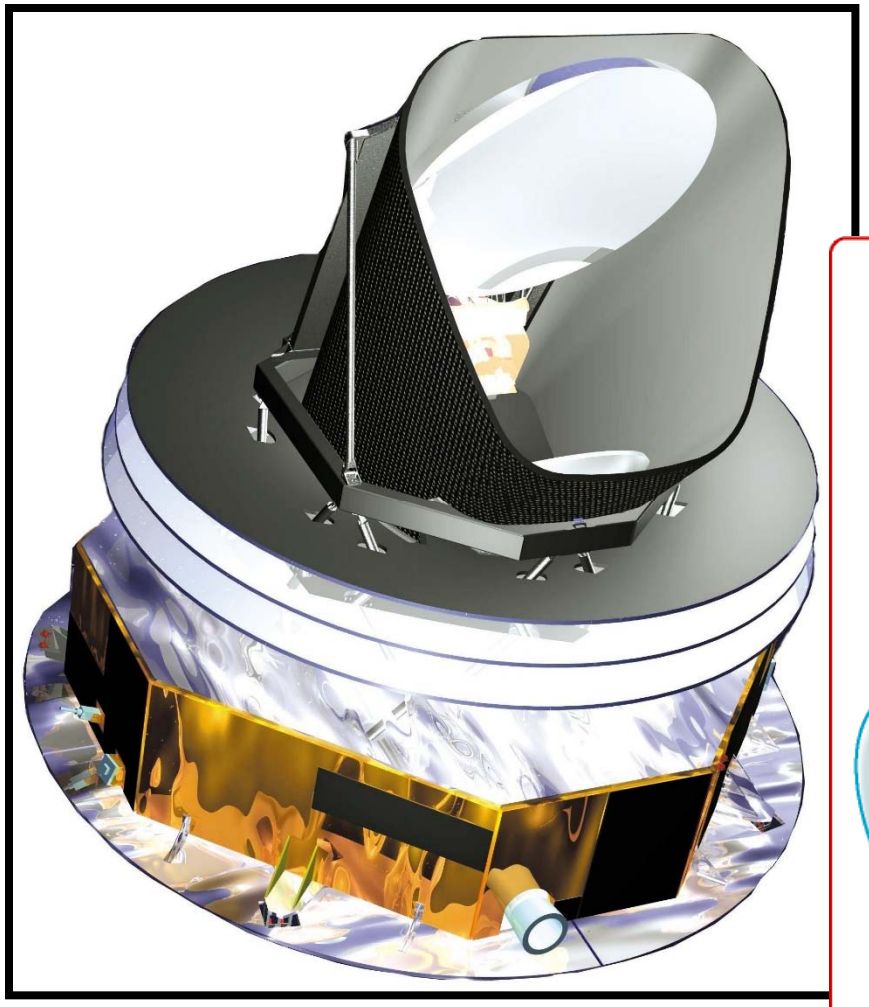

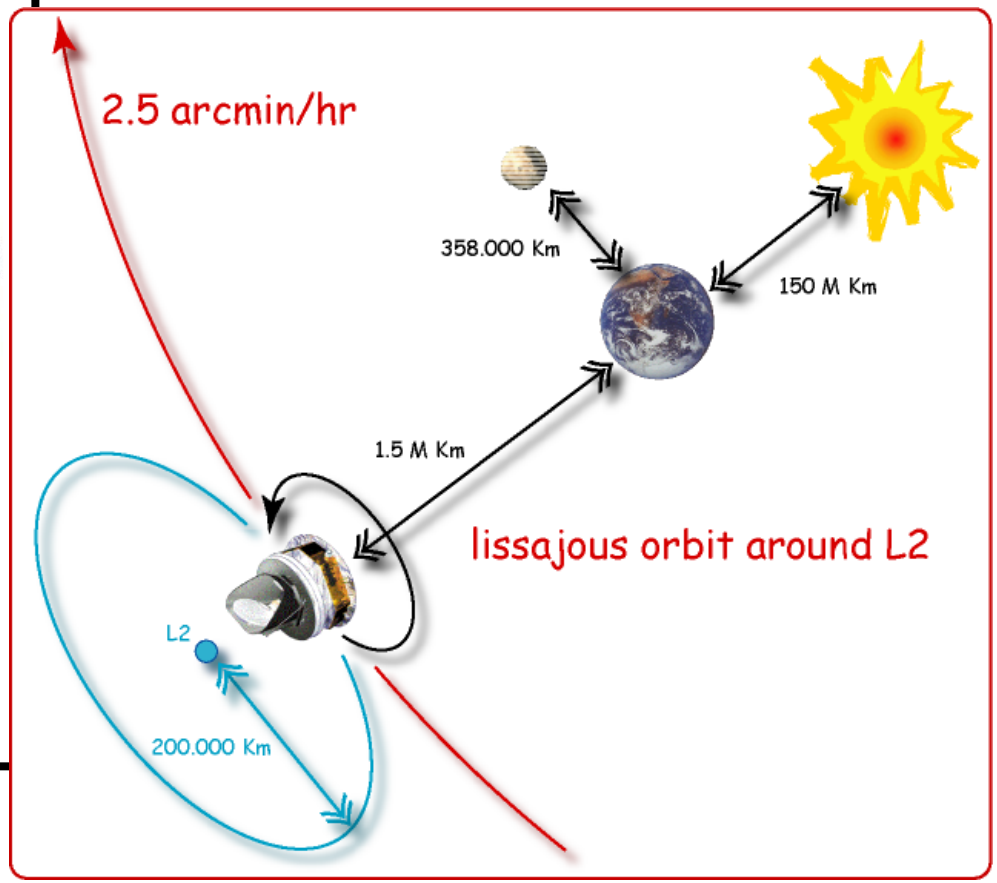

STRAY LIGHT

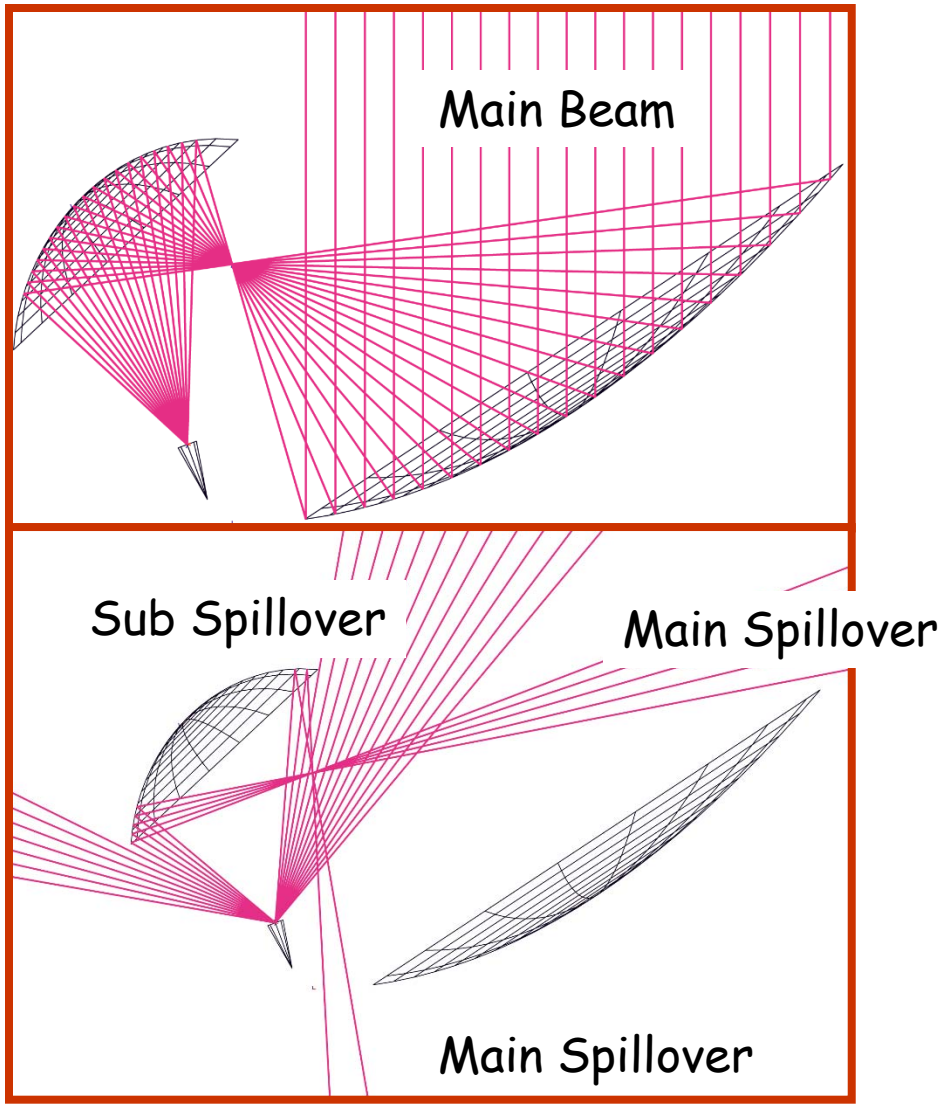

F. Villa, LFI

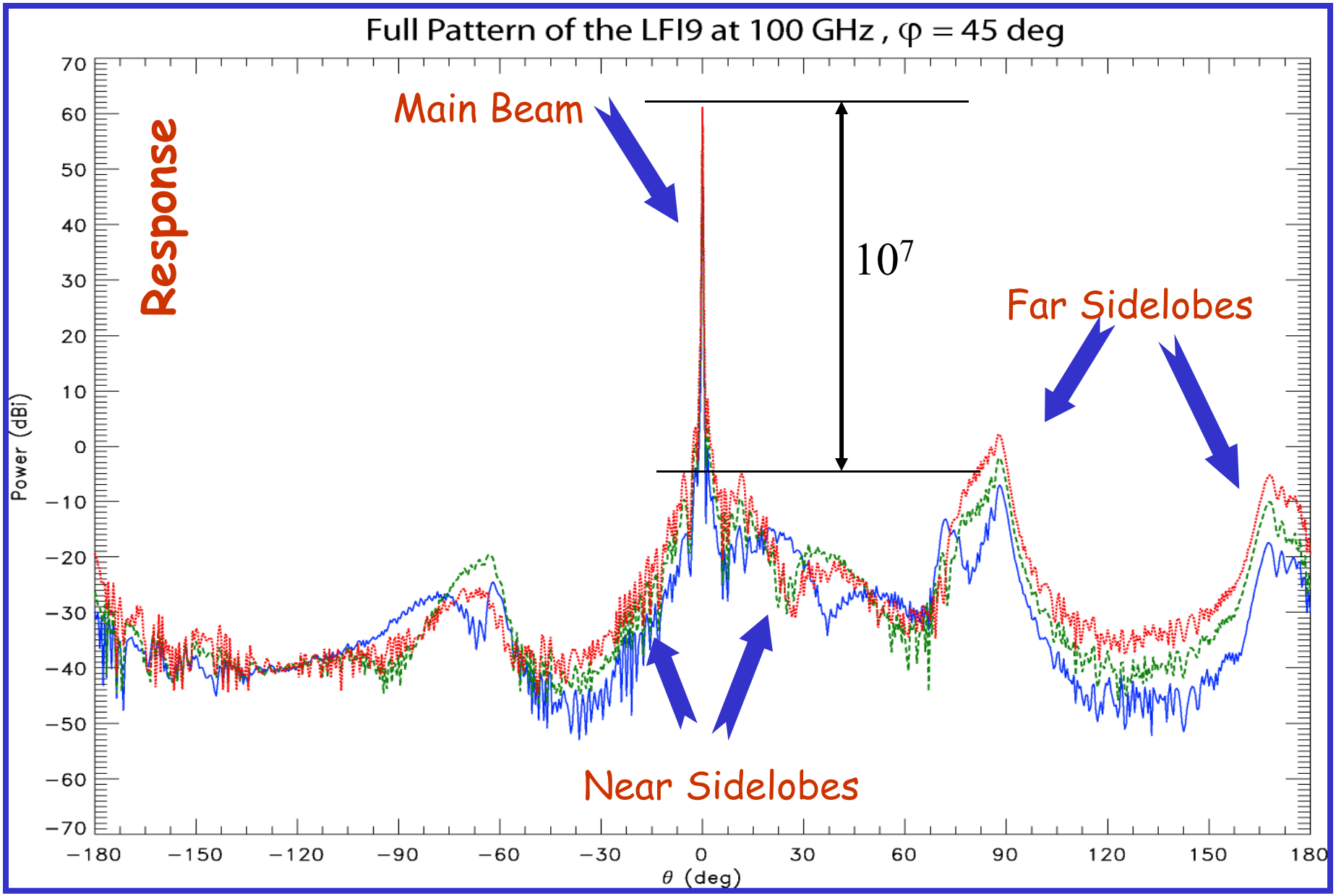

Angle from boresight

F. Villa, LFI

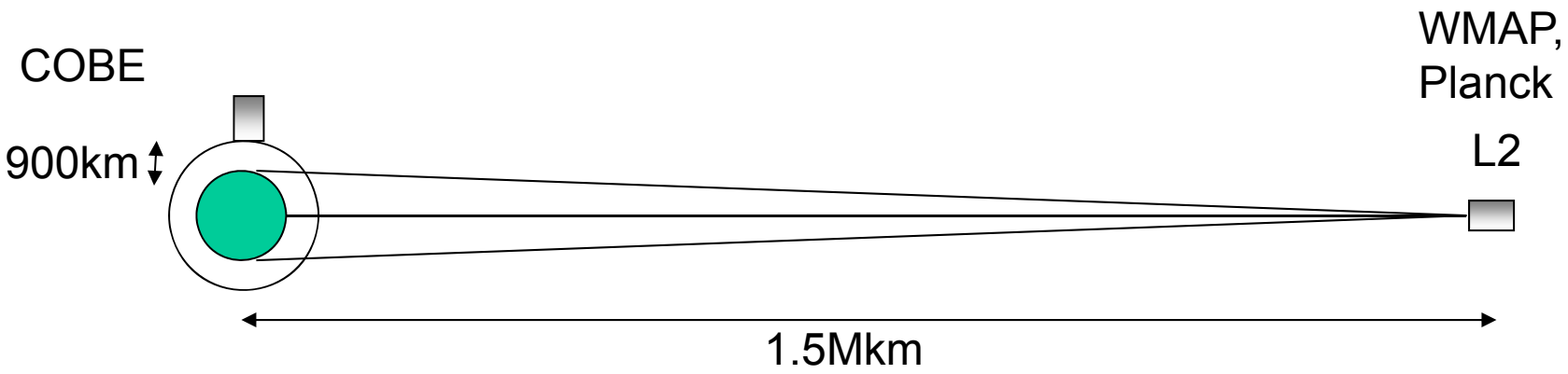

Going to L2 reduces the solid angle occupied by the Earth by a factor $2\pi/2\text{x}10^{-4}=31000$, thus relaxing by the same factor the required off-axis rejection.

FWHM	Ω_{mainlobe}	$<RA_{\text{sidelobes}}>$
10^{o}	$2\text{x}10^{-2}$ srad	$<<1$
1^{o}	$2\text{x}10^{-4}$ srad	$<<0.01$
10’	$7\text{x}10^{-6}$ srad	$<<3\text{x}10^{-4}$
1’	$7\text{x}10^{-8}$ srad	$<<3\text{x}10^{-6}$

Telescopes for the CMB

- After the COBE-DMR results there was a clear the need for meter-sized telescopes for the CMB.
- Working at high frequencies requires smaller mirrors for the same resolution.
- A 1 m mirror at 150 GHz provides 10' resolution, at 15 GHz provides only 1.4° .
- However atmospheric noise at high frequencies is severe.
- So, waiting for a new space mission, two classes of experiments were developed:
  - Ground-based radiometers working at high altitude mountain sites, at λ around 1 cm
  - Balloon-borne bolometric receivers working at λ around 1-2 mm

- Measuring small fluctuations with respect to the isotropic, pure, unpolarized blackbody requires sensitive detectors and advanced measurement methods.

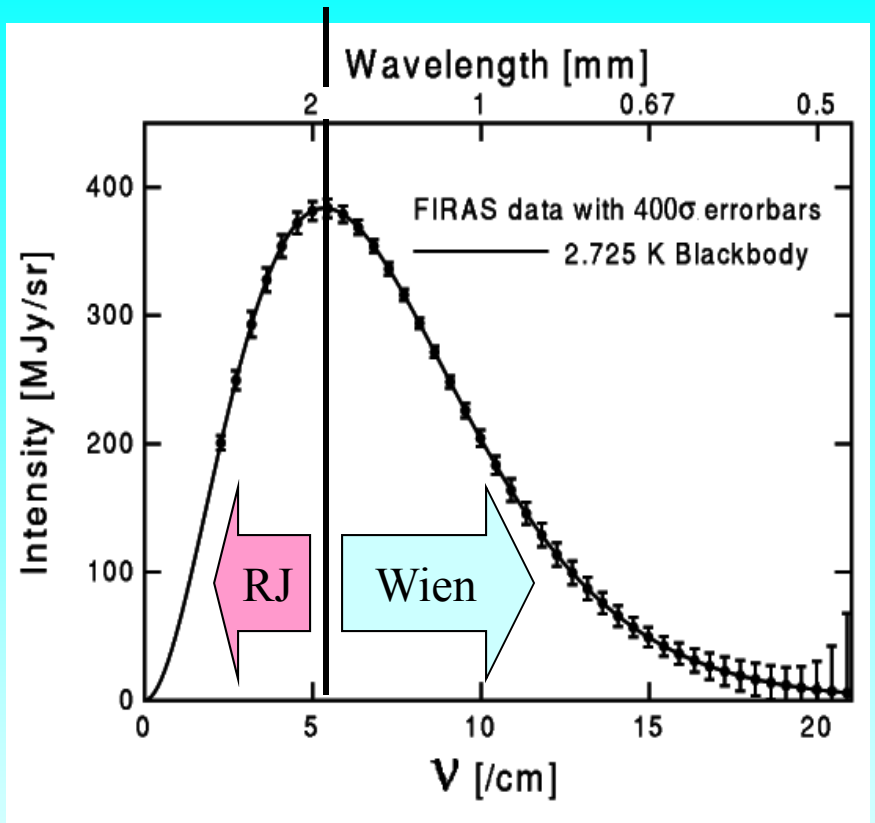

λ=2 mm
E = 0.6 meV

Difficult to build single-photon detectors

$$\nu << \nu_{\max} = 160\ GHz \quad \Rightarrow \quad \text{coherent detectors}$$

$$\nu >> \nu_{\max} = 160\ GHz \quad \Rightarrow \quad \text{bolometers}$$

$$\nu \approx \nu_{\max} = 160\ GHz \quad \Rightarrow \quad ???\ \text{direct detectors}\ ?$$

How to detect CMB photons

- $E(\gamma_{CMB}) < 1$ meV
- many photons per second
- Detection methods:
  - Coherent (antenna + amplifier)
  - Thermal (bolometers)
  - Direct (Cooper pairs in KIDs)
- Fundamental measurement limit: intrinsic noise of the CMB
- Many other limitations (foreground radiation from the instrument and the universe, detector noise, systematic effects in the instrument …)

Radiation Noise

- For thermal radiation (like the CMB) the correct statistics is Bose-Einstein.

$$\langle N \rangle = \frac{g}{e^{(E-\mu)/kT} - 1} \quad ; \quad \langle \Delta N^2 \rangle = T \left. \frac{d\langle N \rangle}{d\mu} \right|_{T,V}$$

$$\Rightarrow \quad \boxed{\langle \Delta N^2 \rangle = \langle N \rangle + \frac{\langle N \rangle^2}{g}}$$

Poisson noise

Wave interference noise

Radiation Noise

- For a blackbody

$$\langle N \rangle = \frac{g}{e^{(E-\mu)/kT} - 1} \quad ; \quad g = 2\frac{\nu^2}{c^3} 4\pi V d\nu$$

$$\langle N \rangle = \frac{8\pi\nu^2}{c^3} \frac{1}{e^{h\nu/kT} - 1} V d\nu$$

$$\Rightarrow \quad \boxed{\langle \Delta N^2 \rangle = \langle N \rangle \left[1 + \frac{1}{e^{h\nu/kT} - 1} \right]}$$

Poisson noise, important at short wavelengths

Wave interference noise, Important at low frequencies

Noise and integration time

- exercise: CMB anisotropy (or polarization) measurement limited only by radiation noise:

$$\Delta B(\nu, T) = \frac{\Delta T}{T} \int_{x_1}^{x_2} \frac{x e^x}{e^x - 1} B(x, T)\, dx$$

$$\sigma\left(\frac{\Delta T}{T}\right) = \frac{\sigma(\Delta B)}{\int_{x_1}^{x_2} \frac{x e^x}{e^x - 1} B(x, T)\, dx}$$

$$\sigma\left(\frac{\Delta T}{T}\right) = \frac{\sqrt{\frac{4 k^5 T^5}{c^2 h^3} A\Omega \int_{x_1}^{x_2} \frac{x^4 e^x}{\left(e^x - 1\right)^2} dx}}{\frac{2 k^4 T^4}{c^2 h^3} A\Omega \int_{x_1}^{x_2} \frac{x^4 e^x}{(e^x - 1)^2} dx} \sqrt{\frac{1}{t}}$$

The ultimate sensitivity plot

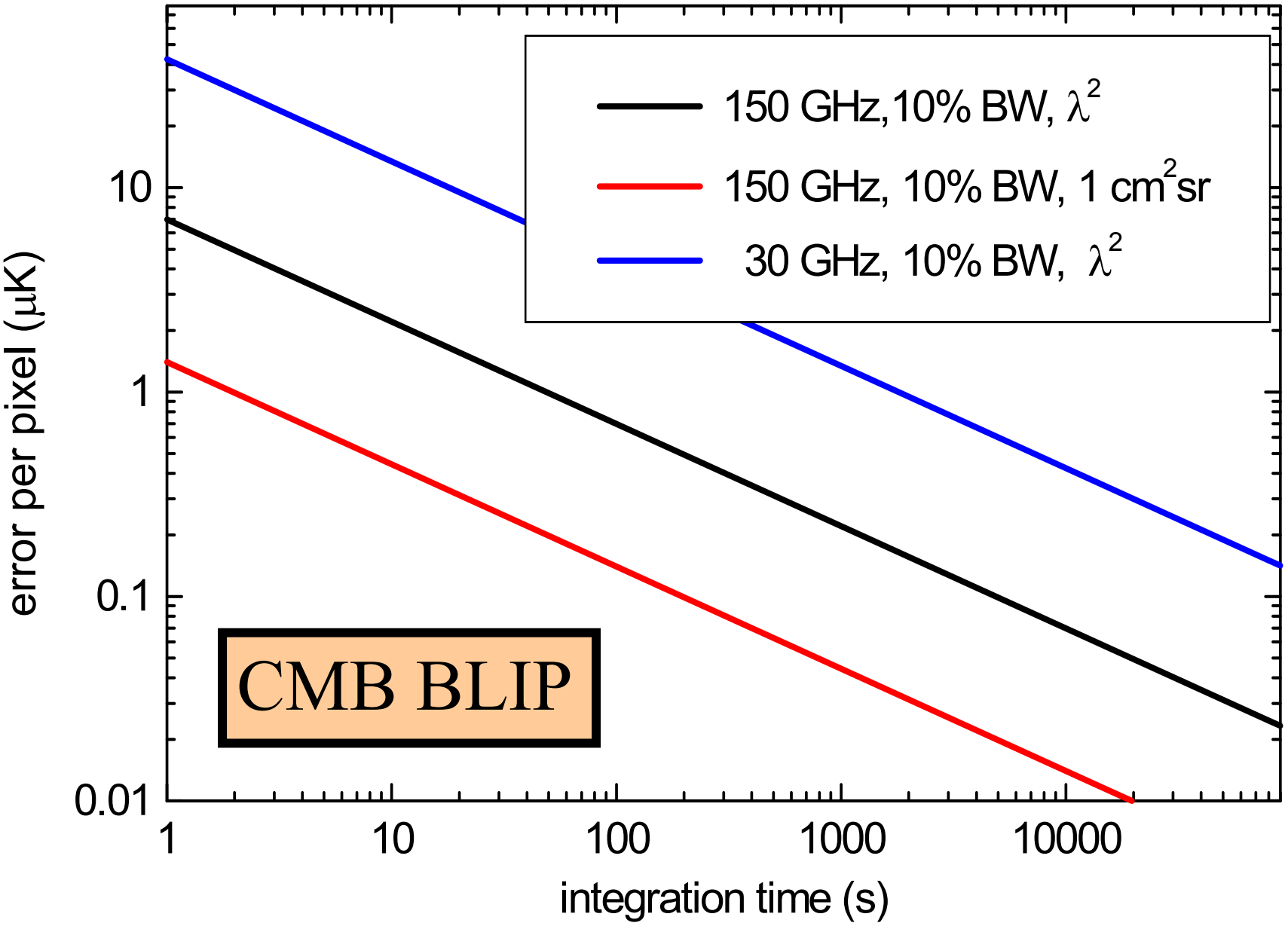

- In the whole sky we have 40000 degree-sized pixels (1 degree = size of causal horizon at recombination).
- Assume that we have a single diffraction-limited detector at 150 GHz, with intrinsic noise lower than the photon-noise from the CMB (NET = 8 μK $s^{1/2}$), and that other noise sources are negligible
- If we need to measure each 5 arcmin-side pixel (to see sub-horizon structures) with 3 μK accuracy (1 ppm), using a single detector it will take order of 40000x12x12x5 s = 1 year.
- How does current technology compare to this *«ideal»* situation ?

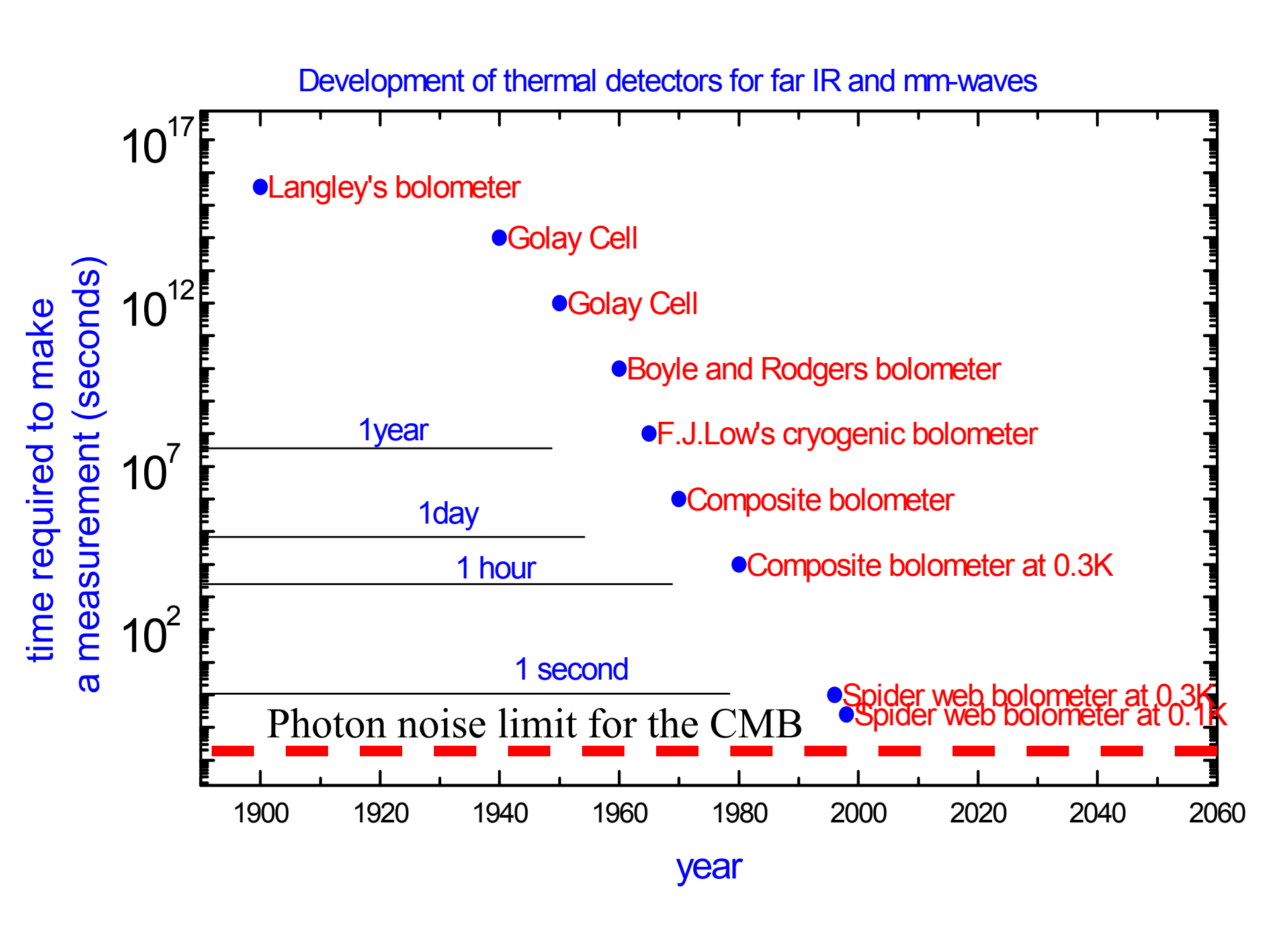
Development of thermal detectors for far IR and mm-waves
time required to make a measurement (seconds)
10^{17}
10^{12}
10^{7}
10^{2}
Langley's bolometer
Golay Cell
Golay Cell
Boyle and Rodgers bolometer
F.J.Low's cryogenic bolometer
Composite bolometer
Composite bolometer at 0.3K
Spider web bolometer at 0.3K
Spider web bolometer at 0.1K
1year
1day
1 hour
1 second
Photon noise limit for the CMB
1900
1920
1940
1960
1980
2000
2020
2040
2060
year

Cryogenic Bolometers

- For FIR & mm-waves spectroscopy we need **very wide band detectors.** Bolometers provide the optimal choice: they are senitive from mm-waves to the visible range.

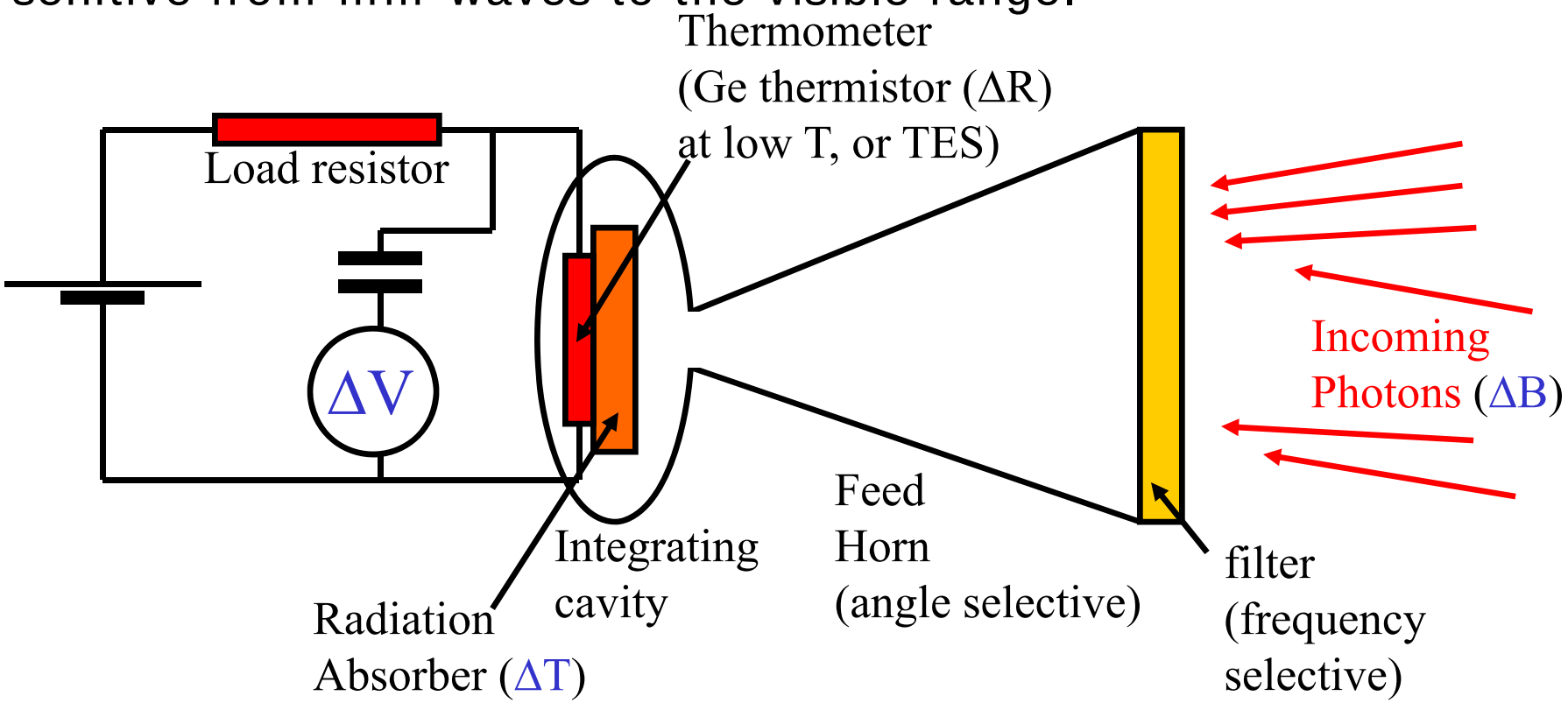

- Fundamental noise sources are Johnson noise in the thermistor ($<\Delta V^2> = 4kTR\Delta f$), temperature fluctuations in the thermistor ($<\Delta W^2> = 4kGT^2\Delta f$), background radiation noise (T_{bkg}^5) → need to reduce the temperature of the detector and the radiative background.

Cryogenic Bolometers

- In steady conditions the temperature rise of the sensor is due to the background radiative power absorbed Q and to the electrical bias power P:

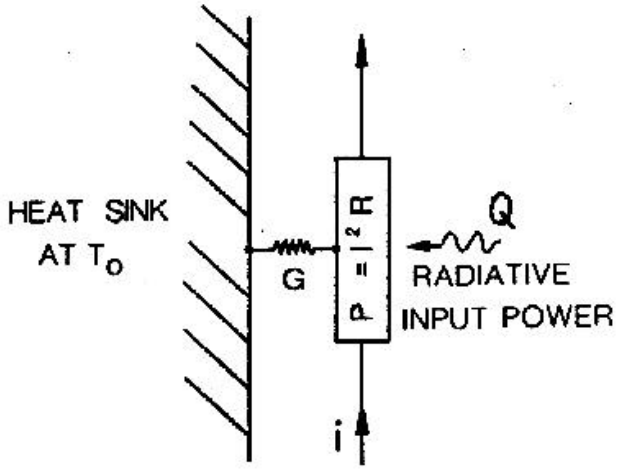

$$G(T - T_0) = Q + P$$

- The effect of the background power is thus equivalent to an increase of the reference temperature:

$$P = G\left[T - (T_0 + \frac{Q}{G})\right] = G(T - T_0')$$

$$T_0' = T_0 + \frac{Q}{G}$$

To optimize sensitivity, we need both a low temperature and a low background (space)

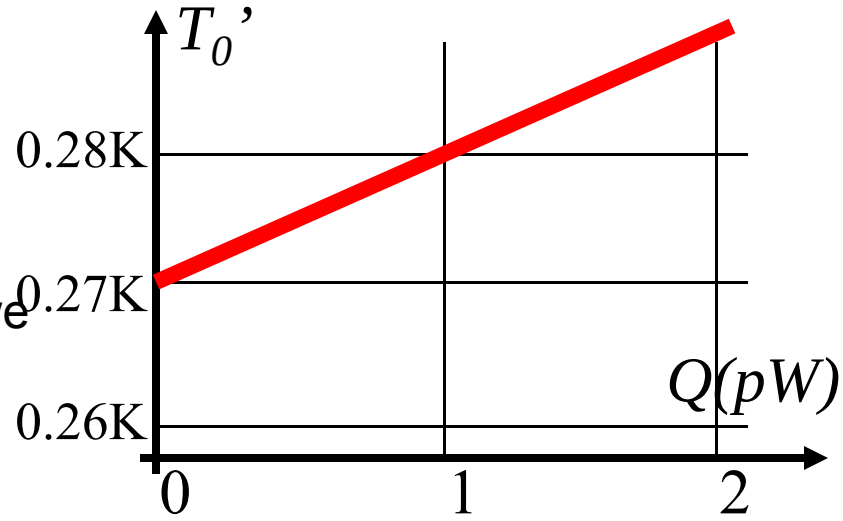

Cryogenic Bolometers

- In presence of an additional power $\Delta Q\, e^{j\omega t}$ (from the sky)

$$C\frac{d\Delta T}{dt}+G_{eff}\Delta T=\Delta Q$$

$$\left|\frac{dT}{dQ}\right|=\frac{1}{G_{eff}\sqrt{1+\tau^2\omega^2}}$$

$$\tau=\frac{C}{G_{eff}}$$

The response depends on the power, not on the wavelength

- There is a tradeoff between high sensitivity and fast response. **The heat capacity C should be minimized** to optimize both.

Small sensor at **low temperature**

- Using a current biased thermistor to readout the temperature change:

$$\alpha=\frac{T}{R(T)}\frac{dR(T)}{dT}\quad\Rightarrow\quad dV=idR=i\alpha RdT/T$$

Responsivity

$$\Re=\frac{dV}{dQ}=i\alpha\frac{R}{T}\frac{dT}{dQ}=\frac{i\alpha R/T}{G_{eff}\sqrt{1+\tau^2\omega^2}}$$

Cryogenic Bolometers

$$\alpha = \frac{T}{R(T)}\frac{dR(T)}{dT}$$

$$\Re = \frac{i\alpha R/T}{G_{eff}\sqrt{1+\tau^2\omega^2}}$$

- A large α is important for high responsivity.
- Ge thermistors: $\frac{\alpha}{T} \approx -10K^{-1}$

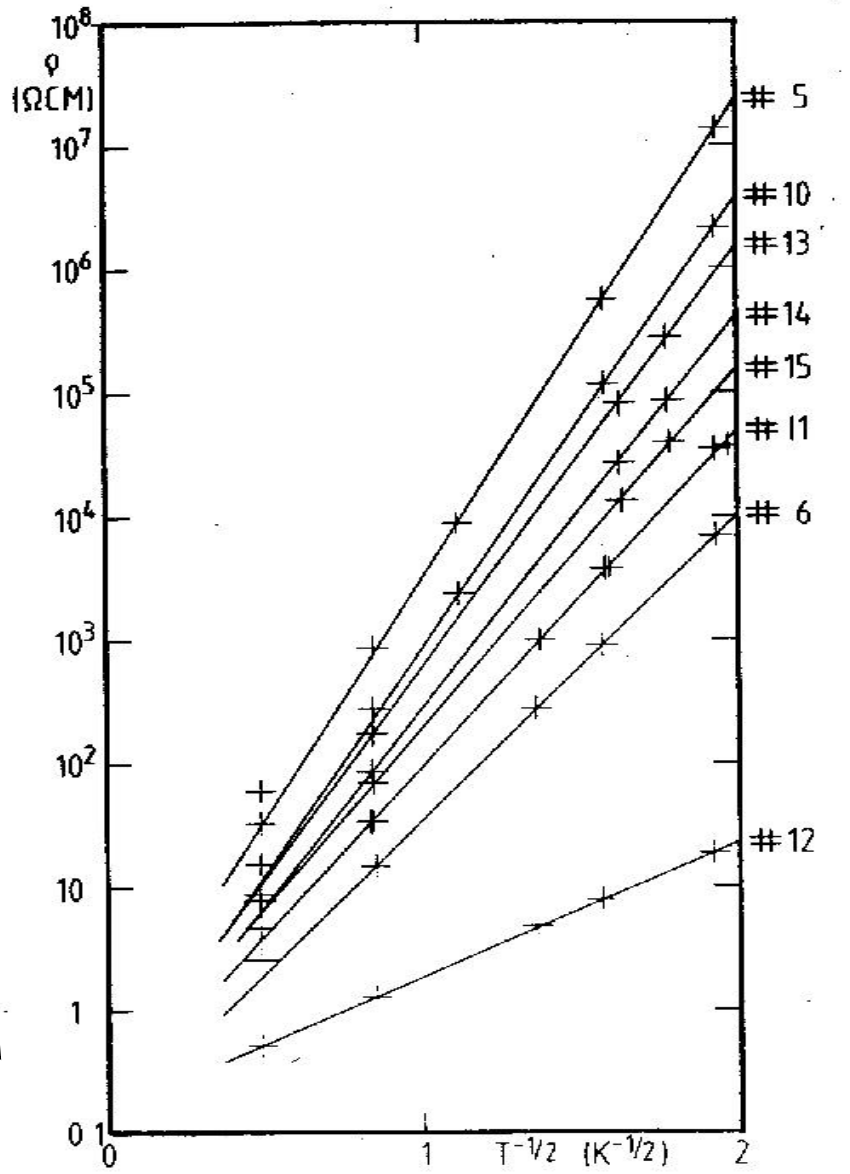

Cryogenic Bolometers

- Johnson noise in the thermistor

$$\frac{d\left\langle \Delta V_J^2 \right\rangle}{df} = 4kTR$$

- Temperature noise

$$\frac{d\left\langle \Delta W_T^2 \right\rangle}{df} = \frac{4kT^2 G_{eff}}{G_{eff}^2 + (2\pi f C)^2}$$

- Photon noise

$$\frac{d\left\langle \Delta W_{Ph}^2 \right\rangle}{df} = \frac{4k^5 T_{BG}^5}{c^2 h^3} \int \varepsilon \frac{x^4 \left(e^x - 1 + \varepsilon\right)}{\left(e^x - 1\right)^2} dx$$

- Total NEP (fundamental):

$$NEP^2 = \frac{1}{\Re^2}\frac{d\left\langle \Delta V_J^2 \right\rangle}{df} + \frac{d\left\langle \Delta W_T^2 \right\rangle}{df} + \frac{d\left\langle \Delta W_{Ph}^2 \right\rangle}{df}$$

Again, need of low temperature and low background

Q

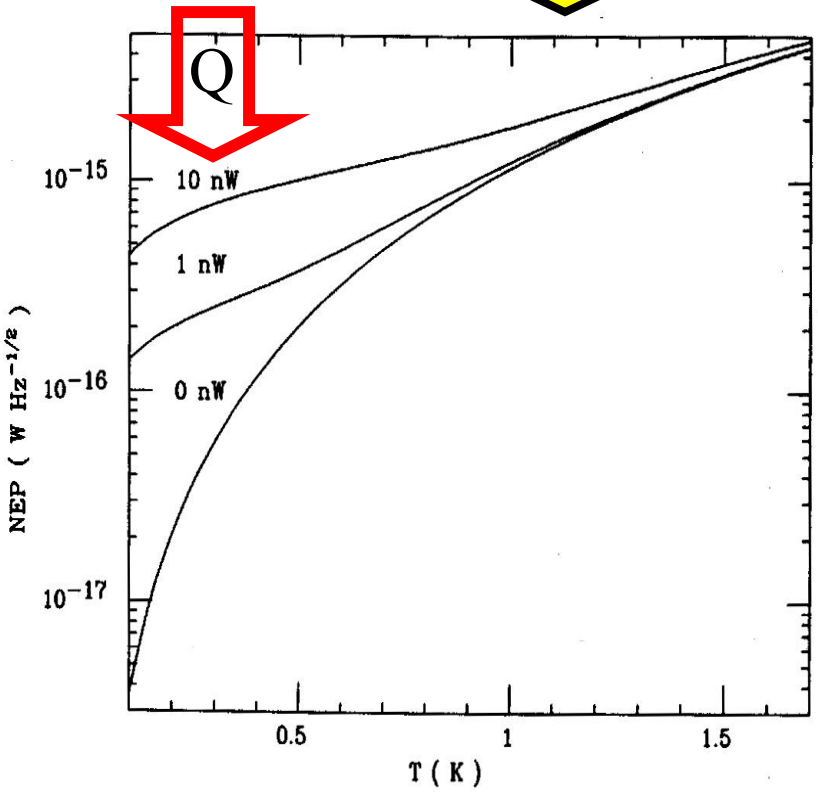

Spider-Web Bolometers

- The absorber is micro machined as a web of metallized Si_3N_4 wires, 2 μm thick, with 0.1 mm pitch.
- This is a good absorber for mm-wave photons and features a very low cross section for cosmic rays. Also, the heat capacity is reduced by a large factor with respect to the solid absorber, and can be made large to absorb many modes.
- NEP ~ 2 10^{-17} W/$Hz^{0.5}$ is achieved @0.3K
- 150μK_{CMB} in 1 s
- Mauskopf *et al.* Appl.Opt. **36**, 765-771, (1997)

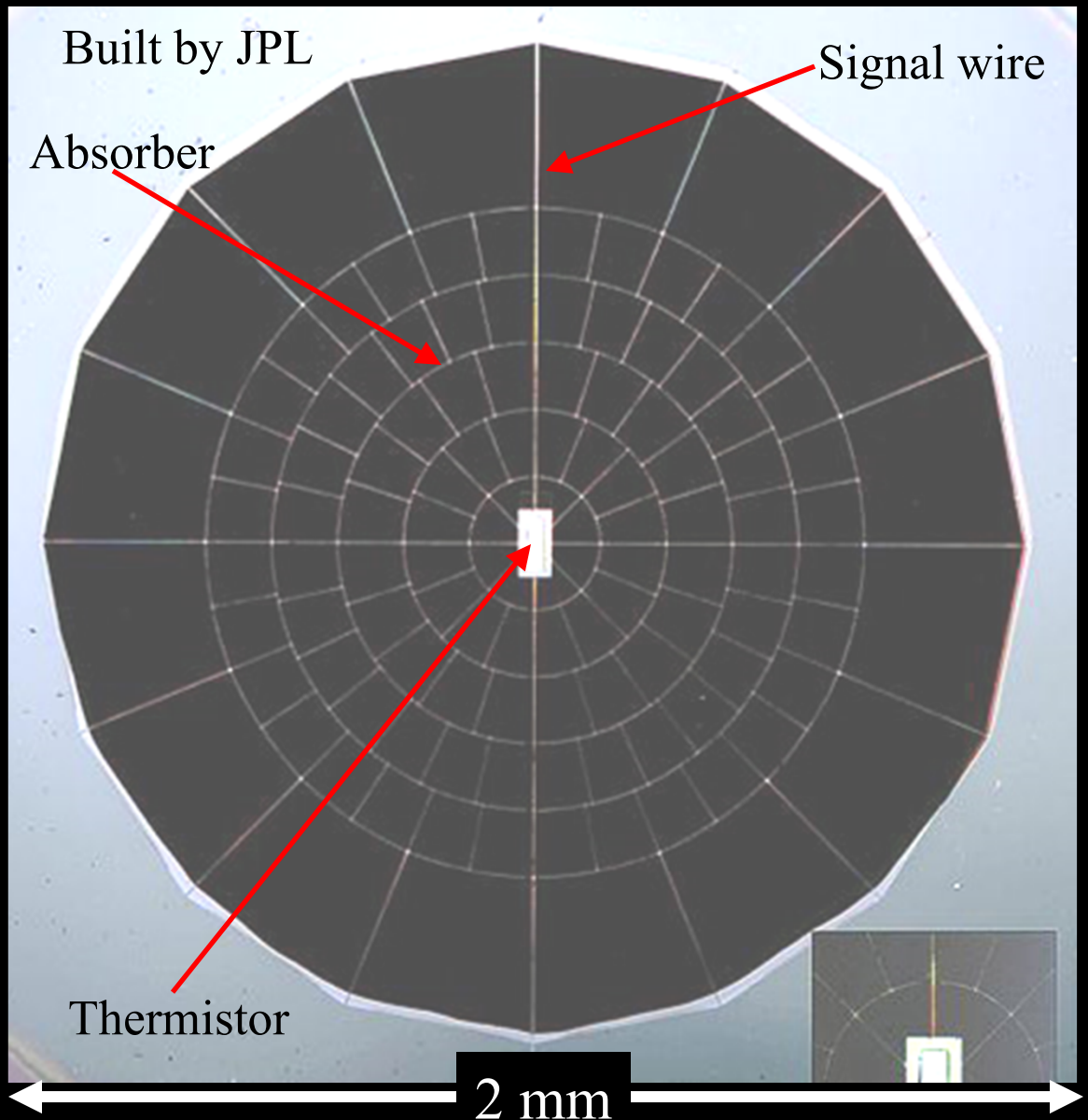

Table 5. In-flight bolometer performance

ν_0 (GHz)	τ (ms)	η_{opt}	G (pW K^{-1})	R (MΩ)	NEP (1 Hz) (10^{-17} W/$\sqrt{\text{Hz}}$)	NET$_{CMB}$ (μK$\sqrt{\text{s}}$)
90	22	0.30	82	5.5	3.2	140
150sm	12.1	0.16	85	5.9	4.2	140
150mm	15.7	0.10	88	5.5	4.0	190
240	8.9	0.07	190	5.7	5.7	210
410	5.7	0.07	445	5.4	12.1	2700

Note. — In-flight bolometer performance. The 150 GHz channels are divided into single mode (150sm) and multimode(150mm). The optical efficiency of the channels decreased significantly from the measured efficiency of each feed structure due to truncation by the Lyot stop. The NEP is that measured in flight, and includes contributions from detector noise, amplifier noise, and photon shot noise.

Crill et al., 2003 – BOOMERanG 1998 bolometers, 300 mK
The same kind of bolometer has been used in Planck @100mK

Measured performance of Planck HFI bolometers **(0.1K)**
(Holmes et al., Appl. Optics, **47**, 5997, 2008)

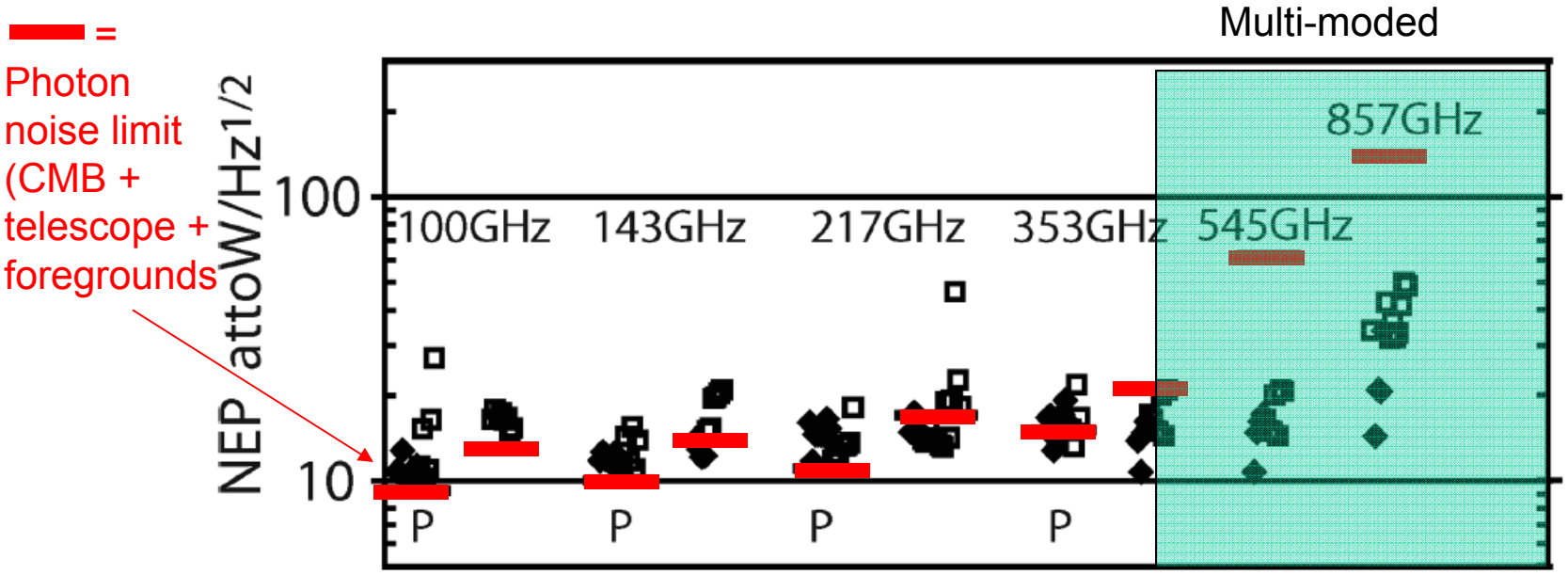

Fig. 1. Measured detector dark NEP including $6.5\,\mathrm{nV}/\sqrt{\mathrm{Hz}}$ amplifier noise at nominal bias for each frequency band. Solid symbols are the NEP for detectors installed in the focal plane. The open symbols are the NEP spare bolometers. The solid lines indicate the photon background limit from a 35 K telescope and astrophysical sources in each band for a 30% bandwidth and 30% in band optical efficiency. Unpolarized detectors at 100 GHz were made and delivered but were replaced by polarized detectors.

- This sensitivity corresponds to 100 μK $s^{1/2}$ for each detector.
- We are far (>10x) from being photon-noise limited from the CMB alone.
- We cannot measure the entire sky at 3 μK/pixel sensitivity (so we will rely on measurements of statistical estimators, like the angular power spectrum), and we need anyway to use detector *arrays* with thousands of pixels.
- Going multi-mode ($A\Omega >> \lambda^2$) can also help, if angular resolution is not the main driver.
- Making arrays requires easily replicable detector technology: nowadays: TESs and KIDs.
- High performance detectors is not all !

Today: Two competing technologies for CMB detectors

- Voltage-biased superconducting transition-edge sensors
  - Thermistor is a superconductor film, operated in the transition (large variation of resistnace for small variation of temperature)
  - Extreme Electrothermal feedback speeds-up the detector
  - Can be produced with litographic techniques, as the rest of the detector, so can be replicated in large arrays at low cost
  - Can be antenna-coupled using planar antennas
  - Readout using squid amplifiers, extreme low noise, multiplexing
  - 1000s pixels arrays already operating at telescopes (SPT, ACT, BICEP, EBEX, SPIDER, ...)
- Kinetic inductance detectors
  - CMB photons break Cooper pairs in a superconductor film, which is the inductive component of a high Q resonator
  - Variation of quasiparticle density detected as variation of the resonance frequency of the resonator
  - Intrinsically multiplexable
  - Litography simpler that in TES (one or two masks)
  - 1000s pixels arrays already operating at telescopes (IRAM, HT ...)
- If we can now make ultrasensitive measurements, it is because of these instrumental developments, which took decades !!!

Large Number of Detectors for Sensitivity : TES bolometers with phased-array antennas (Caltech + JPL) for BICEP2 – 512 detectors

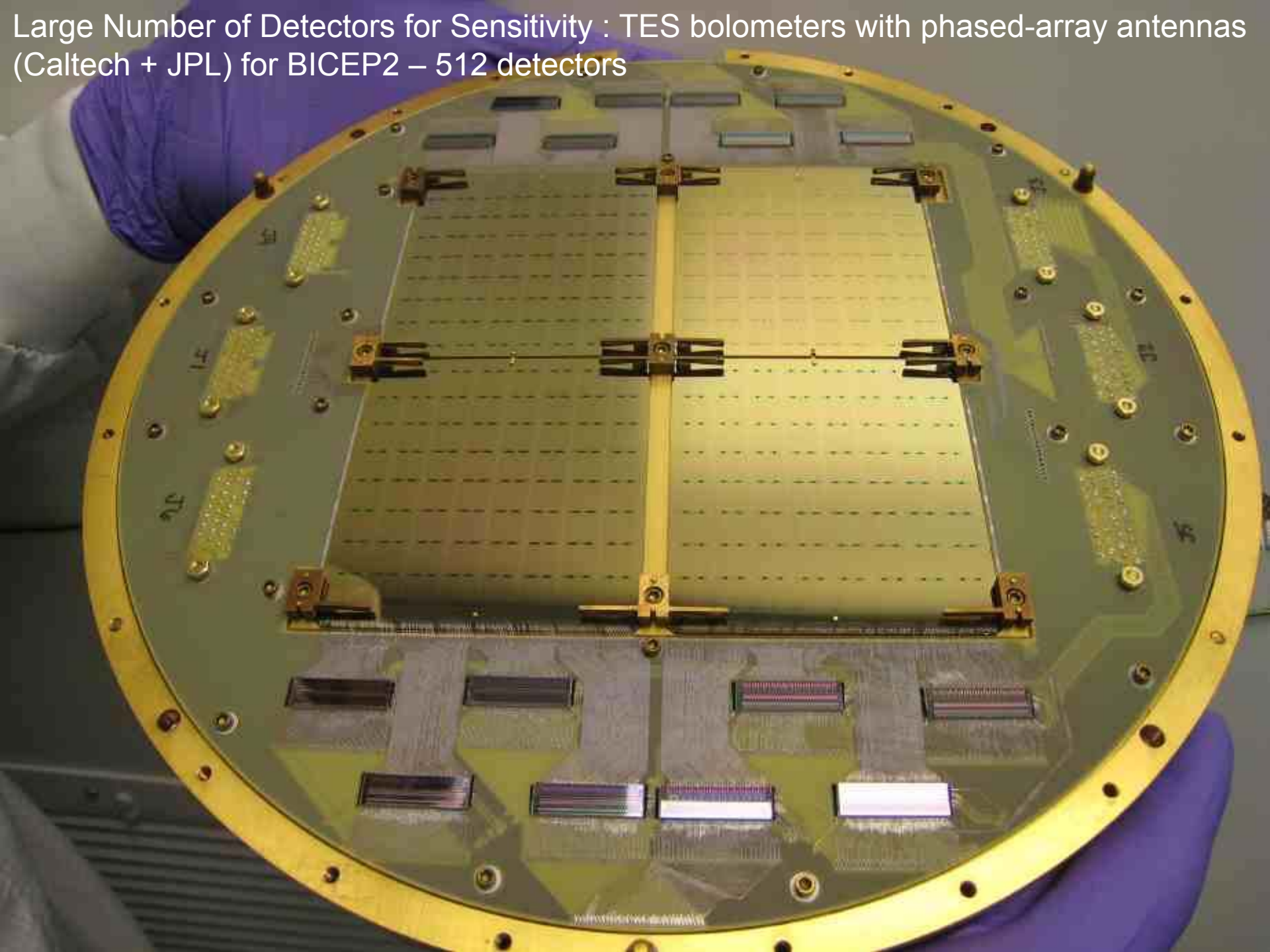

Photon noise from the environment

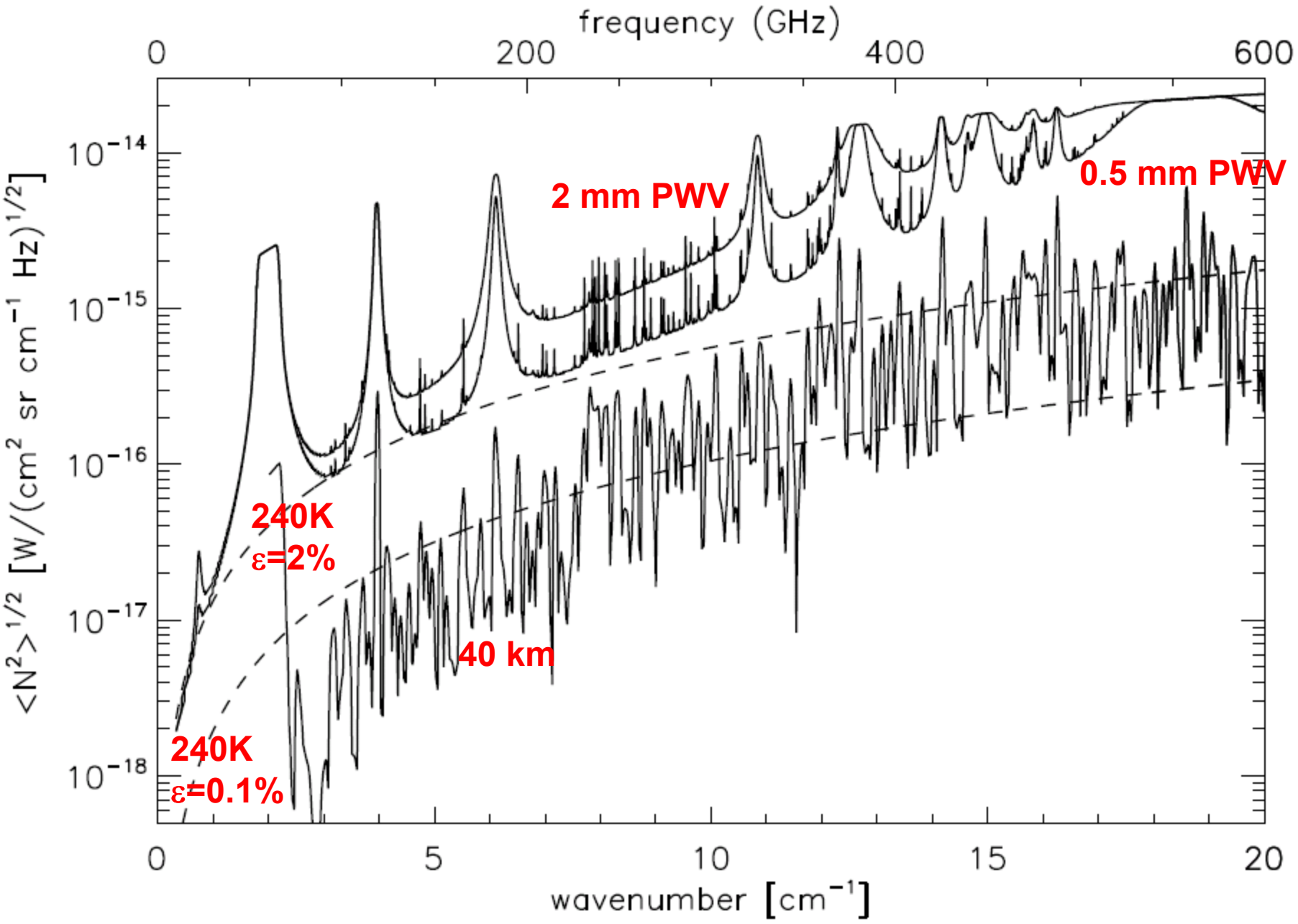

Ground-based

Stratospheric balloons

Space-based

The observable - 1

- The brightness of the CMB is not exactly isotropic in the sky, and has a weak polarization degree, which is anisotropic as well.
- To characterize the angular distribution of a stochastic field on the sky we use the **angular power spectrum**, i.e. the contribution to the variance of the field from different angular scales (represented by different multipoles in an harmonic decomposition of the field).
- The **angular power spectrum of CMB anisotropy** has been now measured very accurately, and is perfectly consistent with the inflation scenario.
- It took decades to get here ..

1980 intermediate scale anisotropy measurements (ULISSE)

1984

100 pixels, sparse samples, higher resolution, constrain σ at different scales

1988

1992

Scanning telescope, 10^4 pixels, map with sub-horizon resolution, constrain TT power spectrum

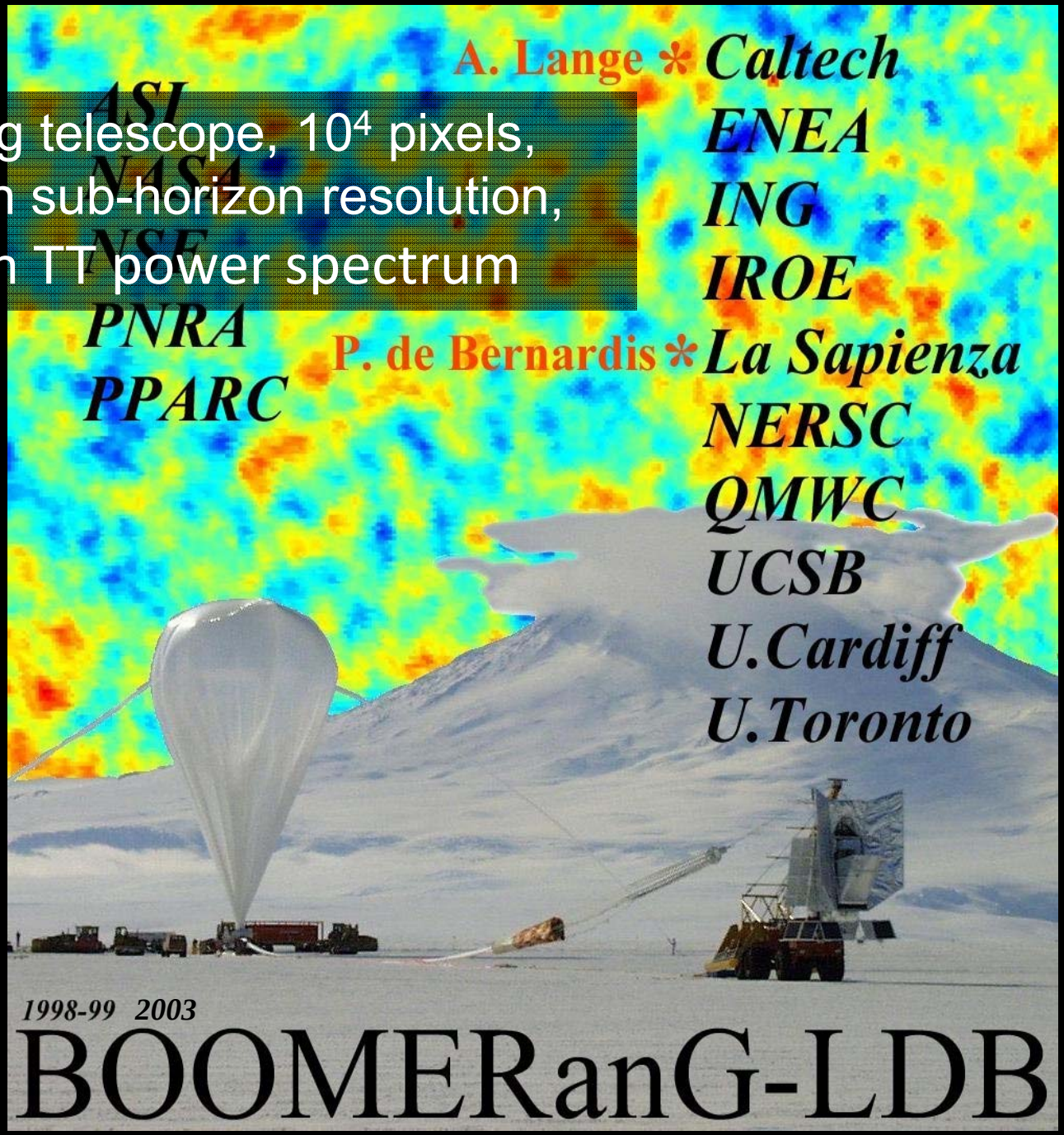

the BOOMERanG ballon-borne telescope

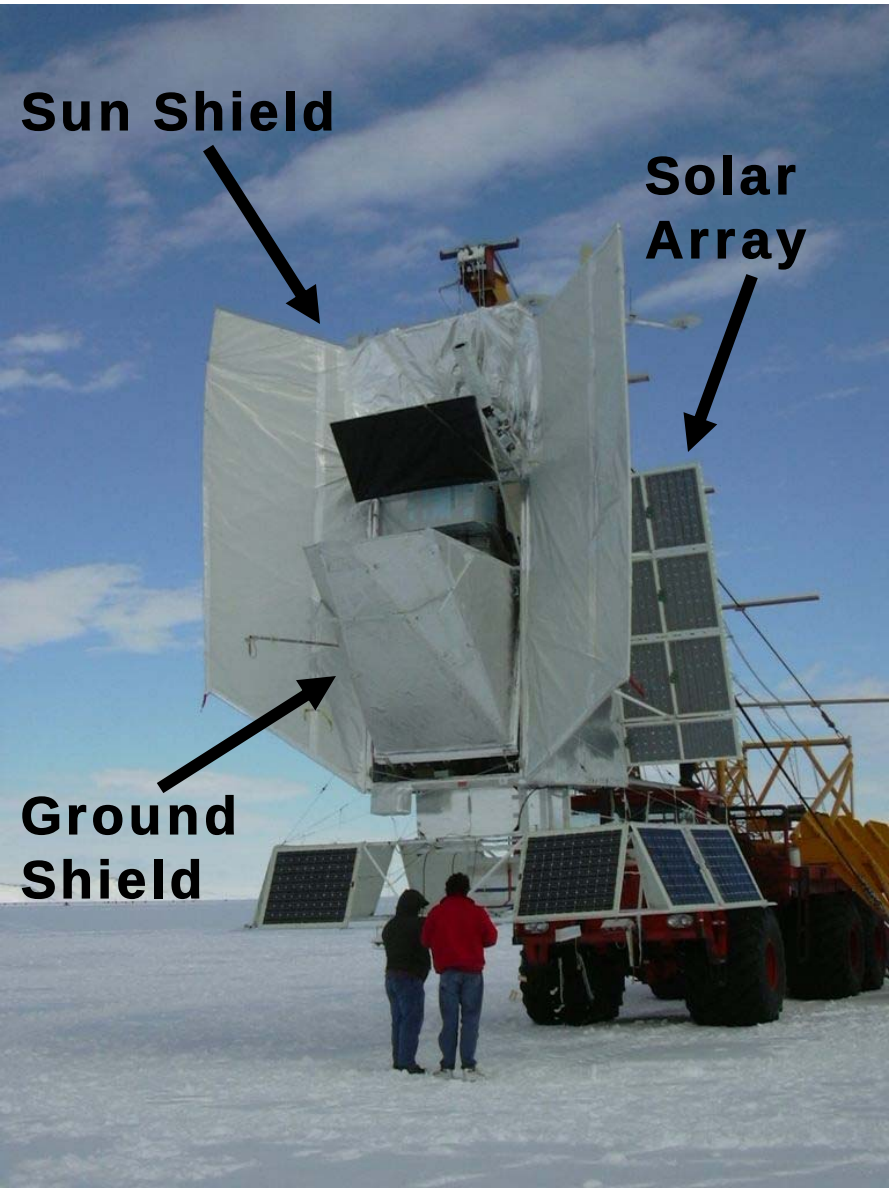

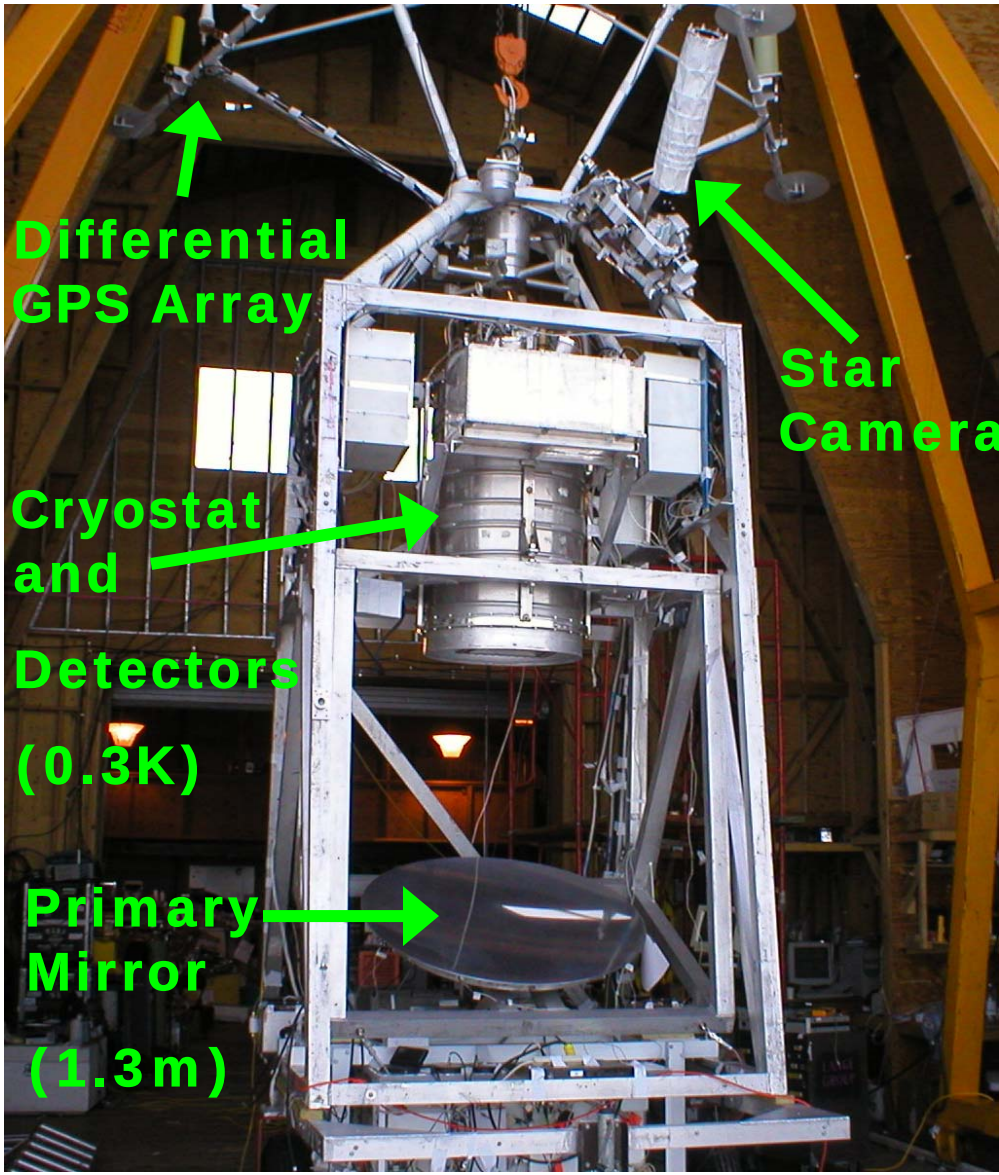

Sensitive at 90, 150, 240, 410 GHz

- The instrument is flown above the Earth atmosphere, at an altitude of 37 km, by means of a stratospheric balloon.
- Long duration flights (LDB, 1-3 weeks) are performad by NASA-NSBF over Antarctica
- BOOMERanG has been flown LDB two times:
- From Dec.28, **1998** to Jan.8, 1999, for CMB anisotropy measurements
- In **2003**, from Jan.6 to Jan.20, for CMB polarization measurements (B2K).

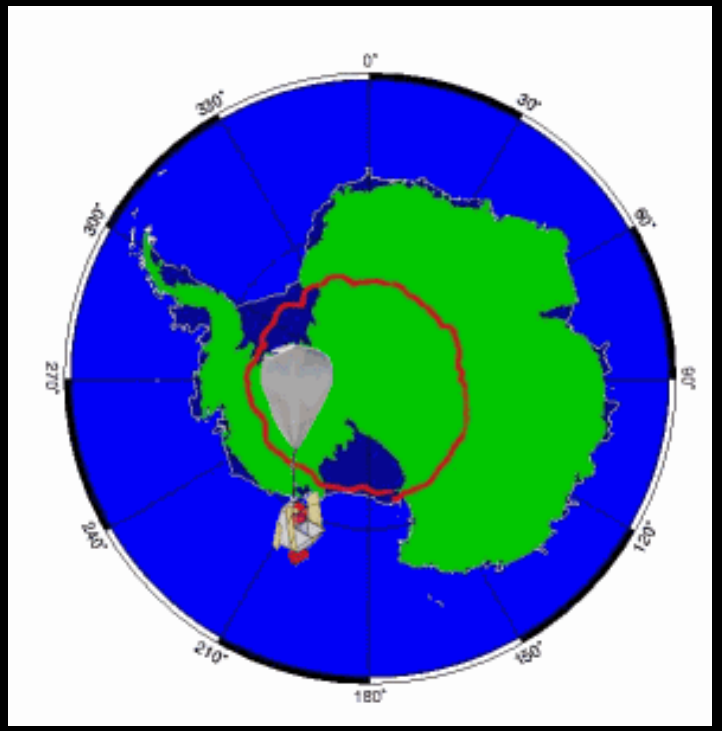

- The image of the sky is obtained by slowly scanning the full payload in azimuth (±30º) at constant elevation

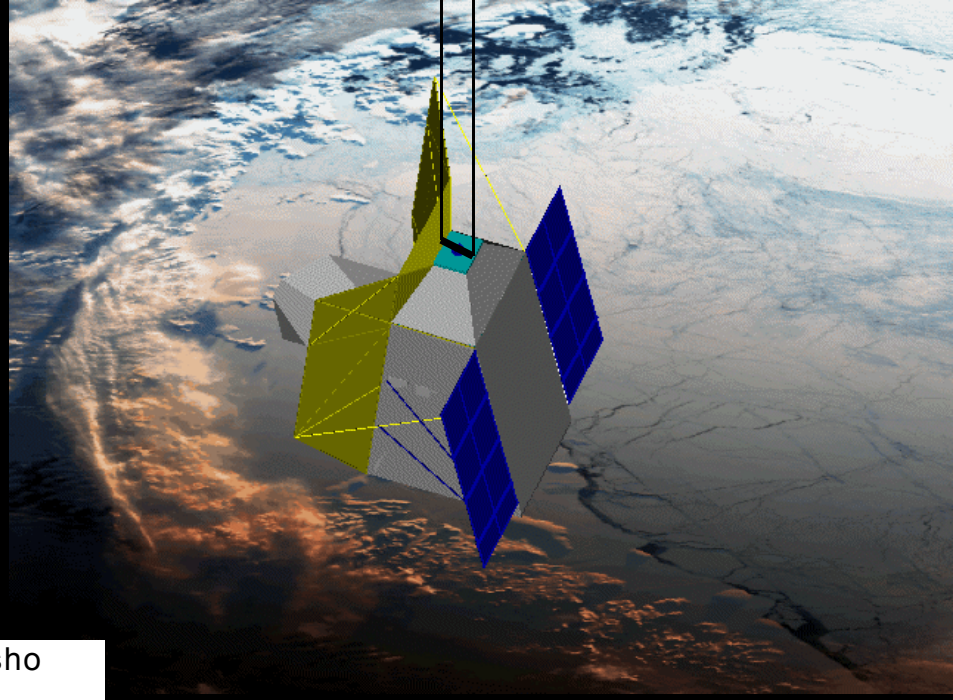

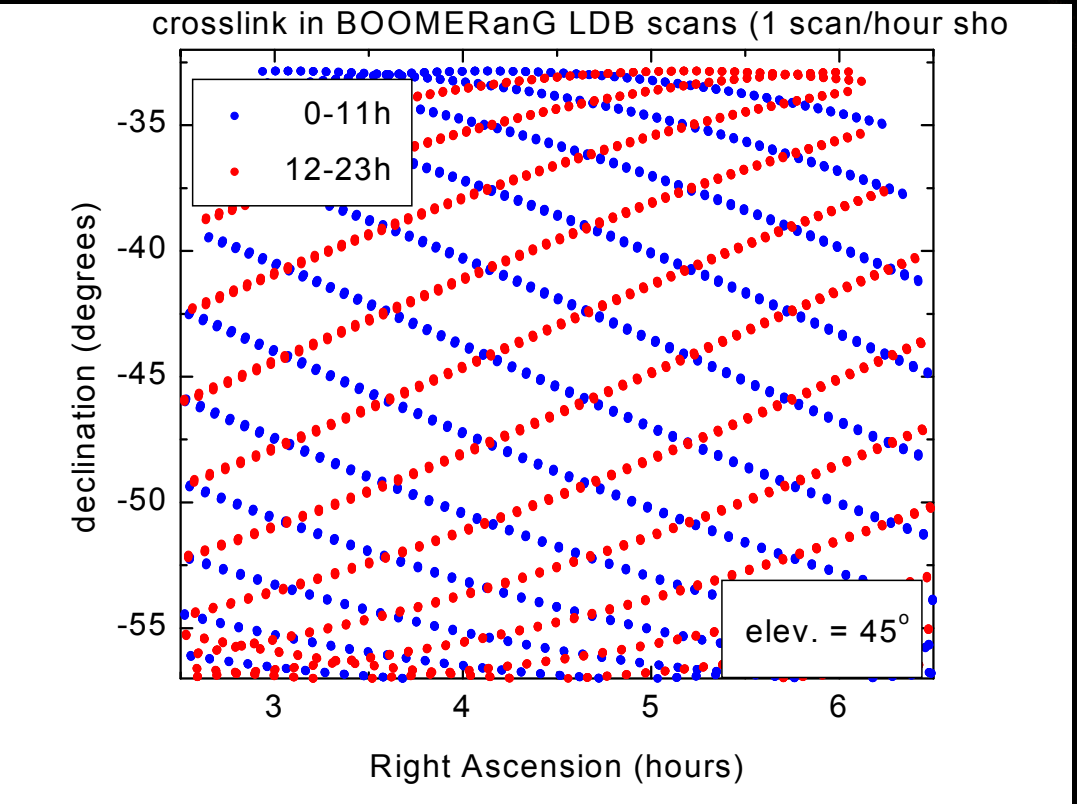

- The scan center constantly tracks the azimuth of the lowest foreground region
- Every day we obtain a fully crosslinked map.
- This is the key for an accurate map of the sky

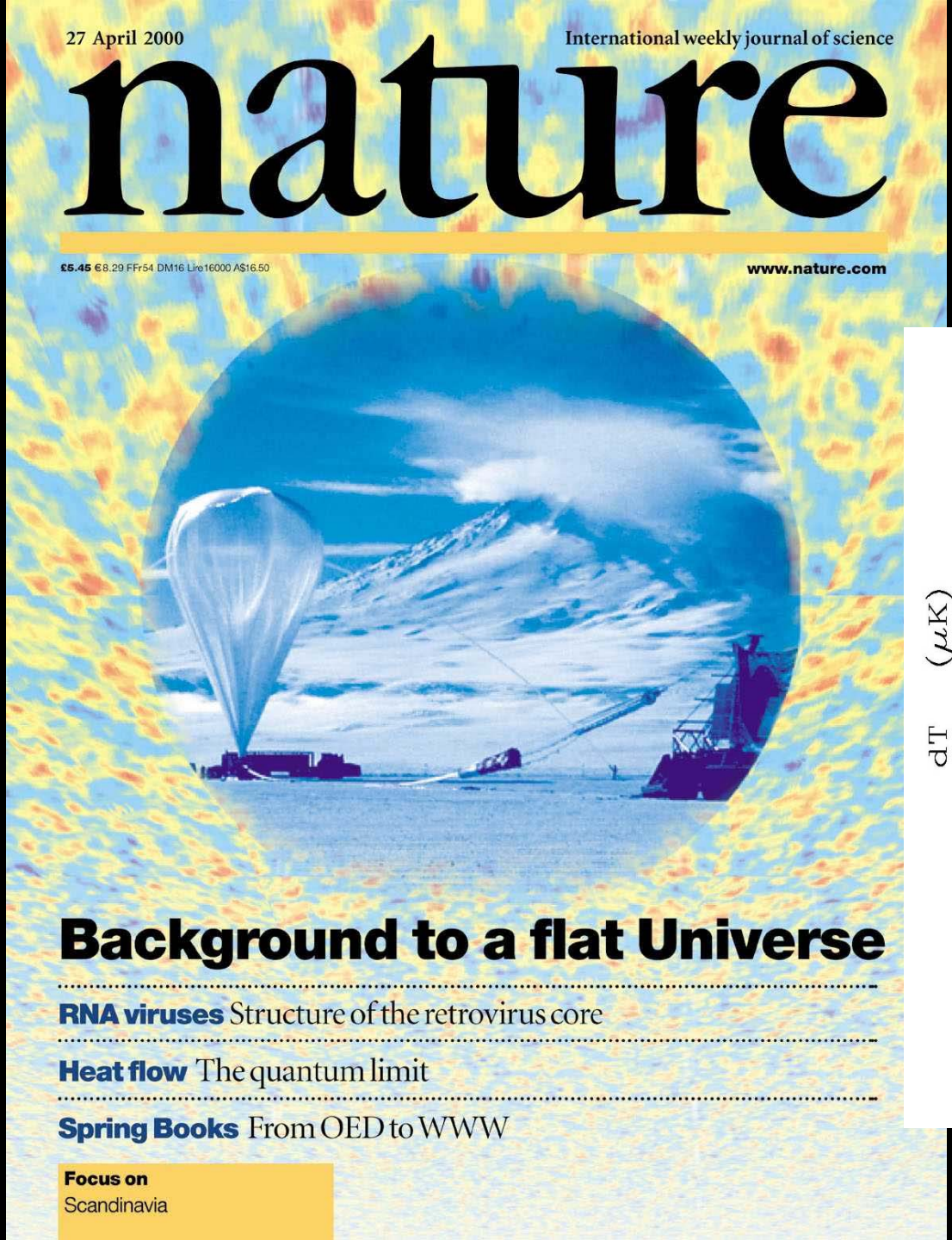

First evidence (2000) from BOOMERanG

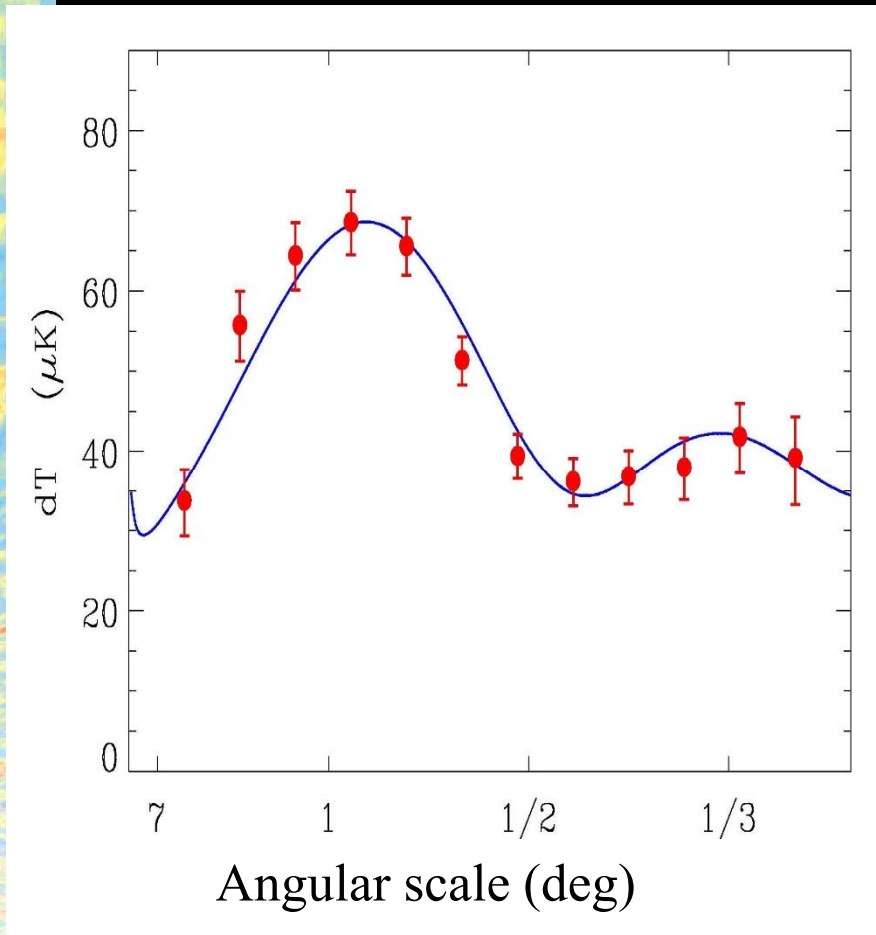

THE ASTROPHYSICAL JOURNAL, 564:559–566, 2002 January 10

MULTIPLE PEAKS IN THE ANGULAR POWER SPECTRUM OF THE COSMIC MICROWAVE BACKGROUND: SIGNIFICANCE AND CONSEQUENCES FOR COSMOLOGY

P. DE BERNARDIS,[1] P. A. R. ADE,[2] J. J. BOCK,[3] J. R. BOND,[4] J. BORRILL,[5] A. BOSCALERI,[6] K. COBLE,[7] C. R. CONTALDI,[4] B. P. CRILL,[8] G. DE TROIA,[1] P. FARESE,[7] K. GANGA,[9] M. GIACOMETTI,[1] E. HIVON,[9] V. V. HRISTOV,[8] A. IACOANGELI,[1] A. H. JAFFE,[10] W. C. JONES,[8] A. E. LANGE,[8] L. MARTINIS,[11] S. MASI,[1] P. MASON,[8] P. D. MAUSKOPF,[12] A. MELCHIORRI,[13] T. MONTROY,[7] C. B. NETTERFIELD,[14] E. PASCALE,[6] F. PIACENTINI,[1] D. POGOSYAN,[4] G. POLENTA,[1] F. PONGETTI,[15] S. PRUNET,[4] G. ROMEO,[15] J. E. RUHL,[7] AND F. SCARAMUZZI[11]

Received 2001 May 18; accepted 2001 September 11

ABSTRACT

Three peaks and two dips have been detected in the power spectrum of the cosmic microwave background by the BOOMERANG experiment, at $l = (213^{+10}_{-13})$, (541^{+20}_{-32}), (845^{+12}_{-25}) and $l = (416^{+22}_{-12})$, (750^{+20}_{-750}), respectively. Using model-independent analyses, we find that all five features are statistically significant, and we measure their location and amplitude. These are consistent with the adiabatic inflationary model. We also calculate the mean and variance of the peak and dip locations and amplitudes in a large seven-dimensional parameter space of such models, which gives good agreement with the model-independent estimates. We forecast where the next few peaks and dips should be found if the basic paradigm is correct. We test the robustness of our results by comparing Bayesian marginalization techniques on this space with likelihood maximization techniques applied to a second seven-dimensional cosmological parameter space, using an independent computational pipeline, and find excellent agreement: $\Omega_{\rm tot} = 1.02^{\pm 0.05}_{-0.06}$ versus 1.04 ± 0.05, $\Omega_b h^2 = 0.022^{+0.004}_{-0.003}$ versus $0.019^{+0.005}_{-0.004}$, and $n_s = 0.96^{+0.09}_{-0.08}$ versus 0.90 ± 0.08. The determination of the best fit by the maximization procedure effectively ignores nonzero optical depth of reionization $\tau_C > 0$, and the difference in primordial spectral index n_s between the two methods is thus a consequence of the strong correlation of n_s with the τ_C.

Subject headings: cosmic microwave background — cosmological parameters — cosmology: observations

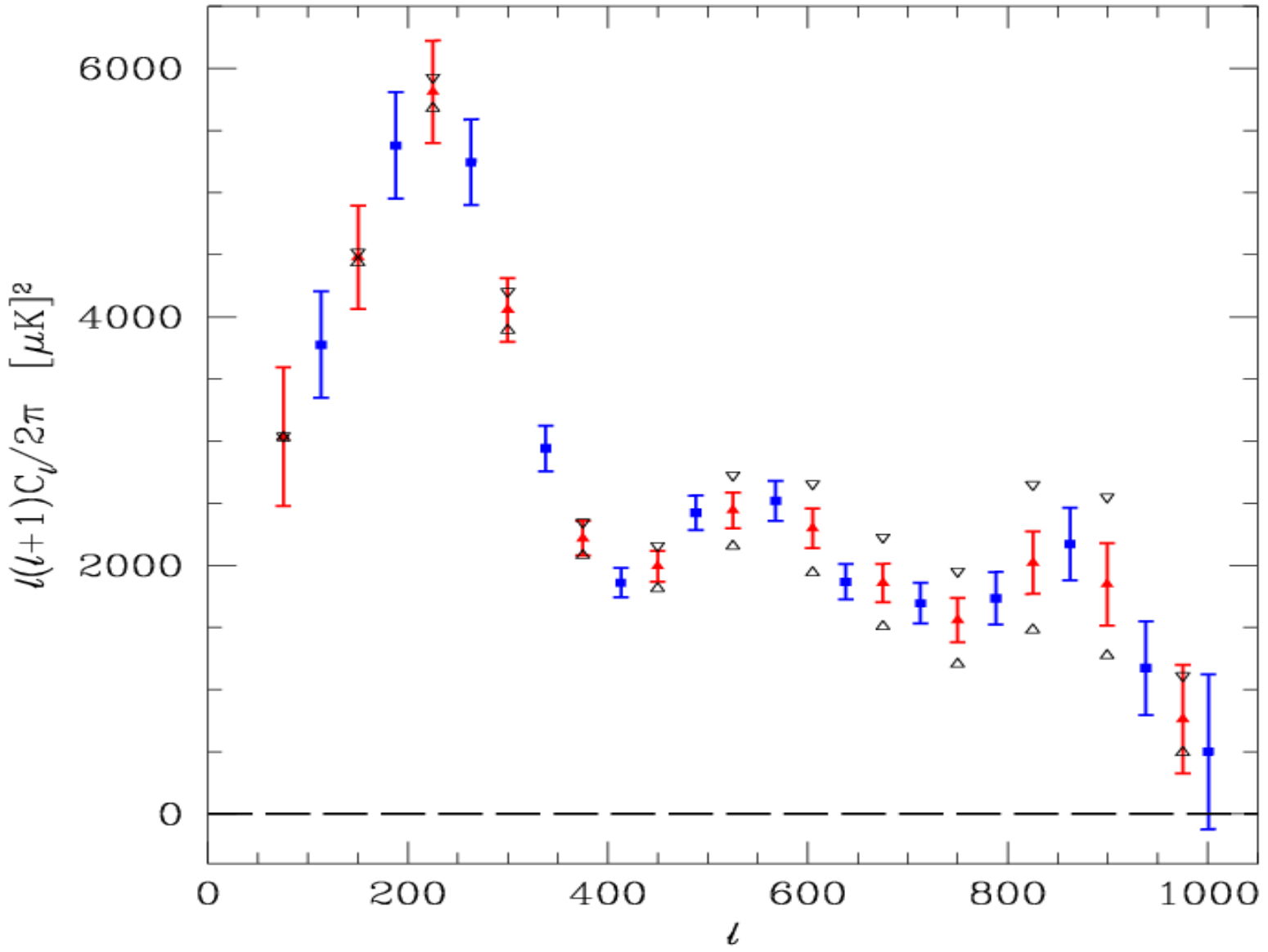

Netterfield et al. 2001, de Bernardis et al. 2002

WMAP (2002)

Wilkinson Microwave Anisotropy Probe

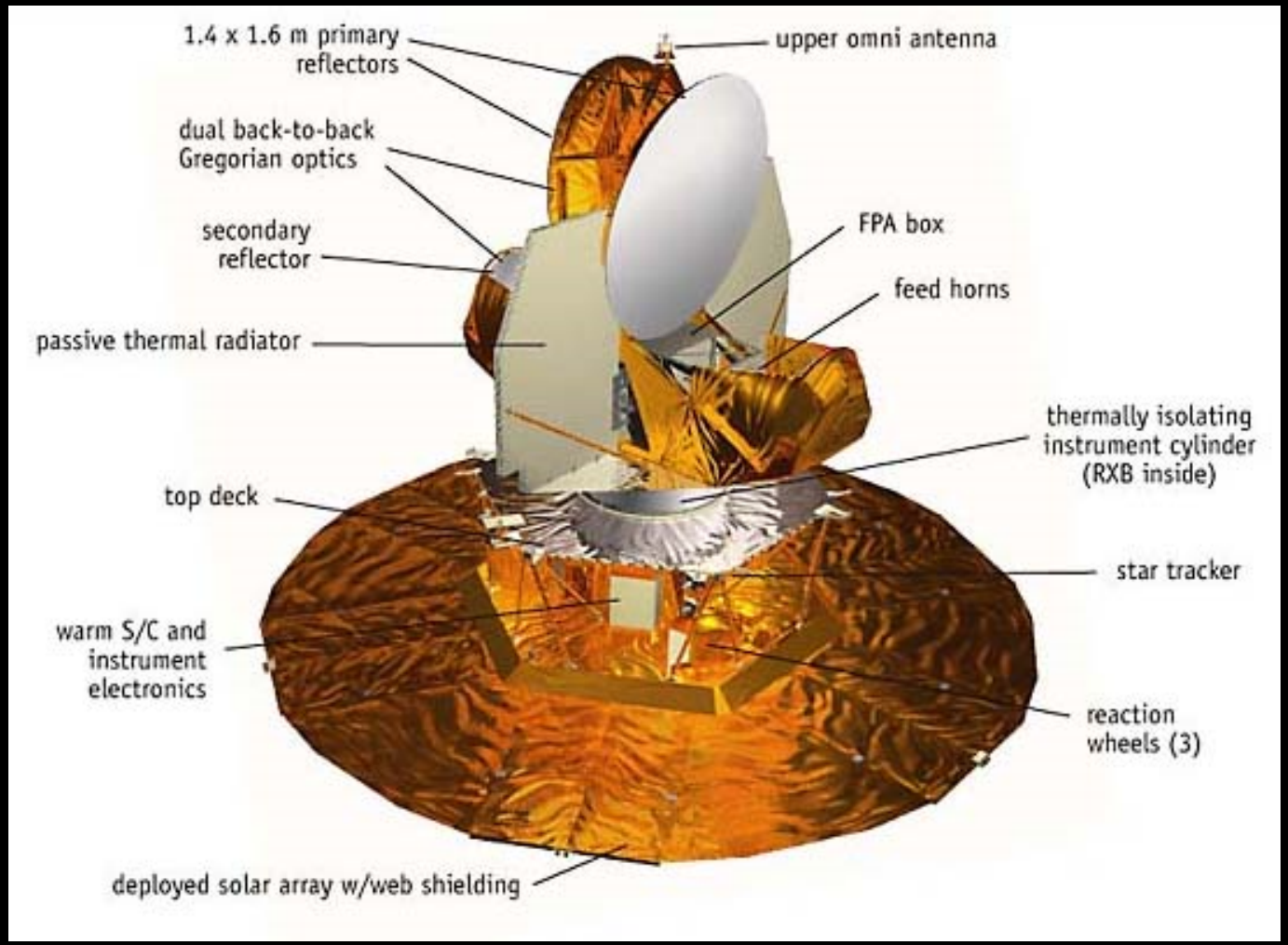

WMAP in L_2 : sun, earth, moon are all well behind the solar shield.

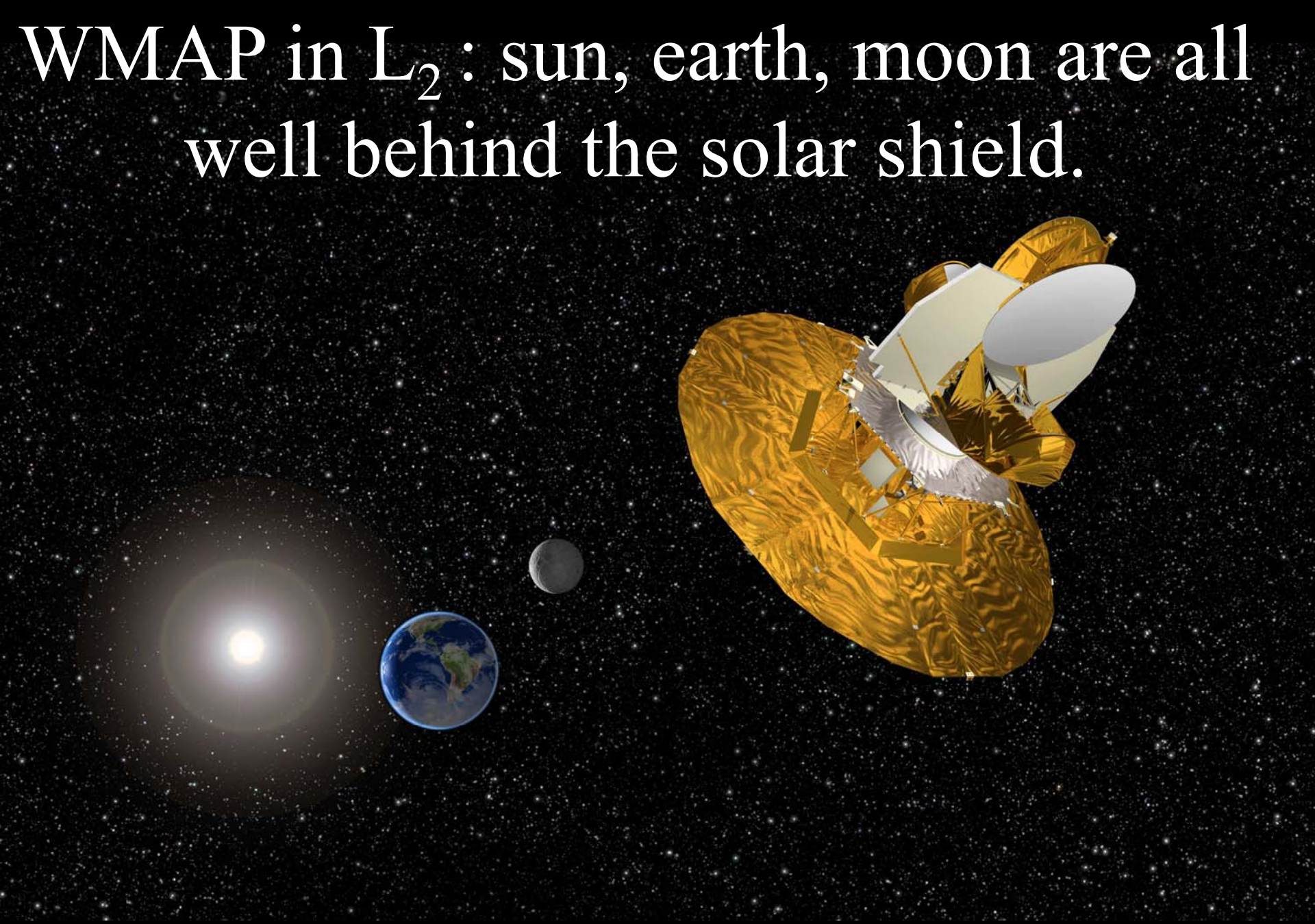

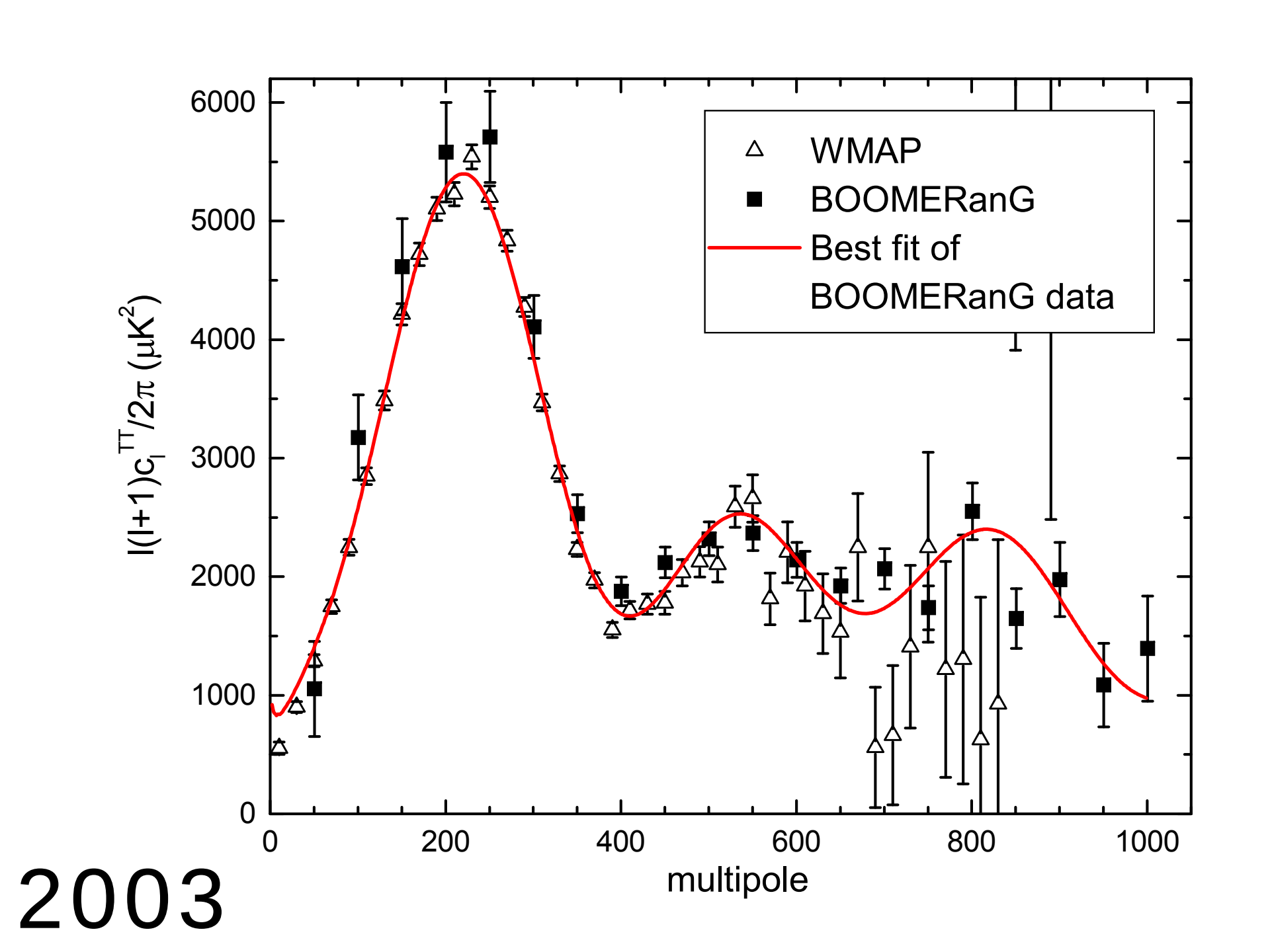
WMAP
BOOMERanG
Best fit of
BOOMERanG data
$l(l+1)c_l^{TT}/2\pi\ (\mu K^2)$
multipole
0
1000
2000
3000
4000
5000
6000
0
200
400
600
800
1000
2003

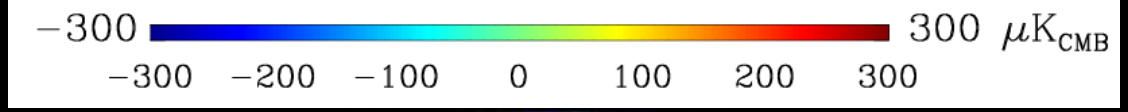

WMAP
Hinshaw et al. 2006
astro-ph/0603451

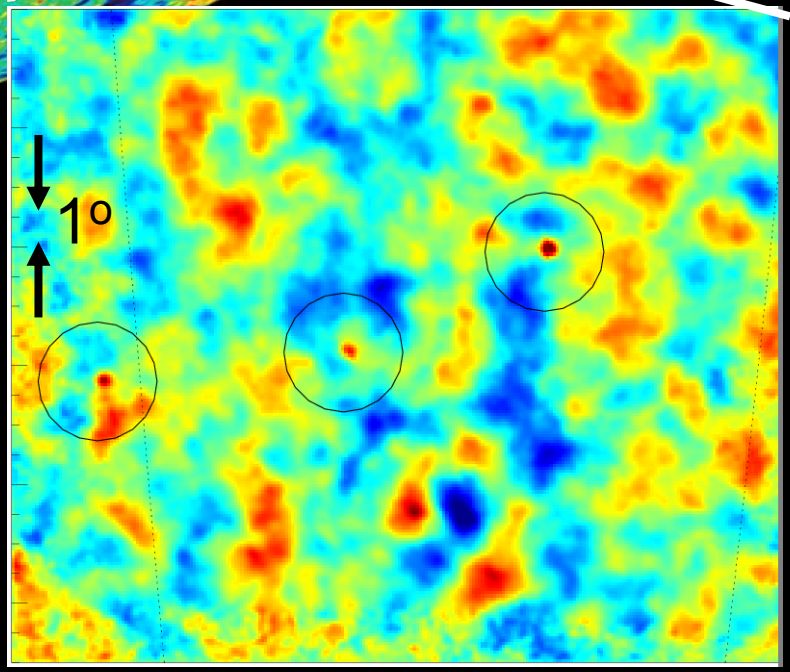

Detailed Views of the Recombination Epoch (z=1088, 13.7 Gyrs ago)

BOOMERanG
Masi et al. 2005
astro-ph/0507509

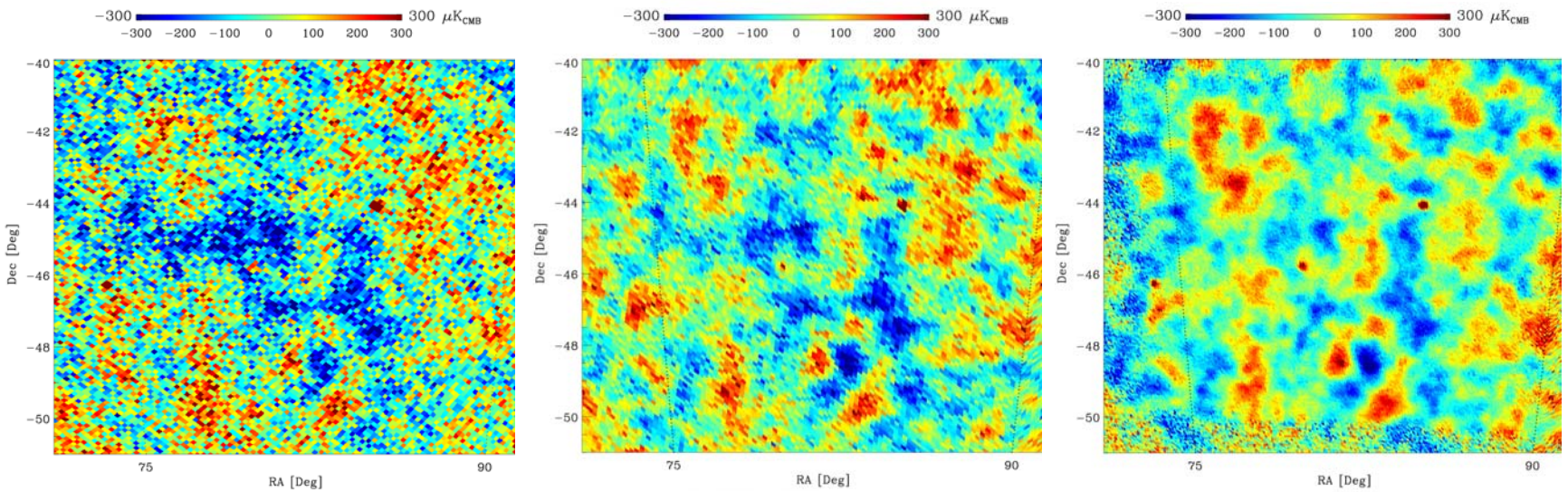

WMAP 3 years
23-94 GHz

BOOMERanG-98
145 GHz

BOOMERanG-03
145 GHz

The consistency of the maps from three *independent* experiments, working at very different frequencies and with very different mesurement methods, is the best evidence that the faint structure observed

- *is not due to instrumental artifacts*
- *has exactly the spectrum of CMB anisotropy, so it is not due to foreground emission*
- The comparison also shows the *extreme sensitivity of cryogenic bolometers* operated at balloon altitude (the B03 map is the result of 5 days of observation)

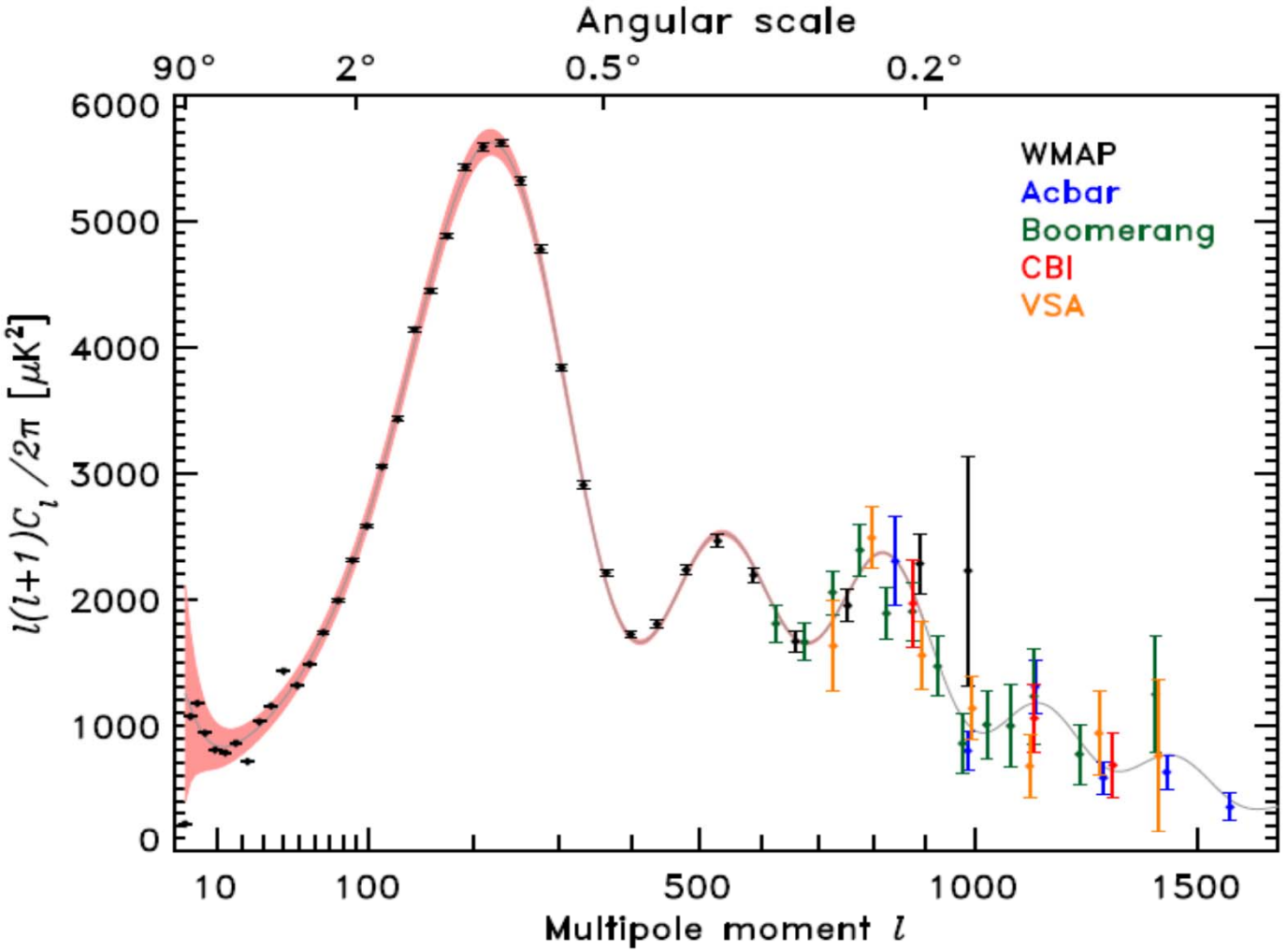

Fig. 18.— The *WMAP* three-year power spectrum (in black) compared to other recent measurements of the CMB angular power spectrum, including Boomerang (Jones et al. 2005), Acbar (Kuo et al. 2004), CBI (Readhead et al. 2004), and VSA (Dickinson et al. 2004). For clarity, the $l < 600$ data from Boomerang and VSA are omitted; as the measurements are consistent with *WMAP*, but with lower weight. These ely confirm the turnover in the 3rd acoustic peak and probe the onset of Silk damping. l sensitivity on sub-degree scales, the *WMAP* data are becoming an increasingly important rce for high-resolution experiments.

2006

Hinshaw et al. 2006

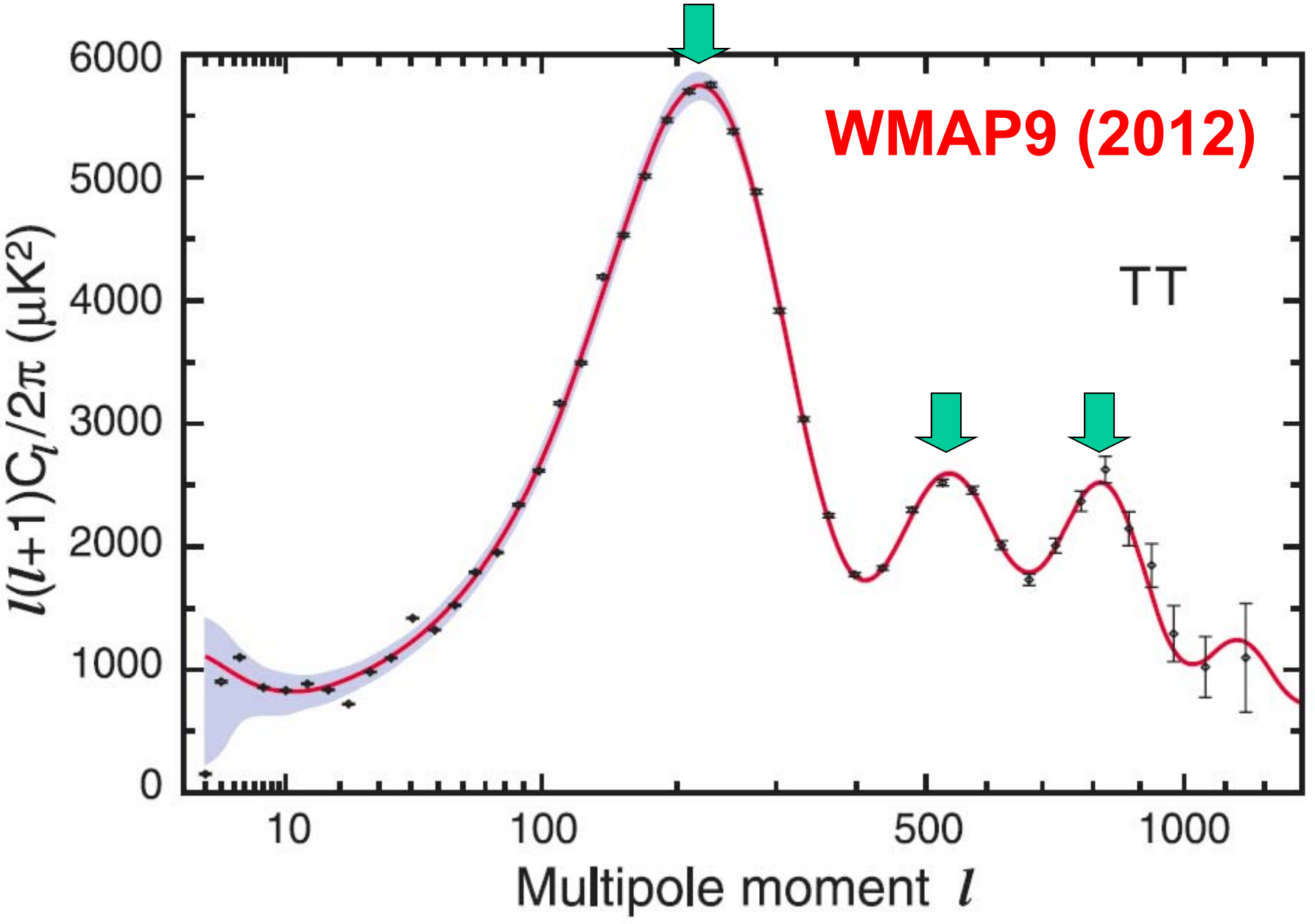
WMAP9 (2012)
TT
$l(l+1)C_l/2\pi$ (μK^2)
6000
5000
4000
3000
2000
1000
0
10
100
500
1000
Multipole moment l

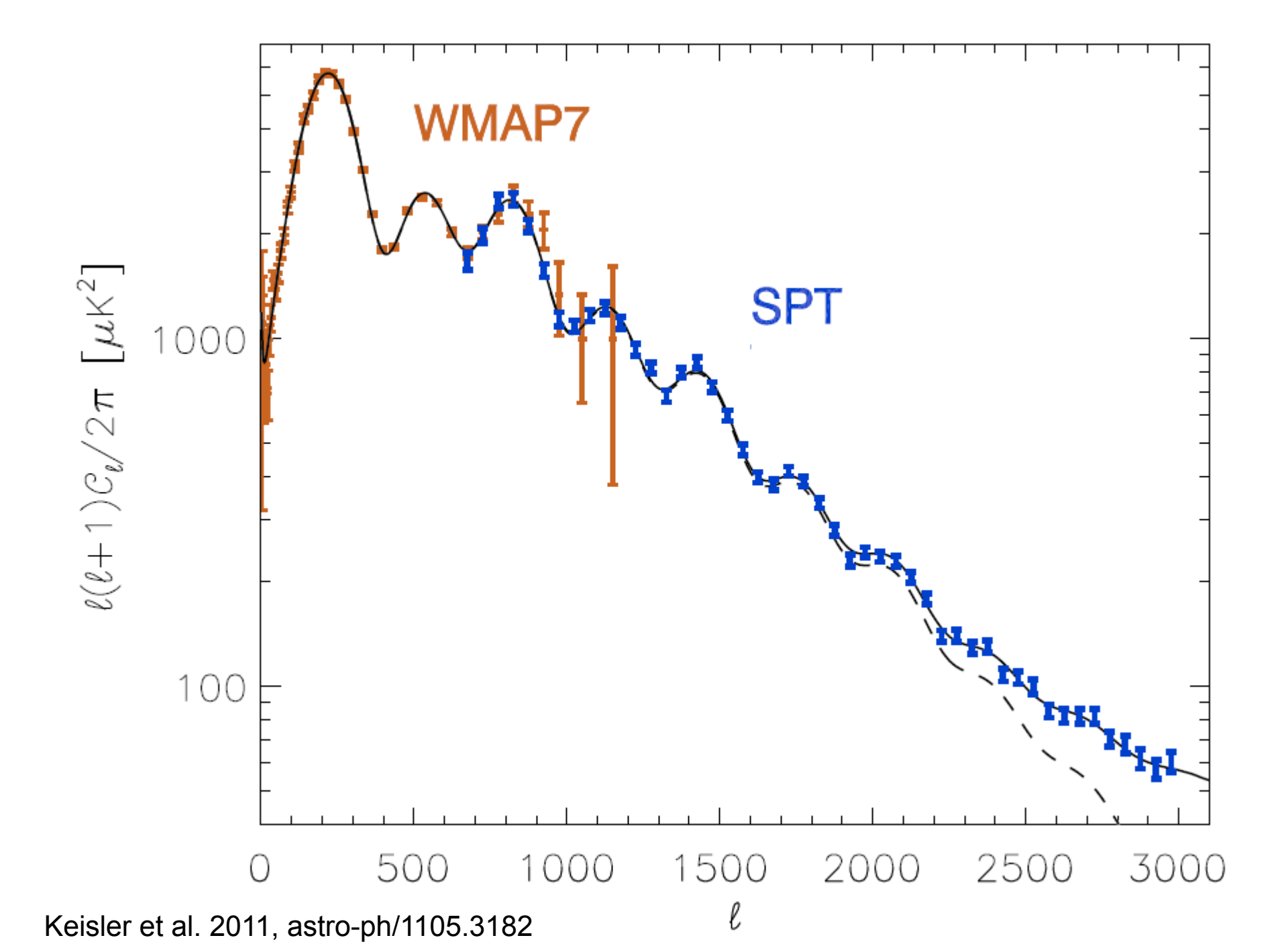

Keisler et al. 2011, astro-ph/1105.3182

Paradigm of CMB anisotropies

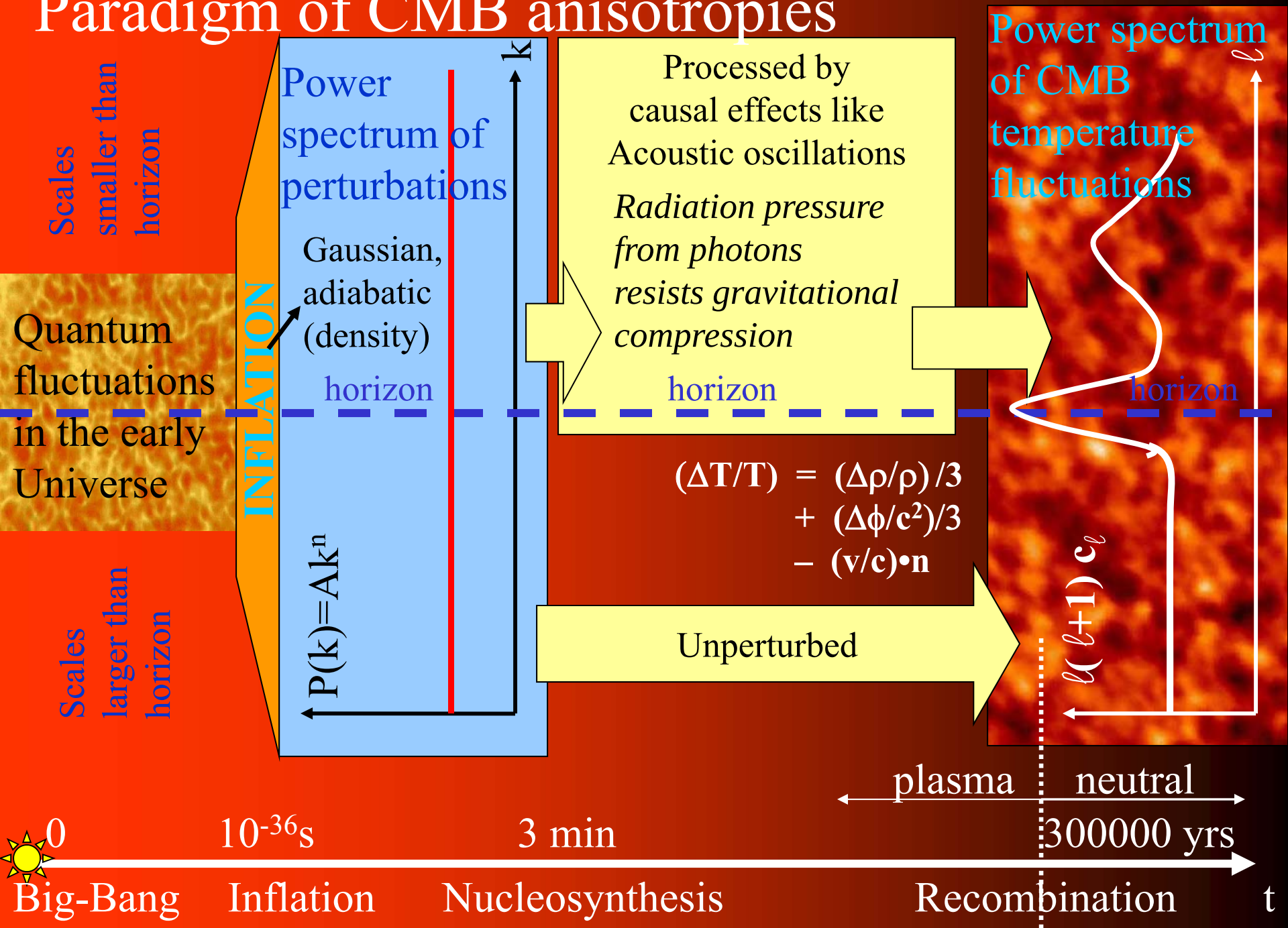

Planck is a very ambitious experiment.

It carries a complex CMB experiment (the state of the art, a few years ago) all the way to L2,

improving the sensitivity wrt WMAP by at least a factor 10,

extending the frequency coverage towards high frequencies by a factor about 10

Customer	**ESA, EUROPEAN SPACE AGENCY**
Prime contractor	*Thales Alenia Space*
Mission	*To study the origins of the Universe by observing the Cosmic Microwave Background (CBM)*
Mass	*Total mass at lift-off 1.921 kg*
Stabilization	*Spin (1rpm)*
Dimensions	*4.2 m (Height)* *4.2 m (Diameter)*
Payload	*1 telescope and 2 scientific instruments (HFI and LFI)*
On-board power	*1 816 W (end of life)*
Life time	*21 months*
Orbital position	*L2 Lagrange Point*

Observing strategy

The payload will work from L2, to avoid the emission of the Earth, of the Moon, of the Sun

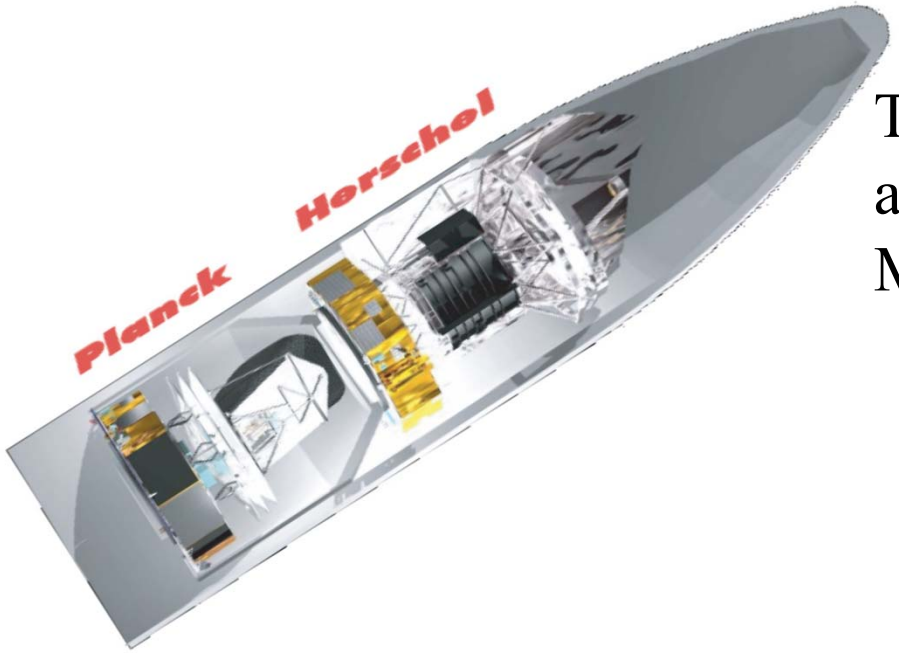

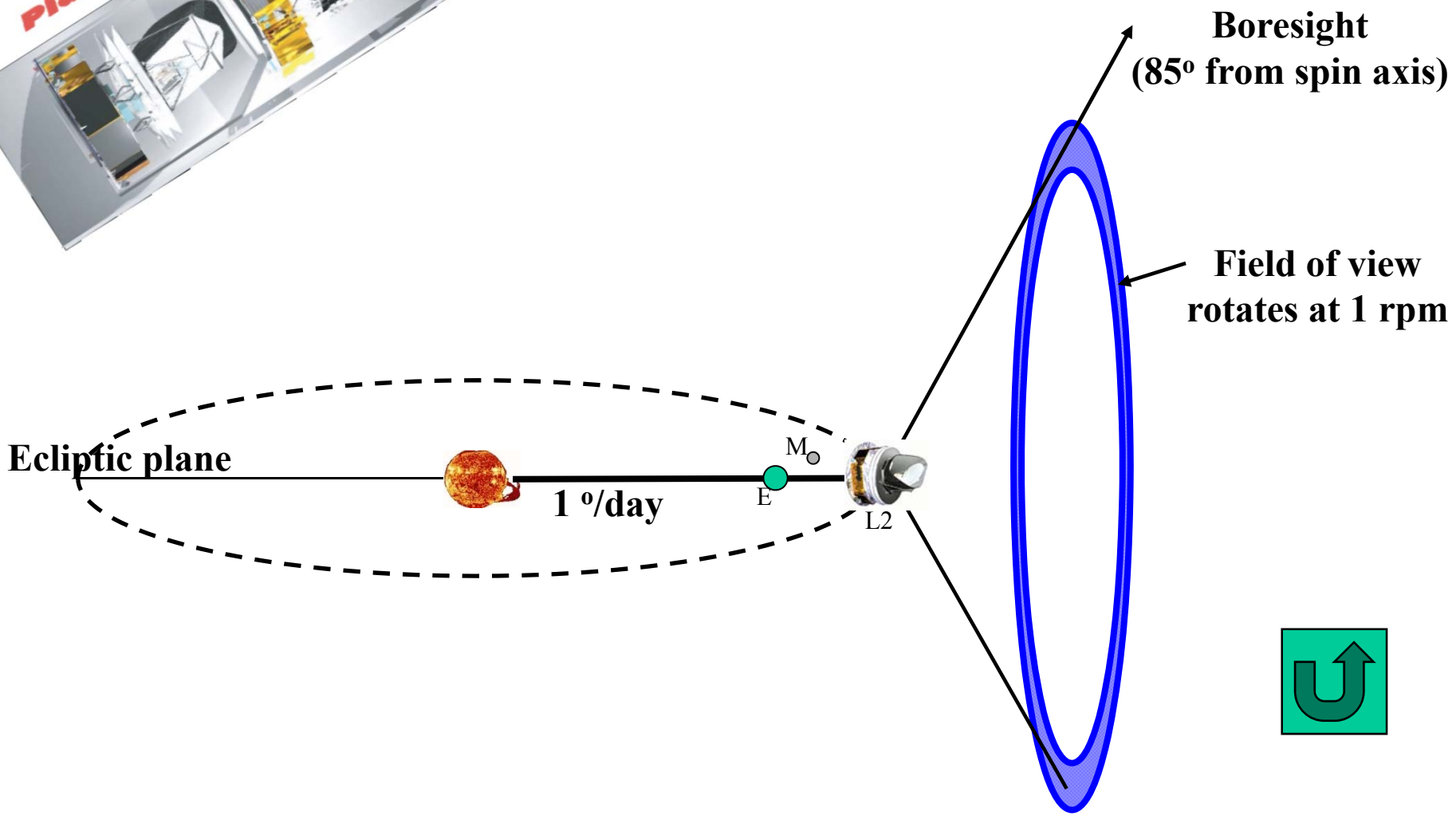

Thermal performance :
Planck collaboration: astro-ph/1101:2023

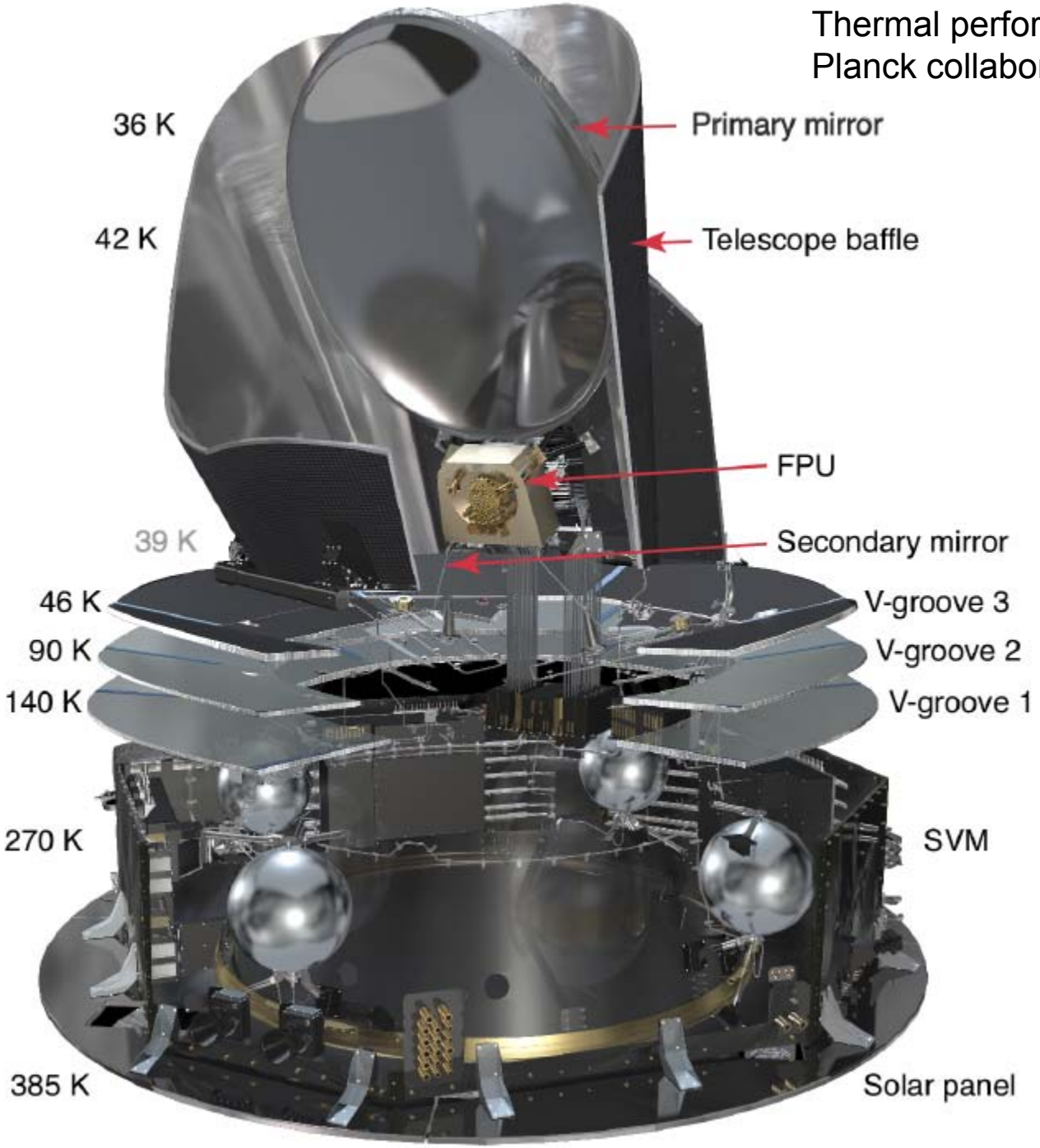

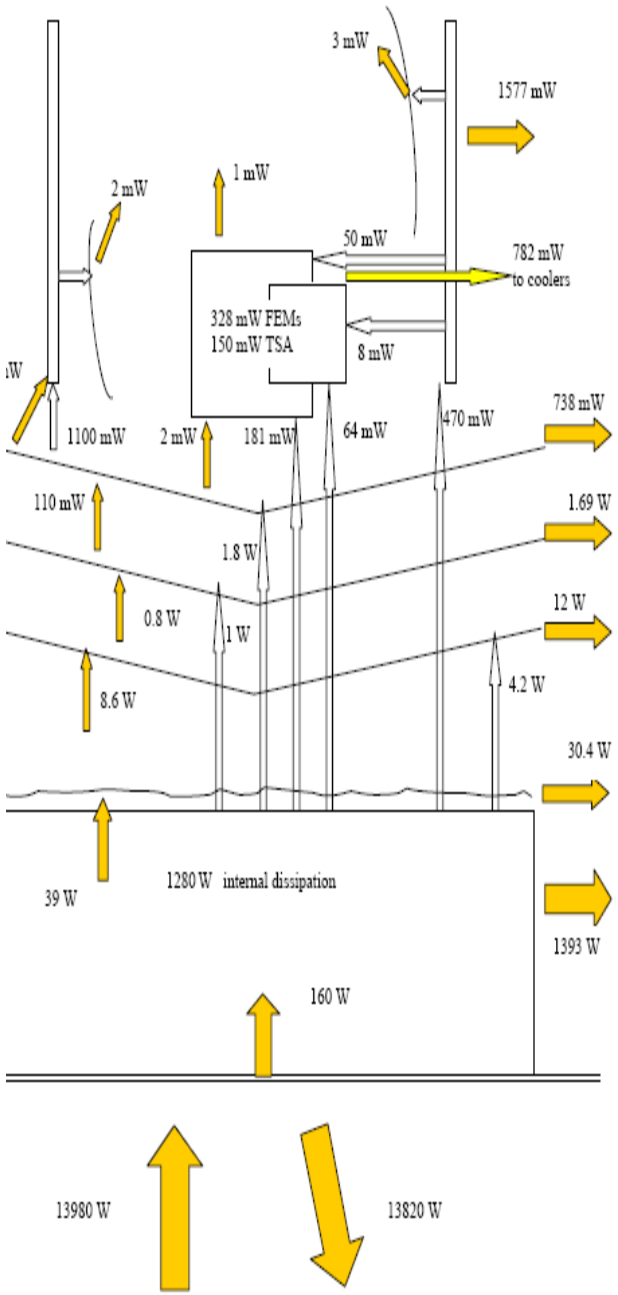

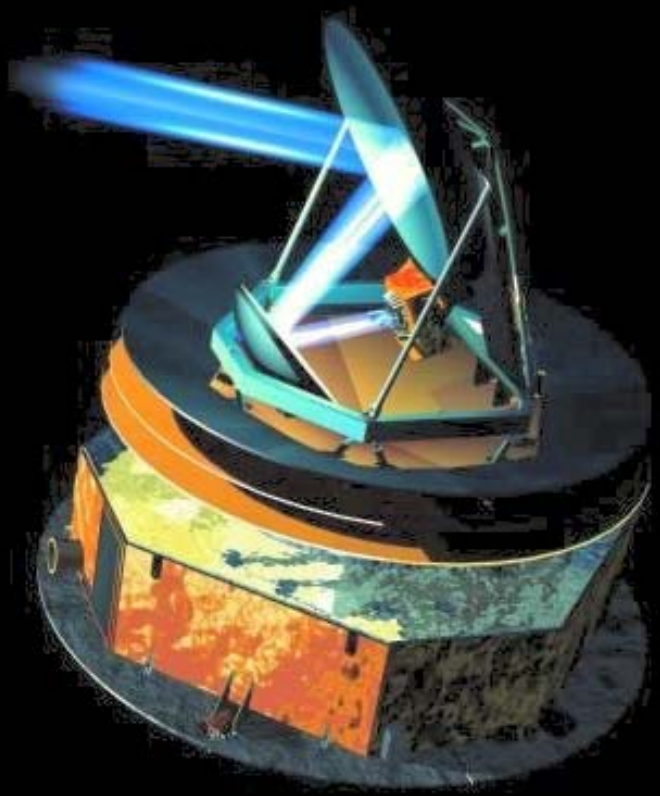

Off-axis telescope,
1.8 m

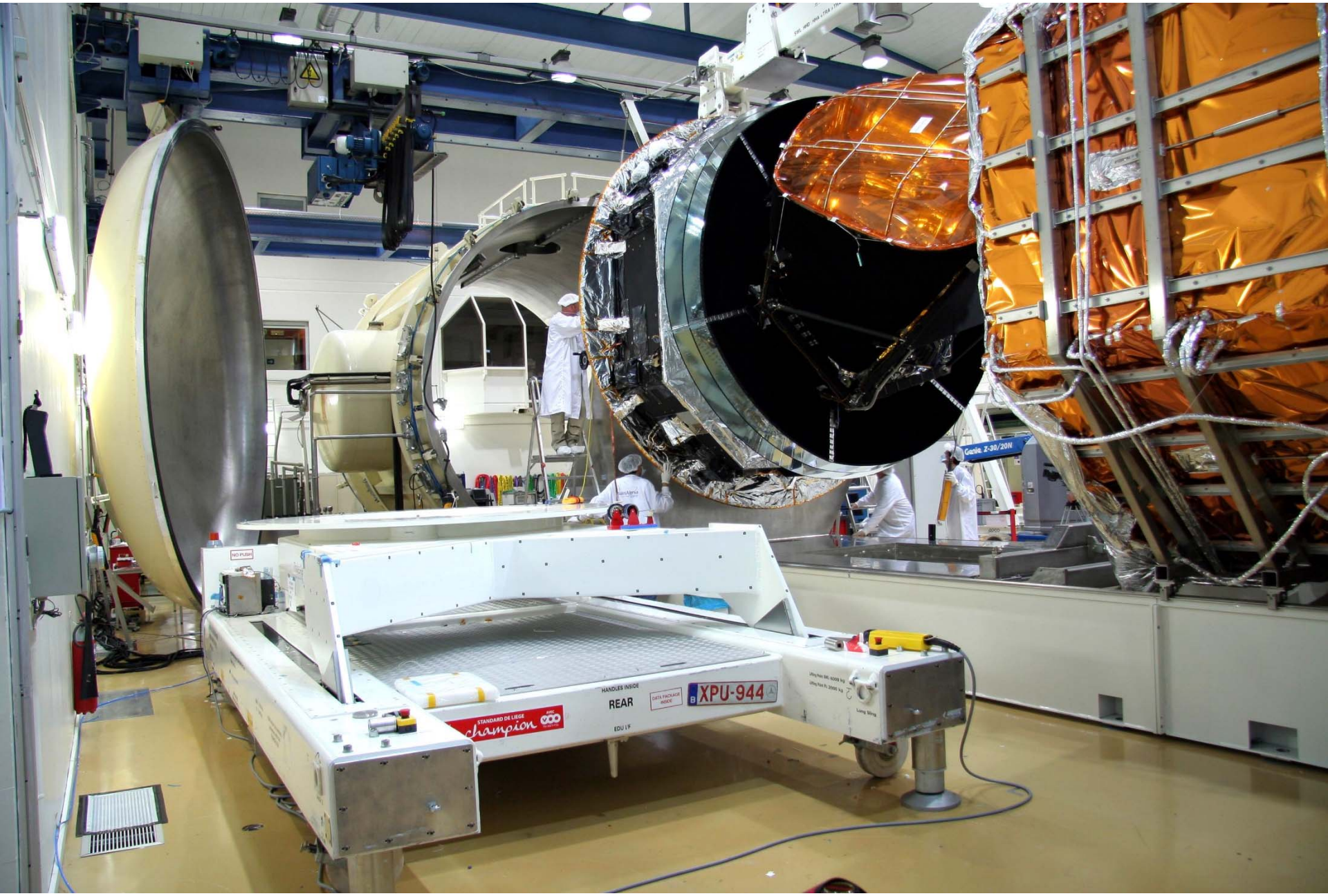
NO PUSH
HANDLES INSIDE
REAR
DATA PACKAGE INSIDE
B XPU-944
EDU I/F
STANDARD DE LIEGE
champion
Genie Z-30/20N

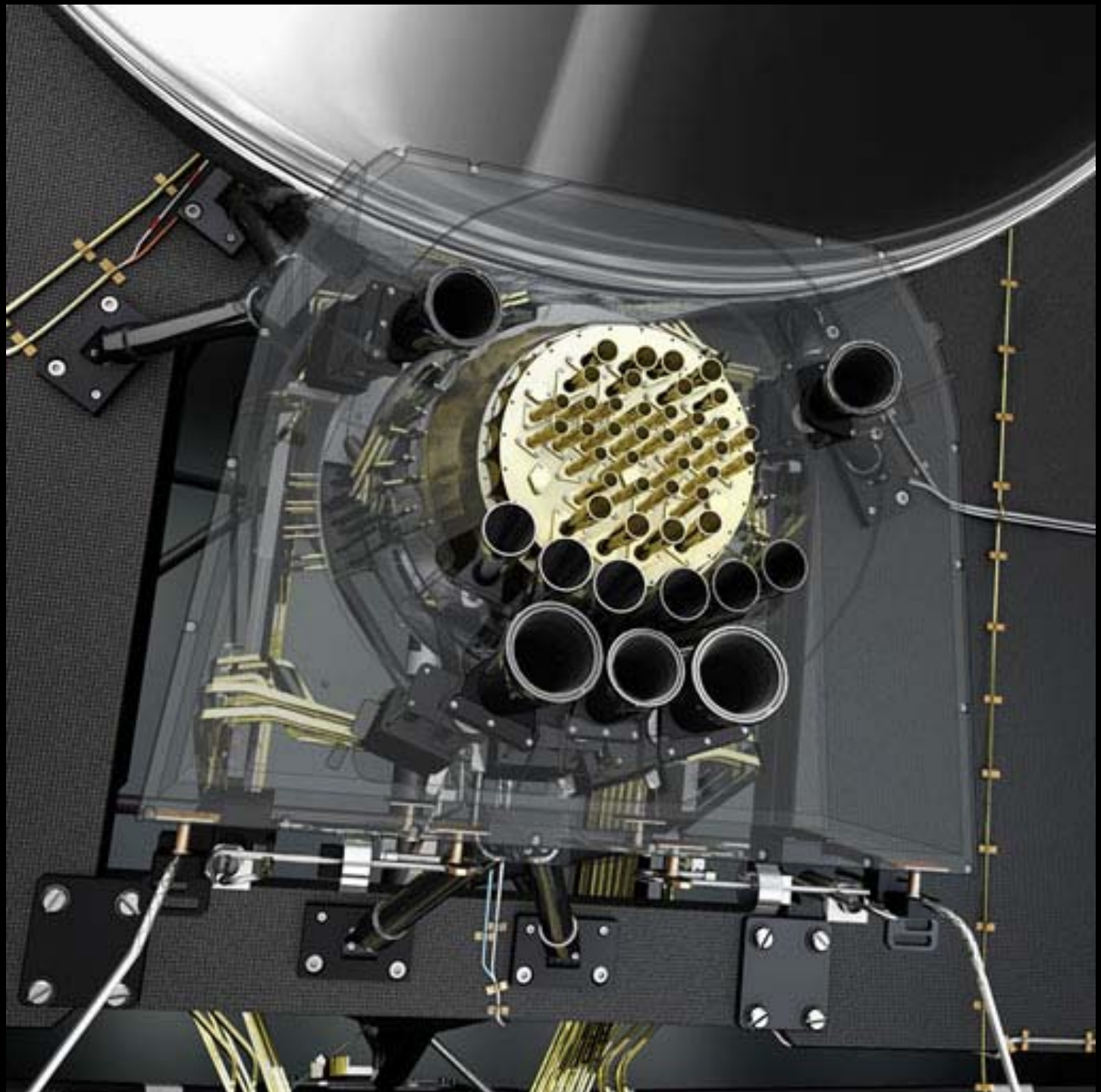

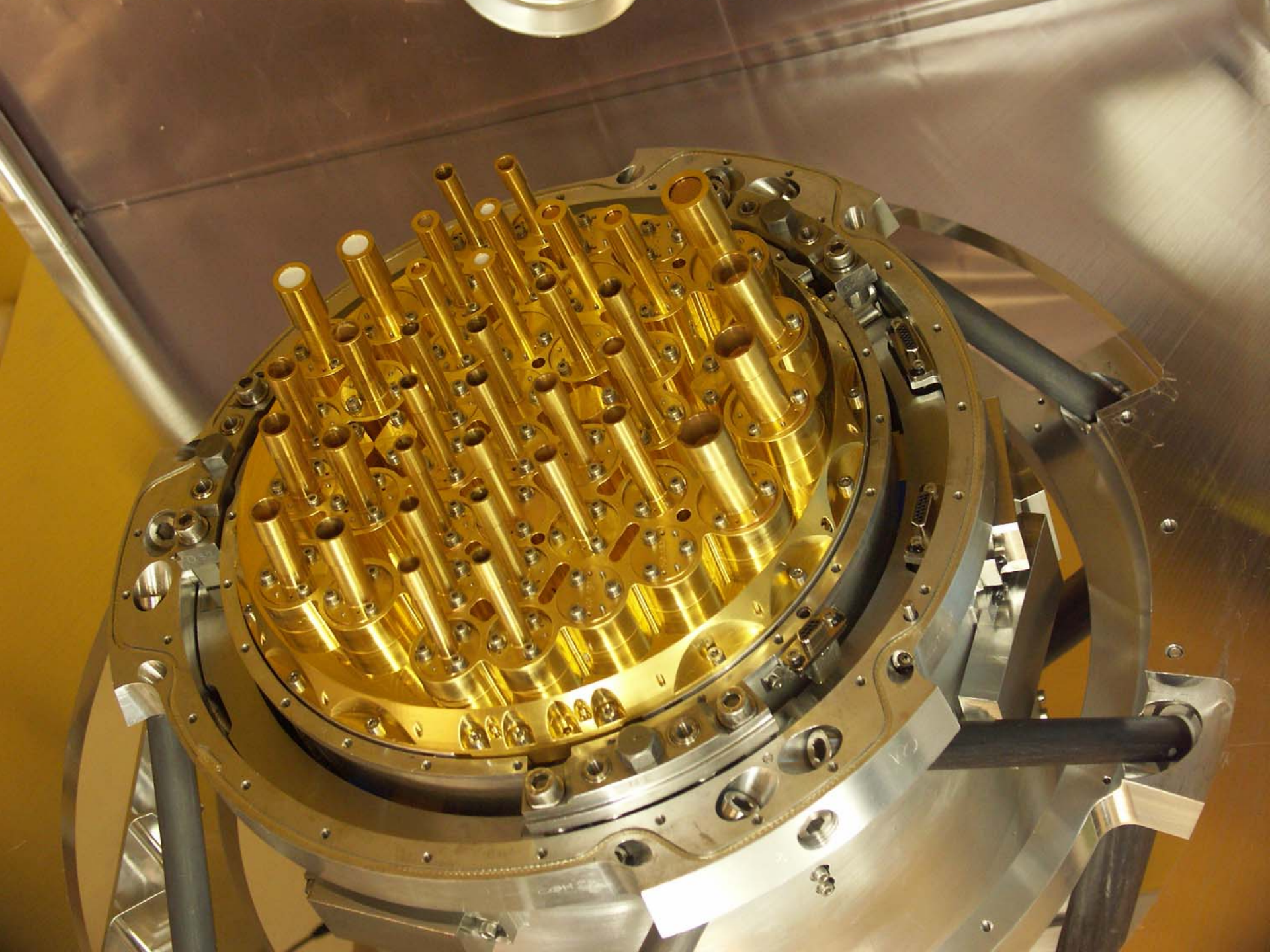

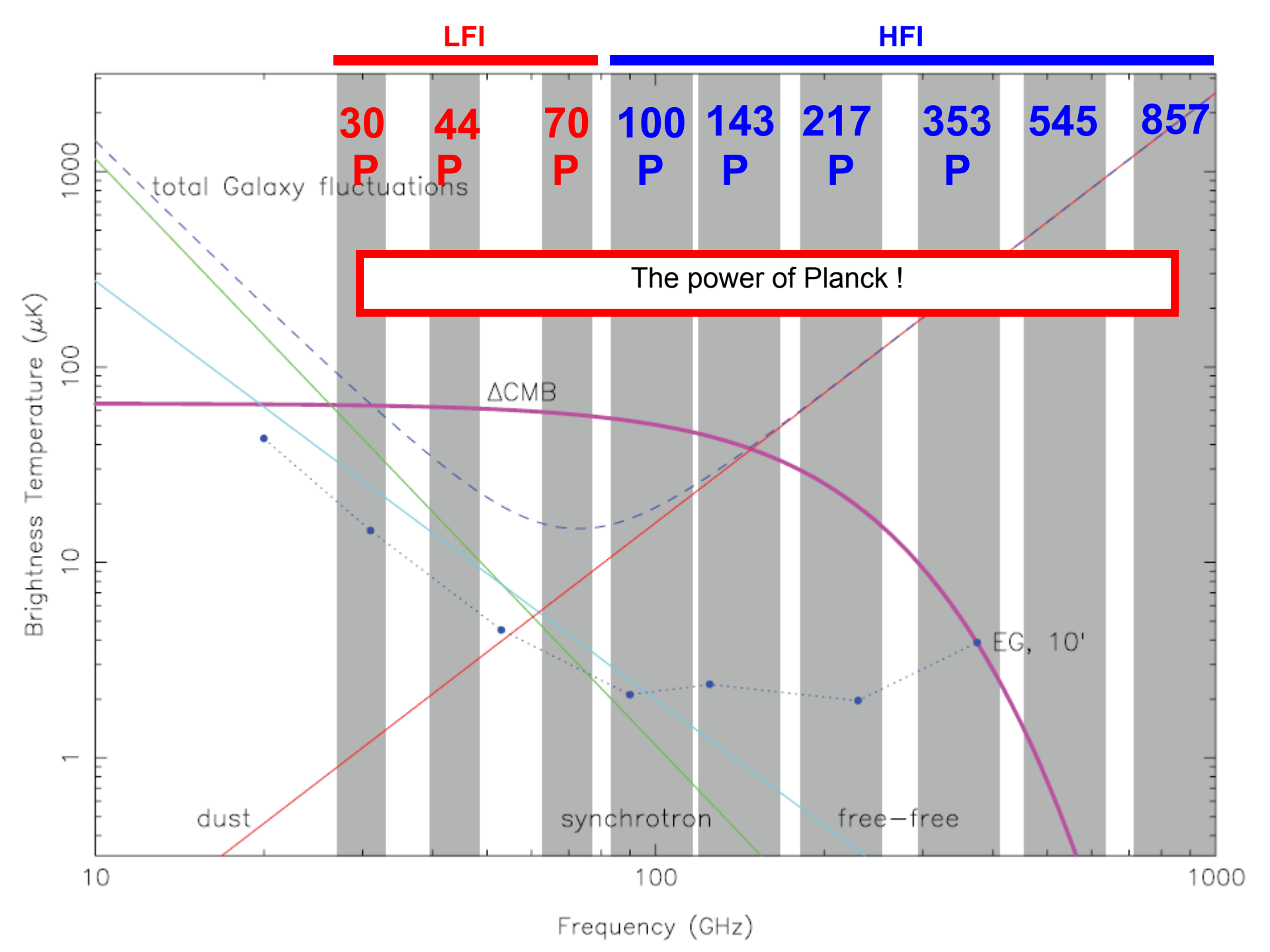
LFI
HFI
30
P
44
P
70
P
100
P
143
P
217
P
353
P
545
857
total Galaxy fluctuations
The power of Planck !
ΔCMB
EG, 10'
dust
synchrotron
free−free
Brightness Temperature (μK)
1000
100
10
1
10
100
1000
Frequency (GHz)

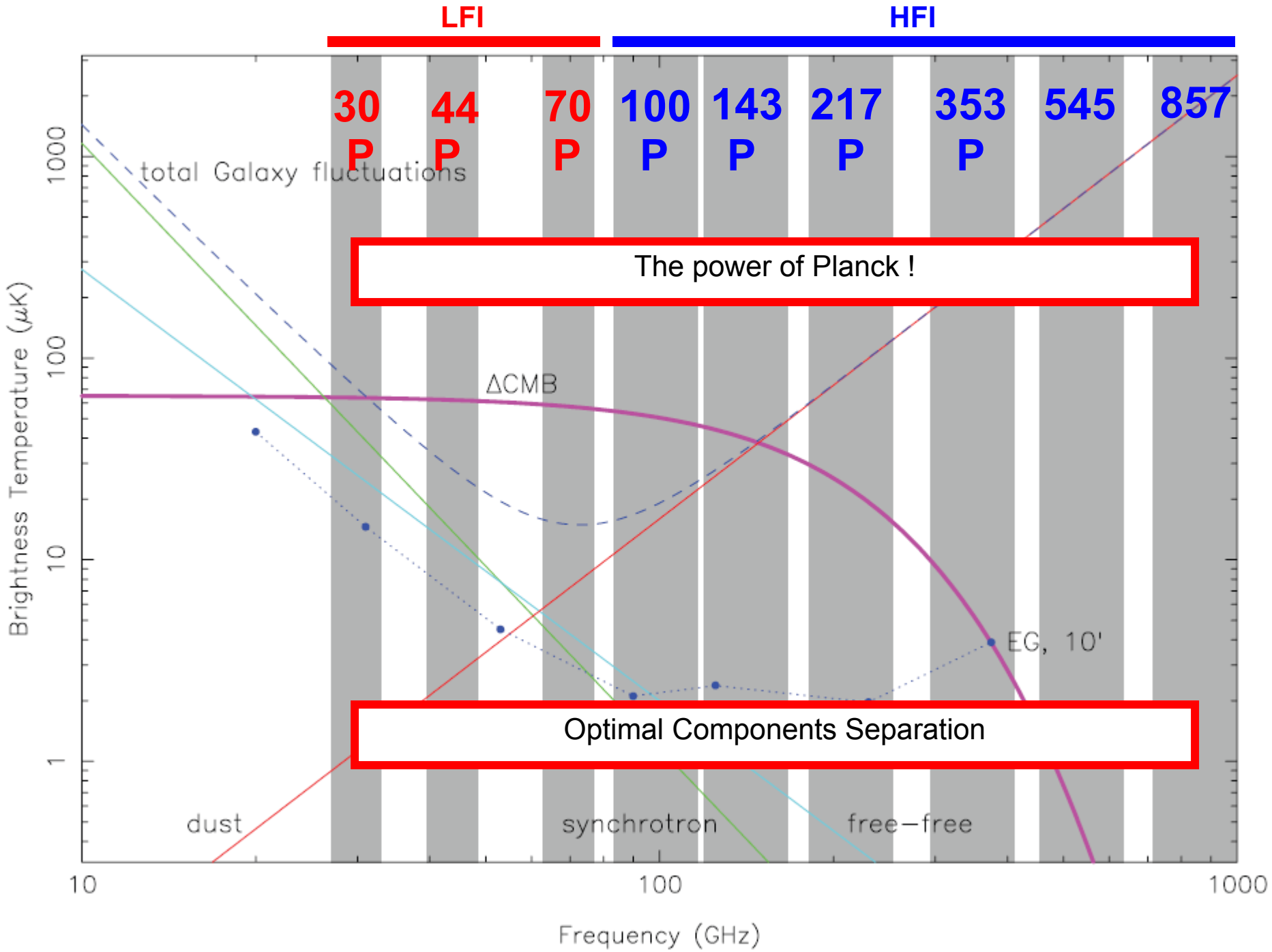
LFI
HFI
30
P
44
P
70
P
100
P
143
P
217
P
353
P
545
857
total Galaxy fluctuations
The power of Planck !
ΔCMB
EG, 10'
Optimal Components Separation
dust
synchrotron
free−free
Brightness Temperature (μK)
1000
100
10
1
10
100
1000
Frequency (GHz)

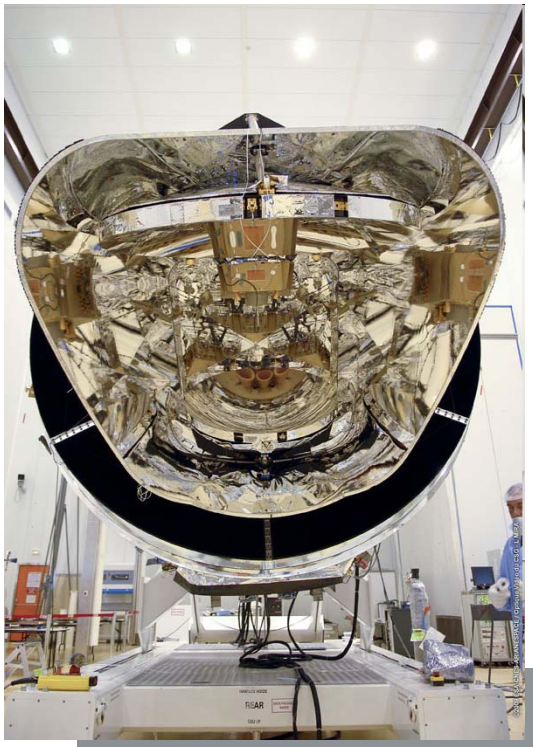

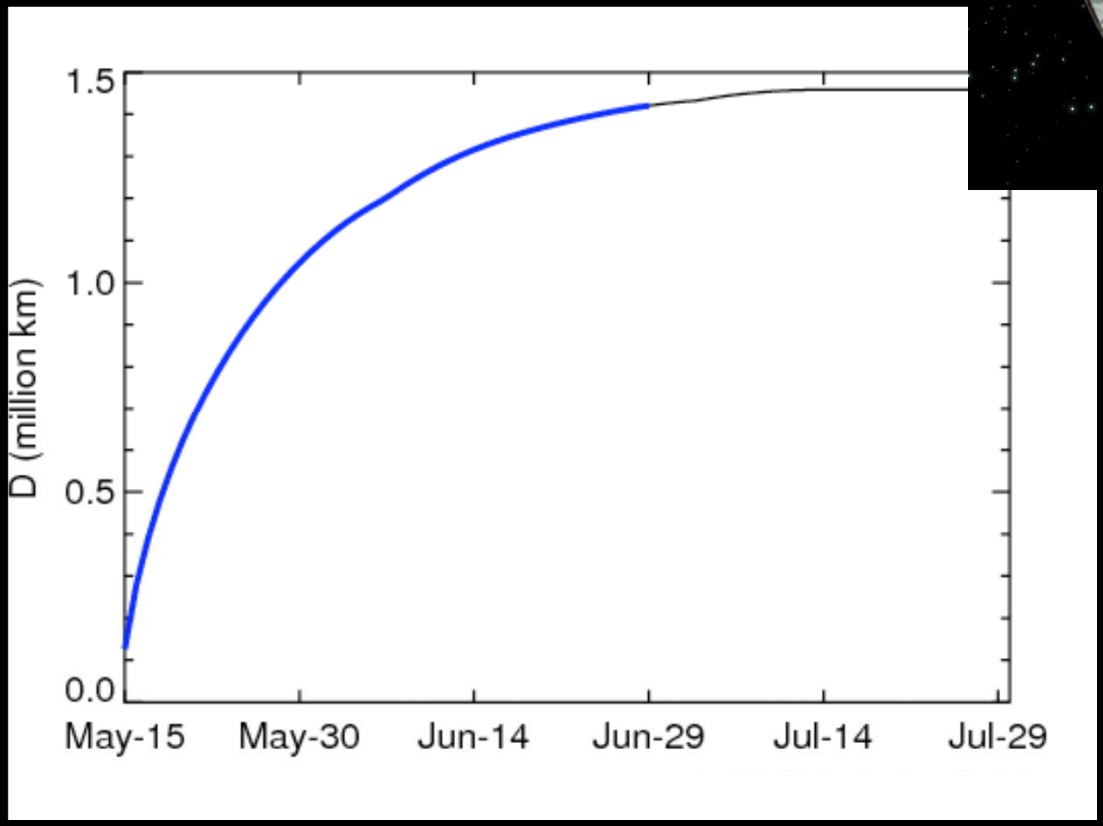
1.5
1.0
0.5
0.0
D (million km)
May-15
May-30
Jun-14
Jun-29
Jul-14
Jul-29

Thermal performance :
Planck collaboration: astro-ph/1101:2023

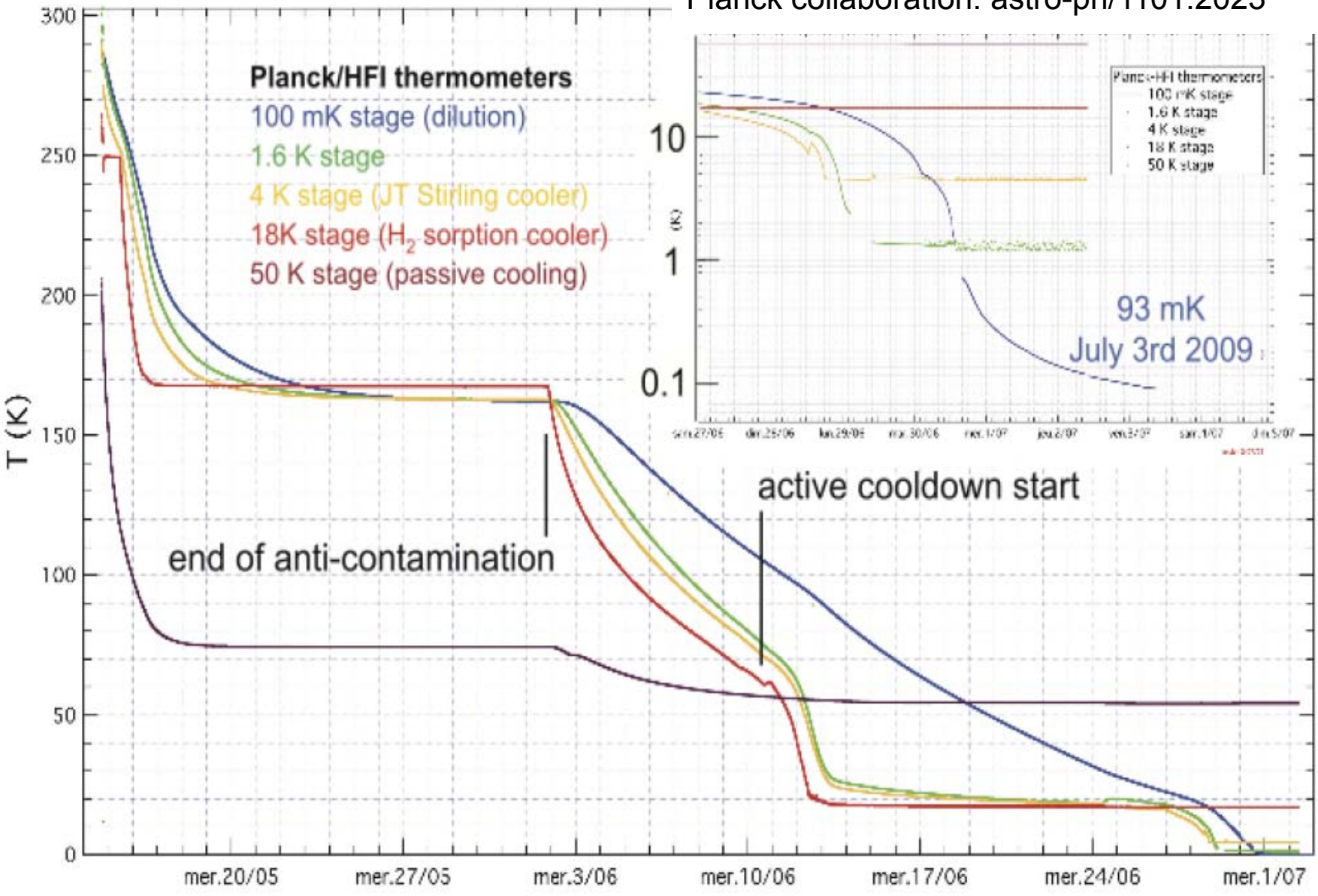

Mission :
Planck collaboration: astro-ph/1101:2022

Table 1. *Planck* coverage statistics.

	30 GHz	100 GHz	545 GHz	
Mean[a]	2293	4575	2278	sec deg^2
Minimum	440	801	375	sec deg^2
< half Mean[b]	14.4	14.6	15.2	%
> 4× Mean[c]	1.6	1.5	1.2	%
> 9× Mean[d]	0.41	0.42	0.41	%

[a] Mean over the whole sky of the integration time cumulated for all detectors (definition as in Table 3) in a given frequency channel.

[b] Fraction of the sky whose coverage is less than half the Mean.

[c] Fraction of the sky whose coverage is larger than four times the Mean.

[d] Fraction of the sky whose coverage is larger than nine times the Mean.

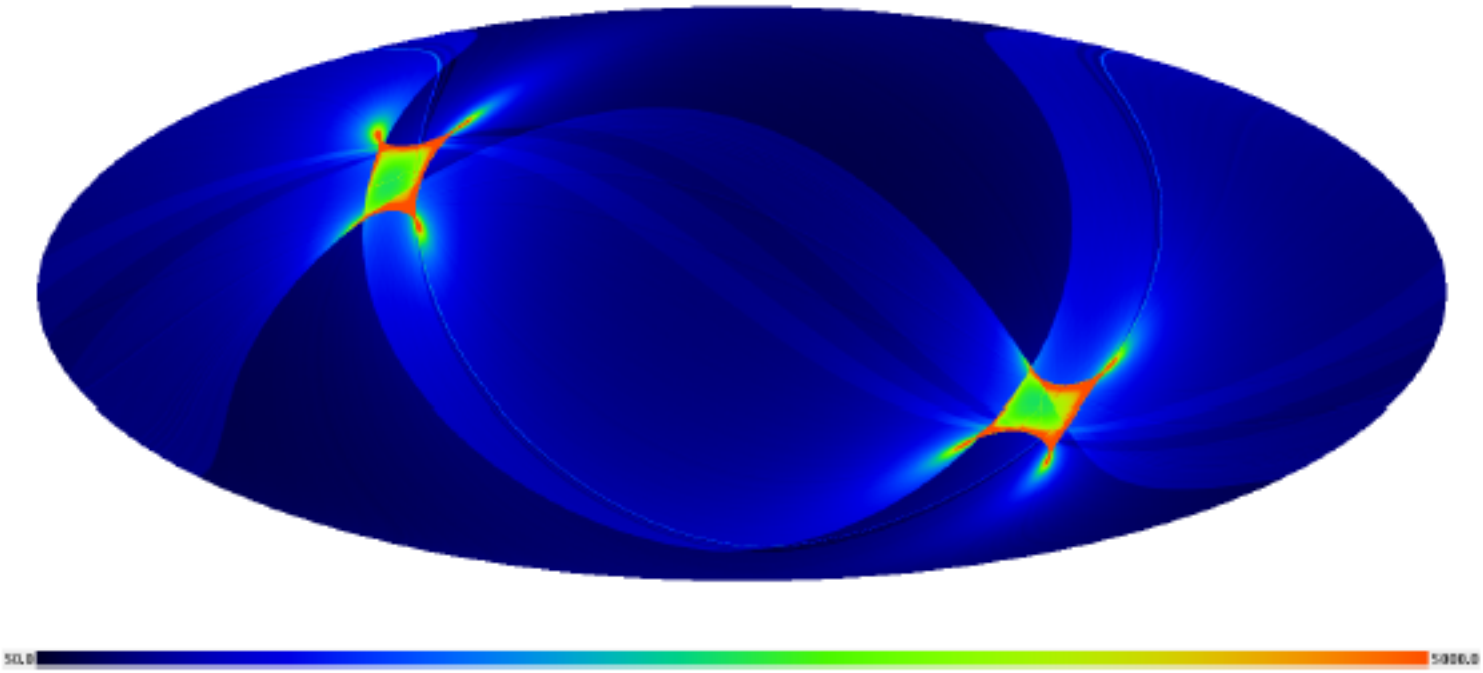

A very **stable** environment

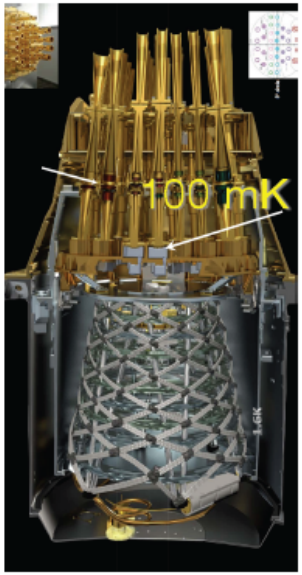

Cryostat:
dilution He3/He4

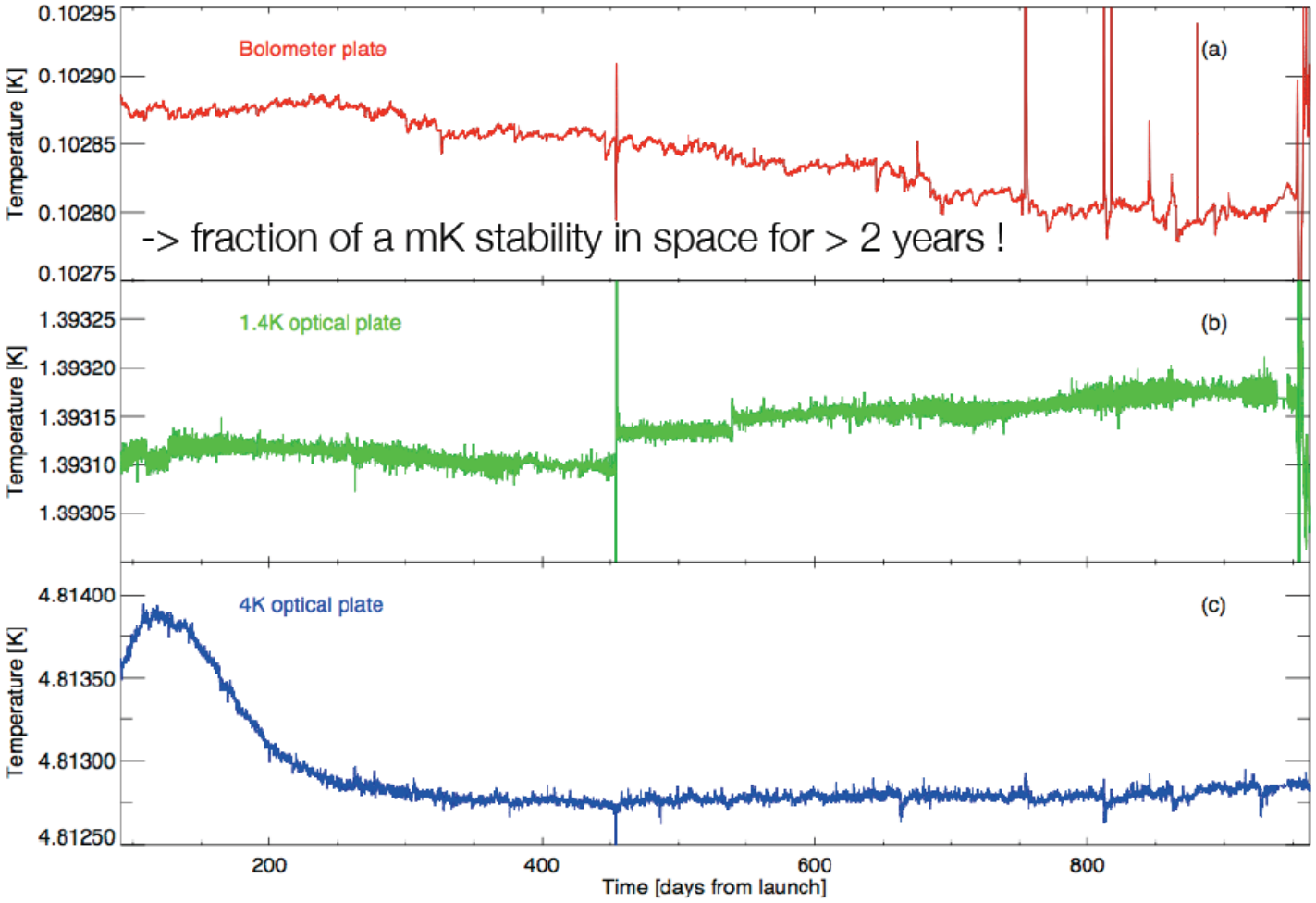

Fig. 7. The impressive stability of the HFI thermal stages during operations. Shown is the temperature evolution of the bolometer stage (*top*), the 1.6 K optical filter stage (*middle*) and the 4-K cooler reference load stage (*bottom*). The horizontal axis displays days since the beginning of the nominal mission.

Raw HFI data

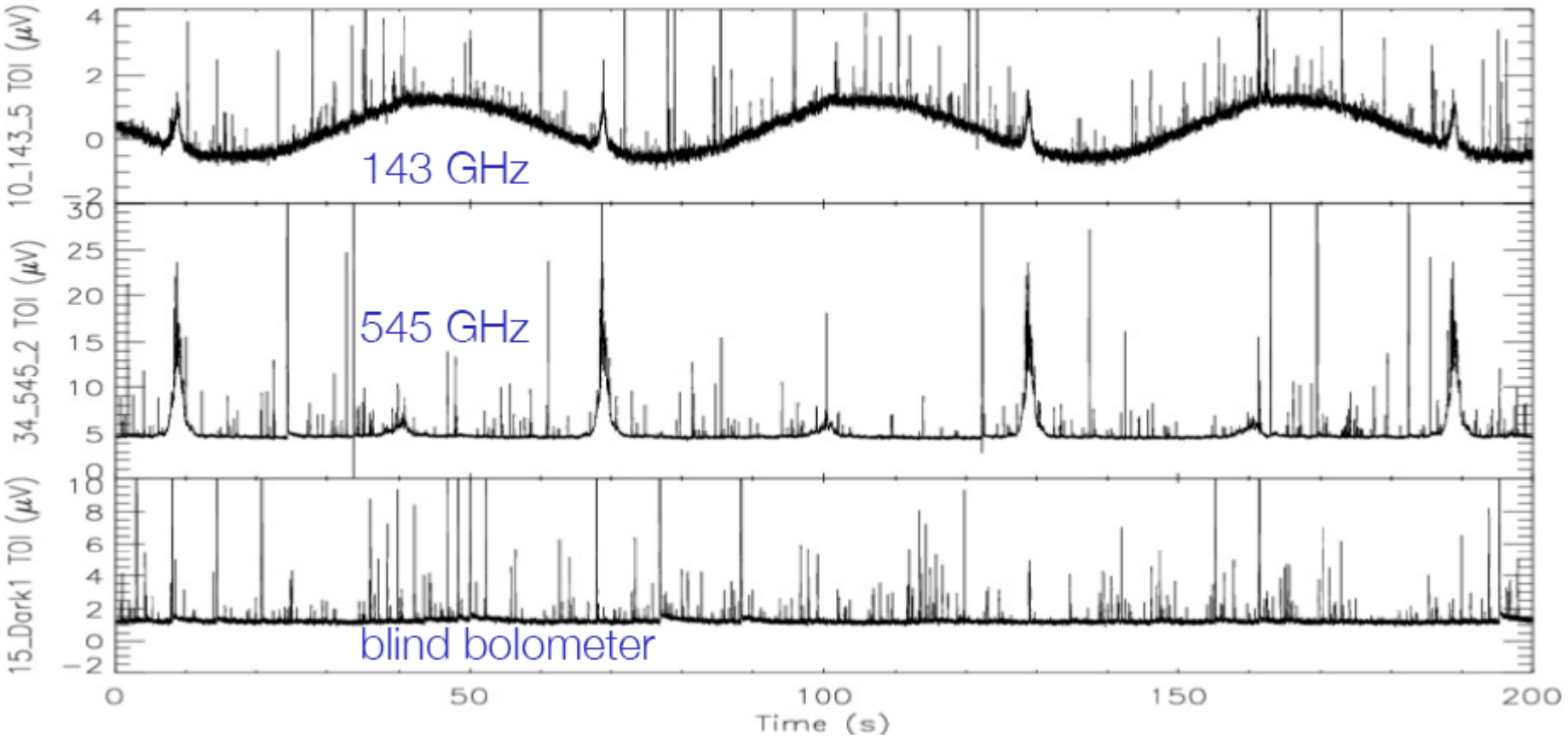
10_143_5 TOI (μV)
34_545_2 TOI (μV)
15_Dark1 TOI (μV)
143 GHz
545 GHz
blind bolometer
Time (s)
0
50
100
150
200

De-spiked HFI data

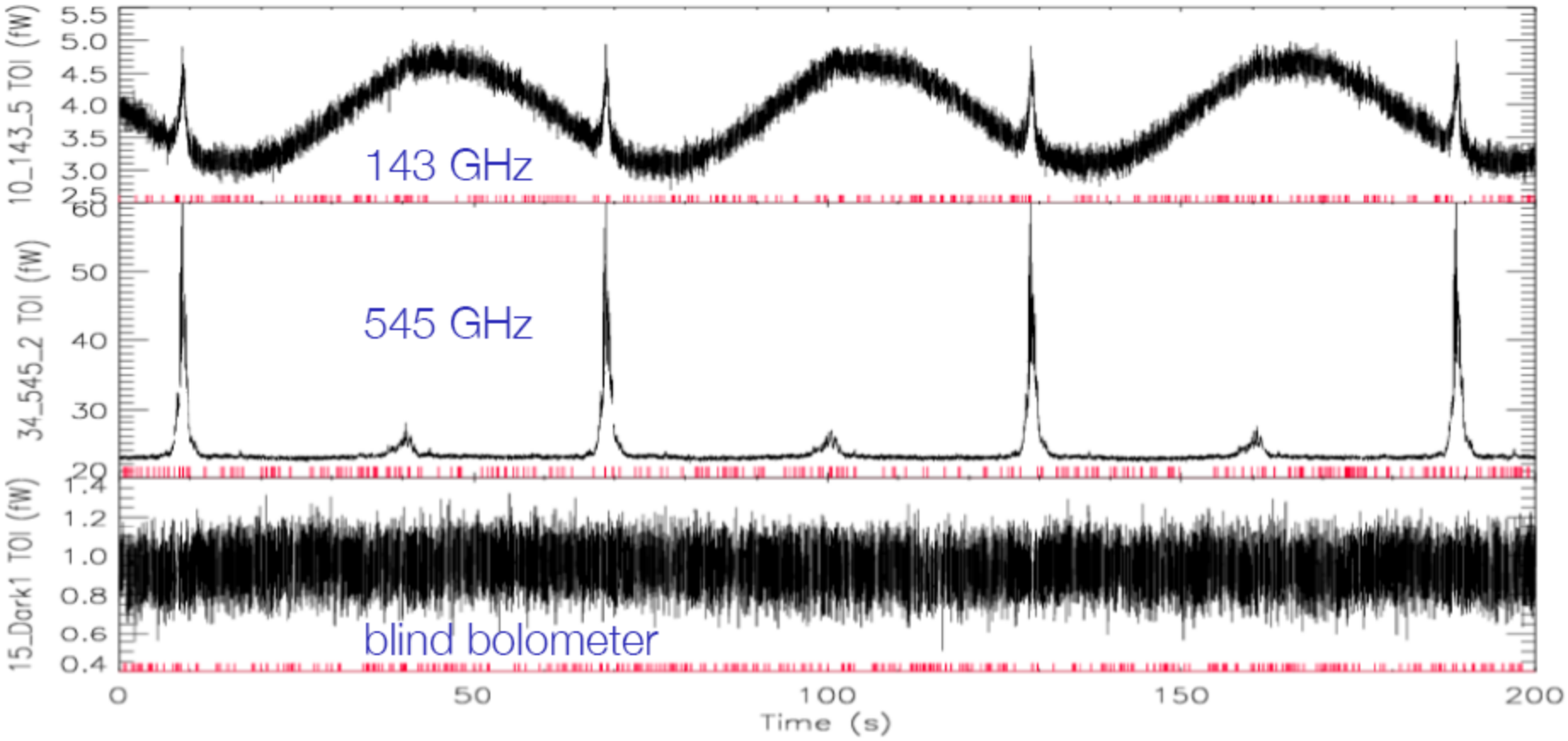

<20% of data flagged

2011 data release

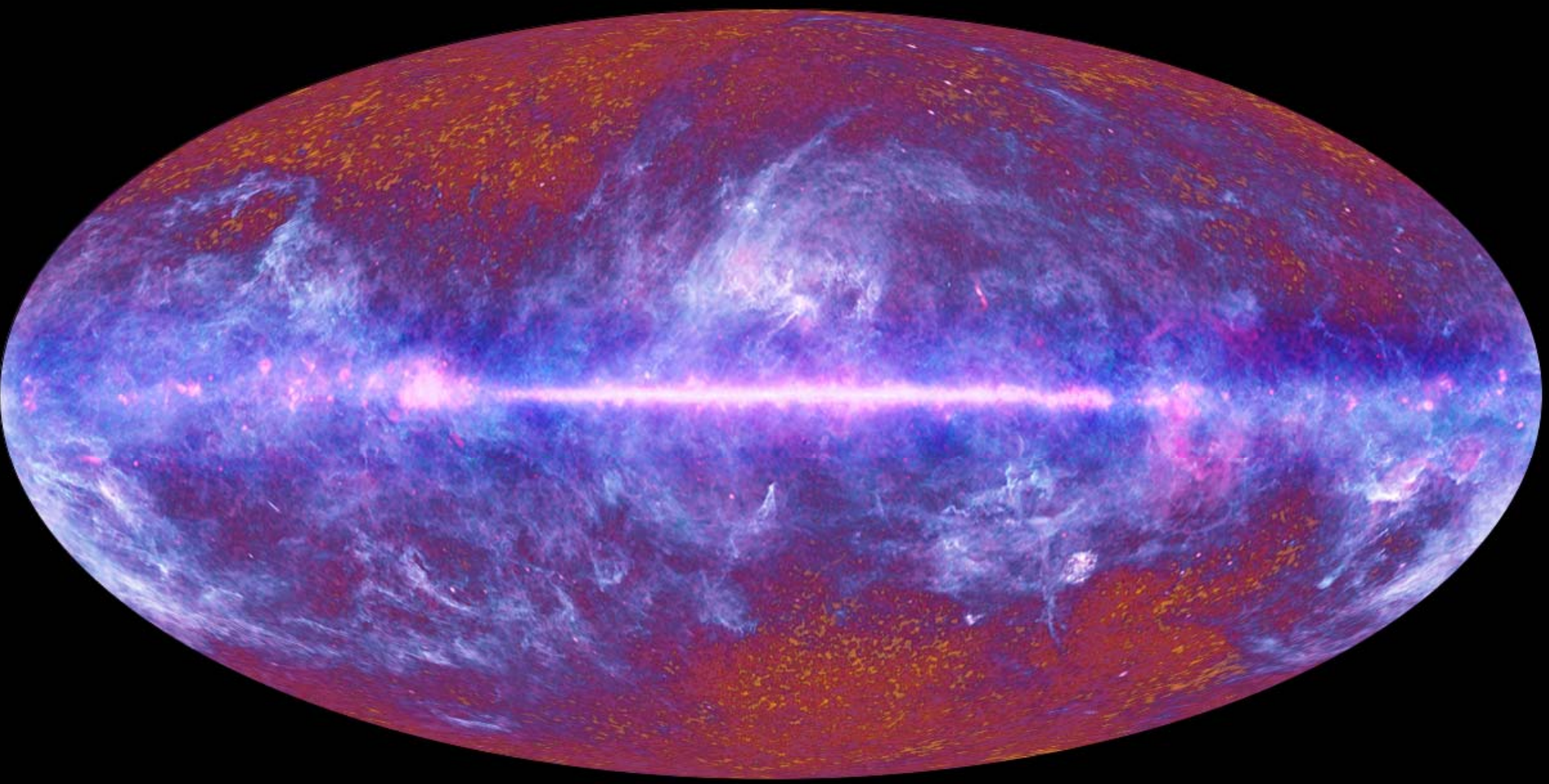

Planck one-year all-sky survey

esa

The 2013 Planck results

- Planck 2013 results. I. Overview of products and results
- Planck 2013 results. II. Low Frequency Instrument data processing
- Planck 2013 results. III. LFI systematic uncertainties
- Planck 2013 results. IV. LFI beams
- Planck 2013 results. V. LFI calibration
- Planck 2013 results. VI. High Frequency Instrument data processing
- Planck 2013 results. VII. HFI time response and beams
- Planck 2013 results. VIII. HFI calibration and mapmaking
- Planck 2013 results. IX. HFI spectral response
- Planck 2013 results. X. HFI energetic particle effects
- Planck 2013 results. XI. Consistency of the data
- Planck 2013 results. XII. Component separation
- Planck 2013 results. XIII. Galactic CO emission
- Planck 2013 results. XIV. Zodiacal emission
- Planck 2013 results. XV. CMB power spectra and likelihood
- Planck 2013 results. XVI. Cosmological parameters
- Planck 2013 results. XVII. Gravitational lensing by large-scale structure
- Planck 2013 results. XVIII. The gravitational lensing-infrared background correlation
- Planck 2013 results. XIX. The integrated Sachs-Wolfe effect
- Planck 2013 results. XX. Cosmology from Sunyaev- Zeldovich cluster counts
- Planck 2013 results. XXI. All-sky Compton-parameter map and characterization
- Planck 2013 results. XXII. Constraints on inflation
- Planck 2013 results. XXIII. Isotropy and statistics of the CMB
- Planck 2013 results. XXIV. Constraints on primordial non-Gaussianity
- Planck 2013 results. XXV. Searches for cosmic strings and other topological defects
- Planck 2013 results. XXVI. Background geometry and topology of the Universe
- Planck 2013 results. XXVII. Special relativistic effects on the CMB dipole
- Planck 2013 results. XXVIII. The Planck Catalogue of Compact Sources
- Planck 2013 results. XXIX. The Planck catalogue of Sunyaev-Zeldovich sources
- Planck 2013 results. Explanatory supplement

29 papers (+1 to come on CIB);
800+ pages
1 Explanatory Supplement
all products available online

The 2013 Planck results

- Planck 2013 results. I. Overview of products and results
- Planck 2013 results. II. Low Frequency Instrument data processing
- Planck 2013 results. III. LFI systematic uncertainties
- Planck 2013 results. IV. LFI beams
- Planck 2013 results. V. LFI calibration
- Planck 2013 results. VI. High Frequency Instrument data processing
- Planck 2013 results. VII. HFI time response and beams
- Planck 2013 results. VIII. HFI calibration and mapmaking
- Planck 2013 results. IX. HFI spectral response
- Planck 2013 results. X. HFI energetic particle effects
- Planck 2013 results. XI. Consistency of the data

Instruments, processing, systematic effects

- Planck 2013 results. XII. Component separation
- Planck 2013 results. XIII. Galactic CO emission
- Planck 2013 results. XIV. Zodiacal emission

Components separation

- Planck 2013 results. XV. CMB power spectra and likelihood
- Planck 2013 results. XVI. Cosmological parameters

Power Spectra, cosmological parameters

- Planck 2013 results. XVII. Gravitational lensing by large-scale structure
- Planck 2013 results. XVIII. The gravitational lensing-infrared background correlation
- Planck 2013 results. XIX. The integrated Sachs-Wolfe effect

Photon propagation effects

- Planck 2013 results. XX. Cosmology from Sunyaev- Zeldovich cluster counts
- Planck 2013 results. XXI. All-sky Compton-parameter map and characterization

The Sunyaev-Zeldovich effect

- Planck 2013 results. XXII. Constraints on inflation
- Planck 2013 results. XXIII. Isotropy and statistics of the CMB
- Planck 2013 results. XXIV. Constraints on primordial non-Gaussianity
- Planck 2013 results. XXV. Searches for cosmic strings and other topological defects
- Planck 2013 results. XXVI. Background geometry and topology of the Universe
- Planck 2013 results. XXVII. Special relativistic effects on the CMB dipole

Constraints on cosmology

- Planck 2013 results. XXVIII. The Planck Catalogue of Compact Sources
- Planck 2013 results. XXIX. The Planck catalogue of Sunyaev-Zeldovich sources
- Planck 2013 results. Explanatory supplement

Products

29 papers (+1 to come on CIB);
800+ pages
1 Explanatory Supplement
all products available online

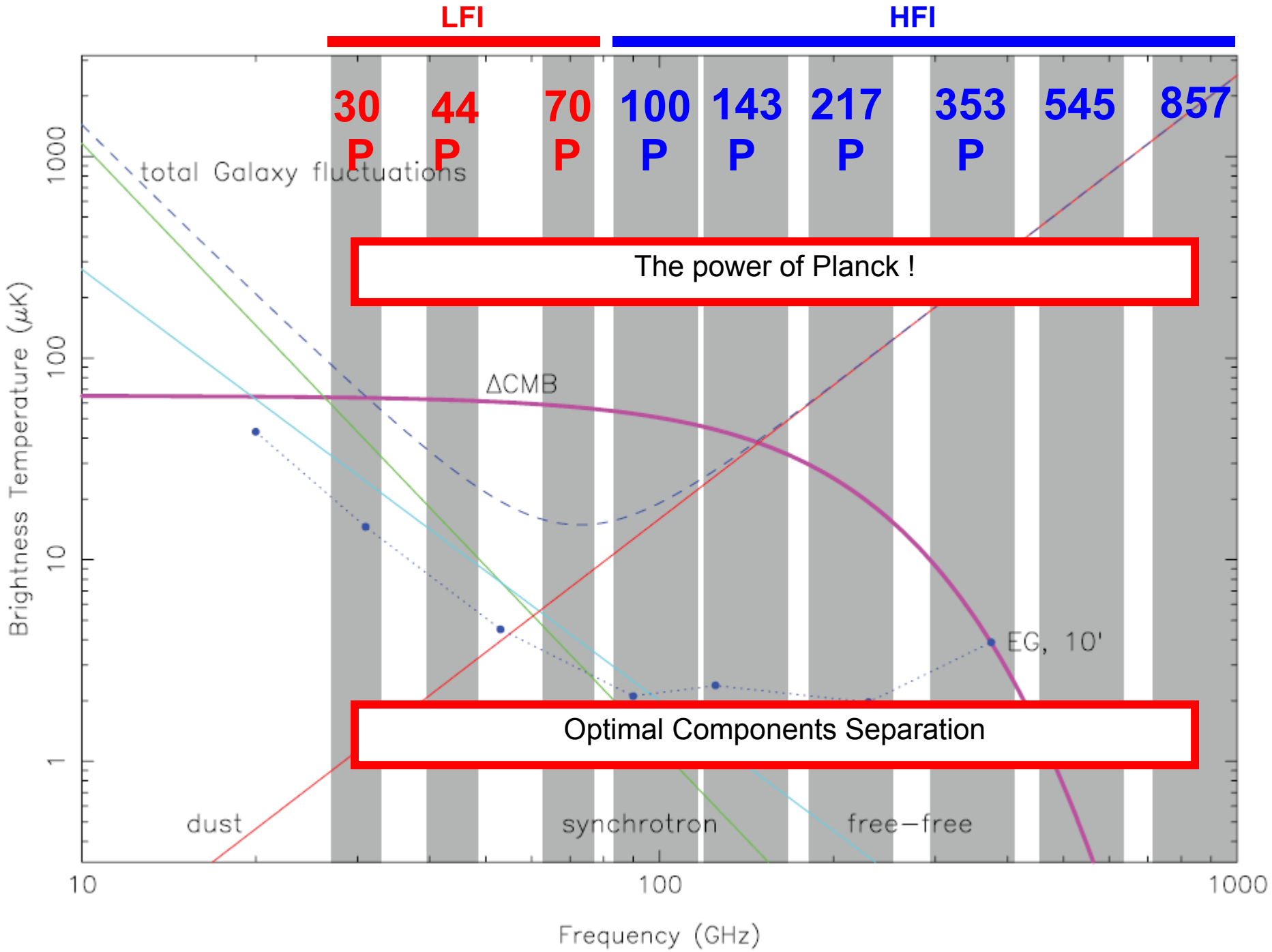
LFI
HFI
30
P
44
P
70
P
100
P
143
P
217
P
353
P
545
857
total Galaxy fluctuations
The power of Planck !
ΔCMB
EG, 10'
Optimal Components Separation
dust
synchrotron
free−free
Brightness Temperature (μK)
1000
100
10
1
10
100
1000
Frequency (GHz)

Planck Legacy Maps

$6x10^6$ pixels (5')

857 GHz

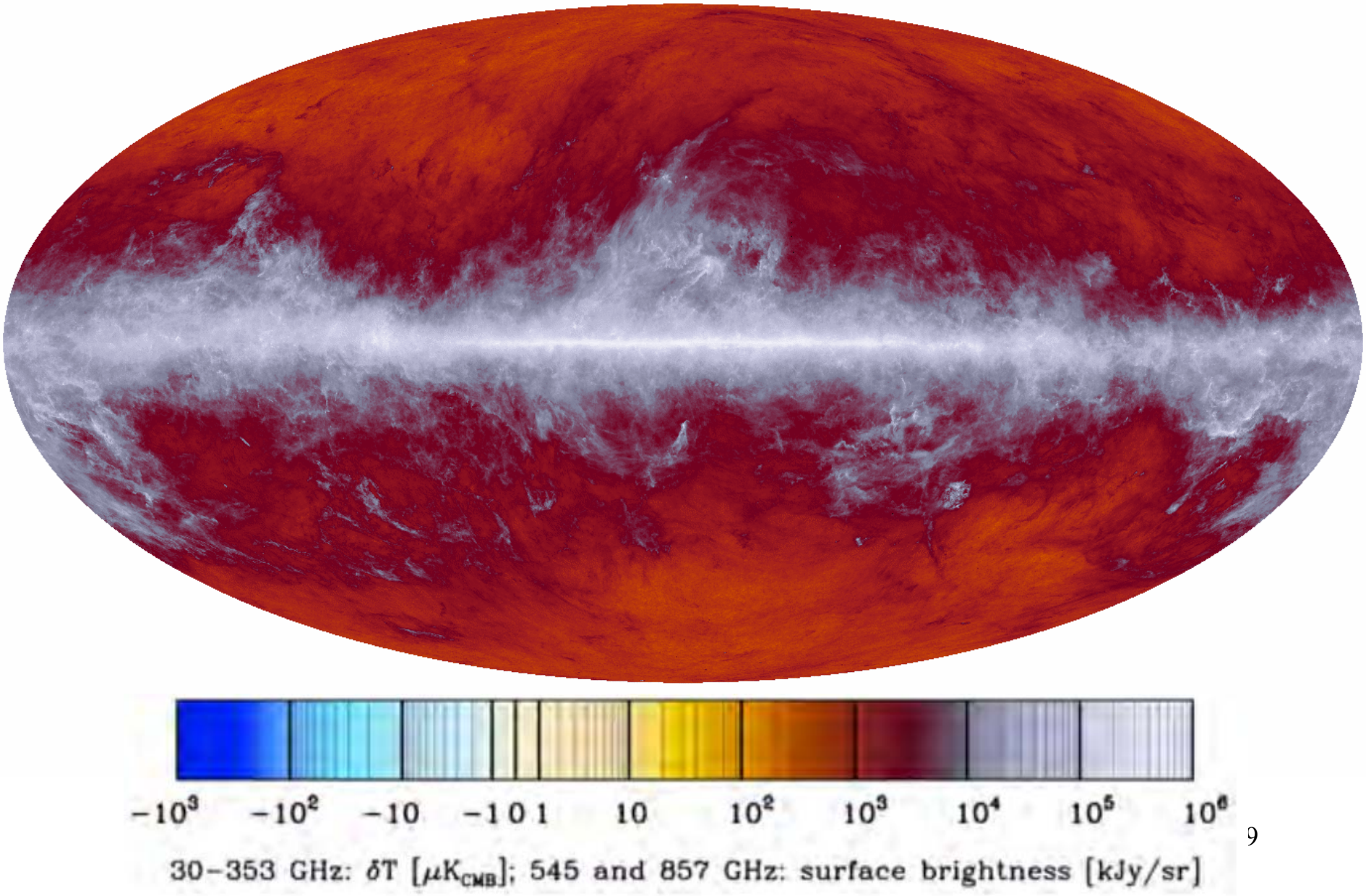

components separation

$$\underbrace{\Delta T(\nu_j,\ell,b)}_{\text{Measured maps}} = \sum_k a_k(\nu_j,\ell,b)\underbrace{C_k(\ell,b)}_{\text{physical components}}$$

k = CMB,dust,synchrotron,…

j = 33, 44, 70 100, 143, 217, 353, 545, 857 GHz

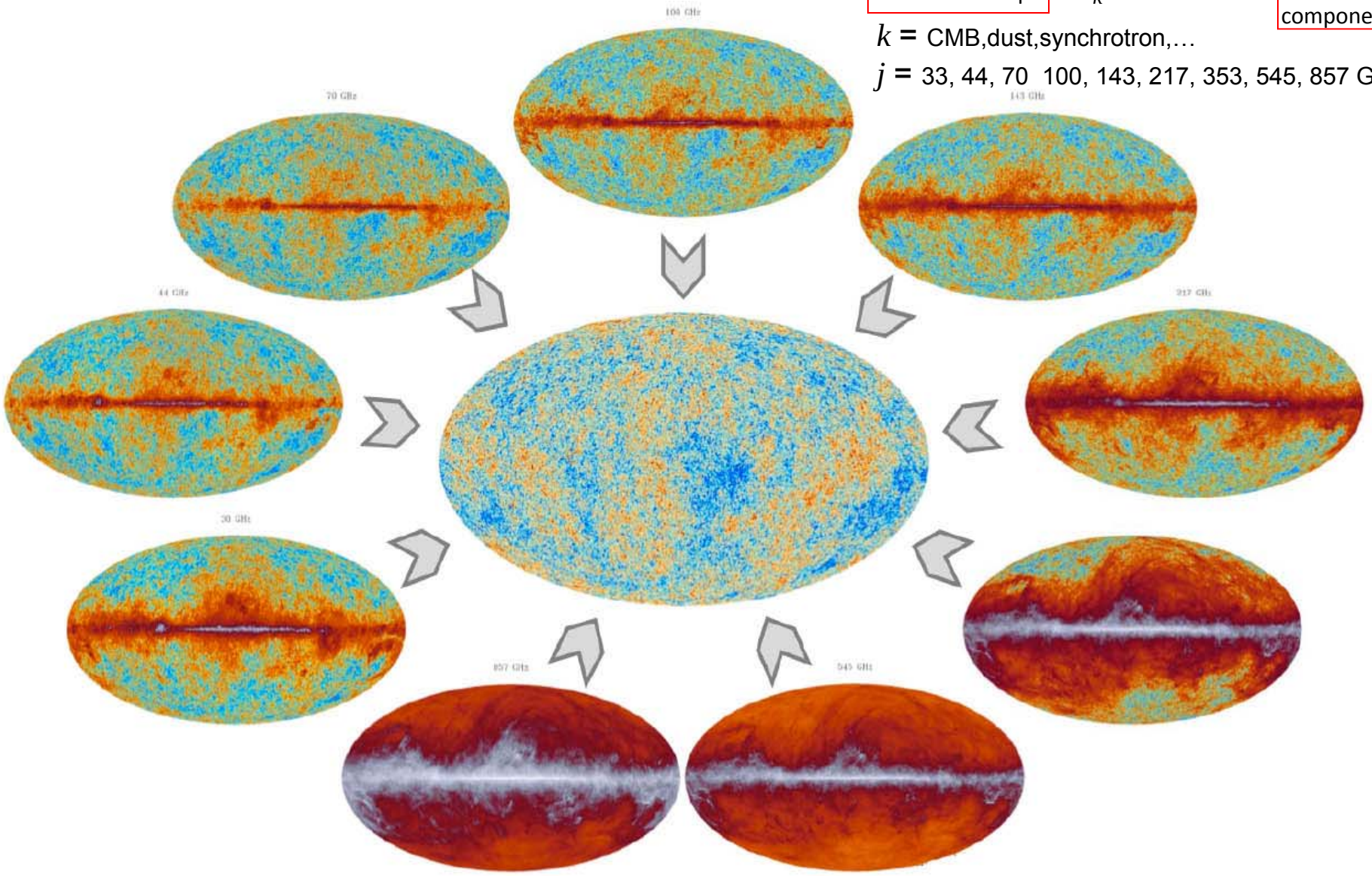

The CMB component

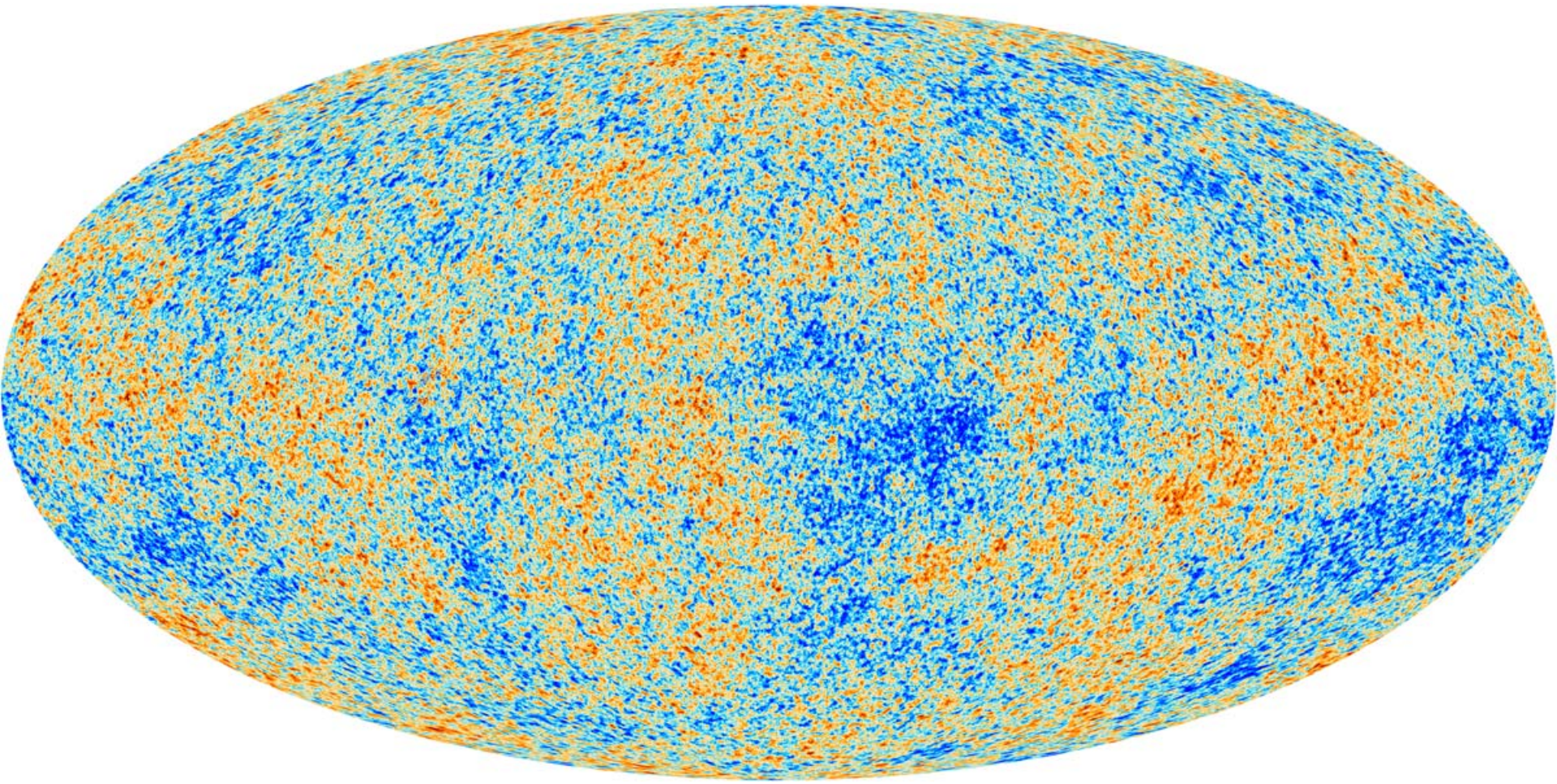

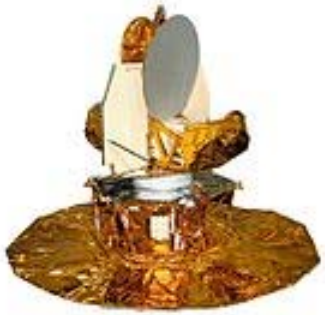

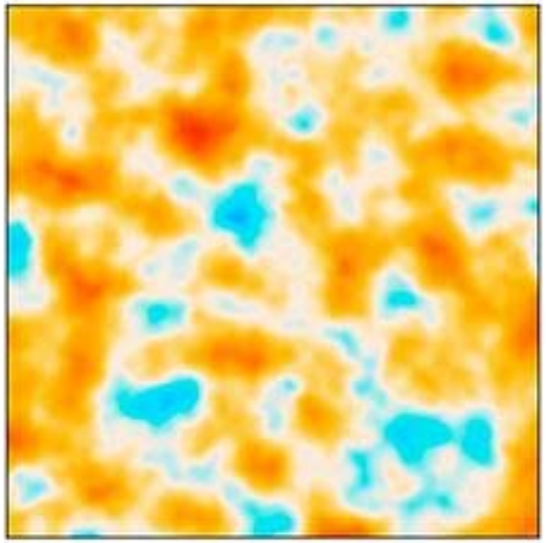

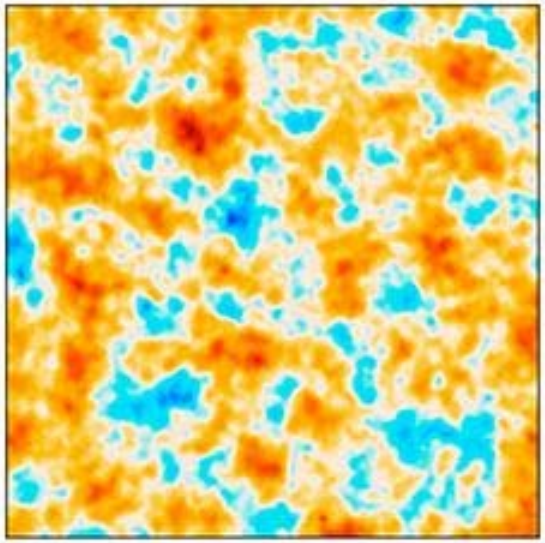

COBE

WMAP

Planck

Best angular resolution
Best control of foregorunds

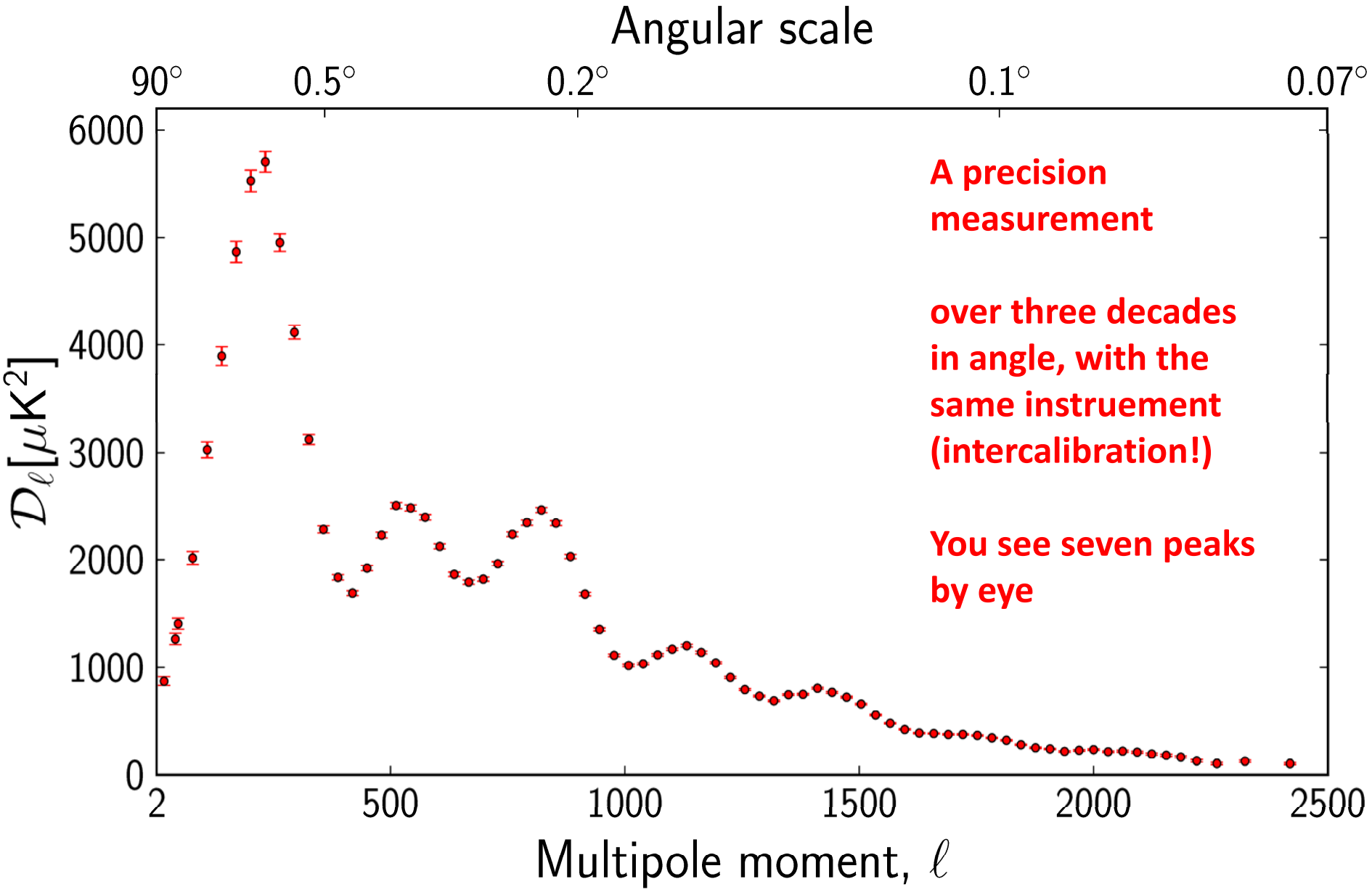
Angular scale
90°
0.5°
0.2°
0.1°
0.07°
6000
5000
4000
3000
2000
1000
0
$\mathcal{D}_\ell [\mu K^2]$
2
500
1000
1500
2000
2500
Multipole moment, ℓ
A precision measurement
over three decades in angle, with the same instruement (intercalibration!)
You see seven peaks by eye

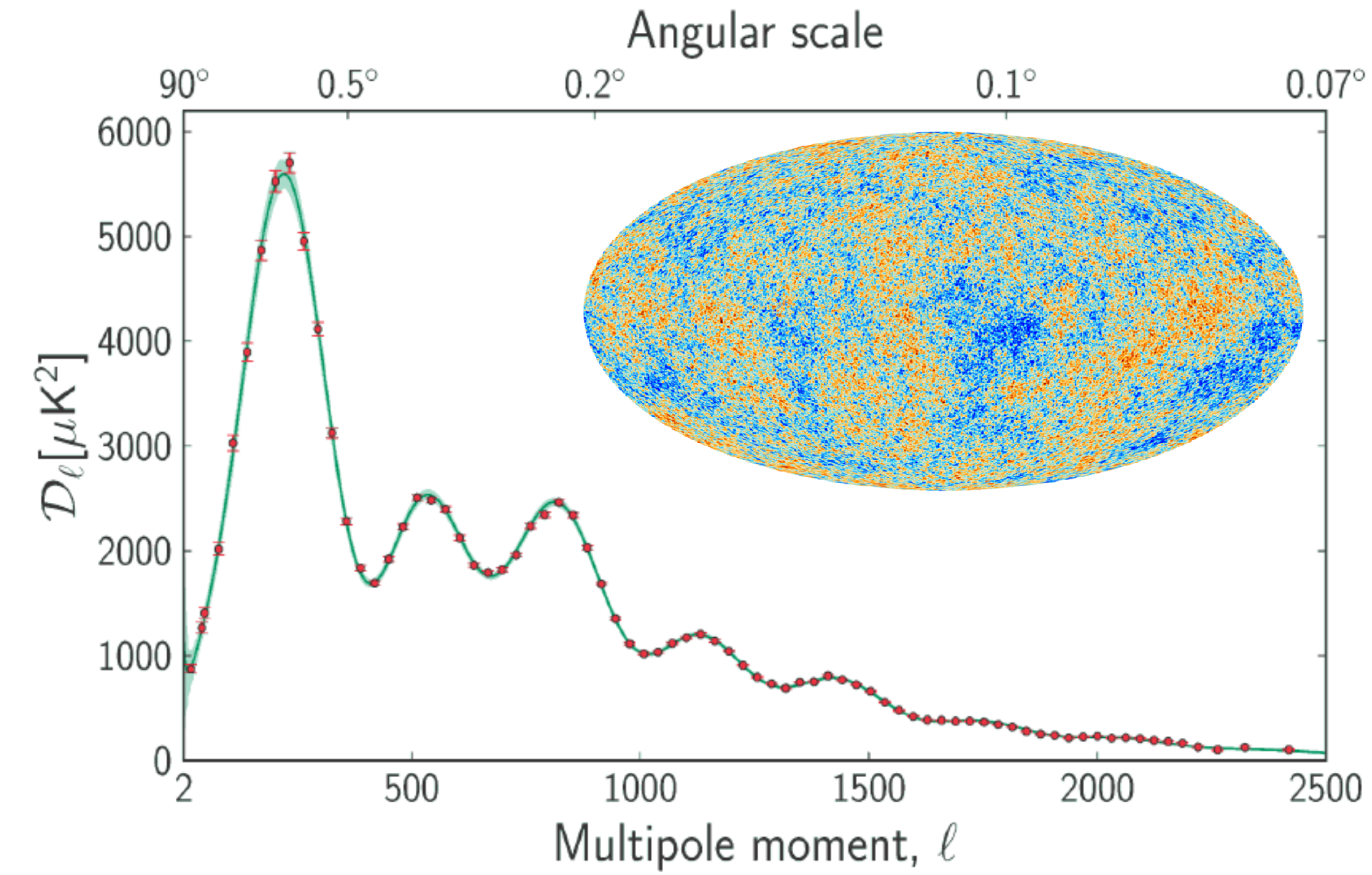

Planck 2013 CMB anisotropy map and angular power spectrum data (red dots with error bars) The green line is the best fit to a 6-parameters model (inflationary Λ-CDM)

CMB polarization (E)

- CMB photons are last scattered at recombination.
- It's a Thomson scattering, and any quadrupole anisotropy in the incoming photons produces a degree of linear polarization in the scattered photons.
- Density perturbation produce a small degree of linear polarization (E-modes)

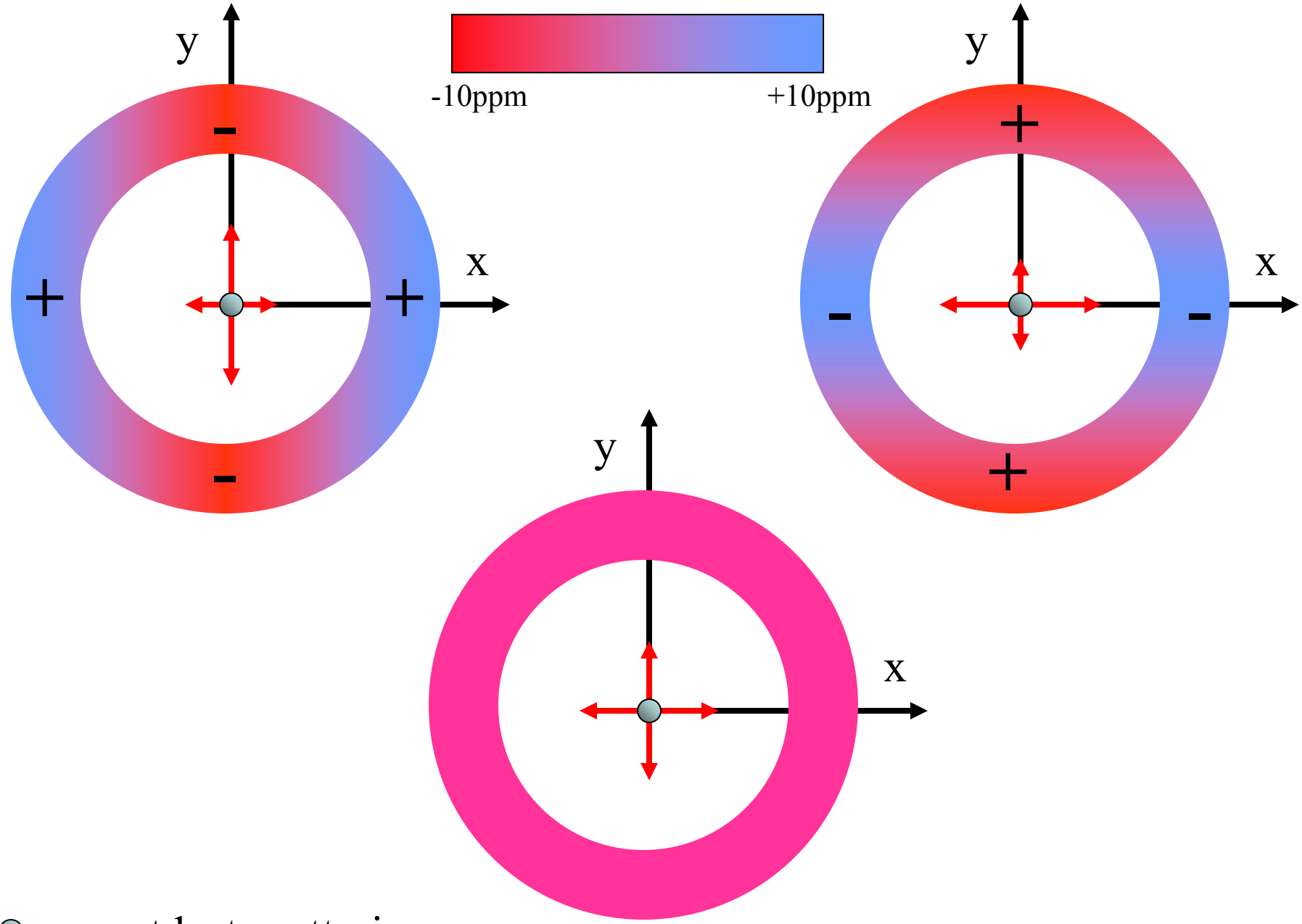
y
x
-10ppm
+10ppm
y
x
y
x
= e- at last scattering

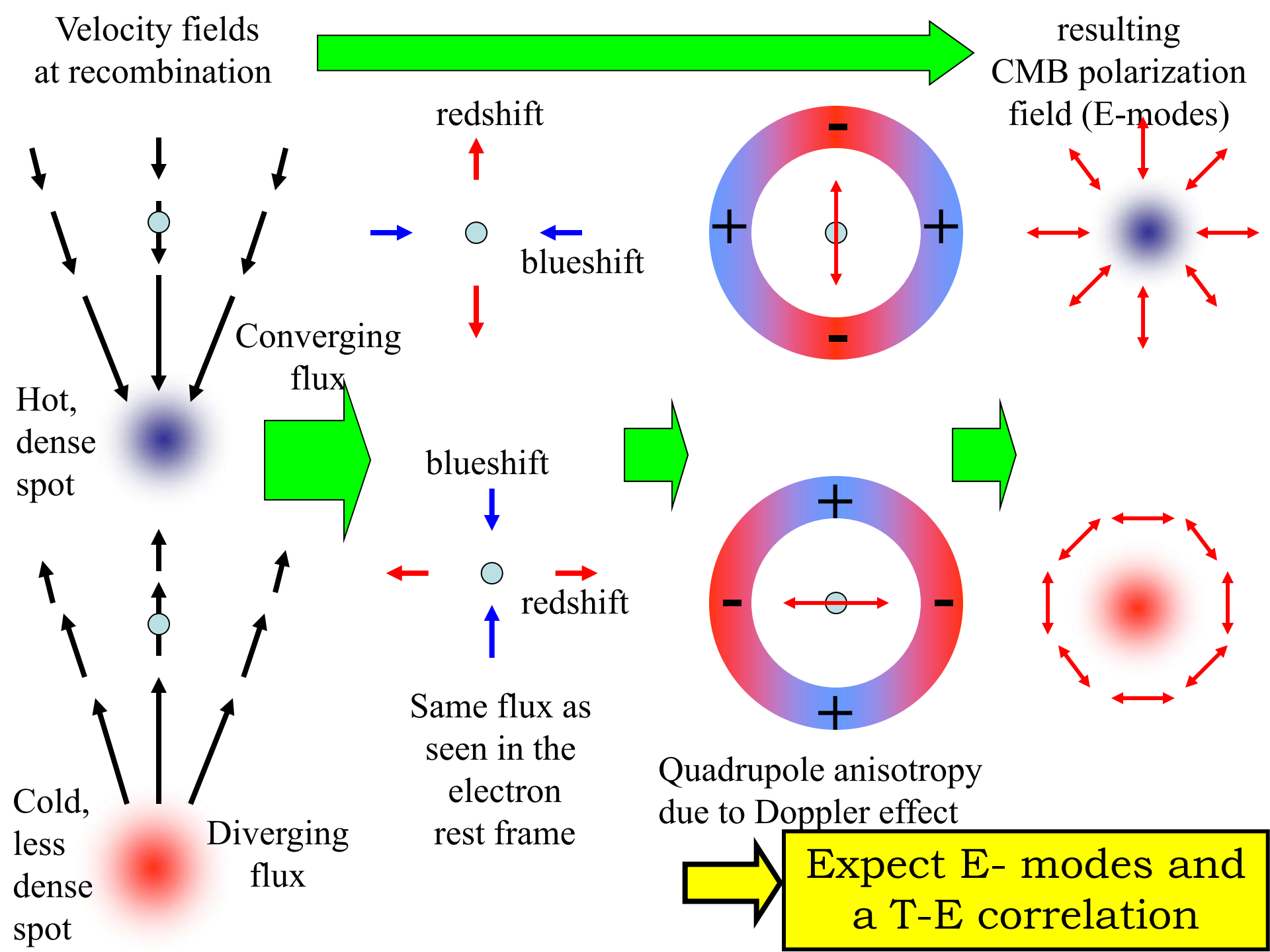
Velocity fields at recombination
resulting CMB polarization field (E-modes)
redshift
blueshift
Converging flux
Hot, dense spot
blueshift
redshift
Same flux as seen in the electron rest frame
Quadrupole anisotropy due to Doppler effect
Cold, less dense spot
Diverging flux
Expect E- modes and a T-E correlation

- E-modes are irrotational
- E modes are related to velocities, while T is related mainly to density
- We expect a power spectrum of the E-modes, <EE>, with maxima and mimina in quadrature with the anisotropy power spectrum <TT>.

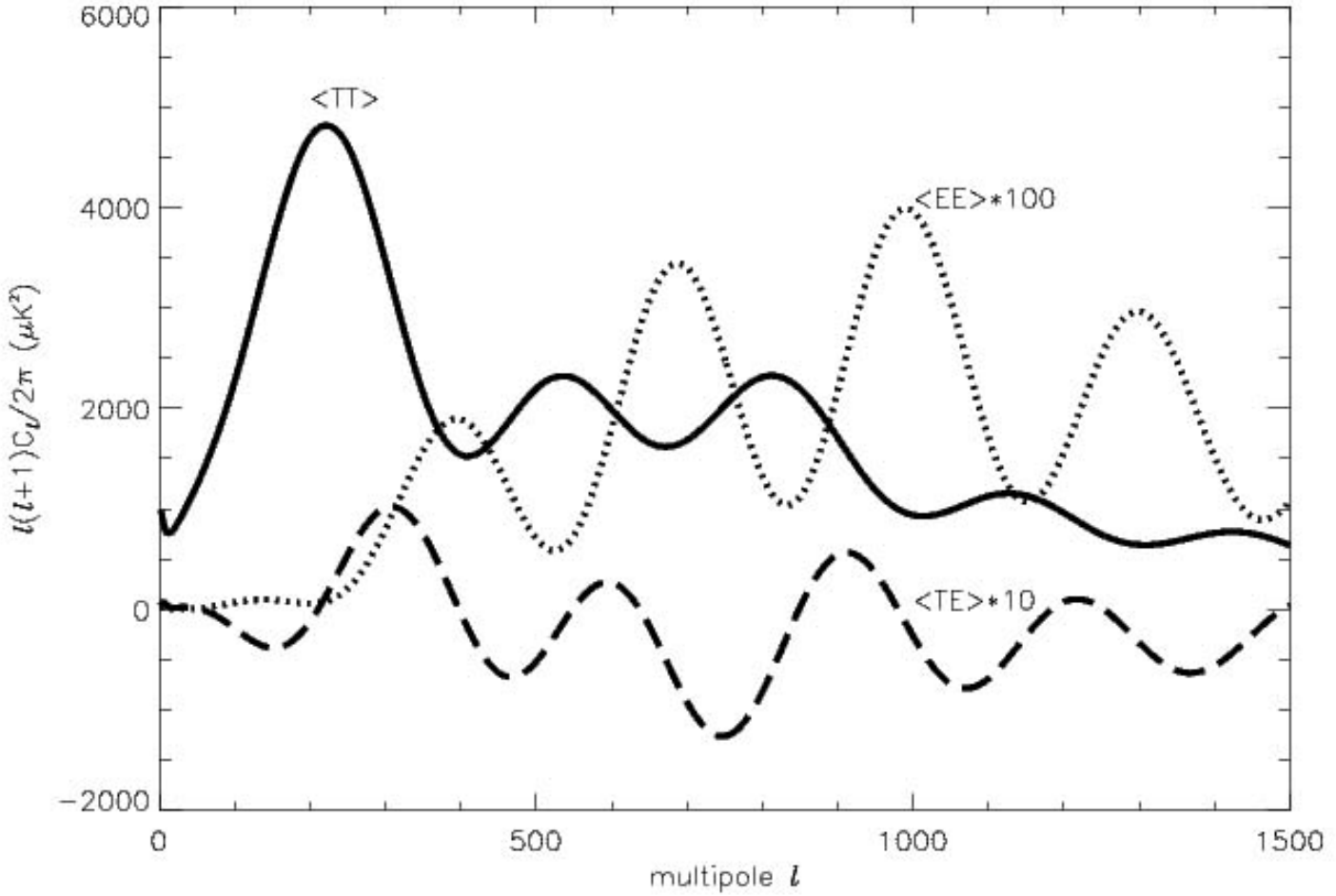

Figure 1.7: Estimated power spectra for the cosmological parameters: $\Omega_b = 0.05$, $\Omega_{cdm} = 0.3$, $\Omega_\Lambda = 0.65$, $\Omega_\nu = 0$, $H_0 = 65$ km/s/Mpc, $\tau = 0.17$. The temperature power spectrum, $\langle TT \rangle = C_\ell^T$, the E-modes power spectrum $\langle EE \rangle = C_\ell^E$ multiplied by a factor 100 to make it visible and the cross power spectrum between temperature and polarization, $\langle TE \rangle = C_\ell^{TE}$ multiplied by a factor 10. The spectra are computed using the publicly available code CMBFAST (http://www.cmbfast.org),

CMB polarization (B)

- CMB photons are last scattered at recombination.
- It's a Thomson scattering, and any quadrupole anisotropy in the incoming photons produces a degree of linear polarization in the scattered photons.
- Tensor perturbations (gravitational waves) produce a small degree of linear polarization with curl properties (B-modes)
- Also, lensing of E-modes does the same at smaller scales

If inflation really happened…

- It stretched geometry of space to nearly Euclidean
- It produced a nearly scale invariant spectrum of density fluctuations
- It produced a stochastic background of gravitational waves.

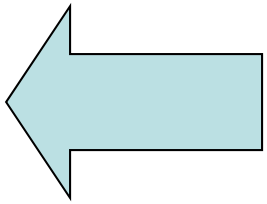

OK

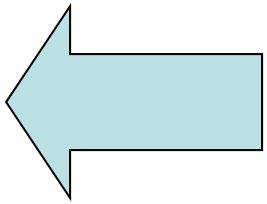

OK

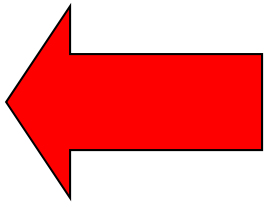

?

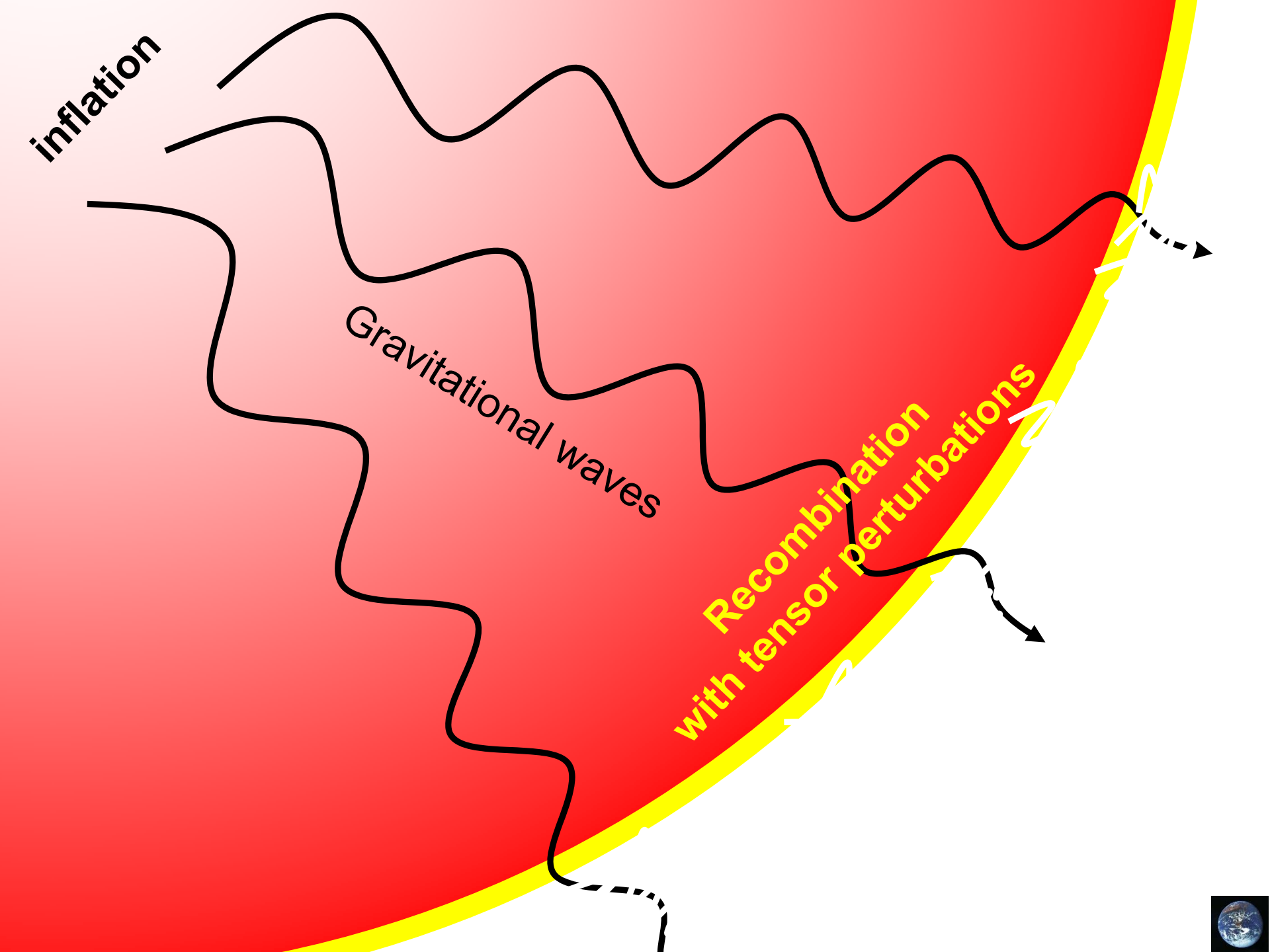
inflation
Gravitational waves
Recombination
with tensor perturbations

Quadrupole from P.G.W.

- If inflation really happened:
  - ✓ It stretched geometry of space to nearly Euclidean
  - ✓ It produced a nearly scale invariant spectrum of gaussian density fluctuations
  - ✓ It produced a stochastic background of gravitational waves: Primordial G.W. The background is so faint that even LISA will not be able to measure it.
- Tensor perturbations also produce quadrupole anisotropy. They generate irrotational (E-modes) **and rotational (B-modes) components** in the CMB polarization field.
- Since B-modes are not produced by scalar fluctuations, they represent a signature of inflation.

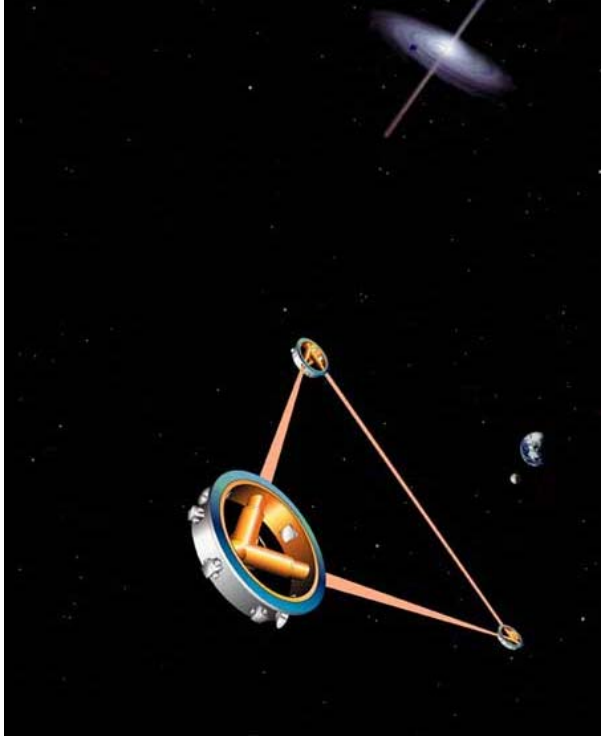

E-modes

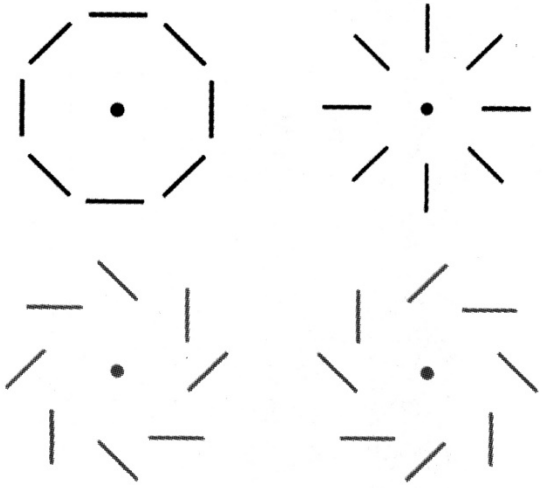

B-modes

B-modes from P.G.W.

- The amplitude of this effect is very small, but depends on the Energy scale of inflation. In fact the amplitude of tensor modes normalized to the scalar ones is:

$$\left(\frac{T}{S}\right)^{1/4} \equiv \left(\frac{C_2^{GW}}{C_2^{Scalar}}\right)^{1/4} \cong \frac{V^{1/4}}{3.7\times10^{16}\,\mathrm{GeV}}$$

Inflation potential

- and

$$\sqrt{\frac{\ell(\ell+1)}{2\pi}C^{B}_{\ell\,\max}} \cong 0.1\mu K\left[\frac{V^{1/4}}{2\times10^{16}\,\mathrm{GeV}}\right]$$

- There are theoretical arguments to expect that the energy scale of inflation is close to the scale of GUT i.e. around 10^{16} GeV.
- The current upper limit on anisotropy at large scales gives $T/S<0.11$ (at 2σ)
- A competing effect is lensing of E-modes, which is important at large multipoles.

E-modes & B-modes

Spin-2 quantity Spin-2 basis

$$(Q \pm iU)(\vec{n}) = \sum_{\ell,m} \left(a^{E}_{\ell m} \pm i a^{B}_{\ell m} \right) {}_{\pm 2}Y_{\ell m}(\vec{n})$$

- From the measurements of the Stokes Parameters ***Q*** and ***U*** of the linear polarization field we can recover both irrotational and rotational a_{lm} by means of modified Legendre transforms:

E-modes produced by scalar and tensor perturbations

$$a^{E}_{\ell m} = \frac{1}{2} \int d\Omega W(\vec{n}) \left[(Q + iU)(\vec{n}) {}_{+2}Y_{\ell m}(\vec{n}) + (Q - iU)(\vec{n}) {}_{-2}Y_{\ell m}(\vec{n}) \right]$$

B-modes produced **only** by tensor perturbations

$$a^{B}_{\ell m} = \frac{1}{2i} \int d\Omega W(\vec{n}) \left[(Q + iU)(\vec{n}) {}_{+2}Y_{\ell m}(\vec{n}) - (Q - iU)(\vec{n}) {}_{-2}Y_{\ell m}(\vec{n}) \right]$$

The signal is extremely weak

- Nobody really knows how to detect this.
  - Pathfinder experiments are needed
- Whatever smart, ambitious experiment we design to detect the B-modes:
  - It needs to be extremely sensitive
  - It needs an extremely careful control of systematic effects
  - It needs careful control of foregrounds
  - It will need independent experiments with orthogonal systematics.
- There is still a long way to go: …

The observable - 2

- Our second observable is the **angular power spectrum of CMB polarization,** and in particular the component produced by tensor fluctuations (**B-modes**).
- In particular, LSPE measures the angular power spectrum **at large angular scales**, i.e. at multipoles (ℓ=2-200), because this is where B-modes from inflation produce maximum signal, while competing effects are weaker.
- This requires an angular resolution around 2° i.e. an aperture diameter of 50 cm for a 20-modes detector at λ2mm (140 GHz)
- The frequency range must cover the peak of CMB brightness (140 GHz) and extend to lower and higher frequencies to monitor local contaminating emission (interstellar dust, synchrotron).

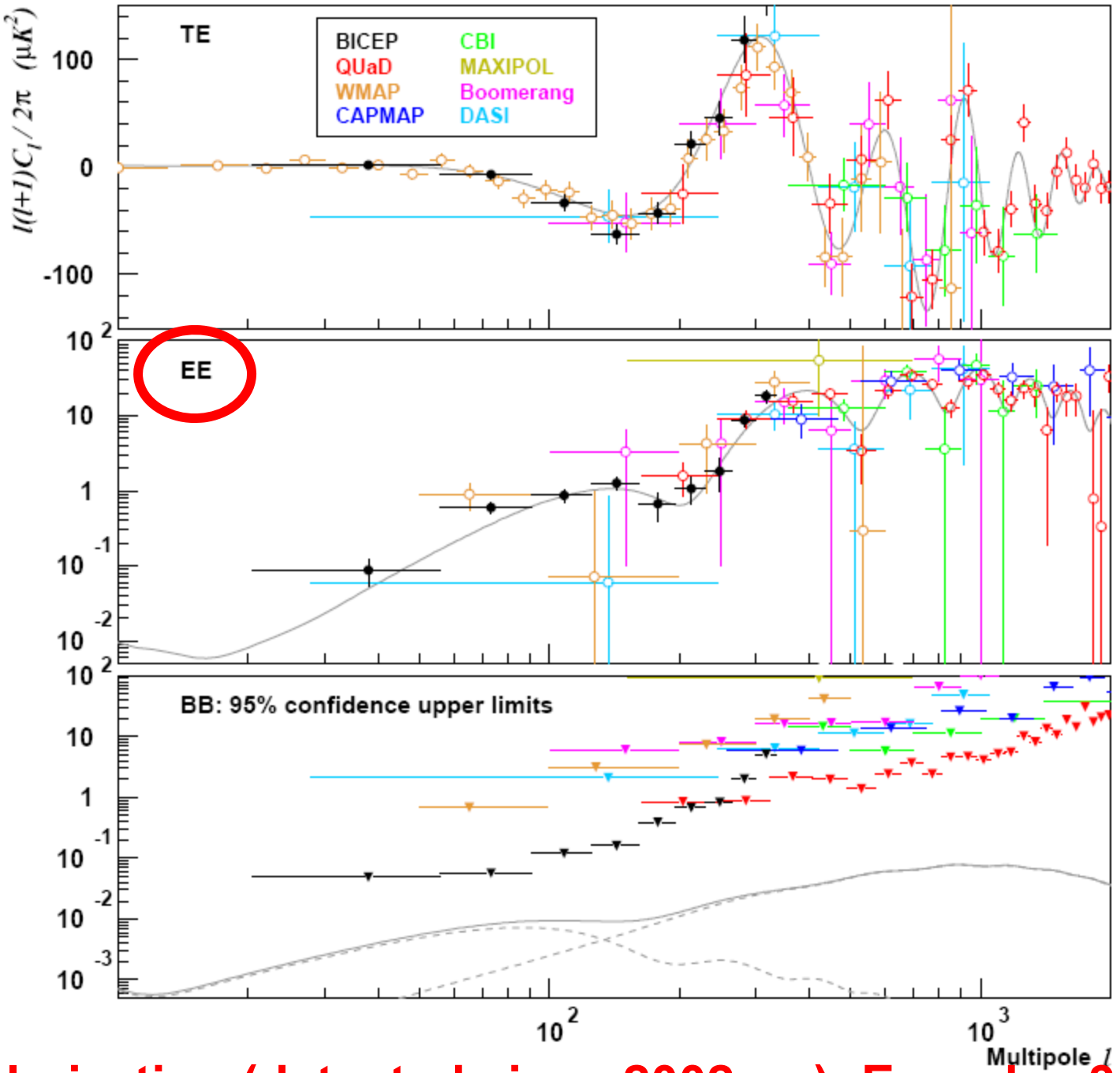

CMB Polarization (detected since 2002 …): E-modes 3 μK

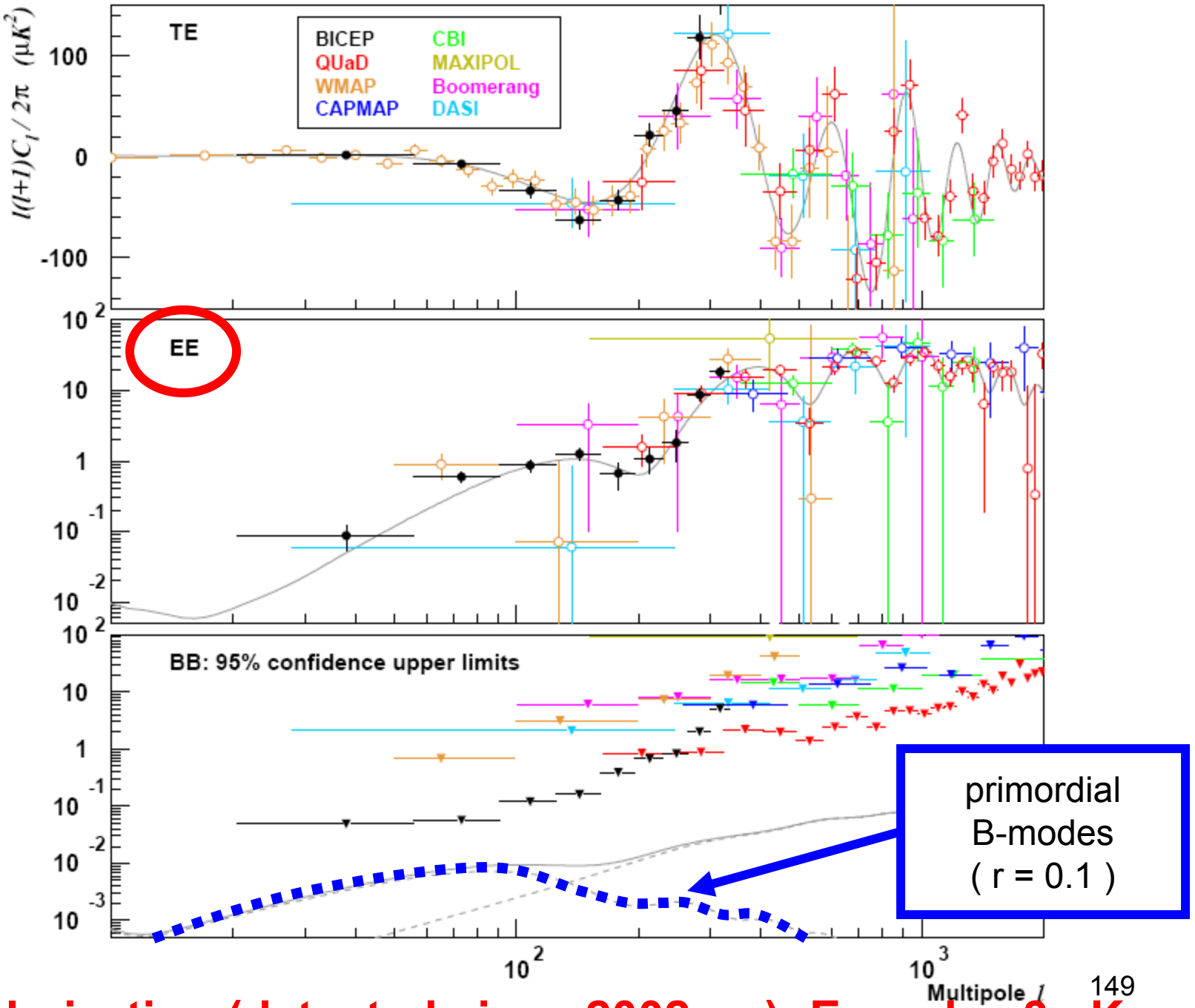

CMB Polarization (detected since 2002 …): E-modes 3 μK

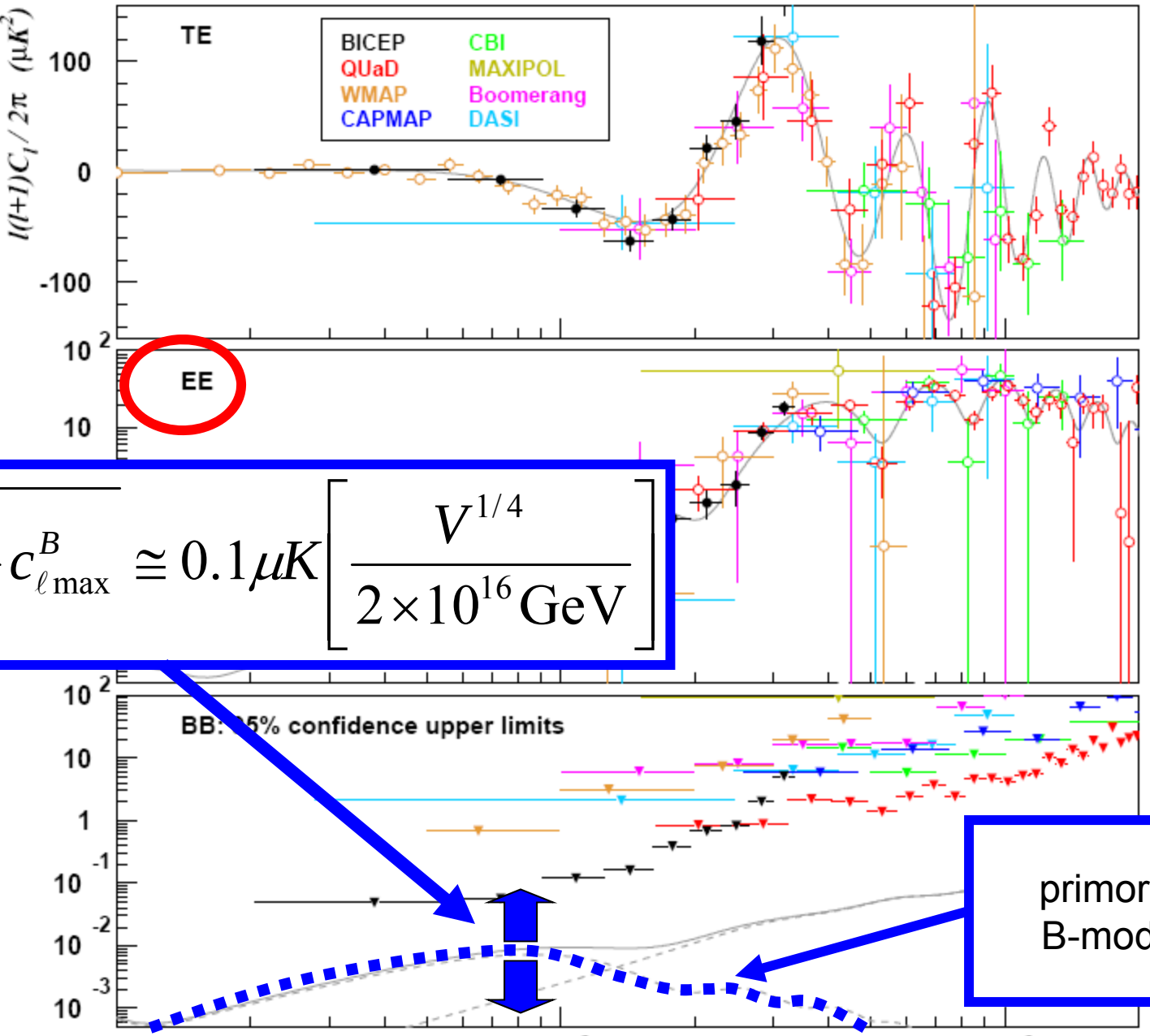

$$\sqrt{\frac{\ell(\ell+1)}{2\pi} c^{B}_{\ell\,\mathrm{max}}} \cong 0.1\mu K \left[\frac{V^{1/4}}{2\times 10^{16}\,\mathrm{GeV}}\right]$$

B-modes depend on the energy-scale of inflation
Maximum signal at large angular scales.

Large Number of Detectors for Sensitivity : TES bolometers with phased-array antennas (Caltech + JPL) for BICEP2

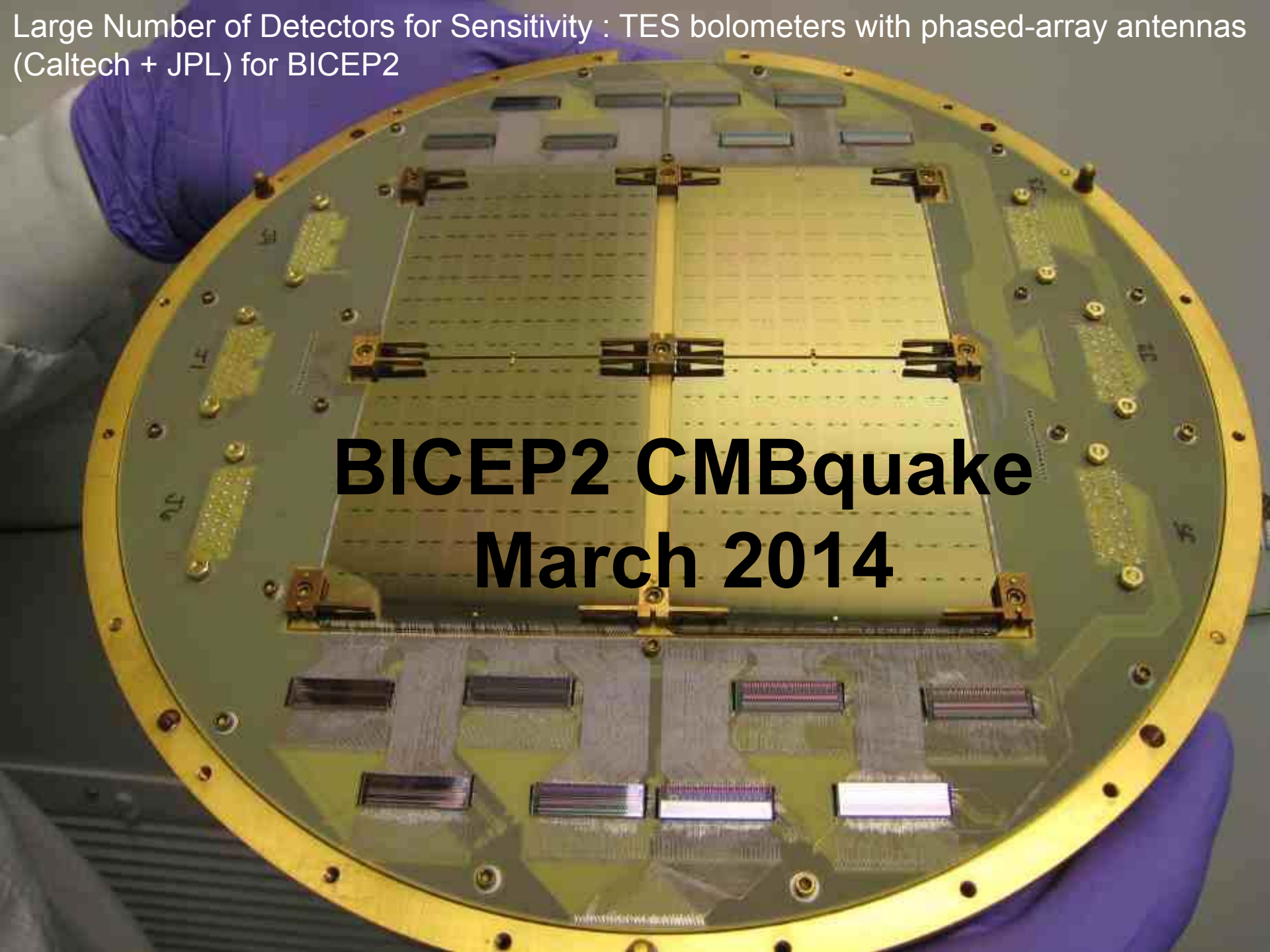

BICEP2/KECK (south pole)

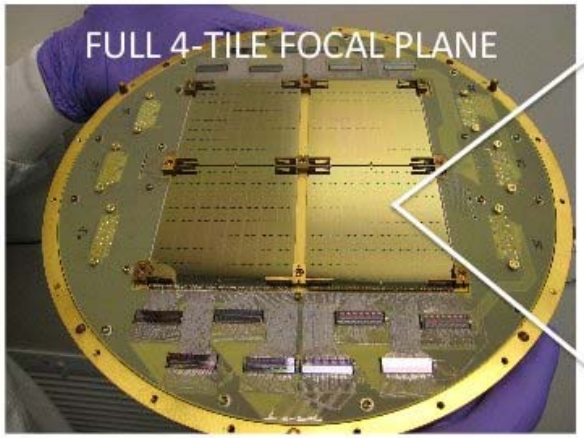

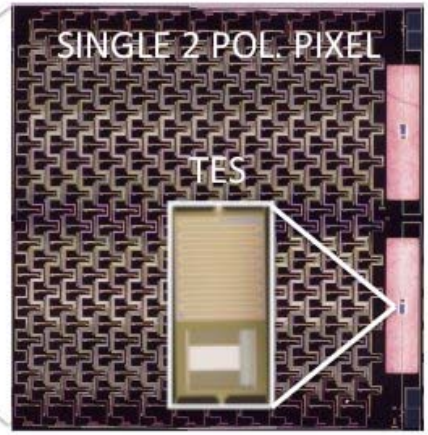

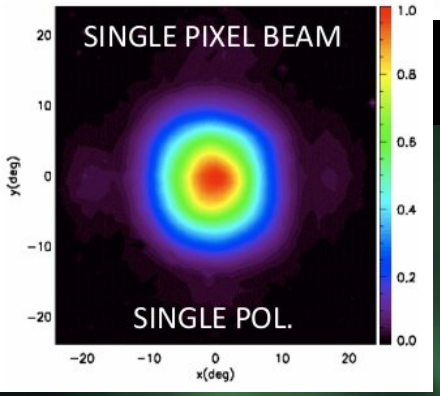

3 dark winters of integration
In the best sky spot (<1000 sq. deg)

BICEP2 : single frequency 150 GHz

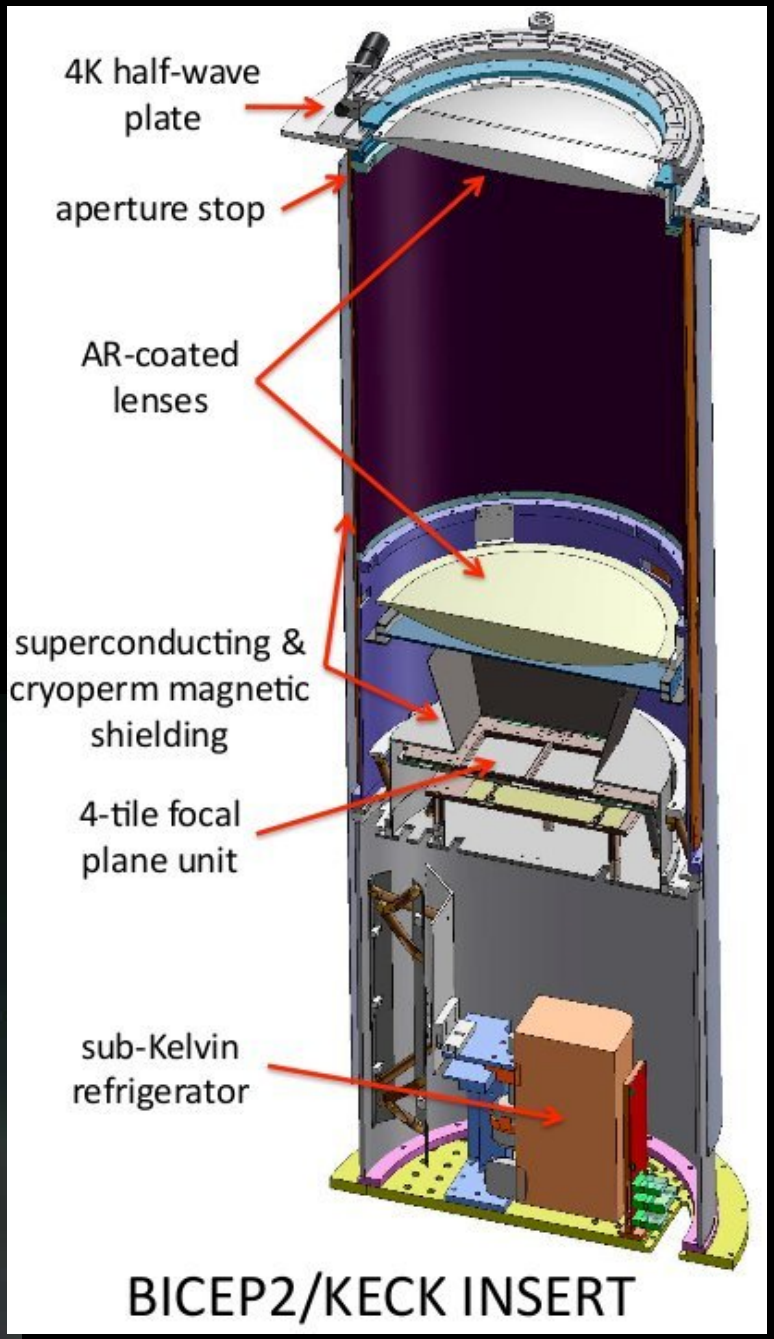

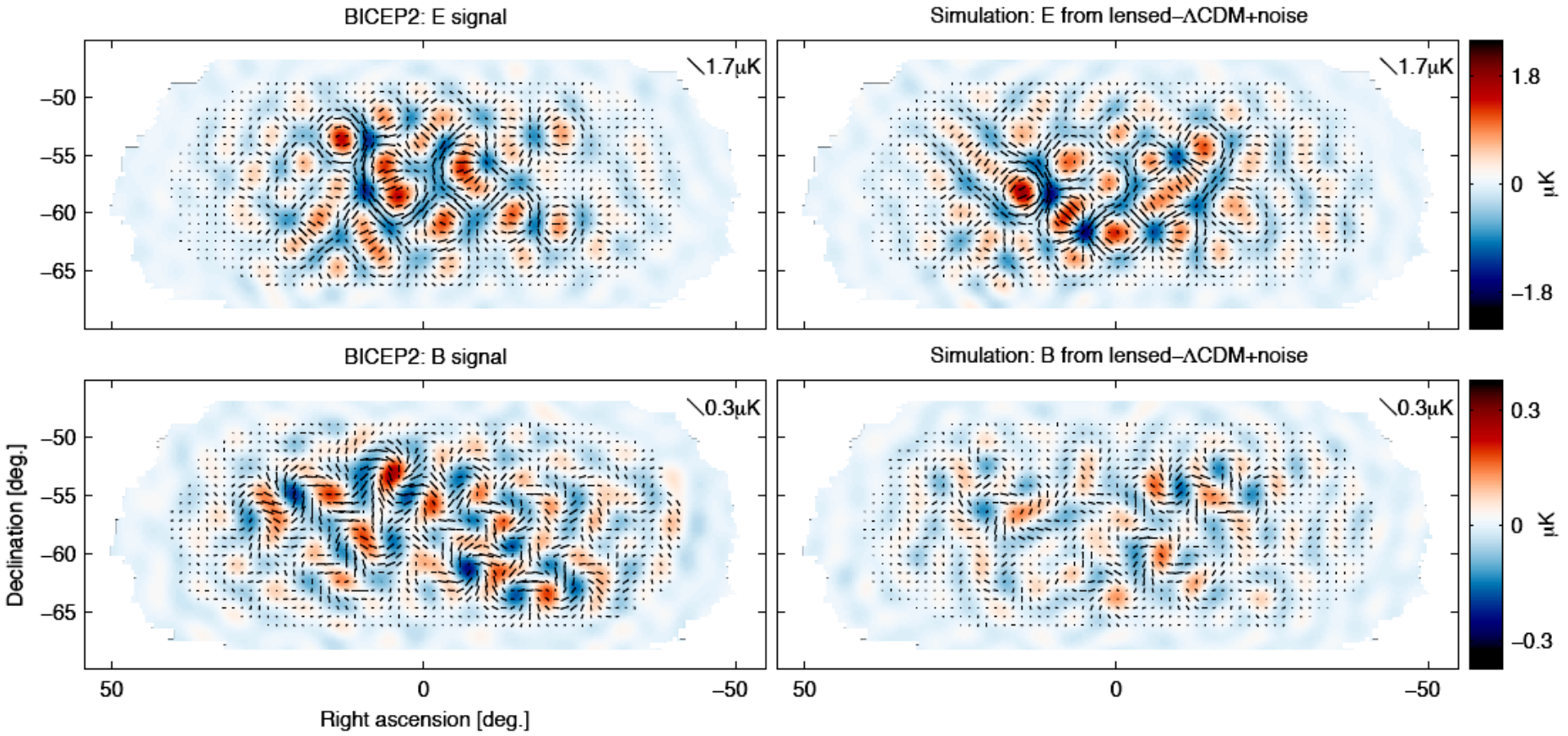

BICEP2 @ south pole :

- 3 dark winters of integration with hundreds of polarization-sensitive bolometers
- Extremely deep map (87 nK deg) of the lowest foreground intensity patch in the sky
- Single frequency (150 GHz)

see astro-ph/1403-3985 and astro-ph/1403-4302

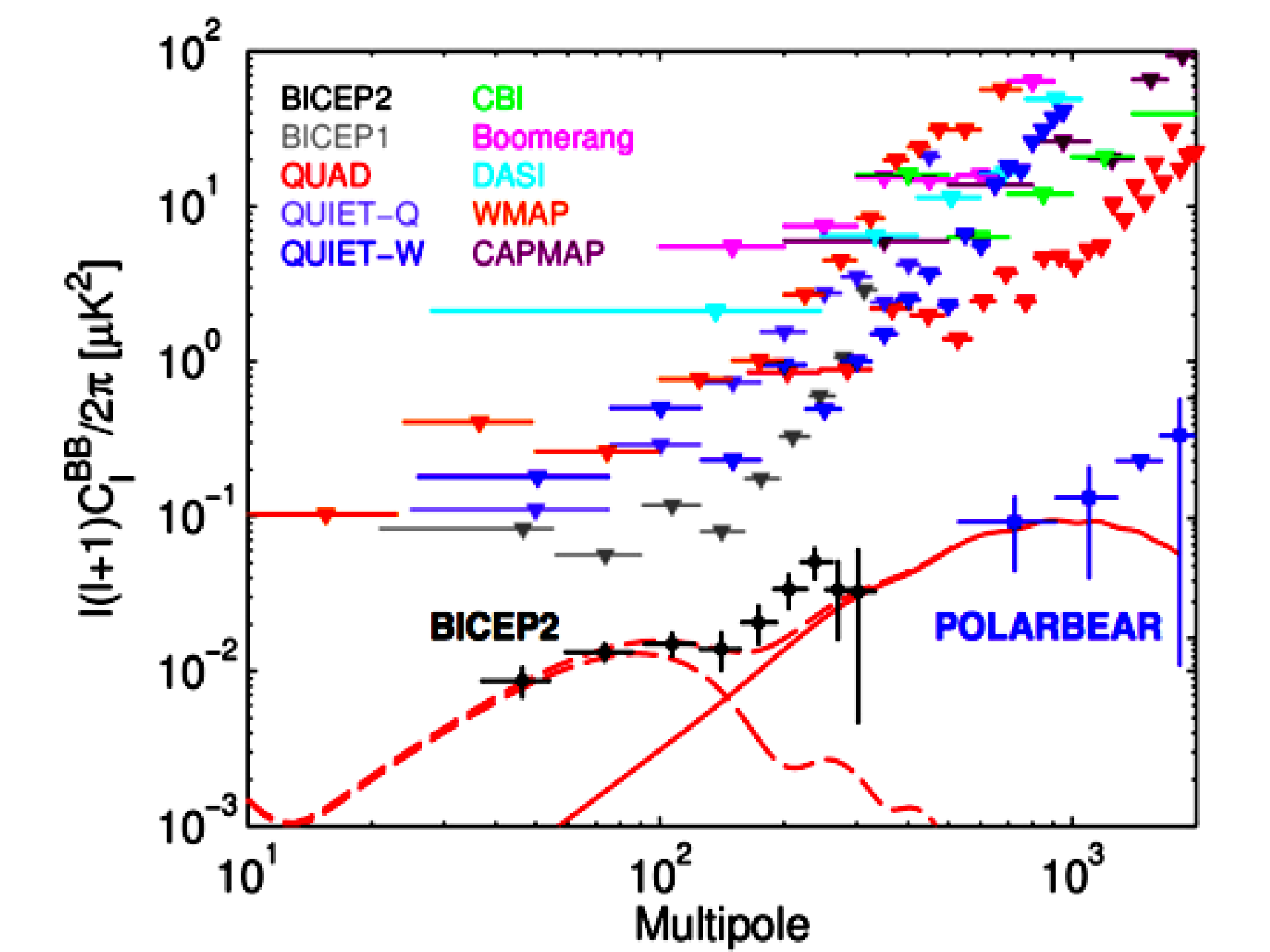
BICEP2
BICEP1
QUAD
QUIET–Q
QUIET–W
CBI
Boomerang
DASI
WMAP
CAPMAP
BICEP2
POLARBEAR
$l(l+1)C_l^{BB}/2\pi$ [μK^2]
Multipole
10^2
10^1
10^0
10^{-1}
10^{-2}
10^{-3}
10^1
10^2
10^3

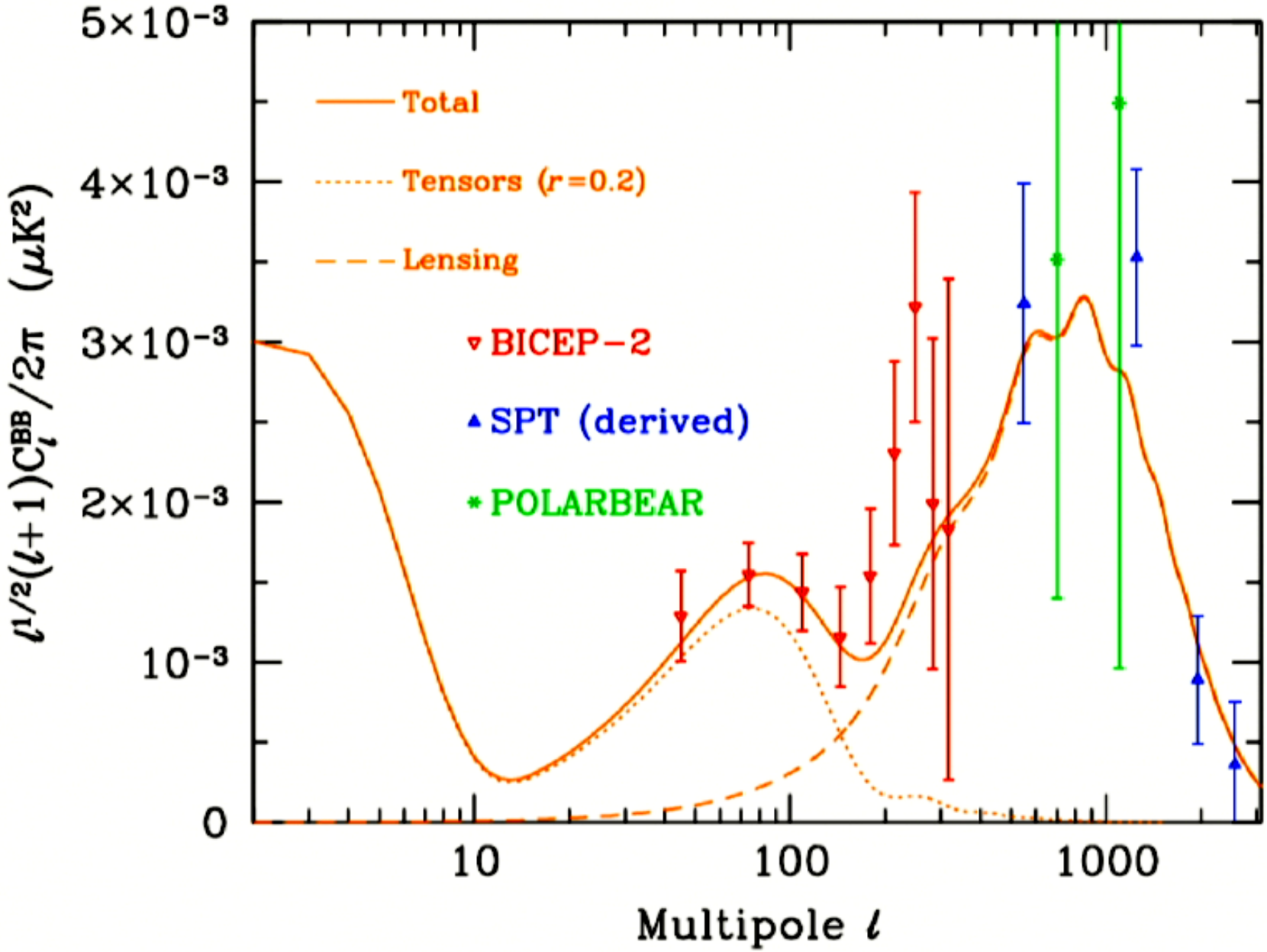
Total
Tensors (r=0.2)
Lensing
BICEP−2
SPT (derived)
POLARBEAR
$\ell^{1/2}(\ell+1)C_\ell^{BB}/2\pi$ (μK^2)
5×10⁻³
4×10⁻³
3×10⁻³
2×10⁻³
10⁻³
0
10
100
1000
Multipole ℓ

BICEP2 results: potentially a huge impact on Cosmology and Fundamental Phsyics

IF the detected B-modes are generated by cosmic inflation:

- What has been measured is the result of pre-inflationary quantum fluctuations in the spacetime metric
- The energy-scale of inflation is 2×10^{16} GeV (quite precise !)
- We can reject several classes of inflation models
- With new instruments and more precise measurements of B-modes we can constrain other parameters of inflation
- high-energy theory is to construct models of new physics near the Planck scale that include inflation.
- knowing the slope of the spectrum of tensor perturbations would provide a new observational constraint of physics in this energy range that CANNOT be probed by any other means

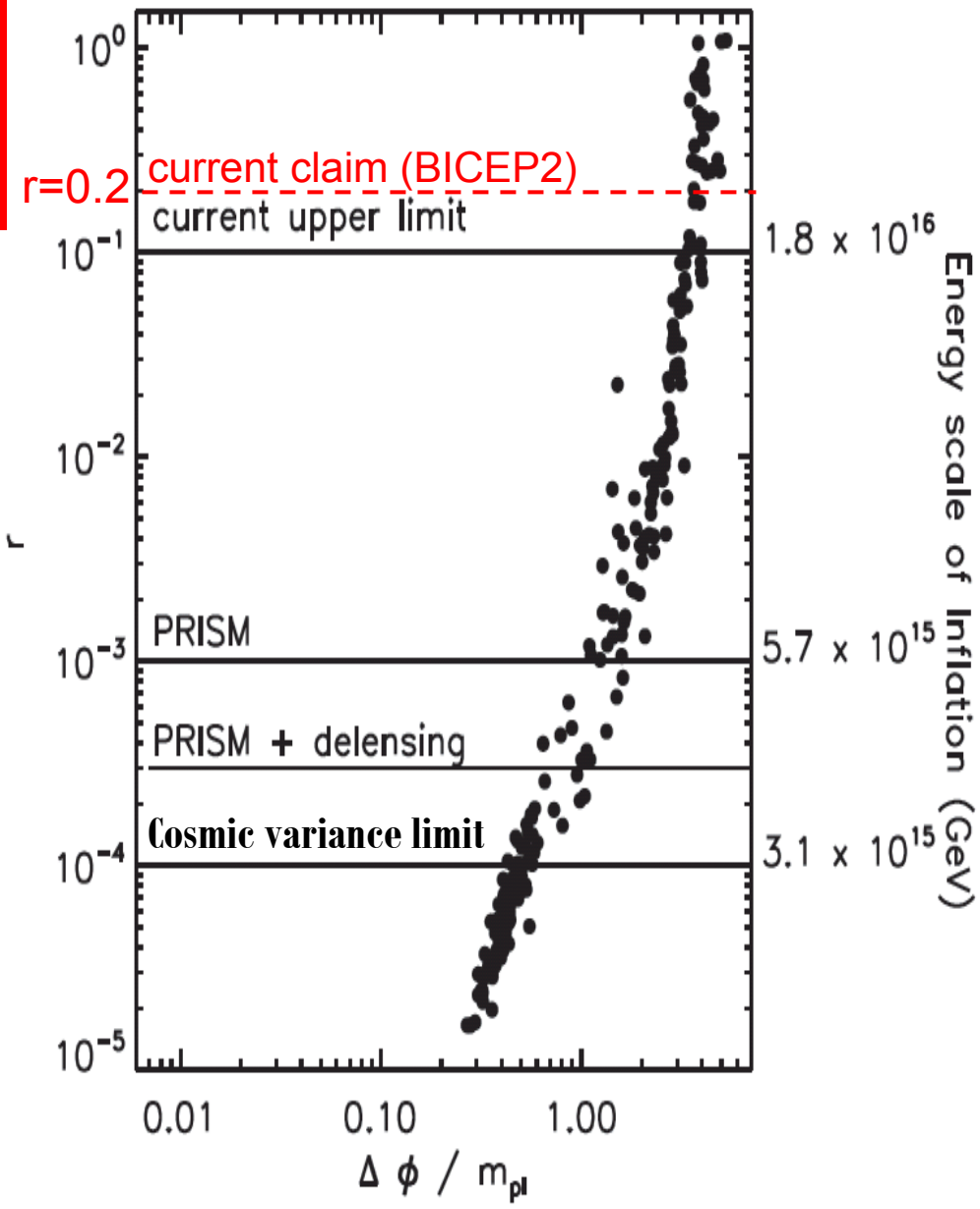

However …

- Extraordinary discoveries require extraordinary evidence
- **Is the BICEP2 B-modes signal really in the sky ?** My personal opinion is YES, despite of the tiny level, there is more than enough evidence for this in the papers. A systematics paper will be published soon, to fully convince.
- **Is the BICEP2 B-modes signal really primordial ?** My personal opinion is that these is NOT enough evidence for this in the papers.

From BICEP2 paper :

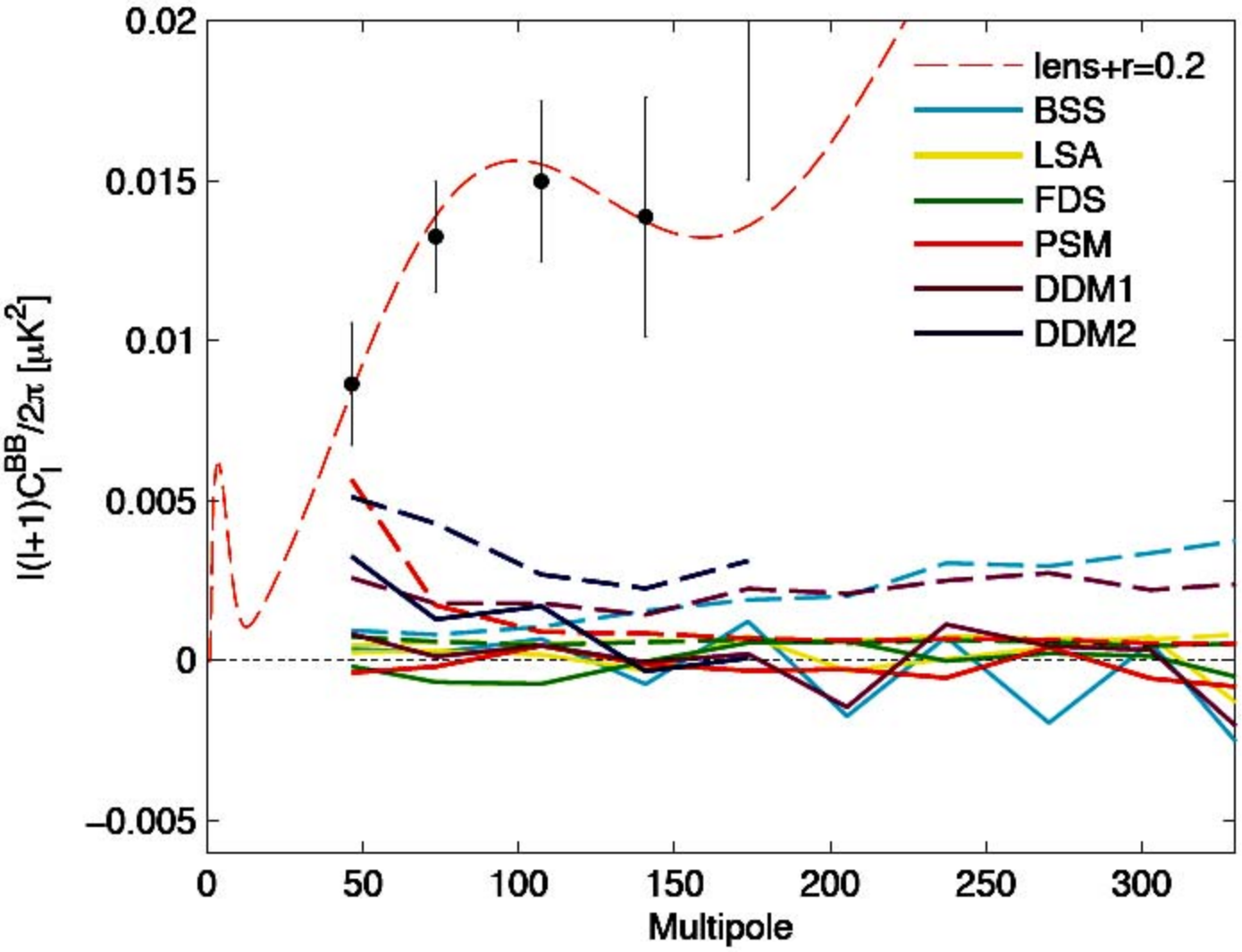

Models for the foregorund signal (mainly interstellar dust)

Interstellar dust polarization

- Interstellar dust grains are elongated and aligned in the magnetic field of our Galaxy
- Dust grains are heated by UVs from stars, and re-emit as grey-body sources in the FIR, with a temperature of 20-30K.

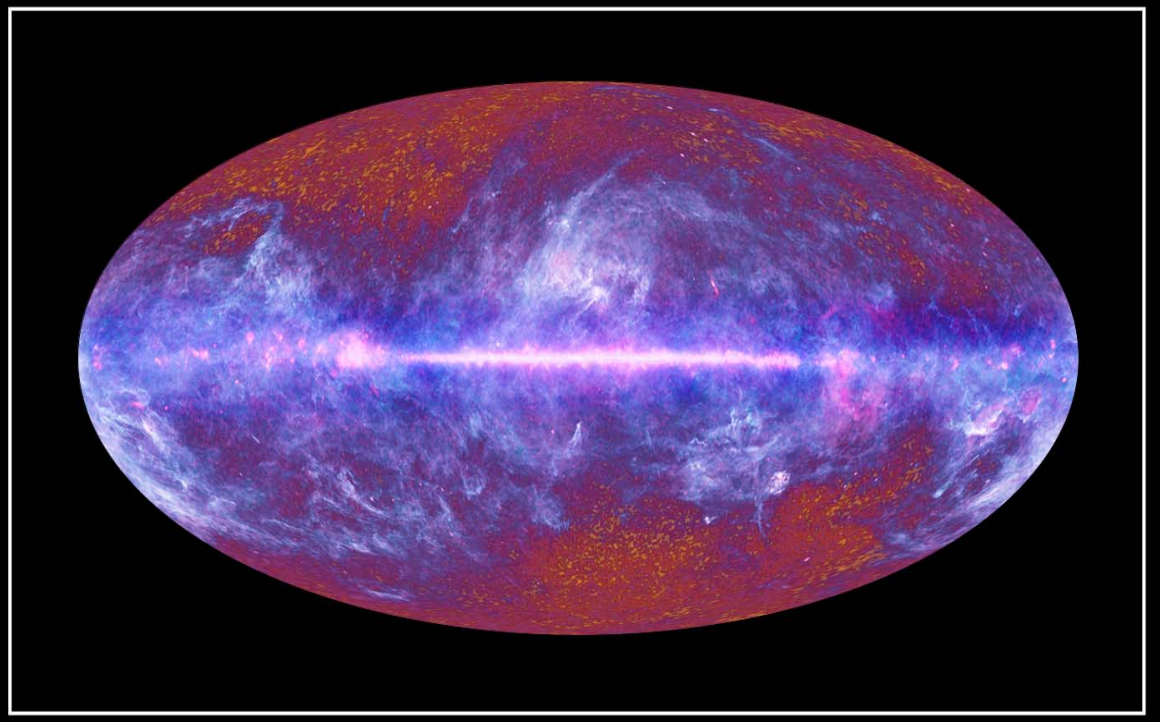

- Due to the alignement, the emission is polarized.
- The polarization fraction depends on the degree of alignment and on the coherence of the B-field along the line of sight
- In high-latitude regions the line of sight crosses only one or a few thin dust clouds, where the magnetic field is likely to be coherent. So lower dust intensity does not imply necessarily low dust polarization.
- Planck polarization data at 340 GHz are very sensitive to polarized dust.
- Other data are very scarce and there are no data are available in the region observed by BICEP2.

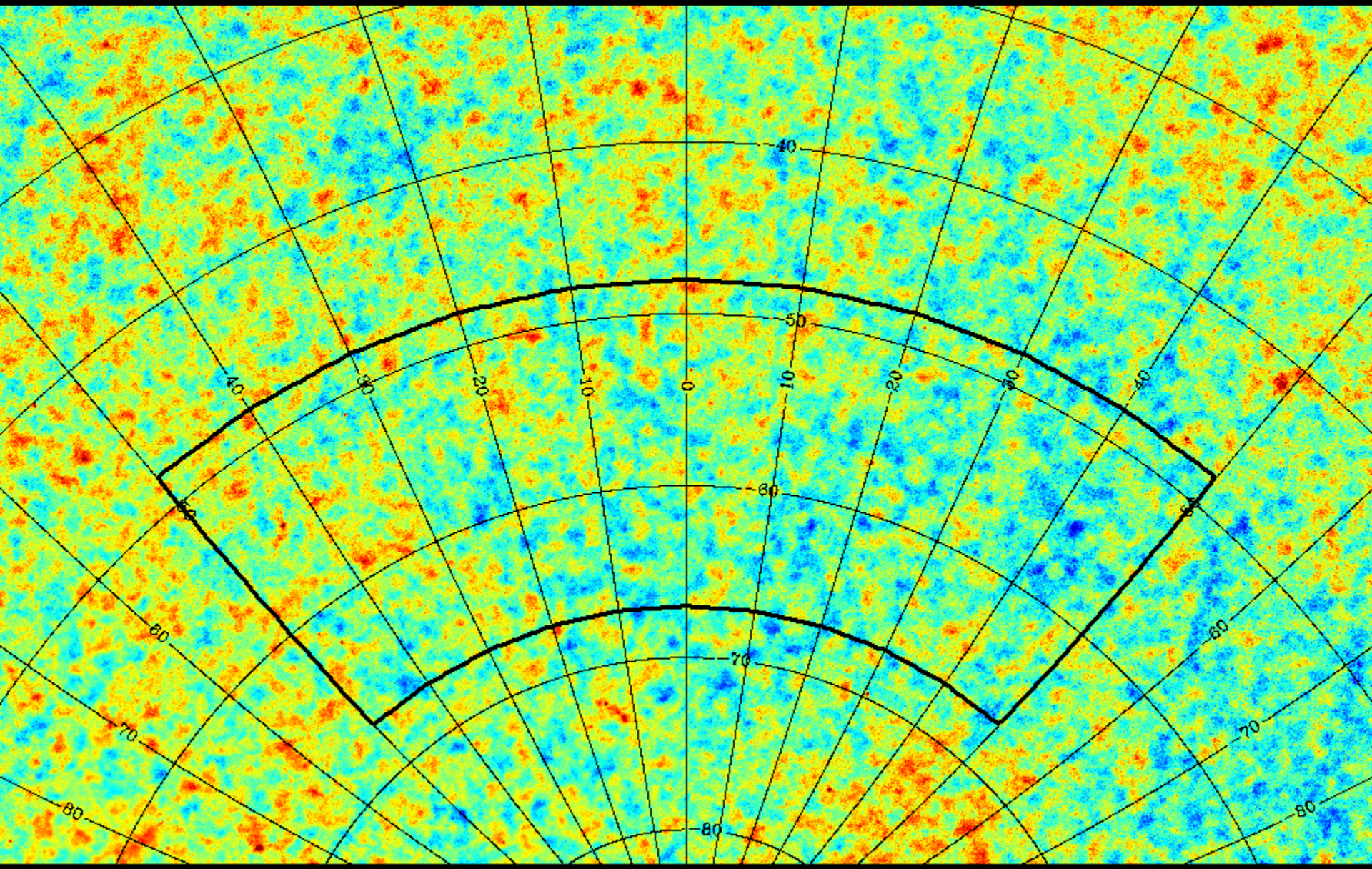

Planck data in the BICEP2 region

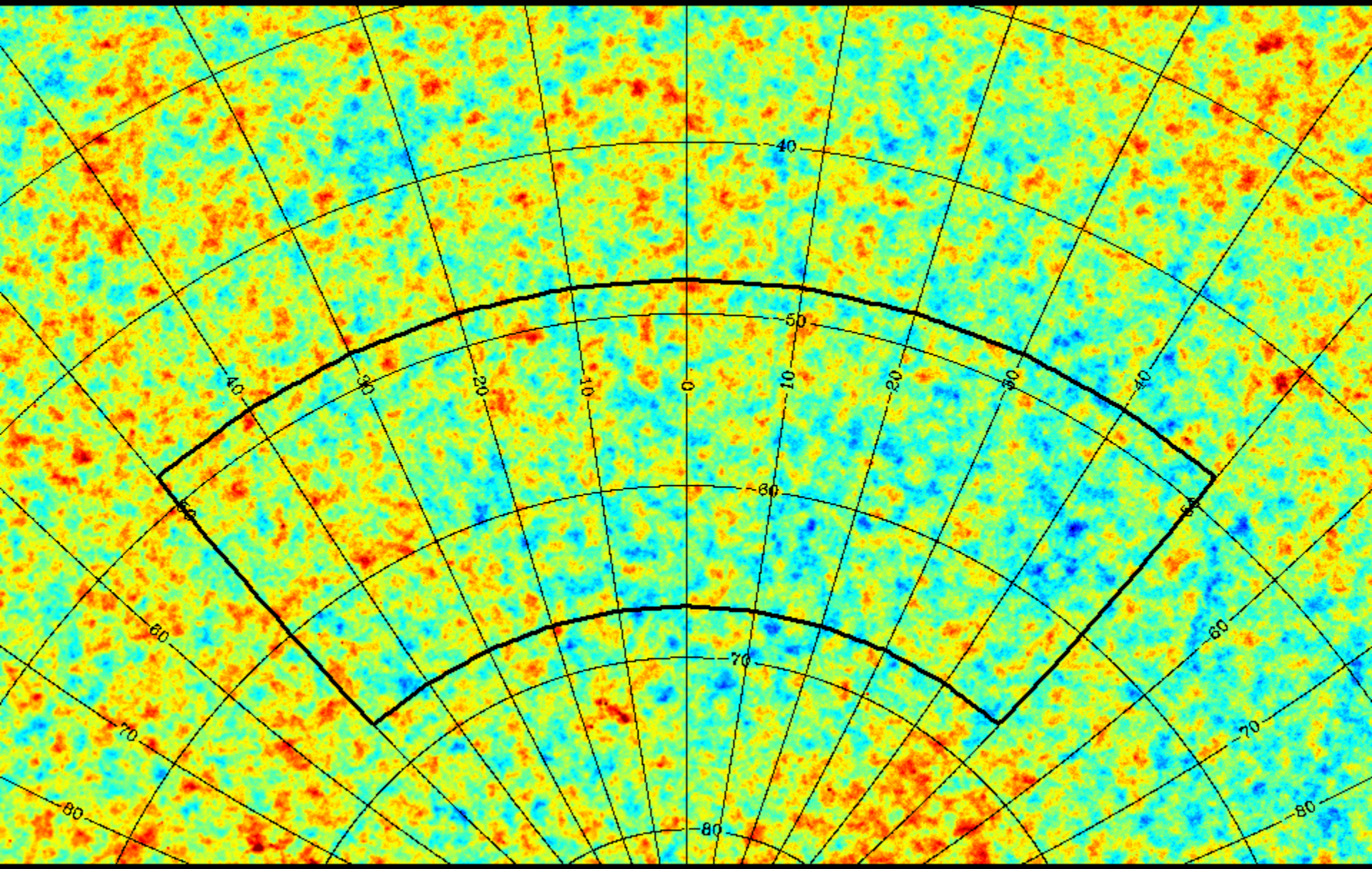

143 GHz

Planck data in the BICEP2 region

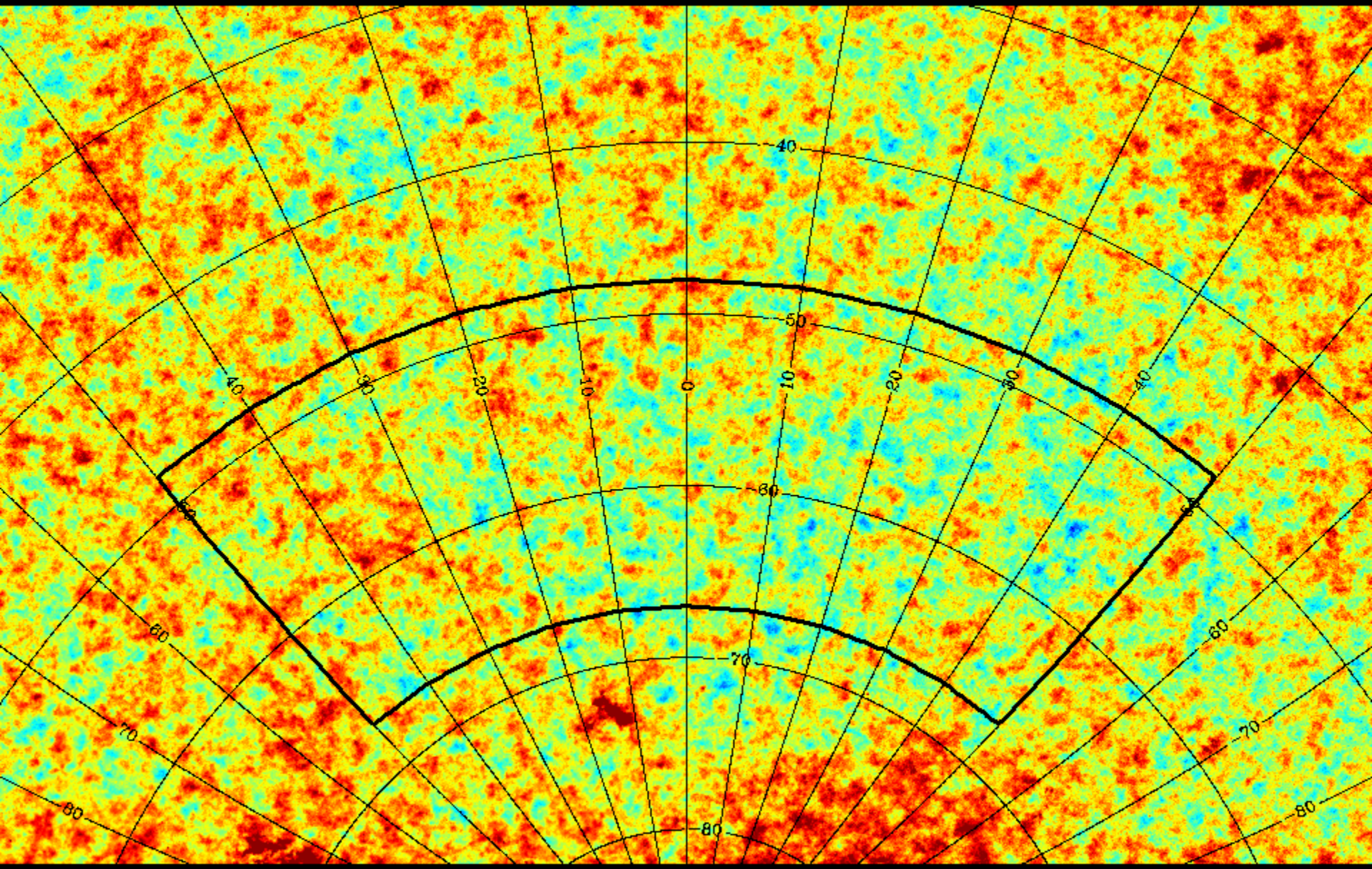

Planck data in the BICEP2 region

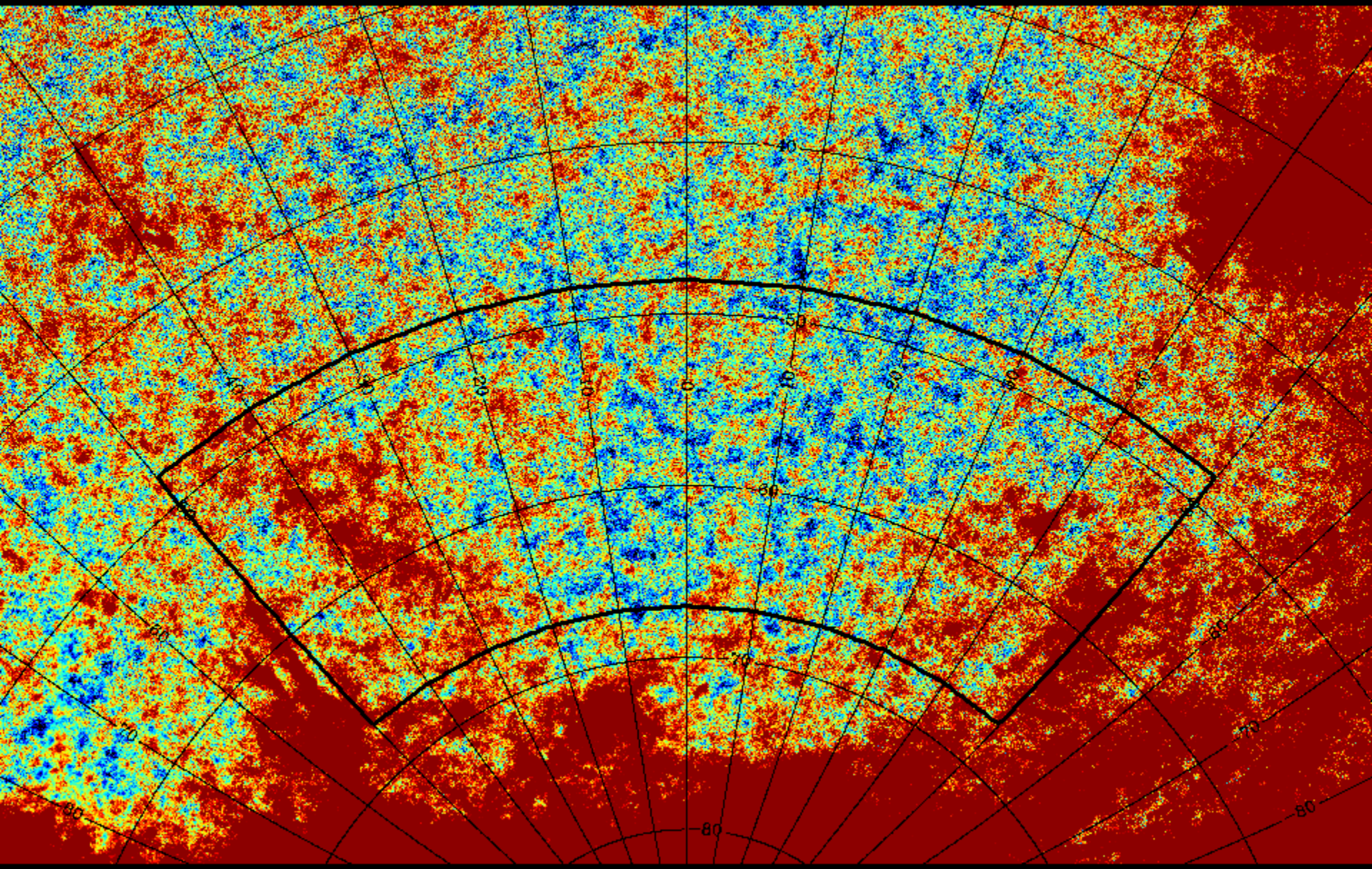

Planck data in the BICEP2 region

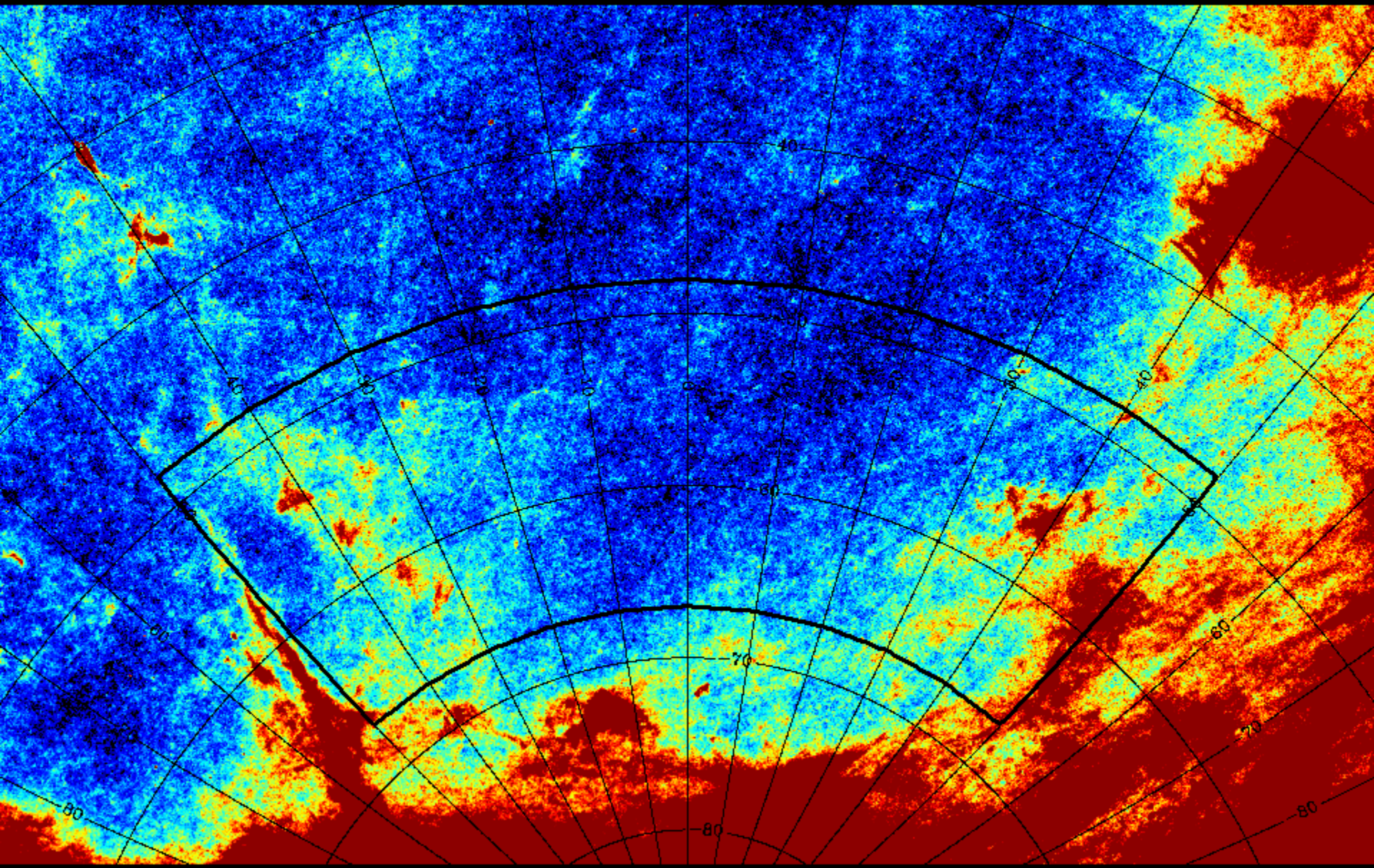

Planck data in the BICEP2 region

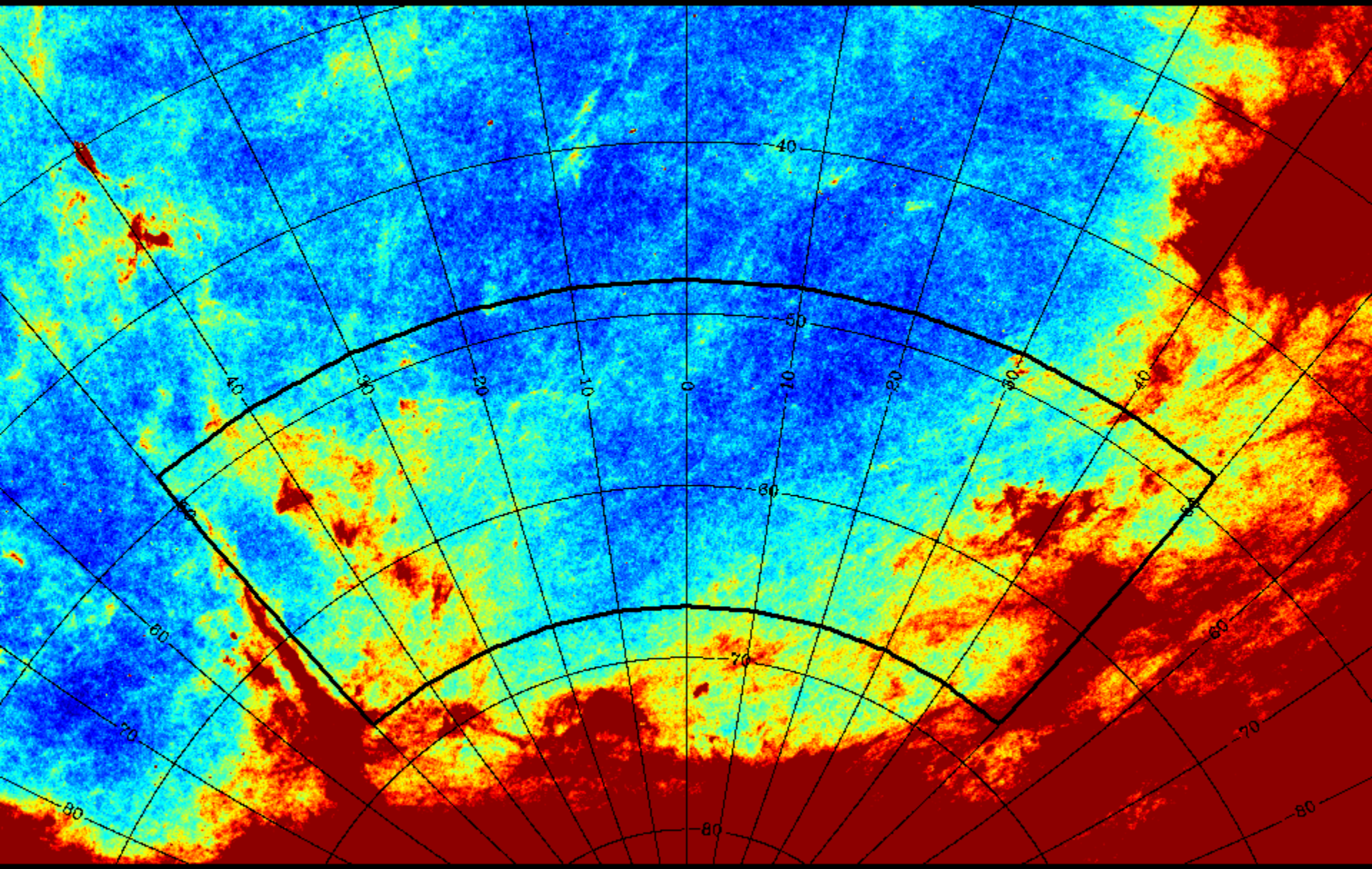

Planck data in the BICEP2 region

Interstellar dust polarization

- Only information available from Planck at the the time of BICEP2 results: two maps shown at a conference (ESLAB 2013, J.P.Bernard talk)

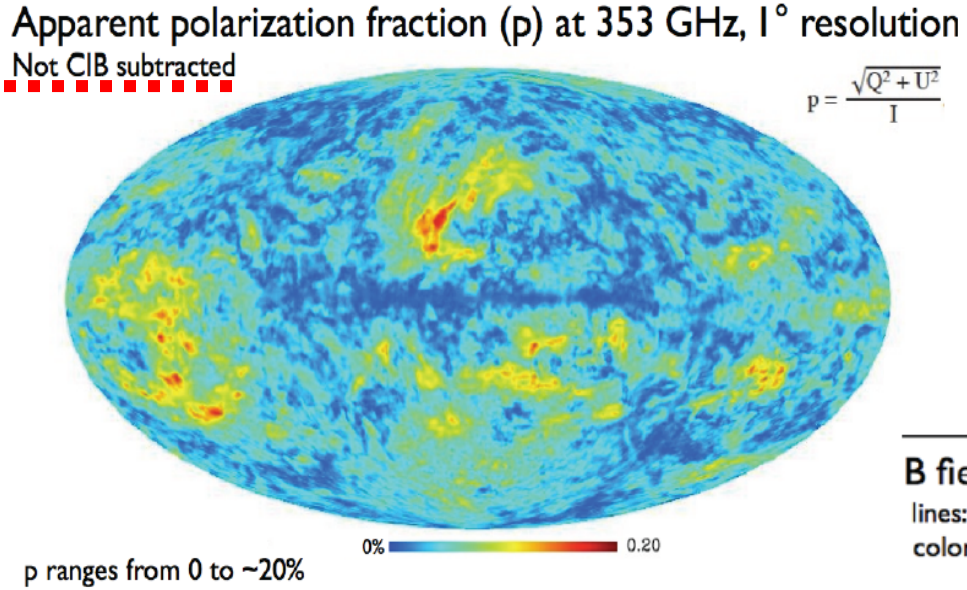

$$p = \frac{\sqrt{Q^2 + U^2}}{I_{dust} + I_{CIB}} < \frac{\sqrt{Q^2 + U^2}}{I_{dust}} = p_{dust}$$

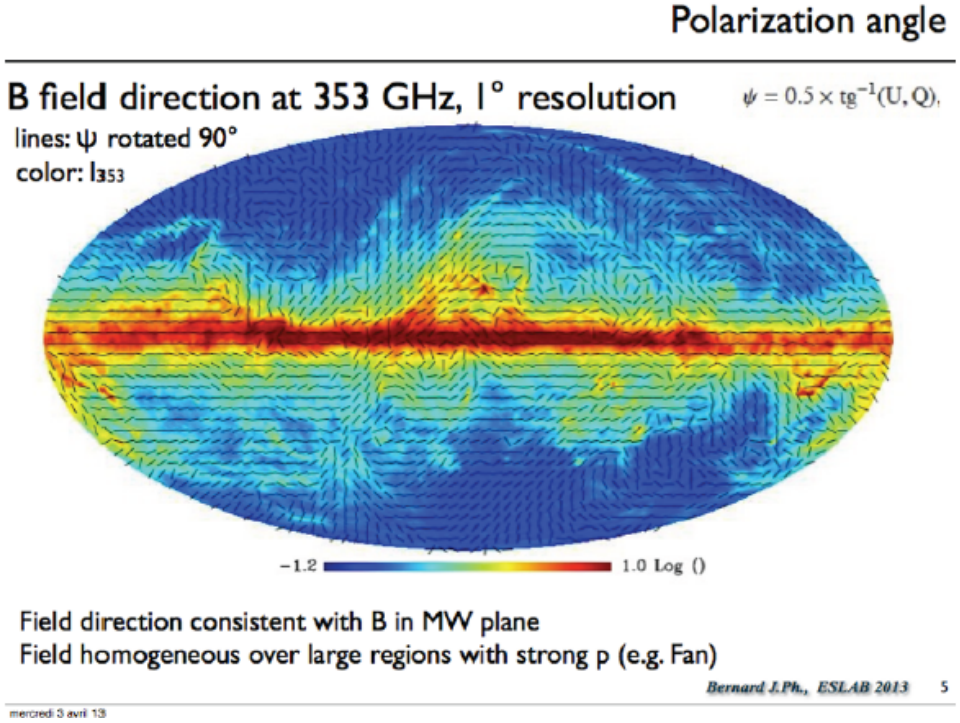

Apparently the BICEP2 team used p as it was from the map, so underestimated the level of polarized dust emission in their region.

Planck intermediate results. XXX. The angular power spectrum of polarized dust emission at intermediate and high Galactic latitudes

(Affiliations can be found after the references)

Preprint online version: 19 September 2014

ABSTRACT

The polarized thermal emission from diffuse Galactic dust is the main foreground present in measurements of the polarization of the cosmic microwave background (CMB) at frequencies above 100 GHz. In this paper we exploit the uniqueness of the *Planck* HFI polarization data from 100 to 353 GHz to measure the polarized dust angular power spectra C_ℓ^{EE} and C_ℓ^{BB} over the multipole range $40 < \ell < 600$ well away from the Galactic plane. These measurements will bring new insights into interstellar dust physics and allow a precise determination of the level of contamination for CMB polarization experiments. Despite the non-Gaussian and anisotropic nature of Galactic dust, we show that general statistical properties of the emission can be characterized accurately over large fractions of the sky using angular power spectra. The polarization power spectra of the dust are well described by power laws in multipole, $C_\ell \propto \ell^\alpha$, with exponents $\alpha^{EE,BB} = -2.42 \pm 0.02$. The amplitudes of the polarization power spectra vary with the average brightness in a way similar to the intensity power spectra. The frequency dependence of the dust polarization spectra is consistent with modified blackbody emission with $\beta_\mathrm{d} = 1.59$ and $T_\mathrm{d} = 19.6$ K down to the lowest *Planck* HFI frequencies. We find a systematic difference between the amplitudes of the Galactic *B*- and *E*-modes, $C_\ell^{BB}/C_\ell^{EE} = 0.5$. We verify that these general properties are preserved towards high Galactic latitudes with low dust column densities. We show that even in the faintest dust-emitting regions there are no "clean" windows in the sky where primordial CMB *B*-mode polarization measurements could be made without subtraction of foreground emission. Finally, we investigate the level of dust polarization in the specific field recently targeted by the BICEP2 experiment. Extrapolation of the *Planck* 353 GHz data to 150 GHz gives a dust power $\mathcal{D}_\ell^{BB} \equiv \ell(\ell+1)C_\ell^{BB}/(2\pi)$ of $1.32 \times 10^{-2}\,\mu\mathrm{K}^2_\mathrm{CMB}$ over the multipole range of the primordial recombination bump ($40 < \ell < 120$); the statistical uncertainty is $\pm 0.29 \times 10^{-2}\,\mu\mathrm{K}^2_\mathrm{CMB}$ and there is an additional uncertainty $(+0.28, -0.24) \times 10^{-2}\,\mu\mathrm{K}^2_\mathrm{CMB}$ from the extrapolation. This level is the same magnitude as reported by BICEP2 over this ℓ range, which highlights the need for assessment of the polarized dust signal even in the cleanest windows of the sky. The present uncertainties are large and will be reduced through an ongoing, joint analysis of the *Planck* and BICEP2 data sets.

Key words. Submillimetre: ISM – Radio continuum: ISM – Polarization – ISM: dust, magnetic fields – cosmic background radiation

- This work was started well before 2013 as part of a group of papers on dust polarization physics; it was delayed due to the difficulty of the analysis, as it concerns the faintest dust emission.
- The work is based entirely on Planck data. - the bulk of the paper is about the characterization of polarized dust emission (both E and B modes) at intermediate and high galactic latitudes.
- It is not about primordial gravitational waves. However, it is of general interest to all B-mode experiments, in particular to find the regions which are cleanest with respect to interstellar dust.
- Only a small part of the paper is specifically related to Bicep2. **The main result with regard to Bicep2 is that the amount of dust in the Bicep2 field is not negligible. It is in fact significantly higher than was assumed in the Bicep2 PRL paper.**
- This fact does not affect the Bicep2 detection of B-modes at 150 GHz. Rather, it affects their interpretation of these signals as arising primarily from primordial gravitational waves. **It is likely that the significance of the Bicep2 detection of primordial B-modes will be reduced, possibly significantly.**
- How much the Bicep2 interpretation is affected - the key question - is not yet clear and will be the outcome of a detailed joint analysis of Bicep2 and Planck data being carried out by the two teams jointly.
- In this work, the contribution of B-modes due to polarized interstellar dust emission is being evaluated using the Planck 353 GHz data mainly.
- This analysis is ongoing and will result in a publication in the same timeframe as the 2014 release of Planck data and results.

Planck intermediate results. XXX. The angular power spectrum of polarized dust emission at intermediate and high Galactic latitudes

(Affiliations can be found after the references)

Preprint online version: 19 September 2014

ABSTRACT

The polarized thermal emission from diffuse Galactic dust is the main foreground present in measurements of the polarization of the cosmic microwave background (CMB) at frequencies above 100 GHz. In this paper we exploit the uniqueness of the *Planck* HFI polarization data from 100 to 353 GHz to measure the polarized dust angular power spectra C_ℓ^{EE} and C_ℓ^{BB} over the multipole range $40 < \ell < 600$ well away from the Galactic plane. These measurements will bring new insights into interstellar dust physics and allow a precise determination of the level of contamination for CMB polarization experiments. Despite the non-Gaussian and anisotropic nature of Galactic dust, we show that general statistical properties of the emission can be characterized accurately over large fractions of the sky using angular power spectra. The polarization power spectra of the dust are well described by power laws in multipole, $C_\ell \propto \ell^\alpha$, with exponents $\alpha^{EE,BB} = -2.42 \pm 0.02$. The amplitudes of the polarization power spectra vary with the average brightness in a way similar to the intensity power spectra. The frequency dependence of the dust polarization spectra is consistent with modified blackbody emission with $\beta_\mathrm{d} = 1.59$ and $T_\mathrm{d} = 19.6$ K down to the lowest *Planck* HFI frequencies. We find a systematic difference between the amplitudes of the Galactic *B*- and *E*-modes, $C_\ell^{BB}/C_\ell^{EE} = 0.5$. We verify that these general properties are preserved towards high Galactic latitudes with low dust column densities. We show that even in the faintest dust-emitting regions there are no "clean" windows in the sky where primordial CMB *B*-mode polarization measurements could be made without subtraction of foreground emission. Finally, we investigate the level of dust polarization in the specific field recently targeted by the BICEP2 experiment. Extrapolation of the *Planck* 353 GHz data to 150 GHz gives a dust power $\mathcal{D}_\ell^{BB} \equiv \ell(\ell+1)C_\ell^{BB}/(2\pi)$ of $1.32 \times 10^{-2}\,\mu\mathrm{K}^2_\mathrm{CMB}$ over the multipole range of the primordial recombination bump ($40 < \ell < 120$); the statistical uncertainty is $\pm 0.29 \times 10^{-2}\,\mu\mathrm{K}^2_\mathrm{CMB}$ and there is an additional uncertainty $(+0.28, -0.24) \times 10^{-2}\,\mu\mathrm{K}^2_\mathrm{CMB}$ from the extrapolation. This level is the same magnitude as reported by BICEP2 over this ℓ range, which highlights the need for assessment of the polarized dust signal even in the cleanest windows of the sky. The present uncertainties are large and will be reduced through an ongoing, joint analysis of the *Planck* and BICEP2 data sets.

Key words. Submillimetre: ISM – Radio continuum: ISM – Polarization – ISM: dust, magnetic fields – cosmic background radiation

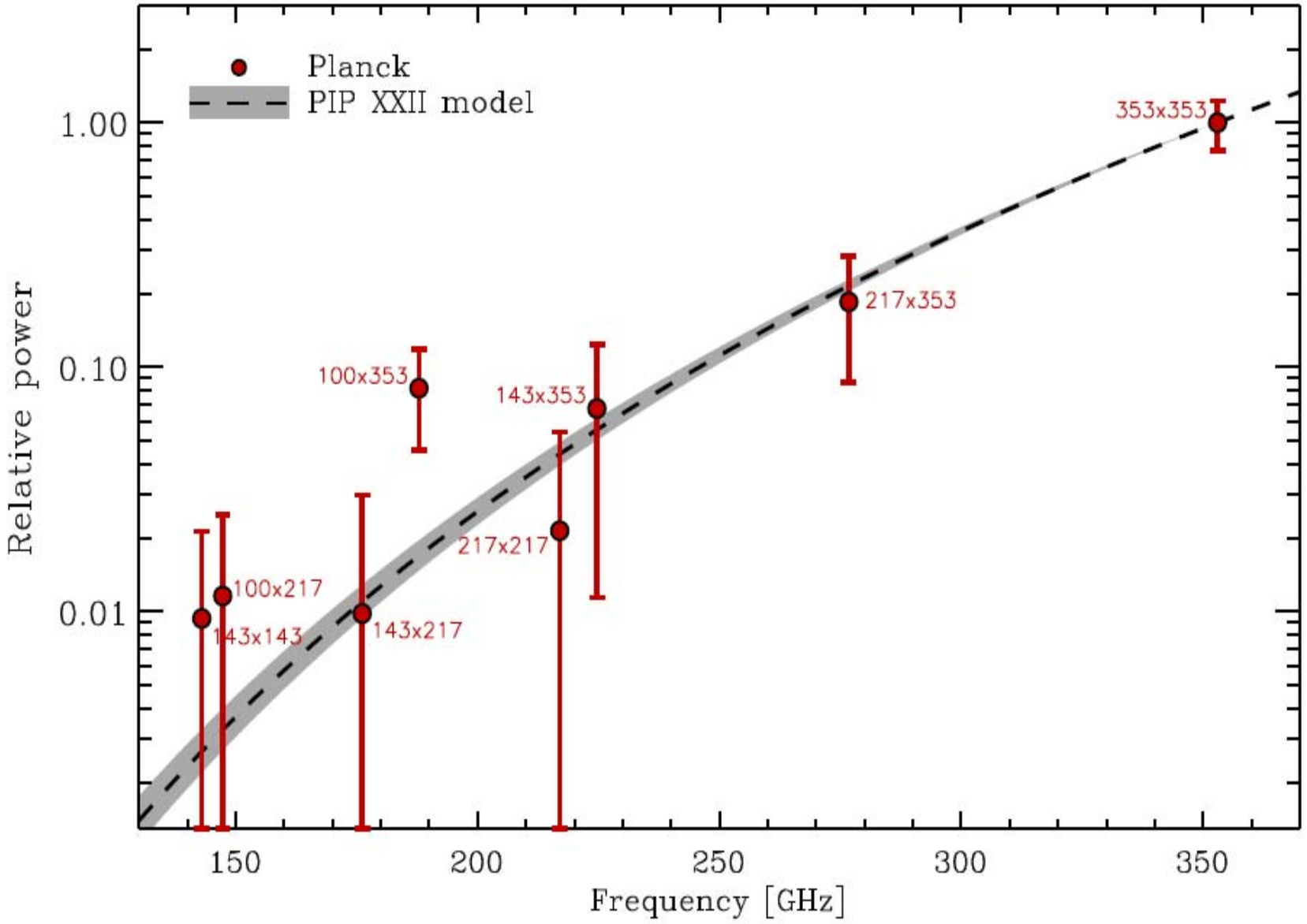
Planck
PIP XXII model
353x353
217x353
100x353
143x353
217x217
100x217
143x143
143x217
1.00
0.10
0.01
Relative power
150
200
250
300
350
Frequency [GHz]

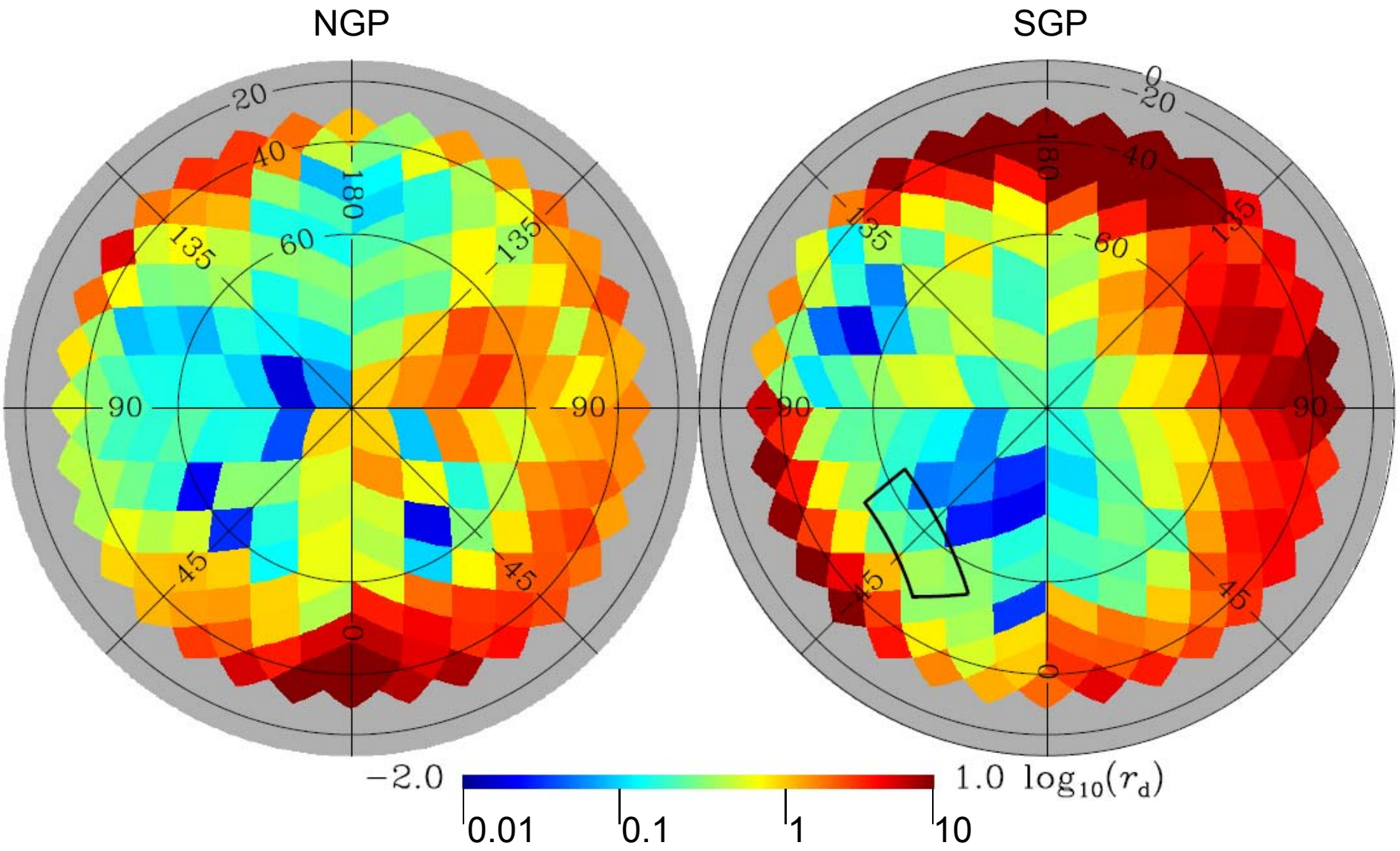

B-modes from dust, as estimated from Planck 343 GHz dust polarization
Planck PIP XXX 1409.5738

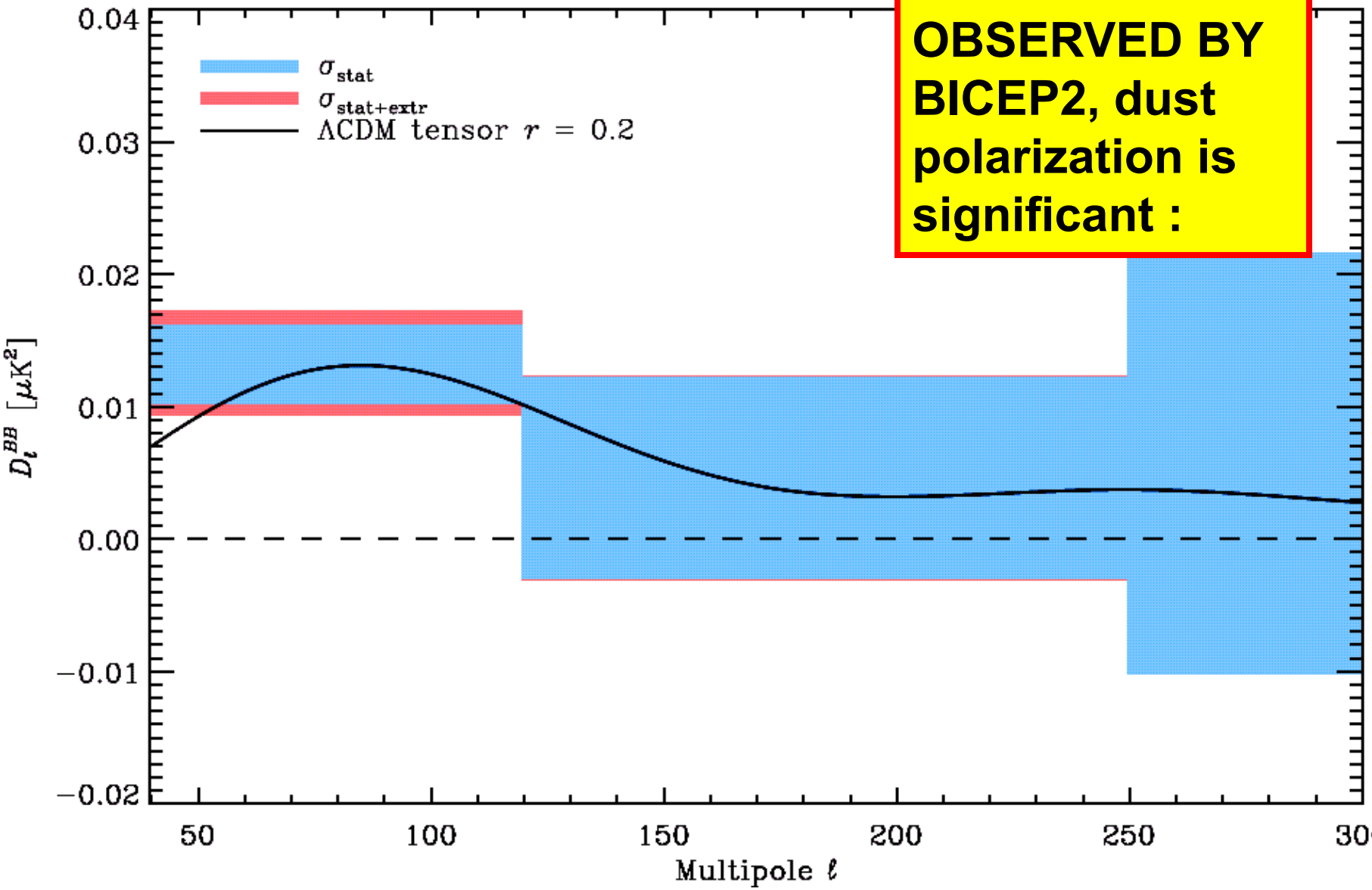

IN THE REGION OBSERVED BY BICEP2, dust polarization is significant :

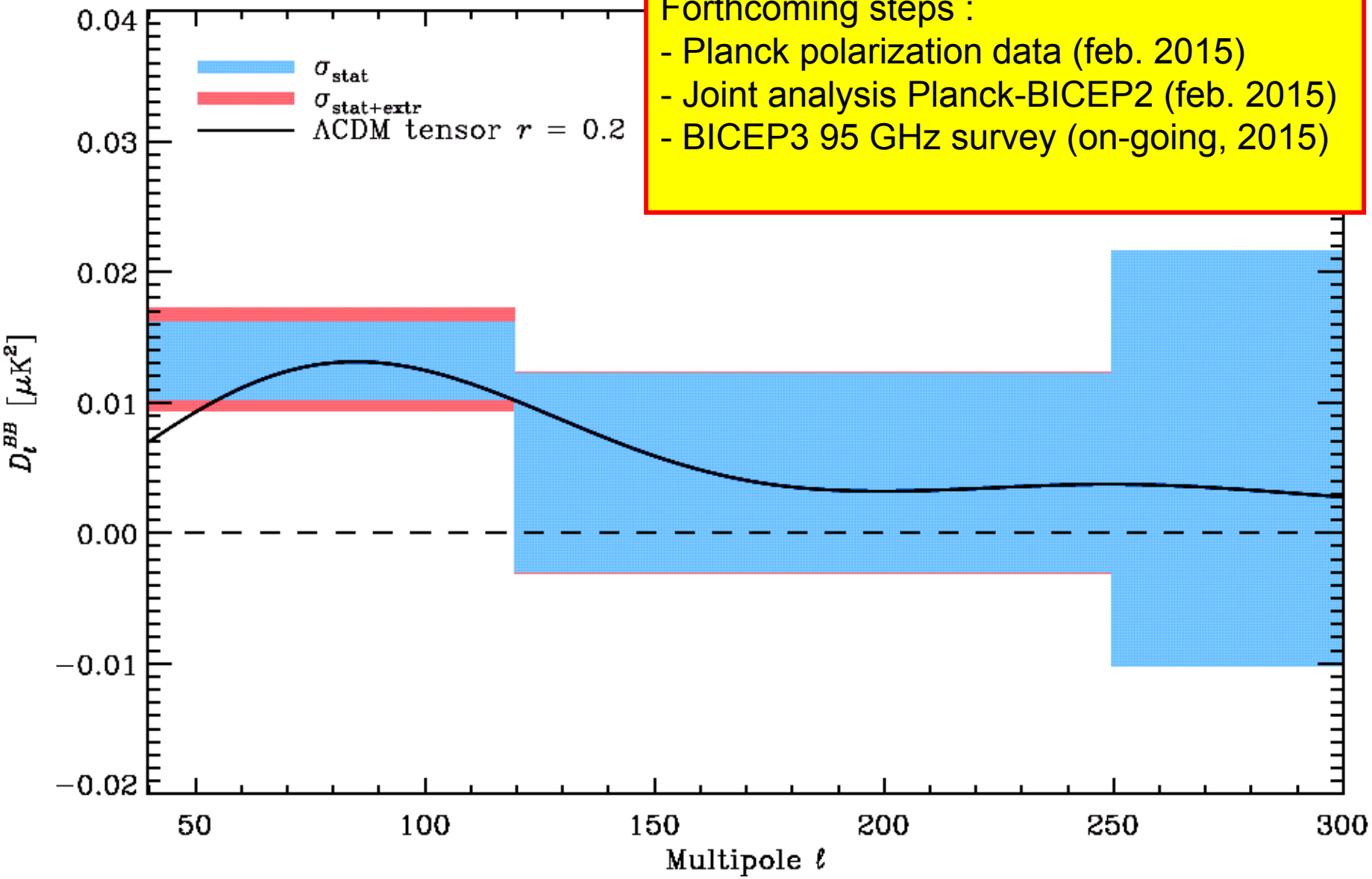
Forthcoming steps :
- Planck polarization data (feb. 2015)
- Joint analysis Planck-BICEP2 (feb. 2015)
- BICEP3 95 GHz survey (on-going, 2015)
σ_{stat}
$\sigma_{stat+extr}$
ΛCDM tensor $r = 0.2$
D_ℓ^{BB} [μK^2]
0.04
0.03
0.02
0.01
0.00
−0.01
−0.02
50
100
150
200
250
300
Multipole ℓ

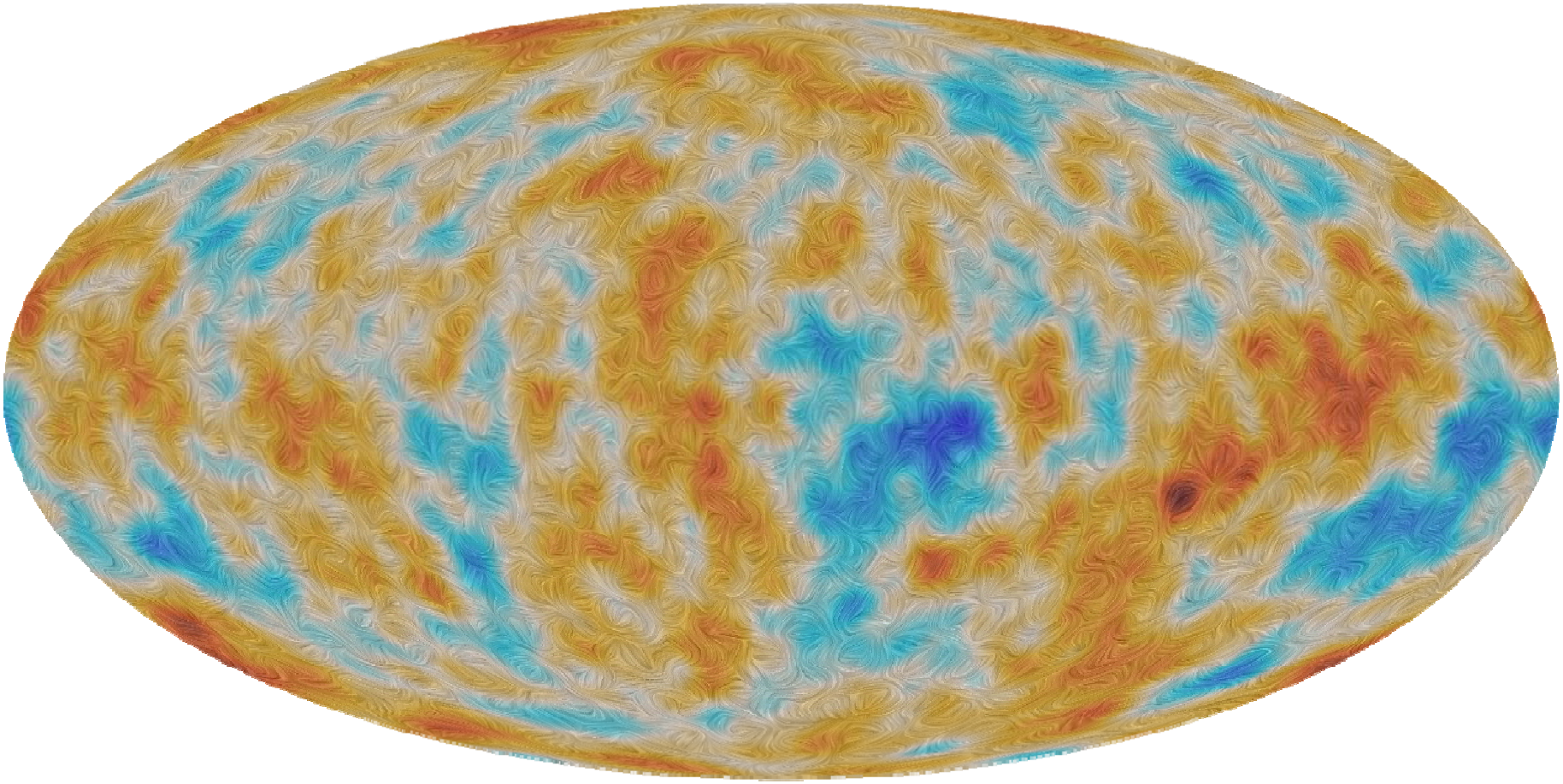

CMB polarization map from Planck (Feb.5, 2015)
$r < 0.1$

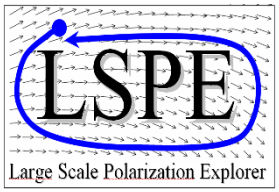

LSPE

the Large-Scale Polarization Explorer

Peter	Ade	University of Cardiff
Giorgio	Amico	Dip. Fisica Sapienza & INFN Roma1
Alessandro	Baldini	INFN Pisa
Paola	Battaglia	Dip. Fisica Università di Milano
Elia Stefano	Battistelli	Dip. Fisica Sapienza & INFN Roma1
Alessandro	Baù	Dip. Fisica Università di Milano Bicocca
Marco	Bersanelli	Dip. Fisica Università di Milano
Michele	Biasotti	Dip. Fisica Uni. Genova & INFN Genova
Andrea	Boscaleri	IFAC - CNR Firenze
Carlo	Bemporad	INFN Pisa
Francesco	Cavaliere	Dip. Fisica Università di Milano
Valentina	Ceriale	Dip. Fisica Uni. Genova & INFN Genova
Eugenio	Coccia	Dip. Fisica Tor Vergata & INFN Roma2
Gabriele	Coppi	Dip. Fisica Sapienza & INFN Roma1
Alessandro	Coppolecchia	Dip. Fisica Sapienza & INFN Roma1
Dario	Corsini	Dip. Fisica Uni. Genova & INFN Genova
Angelo	Cruciani	Dip. Fisica Sapienza & INFN Roma1
Francesco	Cuttaia	INAF - IASF Bologna
Antonello	D' Addabbo	Dip. Fisica Sapienza & INFN Roma1
Giuseppe	D' Alessandro	Dip. Fisica Sapienza & INFN Roma1
Paolo	de Bernardis	Dip. Fisica Sapienza & INFN Roma1
Matteo	De Gerone	Dip. Fisica Uni. Genova & INFN Genova
Marco	De Petris	Dip. Fisica Sapienza & INFN Roma1
Francesco	Del Torto	Dip. Fisica Università di Milano
Viviana	Fafone	Dip. Fisica Tor Vergata & INFN Roma2
Lorenzo	Fiorineschi	Dip. Ing. Ind. Uni. Firenze
Flavio	Fontanelli	Dip. Fisica Uni. Genova & INFN Genova
Christian	Franceschet	Dip. Fisica Università di Milano
Luca	Galli	INFN Pisa
Flavio	Gatti	Dip. Fisica Uni. Genova & INFN Genova
Massimo	Gervasi	Dip. Fisica Università di Milano Bicocca
Anna	Gregorio	Department of Physics - University of Trieste
Daniele	Grosso	Dip. Fisica Uni. Genova & INFN Genova
Riccardo	Gualtieri	Dip. Fisica Sapienza & INFN Roma1
Victor	Haynes	University of Manchester
Marco	Incagli	INFN Pisa
Nicoletta	Krachmalnicoff	Dip. Fisica Università di Milano
Luca	Lamagna	Dip. Fisica Sapienza & INFN Roma1
Bruno	Maffei	University of Manchester
Davide	Maino	Dip. Fisica Università di Milano
Tommaso	Marchetti	Dip. Fisica Sapienza & INFN Roma1
Silvia	Masi	Dip. Fisica Sapienza & INFN Roma1
Aniello	Mennella	Dip. Fisica Università di Milano
Gianluca	Morgante	INAF - IASF Bologna
Federico	Nati	Dip. Fisica Sapienza & INFN Roma1
Ming Wah	Ng	University of Manchester
Luca	Pagano	Dip. Fisica Sapienza & INFN Roma1
Alessandro	Paiella	Dip. Fisica Sapienza & INFN Roma1
Andrea	Passerini	Dip. Fisica Università di Milano Bicocca
Oscar	Peverini	IEIIT - CNR - Torino
Francesco	Piacentini	Dip. Fisica Sapienza & INFN Roma1
Lucio	Piccirillo	University of Manchester
Giampaolo	Pisano	University of Cardiff
Sara	Ricciardi	INAF - IASF Bologna
Paolo	Rissone	Dip. Ing. Ind. Uni. Firenze
Alessio	Rocchi	Dip. Fisica Tor Vergata & INFN Roma2
Giovanni	Romeo	INGV - Roma
Maria	Salatino	Dip. Fisica Sapienza & INFN Roma1
Maura	Sandri	INAF - IASF Bologna
Alessandro	Schillaci	Dip. Fisica Sapienza & INFN Roma1
Giovanni	Signorelli	INFN Pisa
Franco	Spinella	INFN Pisa
Luca	Stringhetti	INAF - IASF Bologna
Andrea	Tartari	Dip. Fisica Università di Milano Bicocca
Riccardo	Tascone	IEIIT - CNR - Torino
Luca	Terenzi	INAF - IASF Bologna
Maurizio	Tomasi	Dip. Fisica Università di Milano
Elisabetta	Tommasi	Italian Space Agency
Carole	Tucker	University of Cardiff
Fabrizio	Villa	INAF - IASF Bologna
Giuseppe	Virone	IEIIT - CNR - Torino
Andrea	Zacchei	INAF Osservatorio Trieste
Mario	Zannoni	Dip. Fisica Università di Milano Bicocca

Scientific Target : B-modes

- Red line : contribution from each multipole to the total mean square fluctuation of the tensor component of CMB polarization (B-modes, r = 1).
- Thin blue line : the cumulative of the B-modes, i.e. the variance measured by an experiment sensitive from multipole 2 to a given multipole ℓ.
- The top blue thick line : the beam function B^2_ℓ for an experiment with a 1.5° FWHM Gaussian beam.
- Despite of the coarse angular resolution such an experiment collects most of the polarization signal from B-modes.

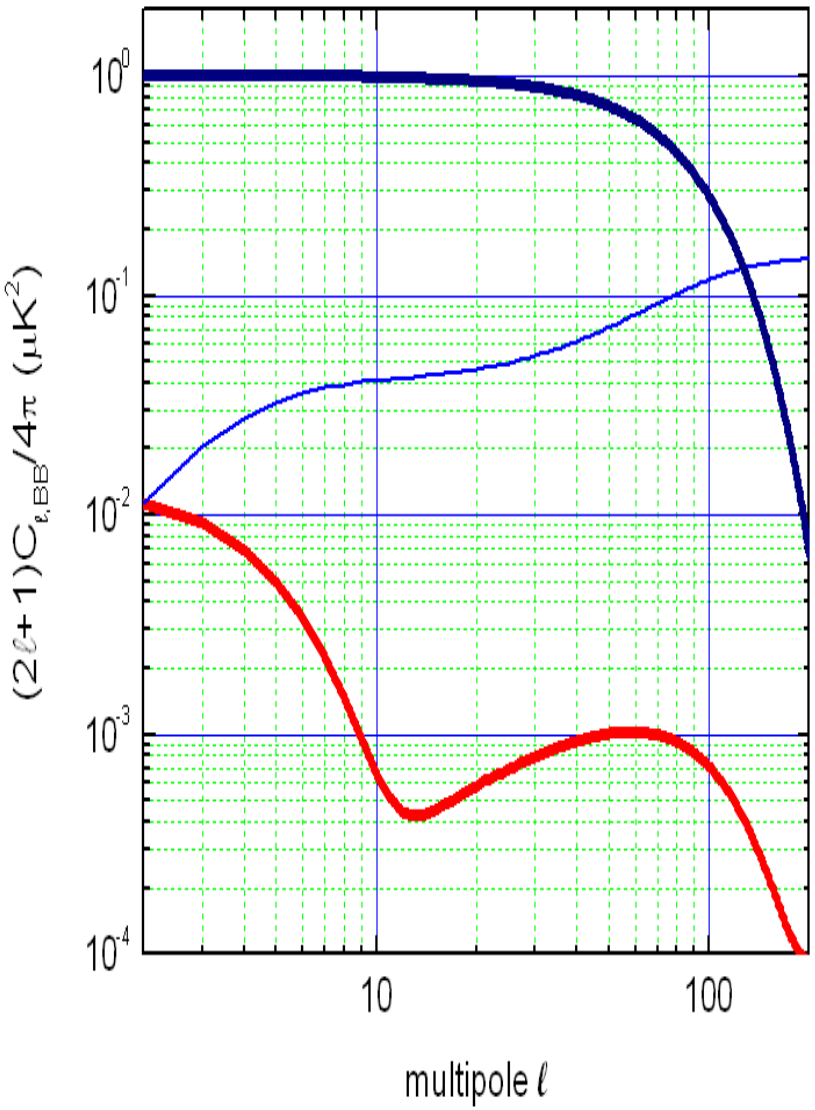

main target : reionization peak

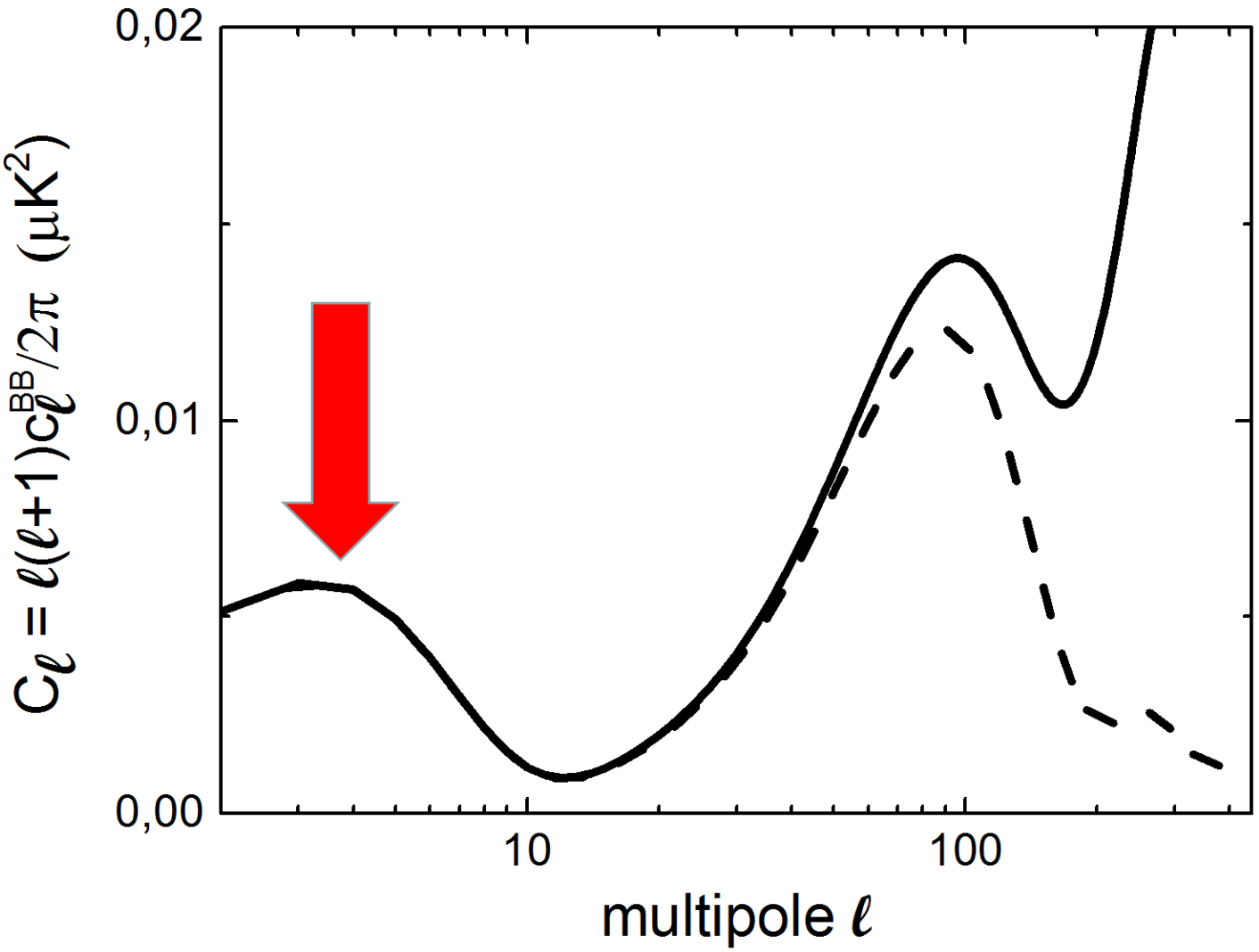

A difficult but important target, to complement measurements of the ℓ=80 peak !

the reionization peak is difficult

- Large angular scales: wide sky coverage required.
- Foreground contamination is high. From *Planck intermediate results XXX: The angular power spectrum of polarized dust emission at intermediate and high Galactic latitude*
  - Dust B-modes in the best 30% of sky at 350 GHz:

$$D_\ell = \ell(\ell+1)C_\ell/2\pi$$

$$D_\ell = 14\mu K^2(\ell/80)^{-0.42}$$

  - Extrapolating to 150 GHz (factor 0.04^2)

$$D_\ell = 2.2\cdot 10^{-2}\mu K^2(\ell/80)^{-0.42}$$

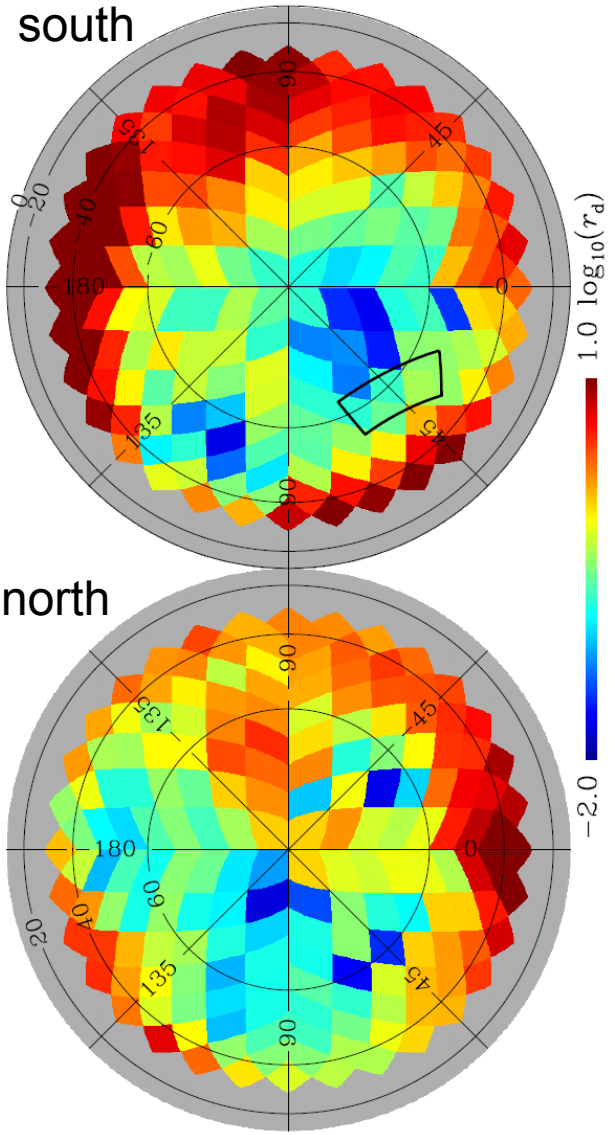

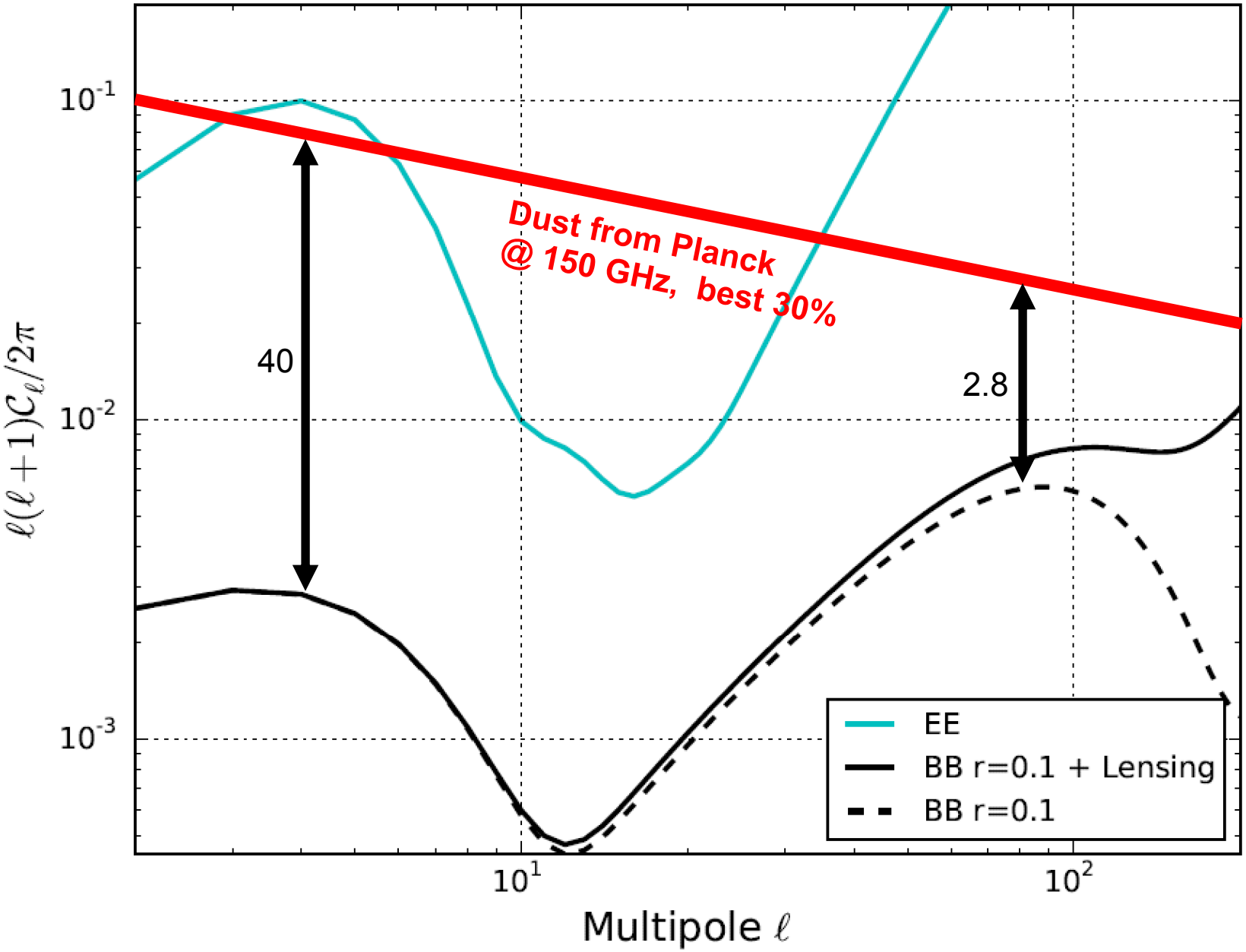
10^{-1}
10^{-2}
10^{-3}
$\ell(\ell+1)C_\ell/2\pi$
Dust from Planck
@ 150 GHz, best 30%
40
2.8
EE
BB r=0.1 + Lensing
BB r=0.1
10^1
10^2
Multipole ℓ

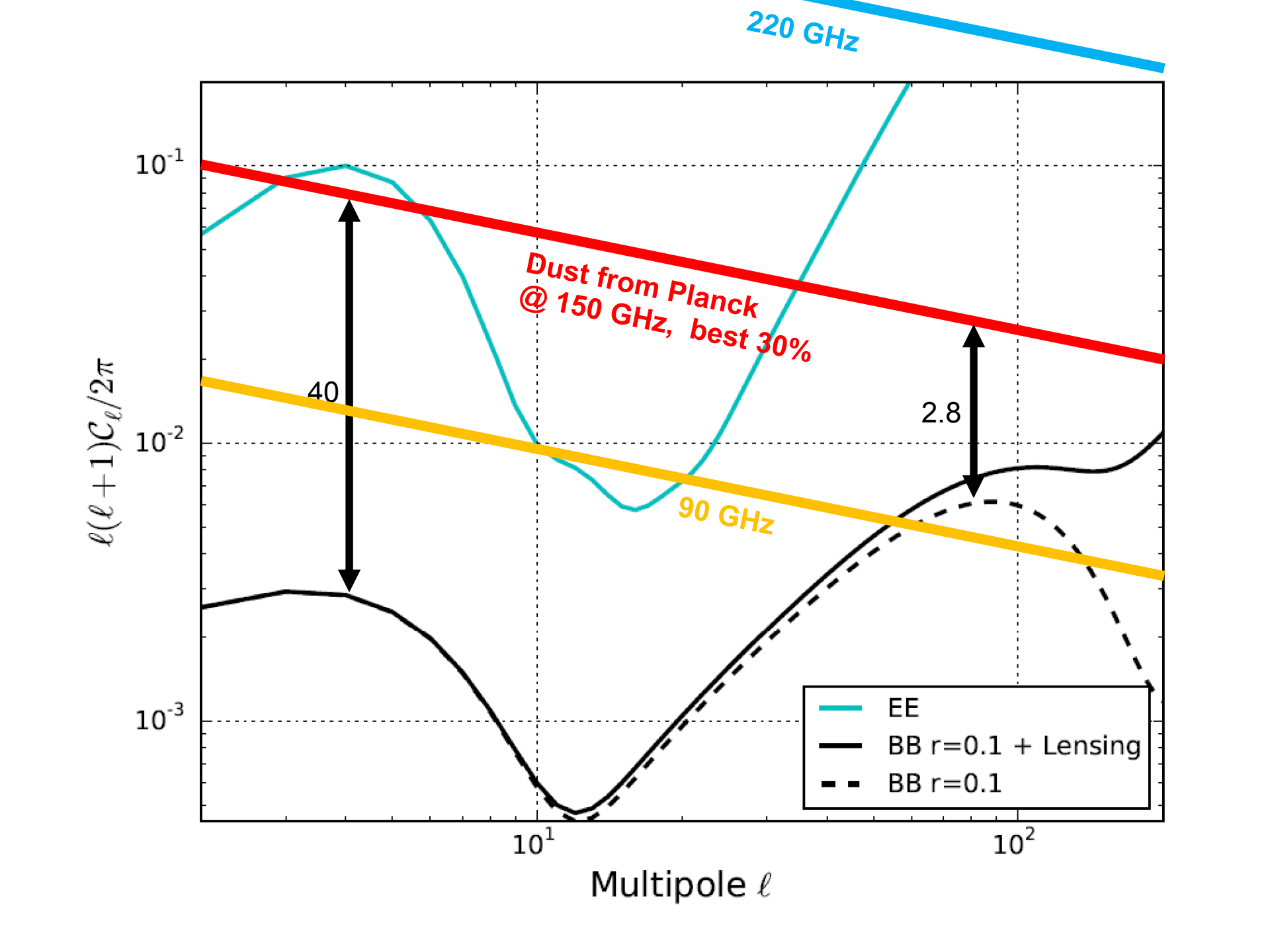
220 GHz
Dust from Planck
@ 150 GHz, best 30%
90 GHz
40
2.8
EE
BB r=0.1 + Lensing
BB r=0.1
10^{-1}
10^{-2}
10^{-3}
10^{1}
10^{2}
$\ell(\ell+1)C_\ell/2\pi$
Multipole ℓ

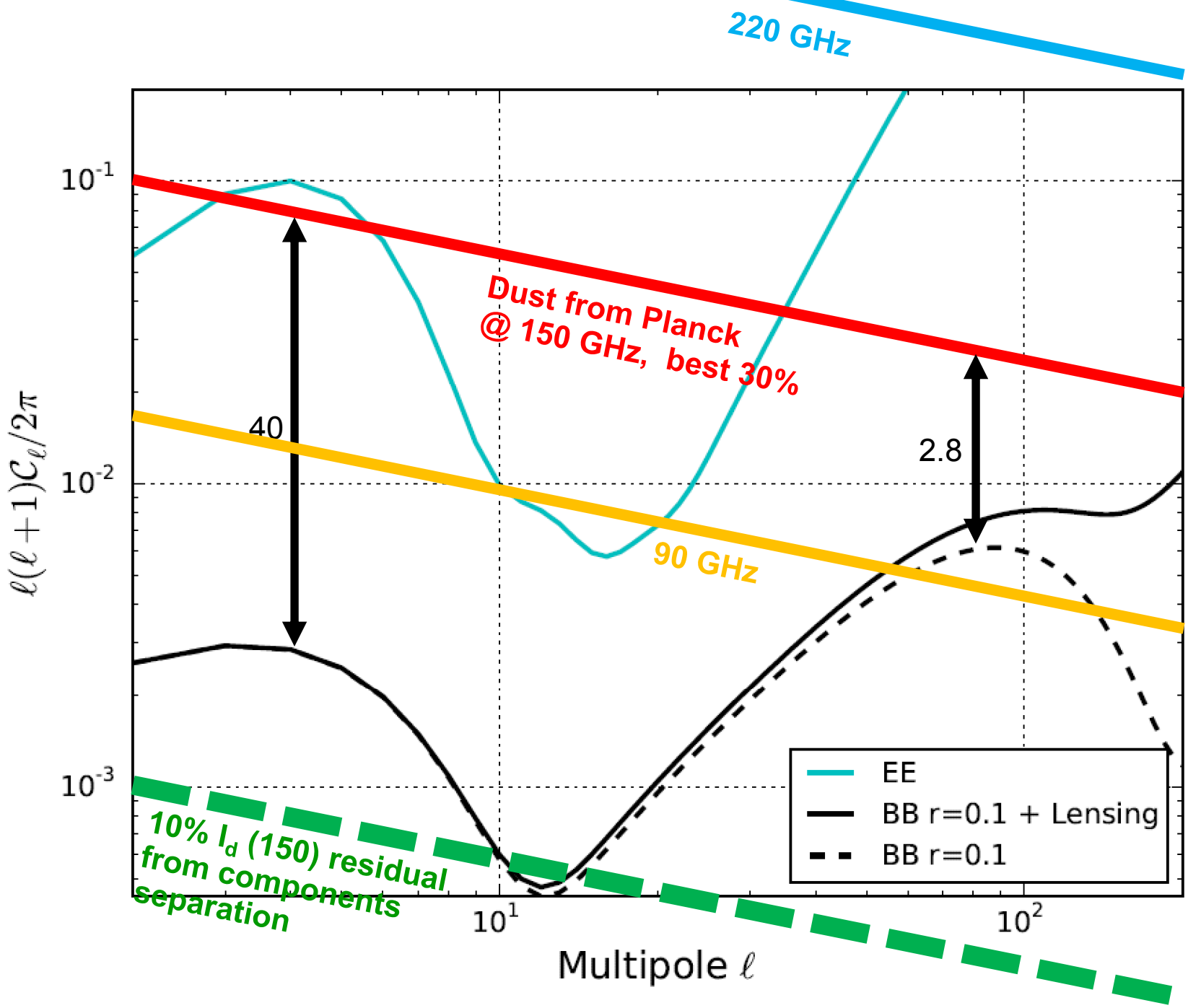
220 GHz
Dust from Planck
@ 150 GHz, best 30%
90 GHz
40
2.8
10% l_d (150) residual
from components
separation
EE
BB r=0.1 + Lensing
BB r=0.1
10^{-1}
10^{-2}
10^{-3}
10^{1}
10^{2}
$\ell(\ell+1)C_\ell/2\pi$
Multipole ℓ

Experiment Strategy

- Large sky coverage and wide frequency coverage call for a space mission. See e.g. COrE+ (just submitted !).
- On a shorter time-scale, experimentation is required to qualify specific instrumentation (optical systems, polarization modulators, detectors …) and methods (sky scan, mapping procedures, polarized foregrounds separation …) and possibly to get detections !
- A *balloon-borne instrument* can
  - avoid atmosperic noise and loading
  - exploit a wide frequency coverage
  - access a large fraction of the sky *during night-time*
  - offer a stable environment *during night-time*
  - reject ground spillover using very large ground-shields

LSPE in a nutshell

- The Large-Scale Polarization Explorer is :
  - an instrument to measure the polarization of the Cosmic Microwave Background at large angular scales
  - using *a spinning stratospheric balloon payload* to avoid atmospheric noise
  - flying *long-duration, in the polar night*
  - using a *polarization modulator* to achieve high stability
- Frequency coverage: 40 – 250 GHz (5 channels, 2 instruments: STRIP & SWIPE)
- Angular resolution: 1.3^{o} FWHM
- Sky coverage: 20-25% of the sky per flight
- Combined sensitivity: 10 μK arcmin per flight
- Current collaboration: Sapienza, UNIMI, UNIMIB, IASFBO-INAF, IFAC-CNR, Uni.Cardiff, Uni.Manchester. INFN-GE, INFN-PI, INFN-RM1, INFN-RM2
- See astro-ph/1208.0298, 1208.0281, 1208.0164 and forthcoming updates

LSPE gondola : frame + pivot + STRIP + SWIPE

Preliminary sketch of the LSPE experiment, without thermal protections.
The total mass is around 2.5 tons, the overall dimensions are 5.8m(w) x 3.2m(d) x 4.6m (h).
A 800000 m^3 balloon is used to lift the instrument at 37 km of altitude.

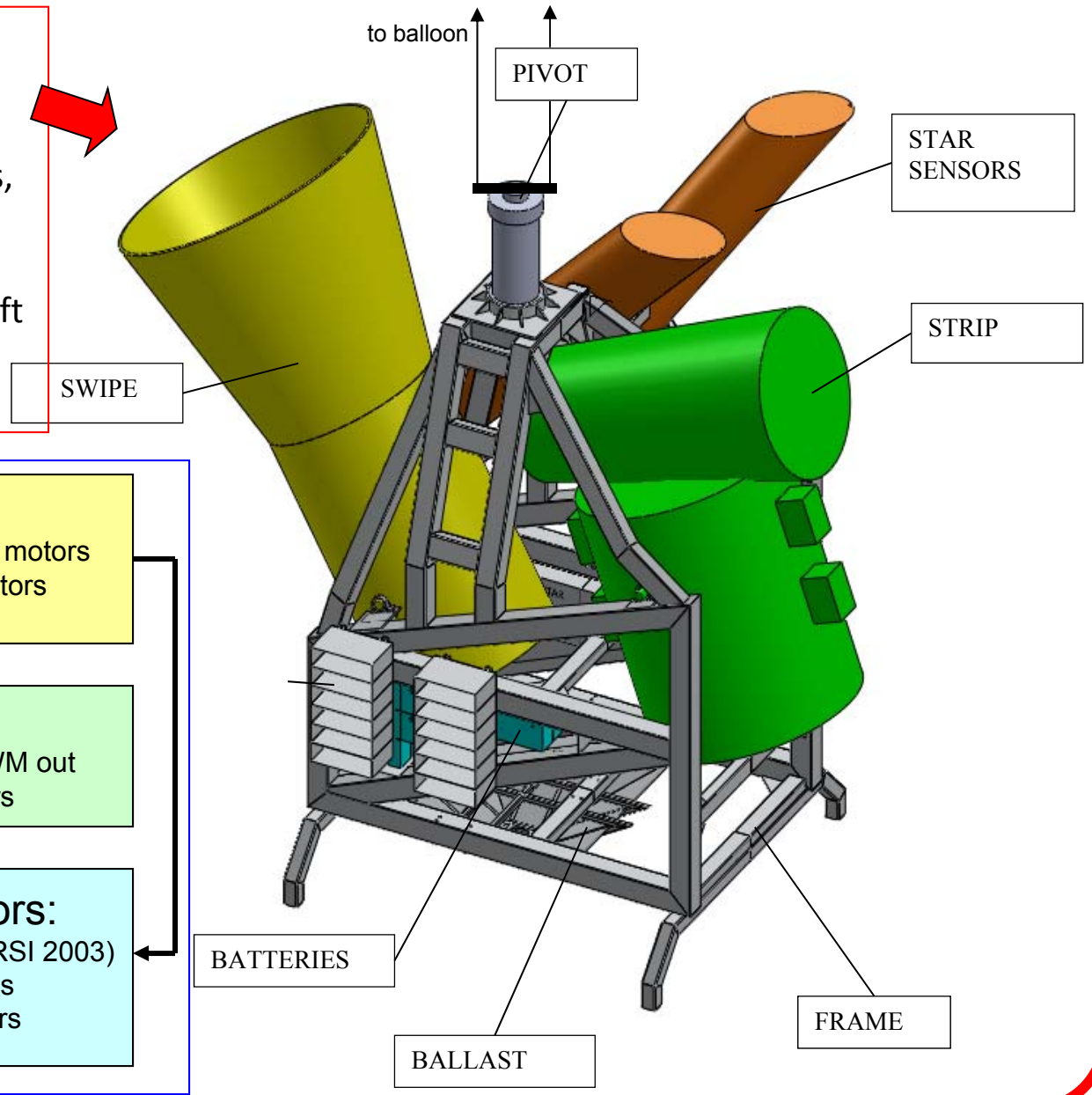

ACS block diagram

Actuators:
Azimuth pivot with torque motors
Linear elevation actuators

Processor:
PC104 with ADC in / PWM out
H-bridges for motors

TM
TC

Attitude sensors:
Star sensors (Nati et al. RSI 2003)
Laser Gyroscopes
Elevation Encoders

Sky coverage of LSPE

(Launch from Longyearbyen, Svalbard)

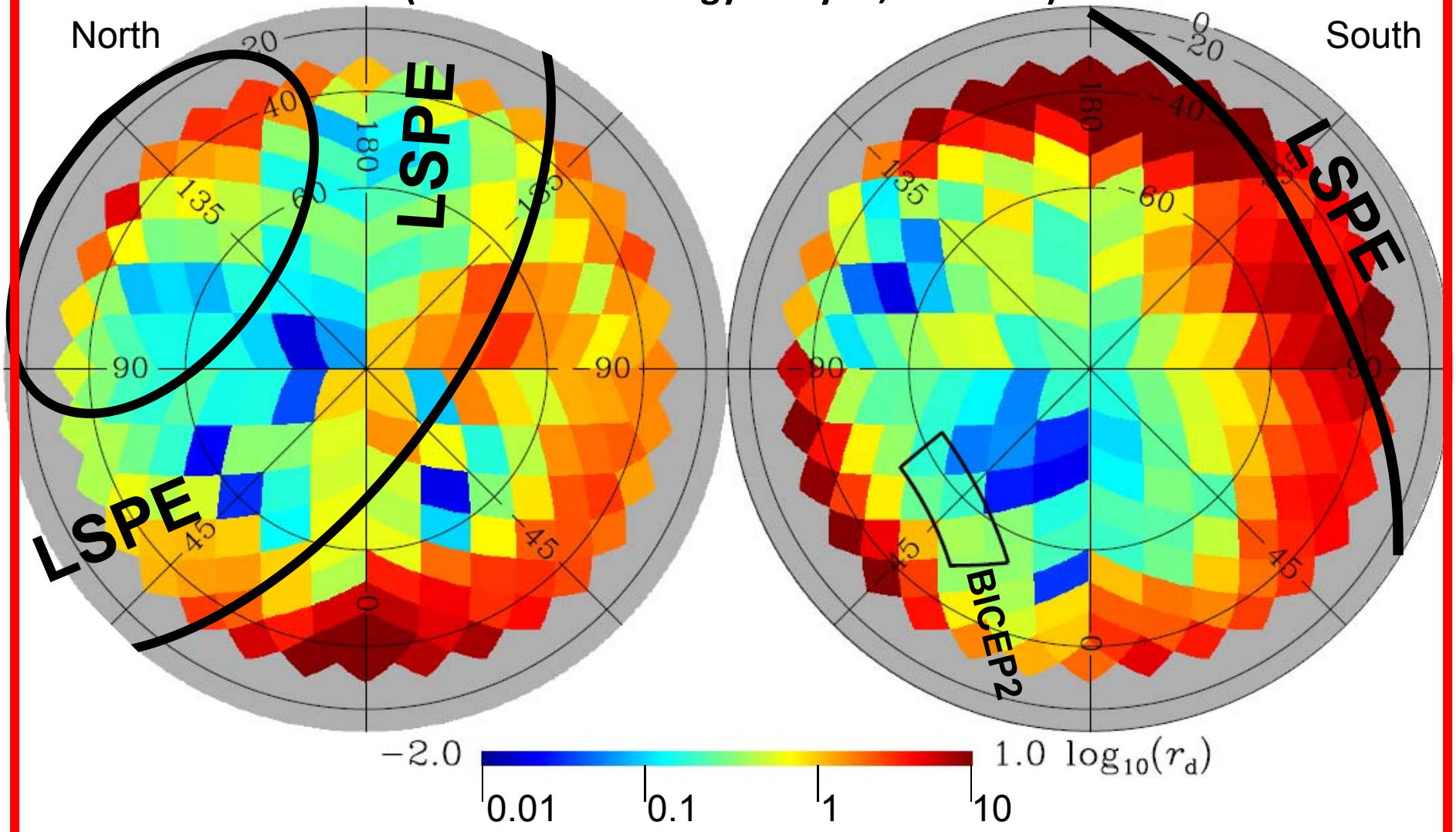

B-modes from dust @140 GHz, as estimated from Planck 343 GHz dust polarization - Planck PIP XXX 1409.5738

The STRIP Instrument

- STRIP is the STRatospheric Italian Polarimeter, aimed at accurate measurements of the low-frequency (44 and 90 GHz) polarized emission, dominated by Galactic synchrotron.
- Its sensitivity at 44 GHz in a single flight is twice better than the final sensitivity of the Planck LFI survey.
- The correlation radiometers are contained in a large cryostat and cooled at 20K by evaporating ^{4}He.

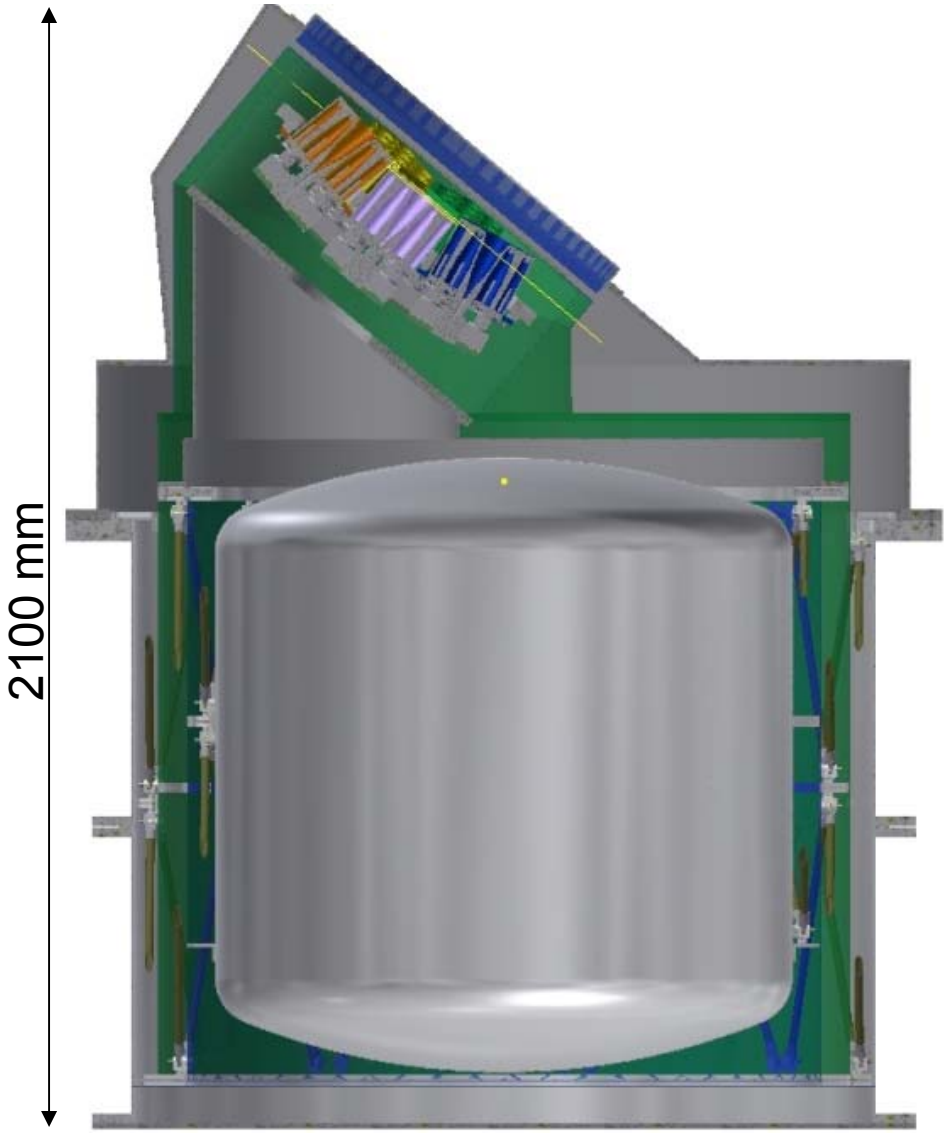

The STRIP Instrument

- The beam is defined by a 600 mm aperture side-fed crossed-Dragone telescope, selected for best polarization purity
- Challenging for spillover, stray-light and obscuration
- Modular Primary and secondary mirrors to reduce fabrication costs
- Lightened structure to reduce weight

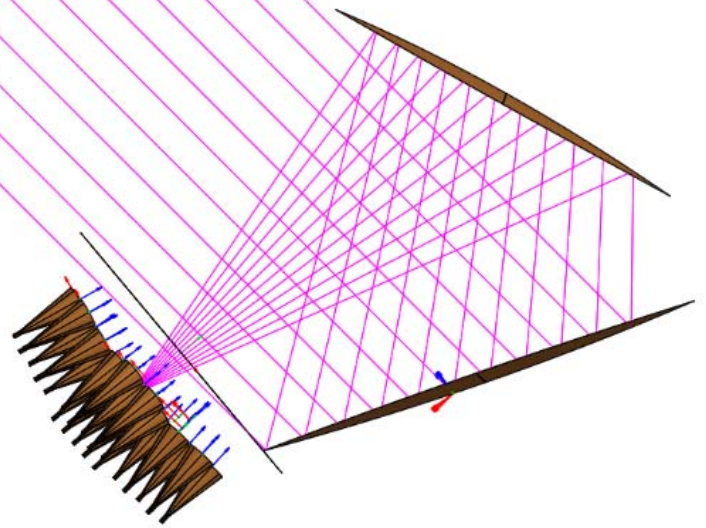

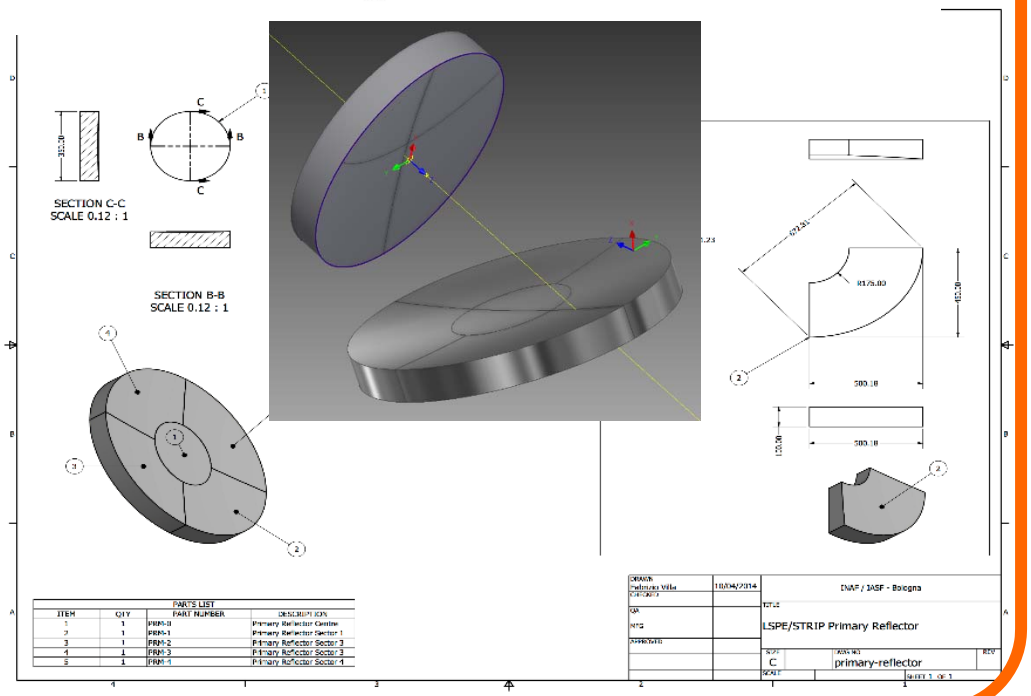

The STRIP Instrument

- In the focal plane, an array of 44 GHz platelet feedhorns (already manufactured) feeds high performance OMTs and LNAs derived from the QUIET exp.
- The measured response of the corrugated feedhorns confirms the expected performance down to -55 dB

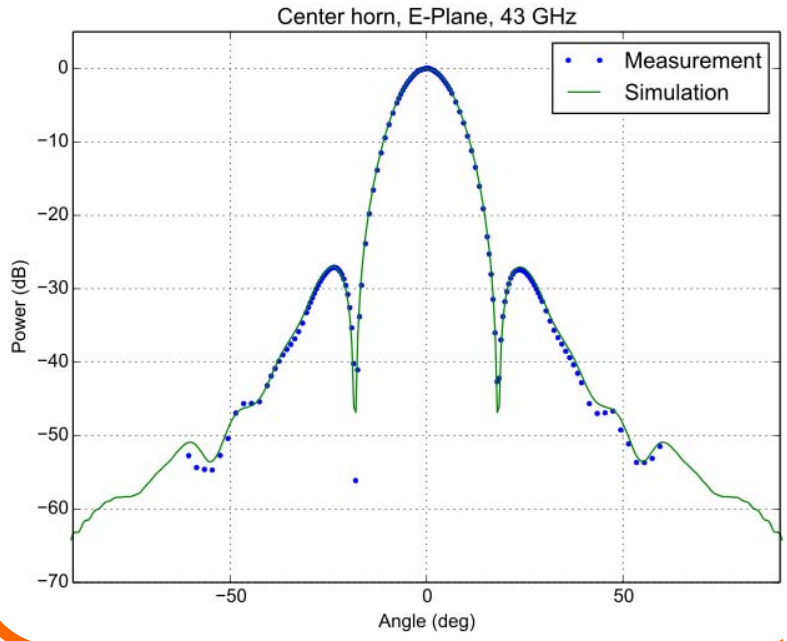

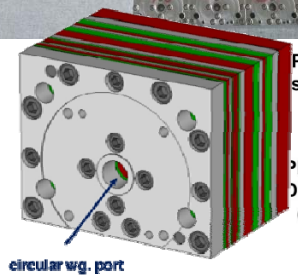

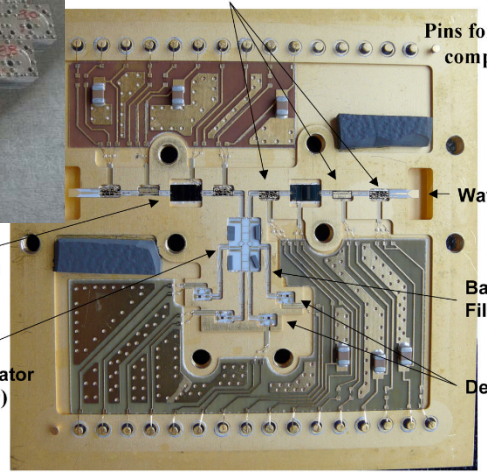

The SWIPE Instrument

- SWIPE is the Short Wavelength Instrument for the Polarization Explorer
- It is a Stokes Polarimeter, based on a simple 50 cm aperture refractive telescope, a cold HWP polarization modulator, a beamsplitting polarizer, and two large focal planes, filled with multimode bolometers at 140, 220, 240 GHz.
- Everything is cooled by a large L^{4}He cryostat and a ^{3}He refrigerator, for operation of the bolometers at 0.3K

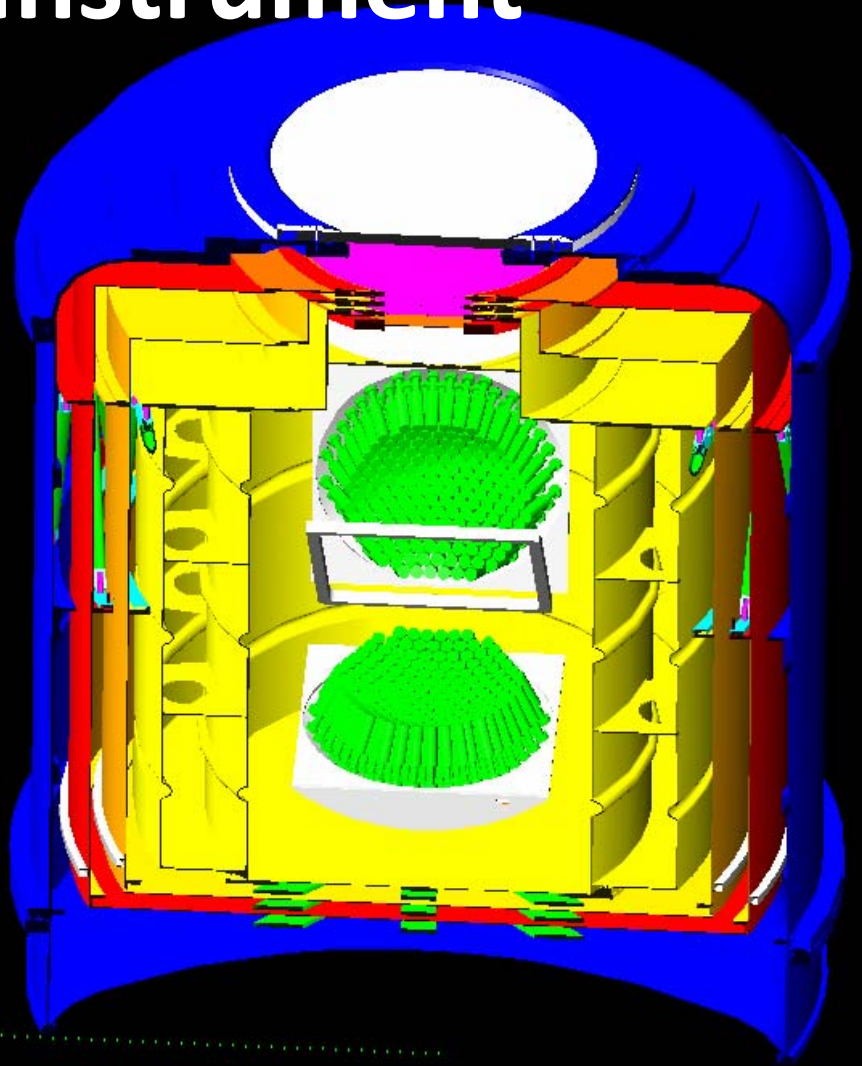

SAPIENZA UNIVERSITÀ DI ROMA
MANCHESTER 1824
CARDIFF UNIVERSITY
PRIFYSGOL CAERDYDD
INFN Istituto Nazionale di Fisica Nucleare

A cryogenic Stokes polarimeter

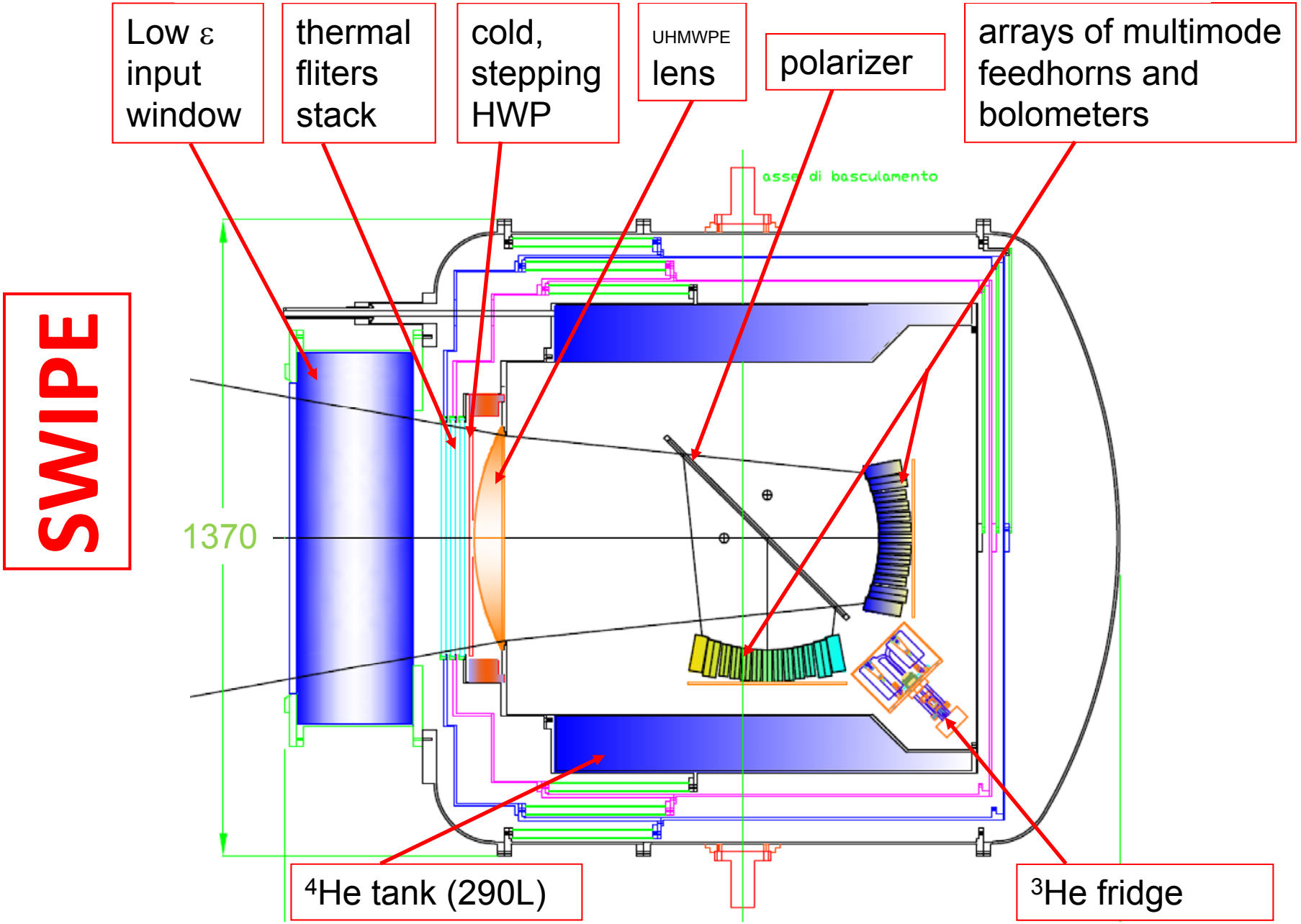

SWIPE – polarization modulator

- Is a cold (2K), large (50 cm useful dia.), wide band metamaterials HWP, placed immediately behind the window and thermal filters stack.
- HWP characteristics for the ordinary and extraordinary rays are well matched: $(T_o-T_e)/T_o < 0.001$, $X_{pol}<0.01$, over the 100-300 GHz band.
- Its orientation is stepped by 11.25° or 22.5° every few scans.

The cryogenic HWP rotator made for the PILOT experiment. The LSPE one will be based on the same design, and scaled up in dimensions (see Salatino et al. A&A 528 A138 2011)

SWIPE – optical system

- Single lens UHMWPE @4K, AR coating, D=480, f=800
- Two curved focal planes populated with multimode bolometric detectors, resulting in 1.2°FWHM beams

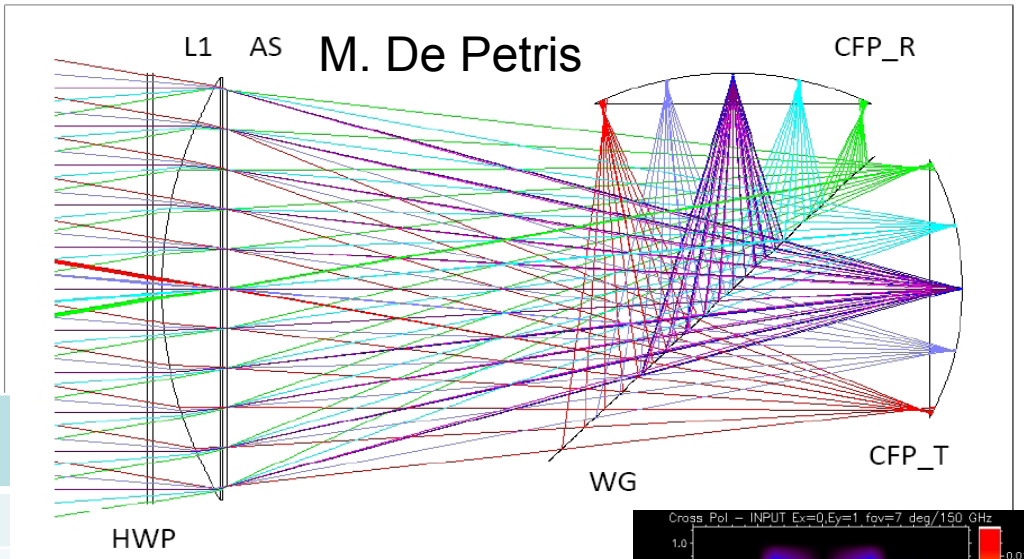

Band (GHz)	Width (%)	Total # detectors	# λ^2 modes
140 GHz	30	110	10
220 GHz	5	110	21
240 GHz	5	110	23

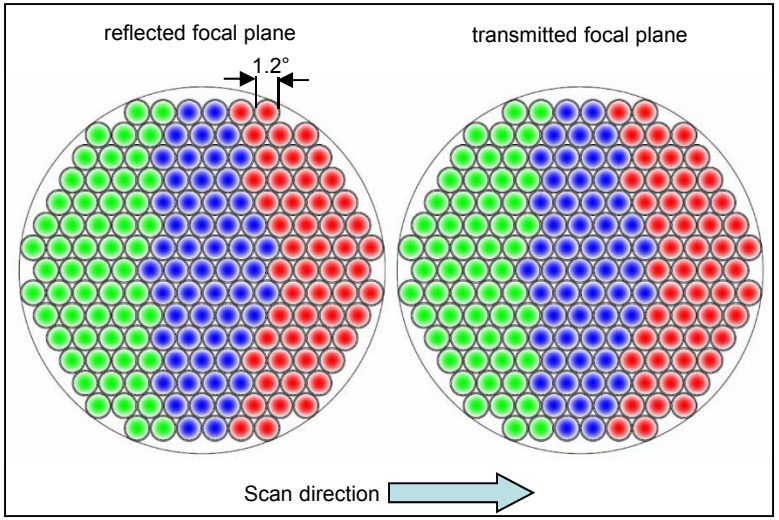

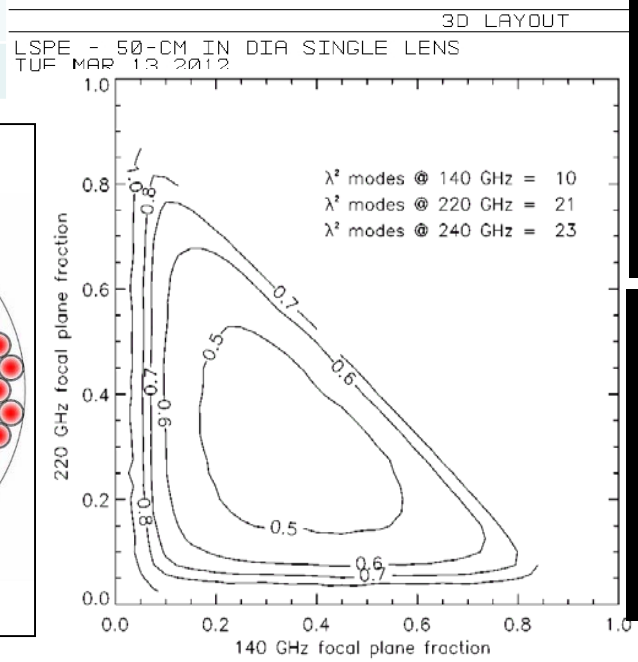

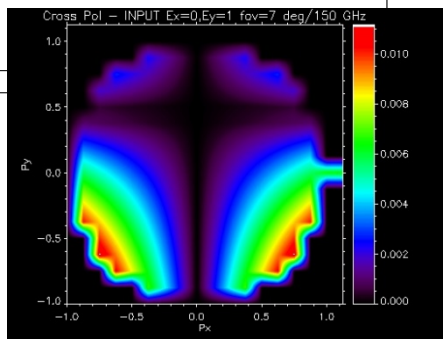

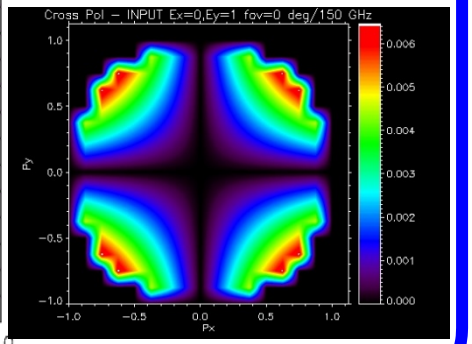

SWIPE – multimode feedhorns

- 20 mm aperture
- High efficiency coupling structure, easy to machine
- Nice top-hat beams
- 10, 21, 23 λ^2 modes @ 140, 220, 240 GHz

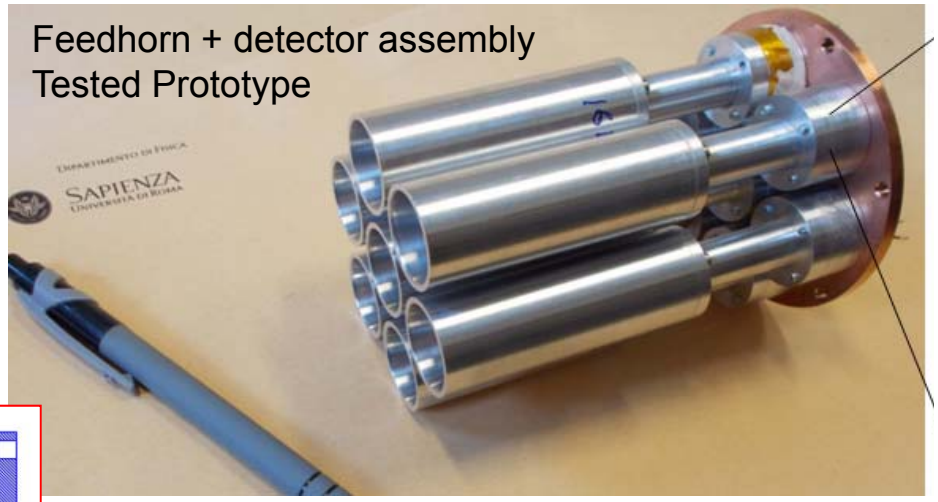

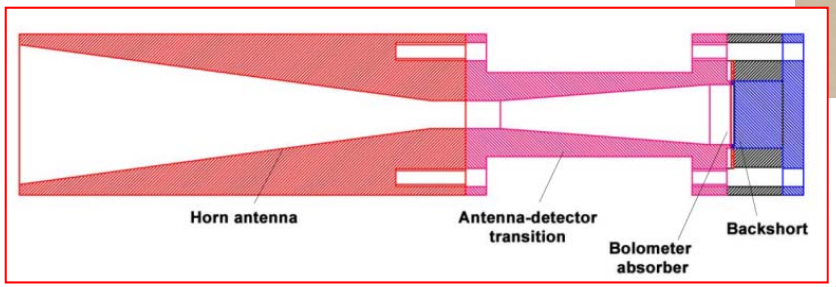

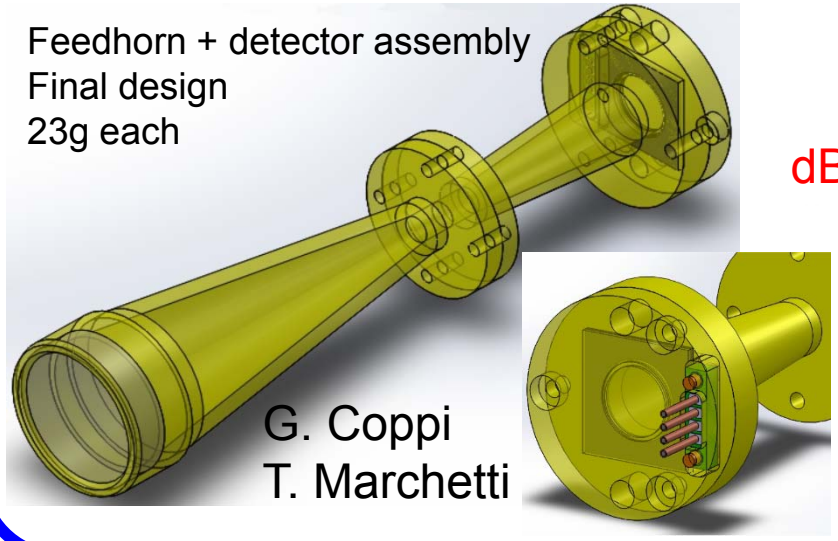

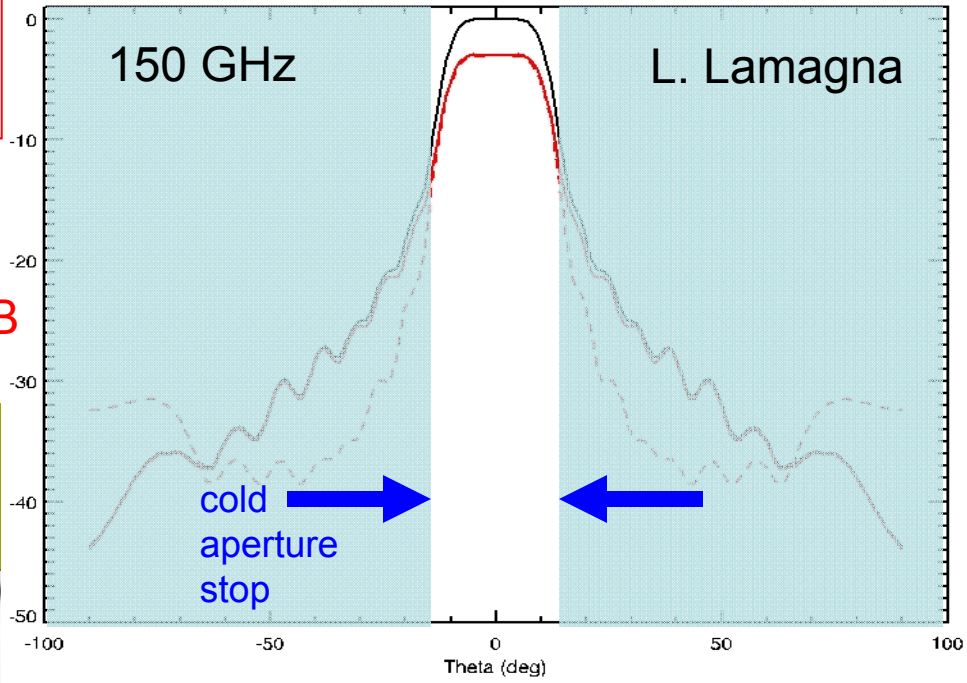

SWIPE - multimode absorbers & TES

- The absorbers are large Si_3N_4 spider-webs (8 mm diameter, multimode)
- Sensors are Ti-Au TES
- Photon noise limited
- τ = 2 ms

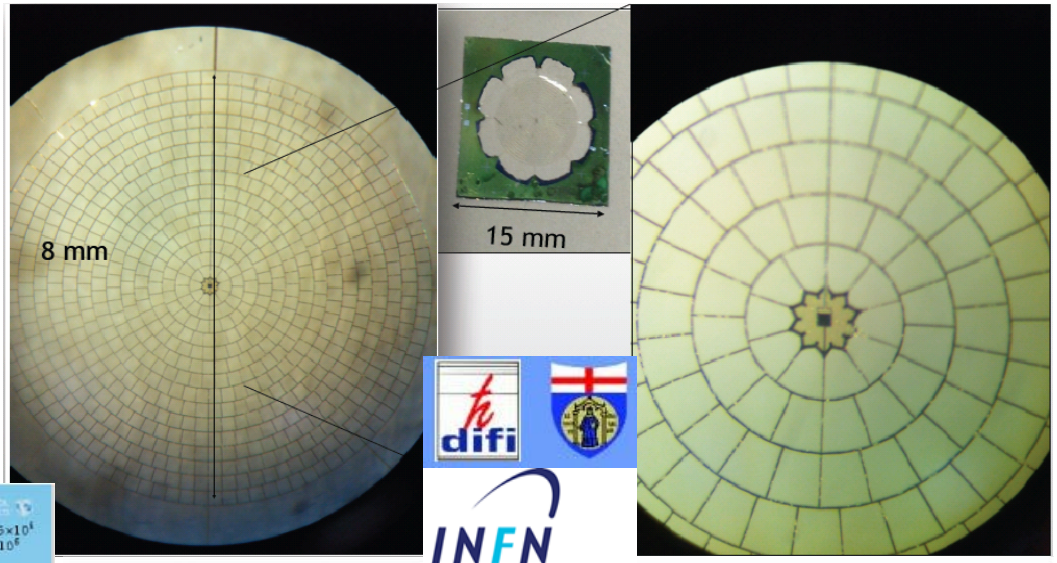

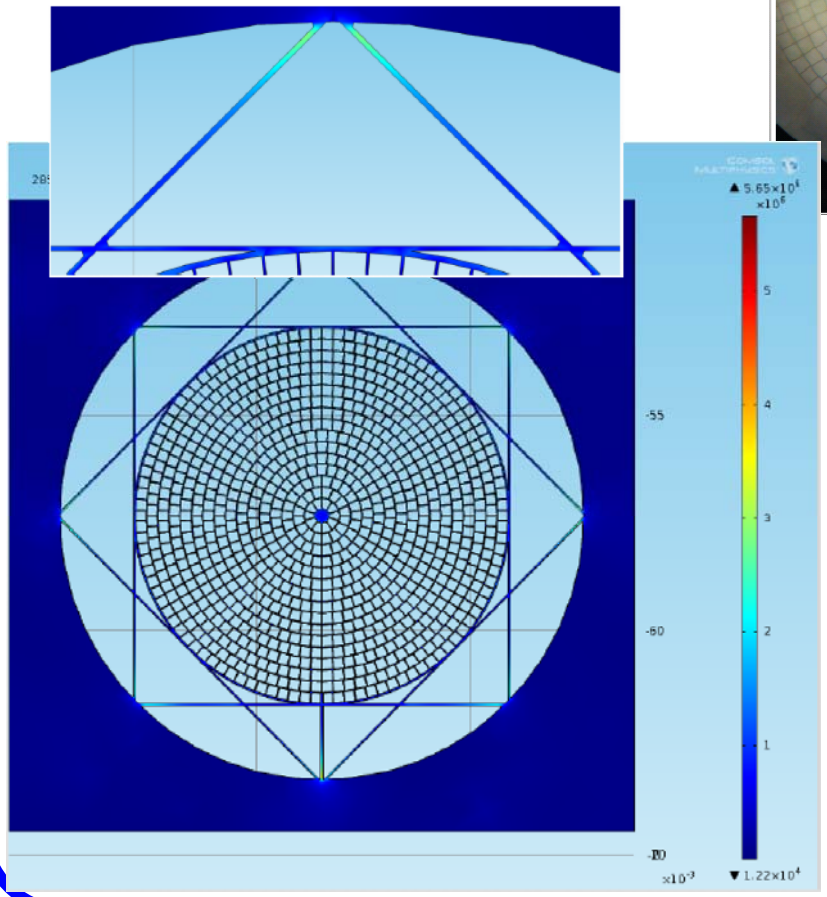

INFN
Istituto Nazionale di Fisica Nucleare

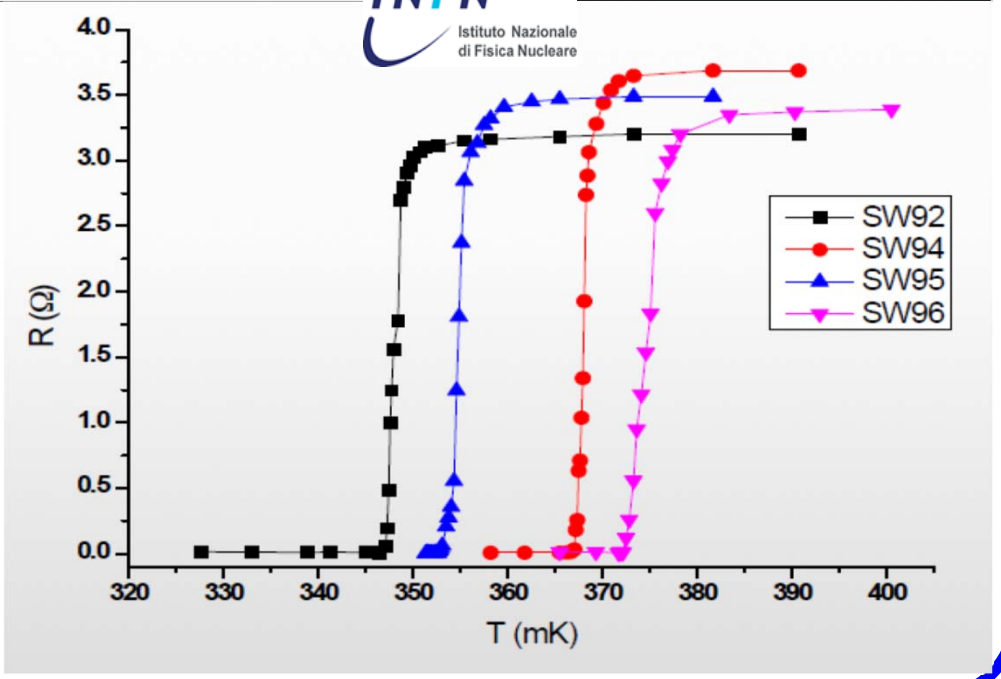

SWIPE - cryostat

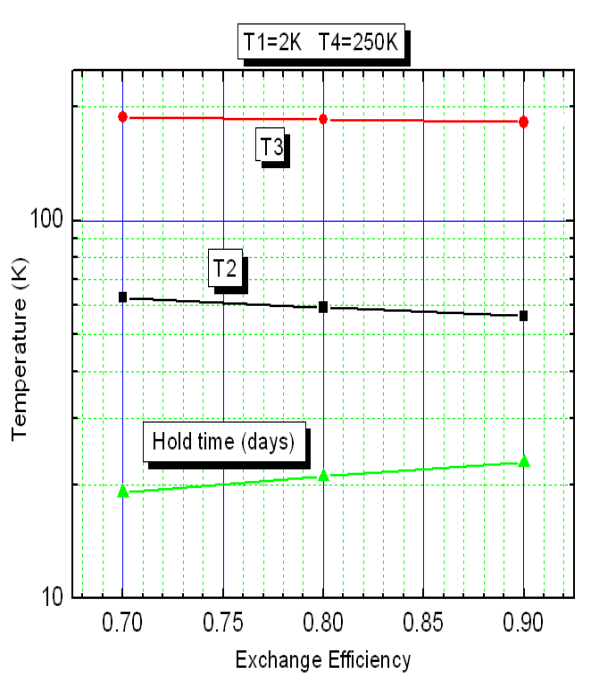

mass = 460 kg

He volume = 0.9 x 290 lt

Hold time = 19 .. 23 days

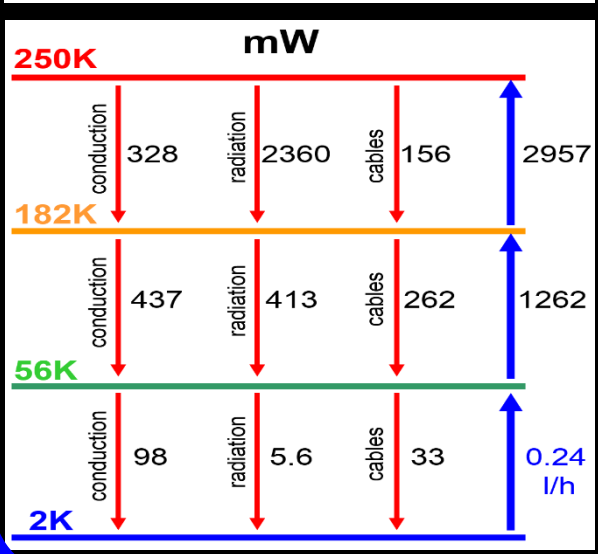

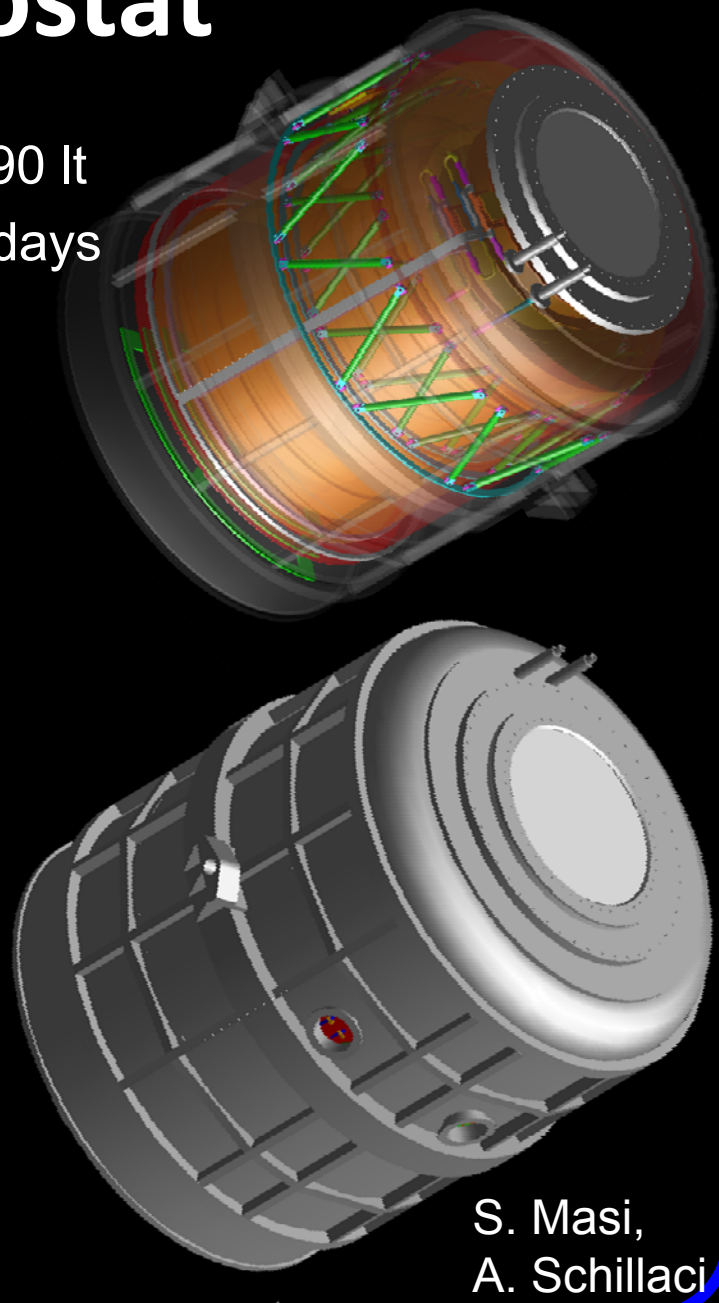

S. Masi,
A. Schillaci

Observations and Calibration Plan

- Scanning strategy: payload spin in azimuth, at 3 rpm (18°/s)
- Coverage of the same sky area by the two instruments
- Elevation changes once a day, at the same time for both instruments
- Specific calibration observations of
  - Jupiter (to map the main beam, see figure below, samples = white dots)

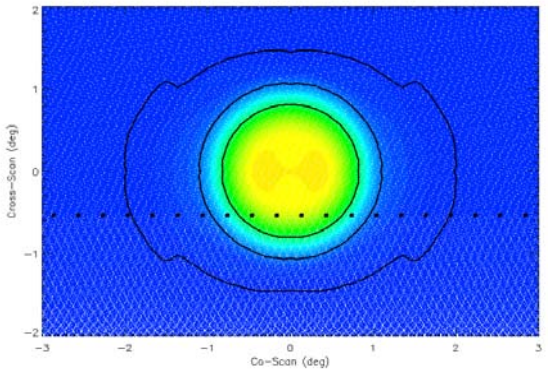

  - the Crab nebula and the Moon Limb (to calibrate the main axis of the polarimeters)
  - the Moon can be used to map sidelobes

LSPE coverage for different sets of elevation changes. The first column reports the boresight elevation range in degrees for the two instruments. Second column, the full coverage. Third column, the coverage after masking the galaxy with the WMAP polarization mask.

Elevation	Coverage	Unmasked
SWIPE [30-40]	31%	23%
SWIPE [40-50]	27%	20%
SWIPE 35	24%	19%
SWIPE 45	22%	18%
SWIPE [30-50]	35%	26%
STRIP 45	27%	20%
STRIP 30	33%	24%

		STRIP			SWIPE	
Source	Culmination (deg)	S/N per sample at 44 GHz	S/N per sample at 90 GHz		S/N per sample at 145 GHz	S/N per sample at 245 GHz
Moon	30	37500	200000		700000	2000000
Crab	34	20	18		23	28
~~Mars~~	0	0.30	1.6		5.6	18
Jupiter	27	15	80		275	850
~~Saturn~~	-6	1.4	7		24	70
~~Uranus~~	16	0.05	0.24		0.8	2.5

Sources culmination angle, and expected S/N per sample. Sampling rate is set at 60 Hz. We assume full Moon, as it is when it is observable by LSPE. The Crab flux is based on the free-free spectrum reported in Macías-Pérez, et al. Ap. J., 711, 417 (2010)

Performance Forecast

- The presence of the HWP allows to fully exploit the sensitivity of LSPE-SWIPE.
- Realistic simulations to assess systematic effects (mainly beam asymmetries) which become irrelevant if the HWP is used.
- The final sensitivity target for *r* is around 0.02

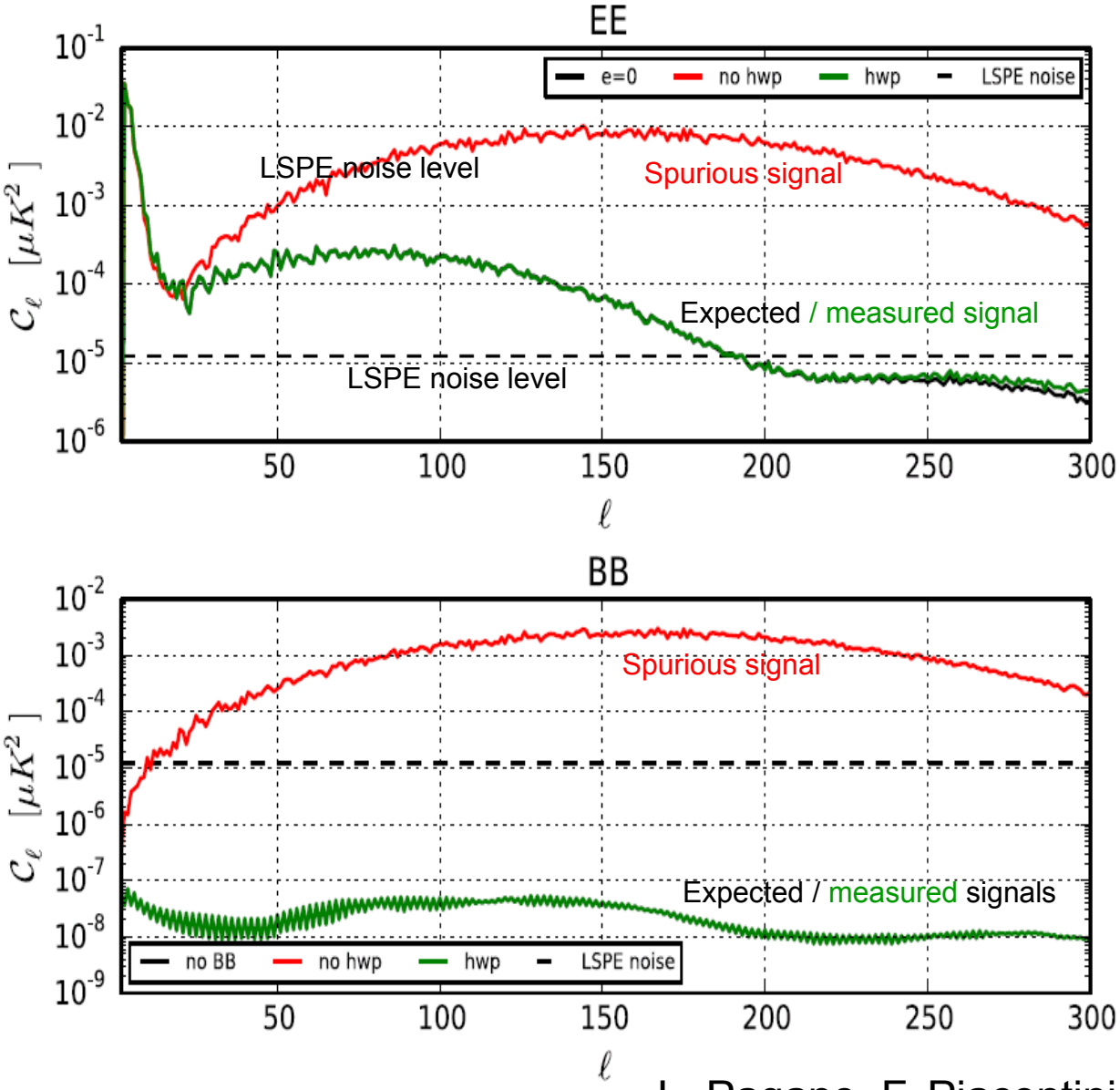

L. Pagano, F. Piacentini

SWIPE Performance Forecast (1st flight)

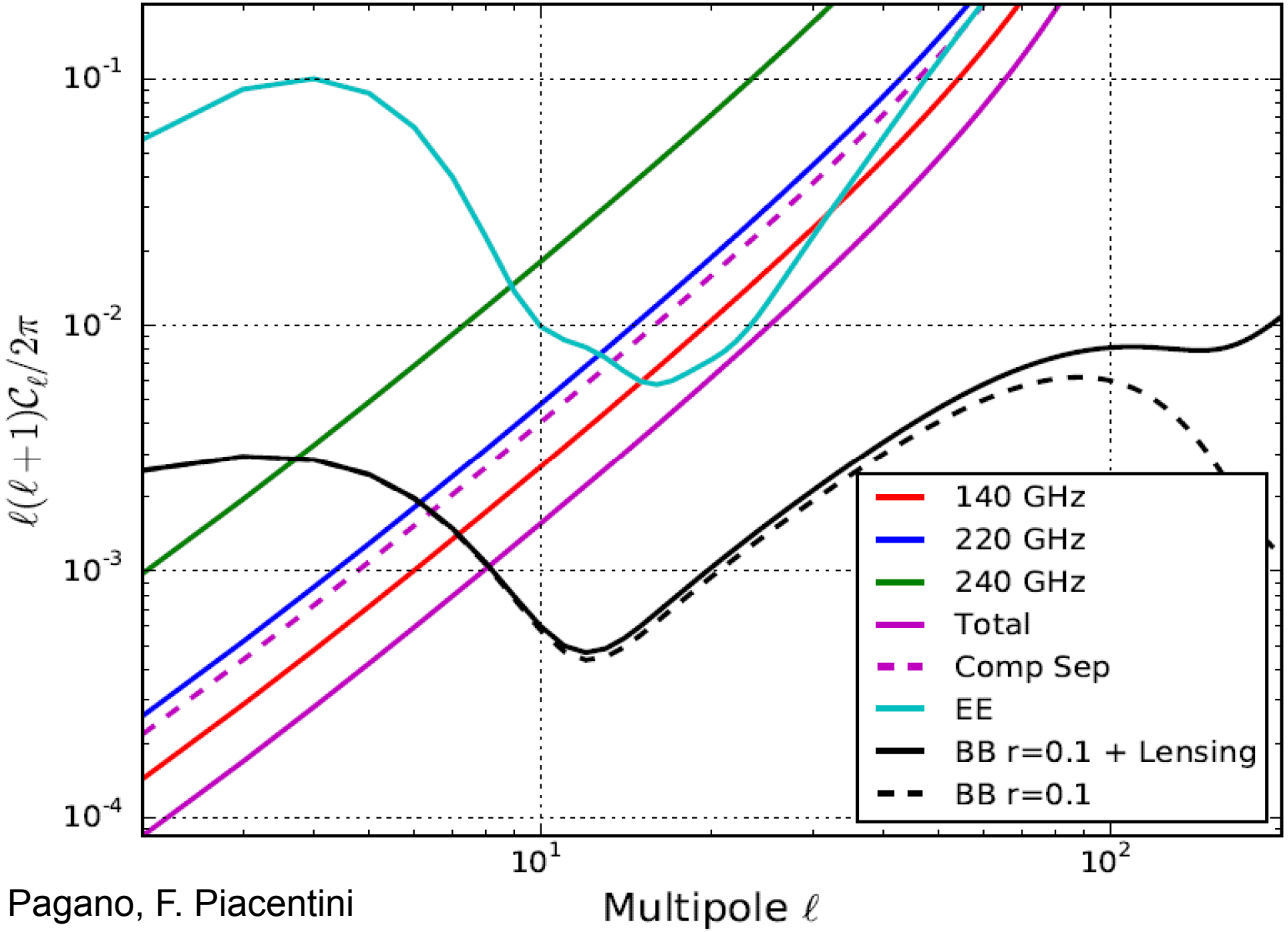

L. Pagano, F. Piacentini

SWIPE Performance Forecast (1st flight)

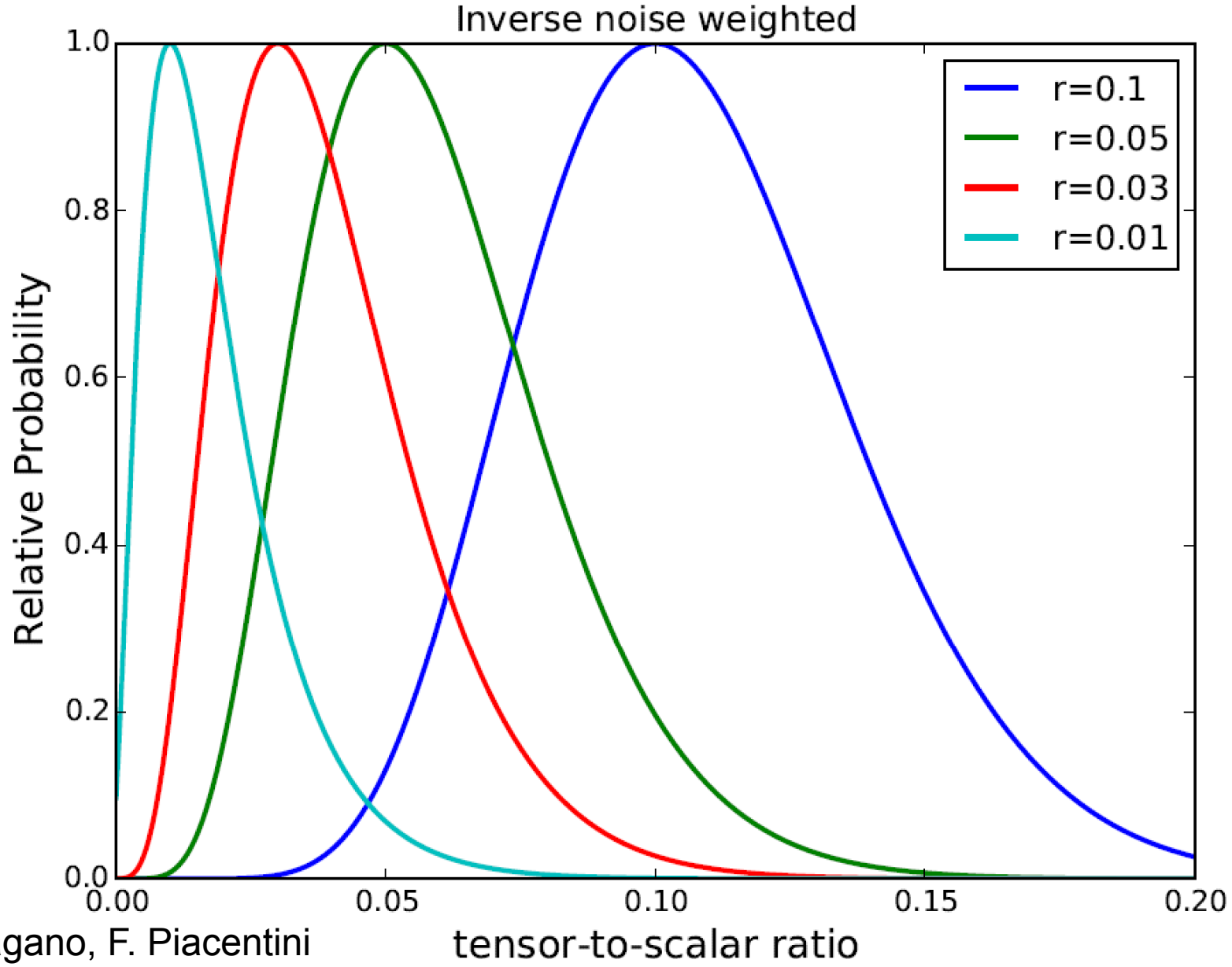

L. Pagano, F. Piacentini

Mission

- The experiment is flown as a stratospheric balloon payload during the polar night, in a long duration flight launched from Longyearbyen (Svalbard). In this way it can access most of the northern sky in a single flight,
  - without contamination from the sun in the sidelobes
  - within a very stable (cold!) environment
  - Accumulating more than 14 days of integration at float (38 km altitude).
- Flight scheduled by ASI for end of 2016

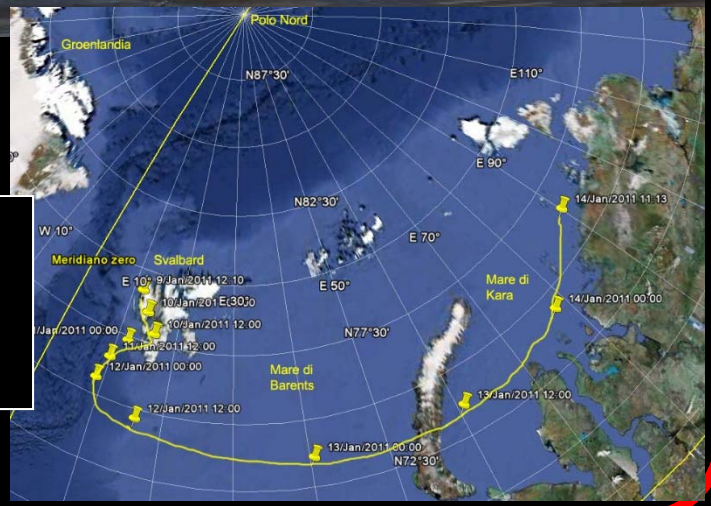

Bottom: Ground path of a small pathfinder test flight performed in January 2011, in the middle of the polar night. The eastward trajectory is evident.. **Top:** Launch of a heavy-lift balloon from the Longyearbyen airport (Svalbard Islands, latitude 78ºN).

See Peterzen, S., Masi, S., et al., "Long Duration Balloon flights development ", Mem. S. A. It., 79, 792-798 (2008) for further information on balloon flights from the Svalbard.

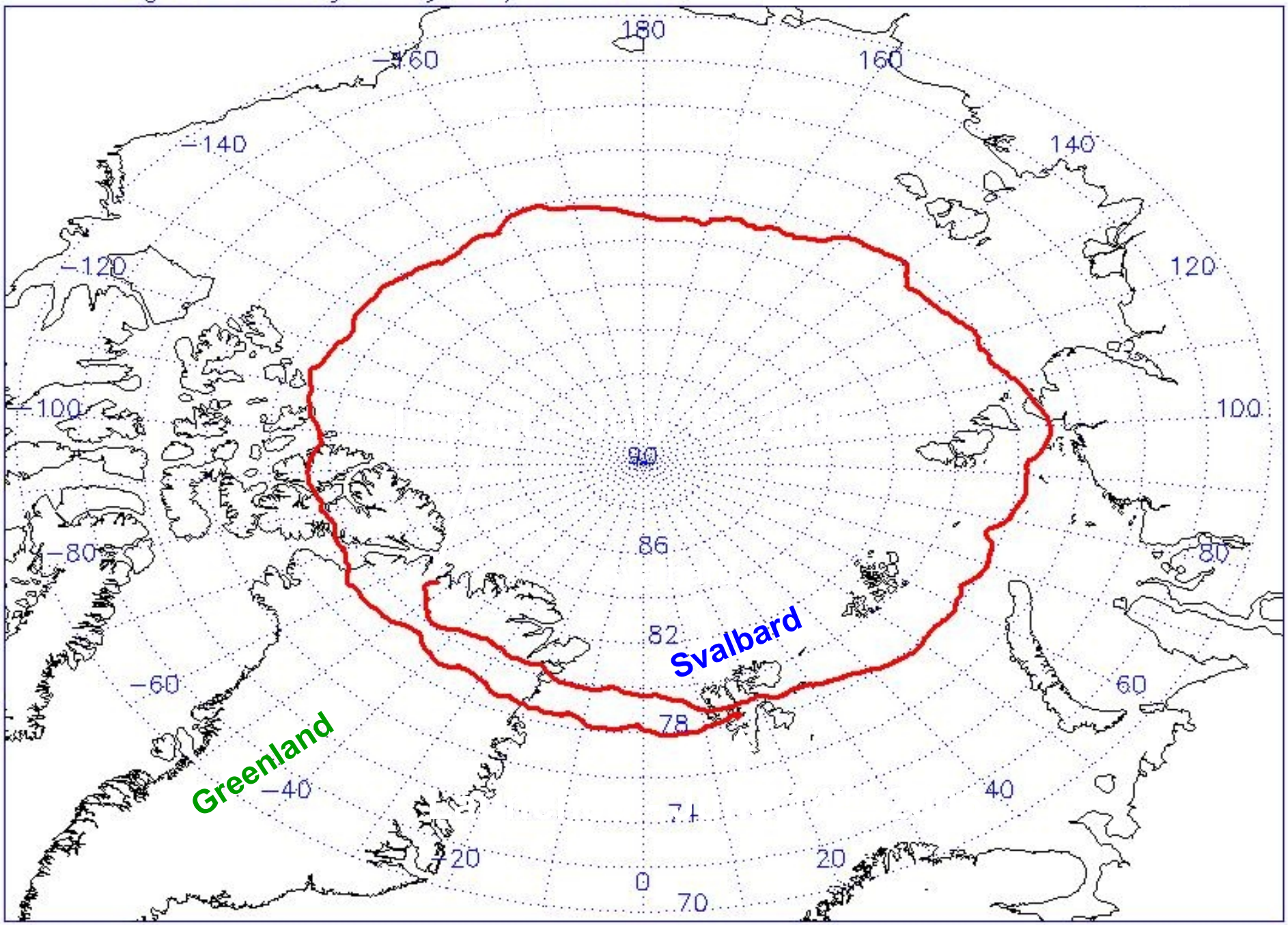
Pegaso–E trajectory 02/07 10:14
180
–160
160
–140
140
–120
120
–100
100
–80
80
–60
60
–40
40
–20
20
0
90
86
82
78
74
70
Svalbard
Greenland

sample flight profile

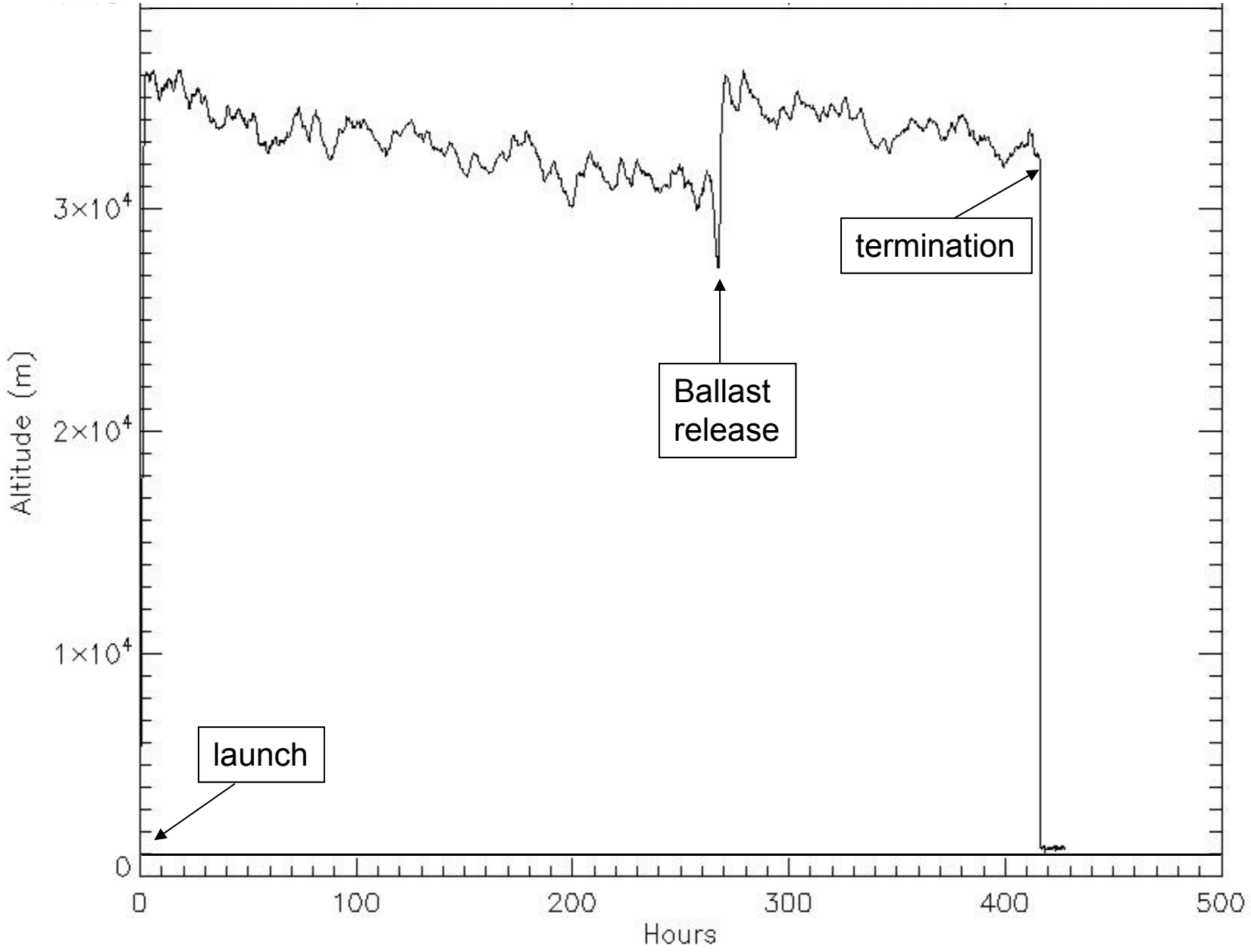

Night Time Long Duration Stratospheric Balloon Flights

1° LDB launched on Jan. 9°, 2011
From CNR Dirigibile Italia base
With support from ISTAR, AWIPEV
Ny Alesund, Svalbard Islands

5 days at 32 Km, Eastward path

Payload prepared by La Sapienza

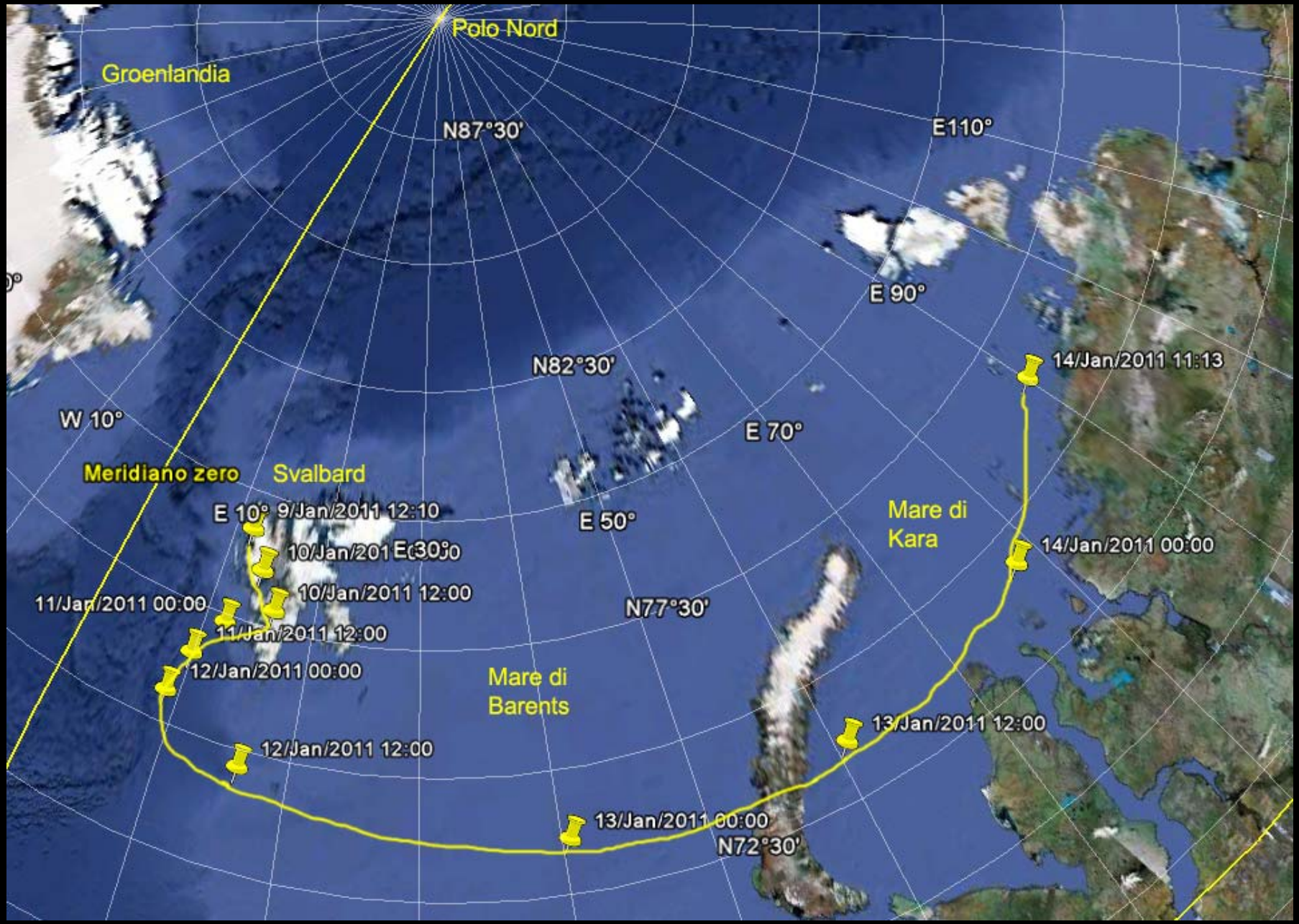
Polo Nord
Groenlandia
N87°30'
E110°
E 90°
N82°30'
14/Jan/2011 11:13
W 10°
E 70°
Meridiano zero
Svalbard
E 10°
9/Jan/2011 12:10
E 50°
Mare di
Kara
10/Jan/201
E 30°
14/Jan/2011 00:00
10/Jan/2011 12:00
11/Jan/2011 00:00
N77°30'
11/Jan/2011 12:00
12/Jan/2011 00:00
Mare di
Barents
13/Jan/2011 12:00
12/Jan/2011 12:00
13/Jan/2011 00:00
N72°30'

References

- The LSPE collaboration: *"The Large-Scale Polarization Explorer (LSPE)" Proc. SPIE* 8446, Ground-based and Airborne Instrumentation for Astronomy IV, 84467A (2012); doi: 10.1117/12.926095; astro-ph/1208.0281
- P. de Bernardis, et al. *"SWIPE: a bolometric polarimeter for the Large-Scale Polarization Explorer" Proc. SPIE* 8452, Millimeter, Submillimeter, and Far-Infrared Detectors and Instrumentation for Astronomy VI, 84523F (October 5, 2012); doi: 10.1117/12.926569; astro-ph/1208.0282 (2012).
- M. Bersanelli, et al. *"A coherent polarimeter array for the Large Scale Polarization Explorer balloon experiment" Proc. SPIE* 8452, Proc. SPIE 8446, Ground-based and Airborne Instrumentation for Astronomy IV, 84467C (24 September 2012); doi: 10.1117/12.925688 ; astro-ph/1208.0164 (2012).
- P. de Bernardis, S. Masi, for the OLIMPO and LSPE teams, "*Precision CMB measurements with long-duration stratospheric balloons: activities in the Arctic*", In Astrophysics from Antarctica - IAU Symposium **288**, Proceedings of the Internatonal Astronomical Union, 8, 208-213 (2013) M. G. Burton, X. Cui & N. F. H. Tothill, eds., Cambridge. doi: 10.1017/S1743921312016894
- Peterzen, S., Masi, S., et al., *"Long Duration Balloon flights development ",* Mem. S. A. It., 79, 792-798 (2008)
- F. Nati, A. Benoit, P. de Bernardis, A. Iacoangeli, S. Masi, D. Yvon, *A fast and reliable star sensor for spinning balloon payloads*, Review of Scientific Instruments, **74**, 4169-4175, (2003)

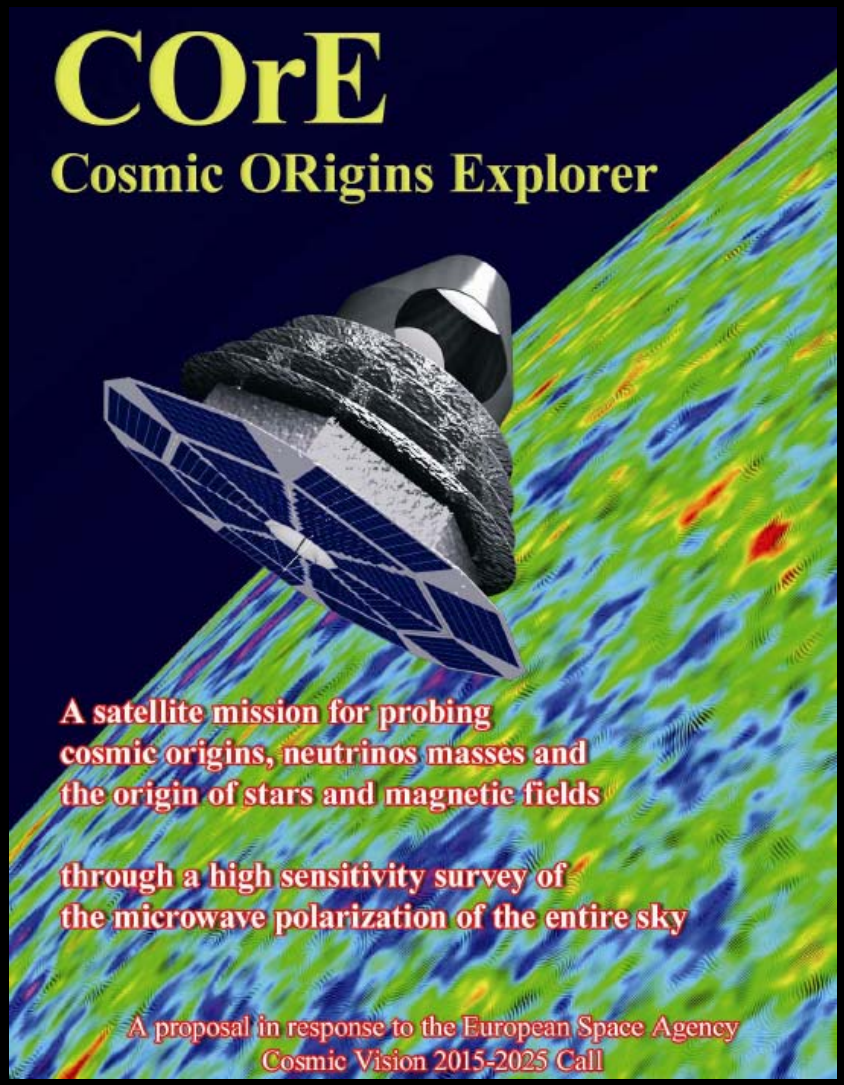

Call for medium missions – 2010-dec-03

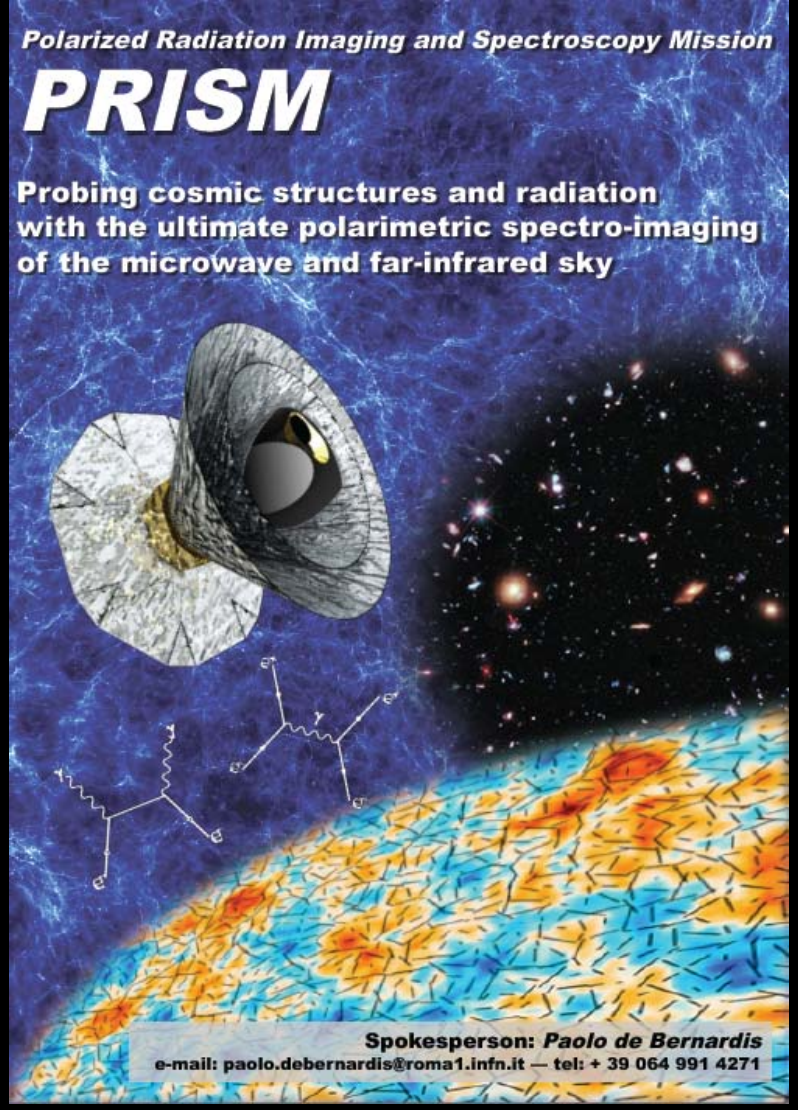

Call for science themes for Large Missions 2013-may-24

ESA call for M4 medium mission –

COrE+ submitted 15/1/2015, soon on the archive

COrE+ : The *COsmic Origins Explorer +*

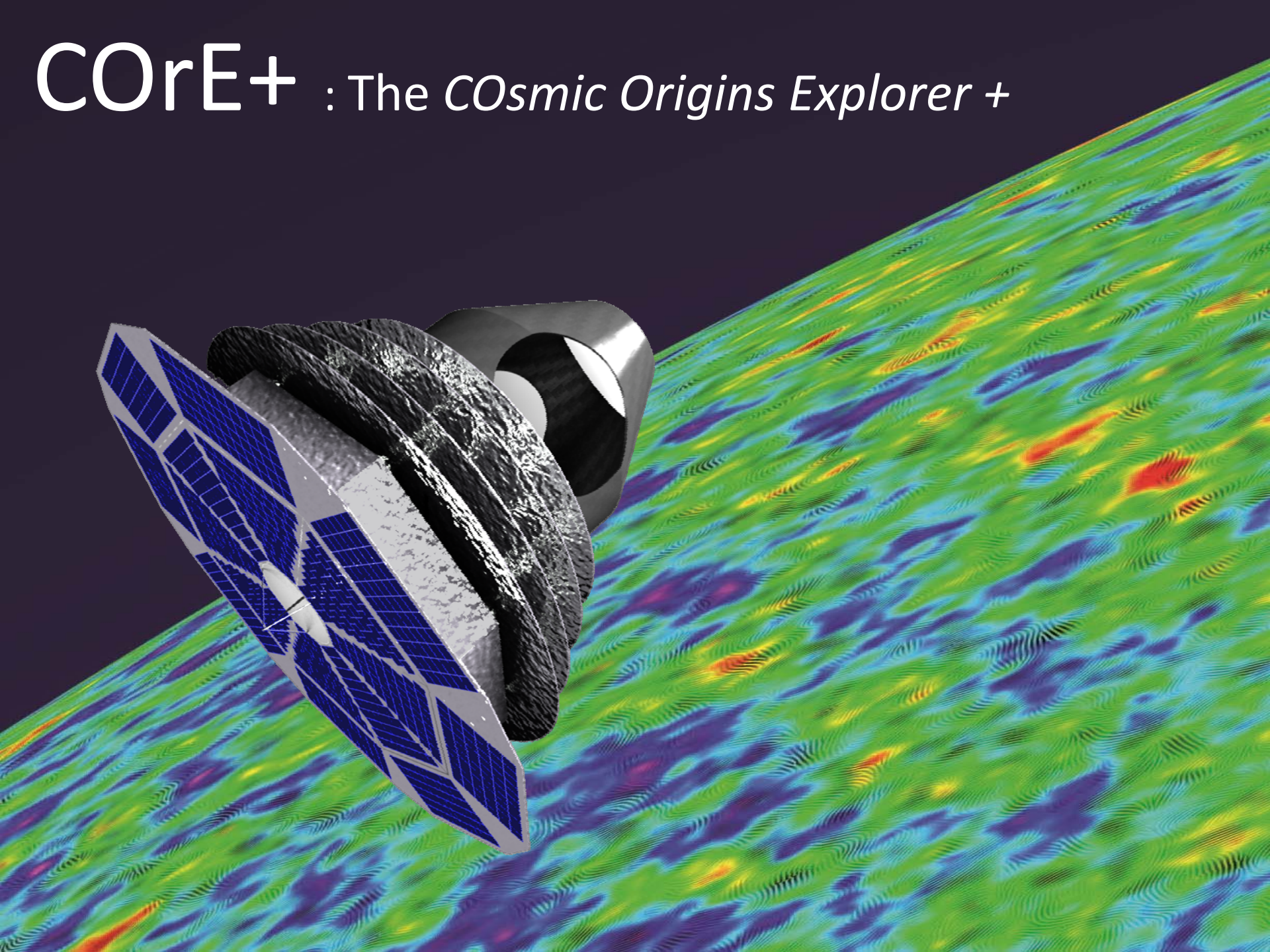

The Motivation

- **Planck** is the nearly-ultimate mission for the measurement of CMB temperature **anisotropy**
- **COrE+** targets at extracting ***nearly all*** the information present in CMB temperature ***and polarization*** anisotropy. This includes:
  - B-modes and inflation physics
  - Lensing potential and dark matter distribution
  - Neutrino masses & hierarchy
  - Extension of the standard model

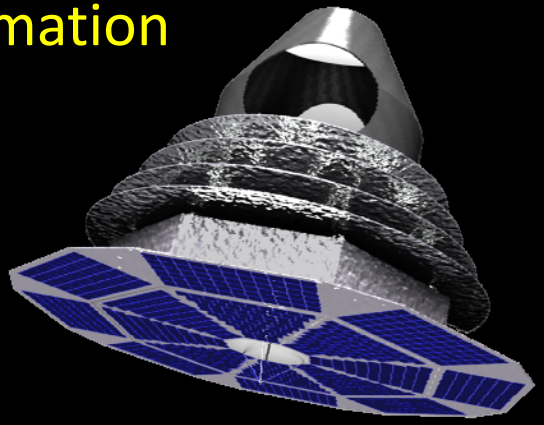

- To do this we have to remove instrumental effects and polarized foregrounds ***at an unprecedented level of precision***.
- At a level that cannot be reached from the ground, with balloons, with small space missions.

Temperature & Polarisation CMB C_l

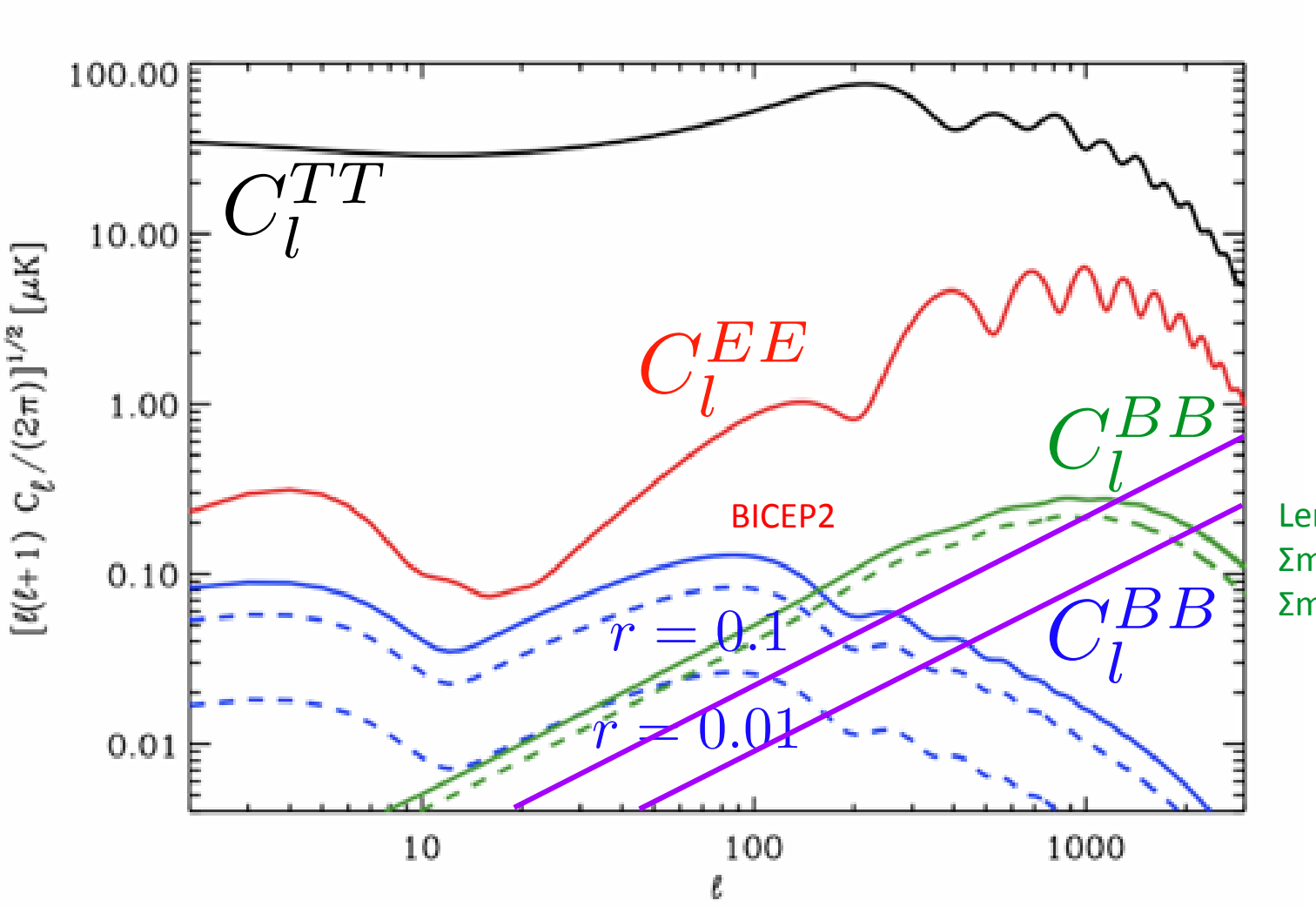

Foregrounds are complex and polarized

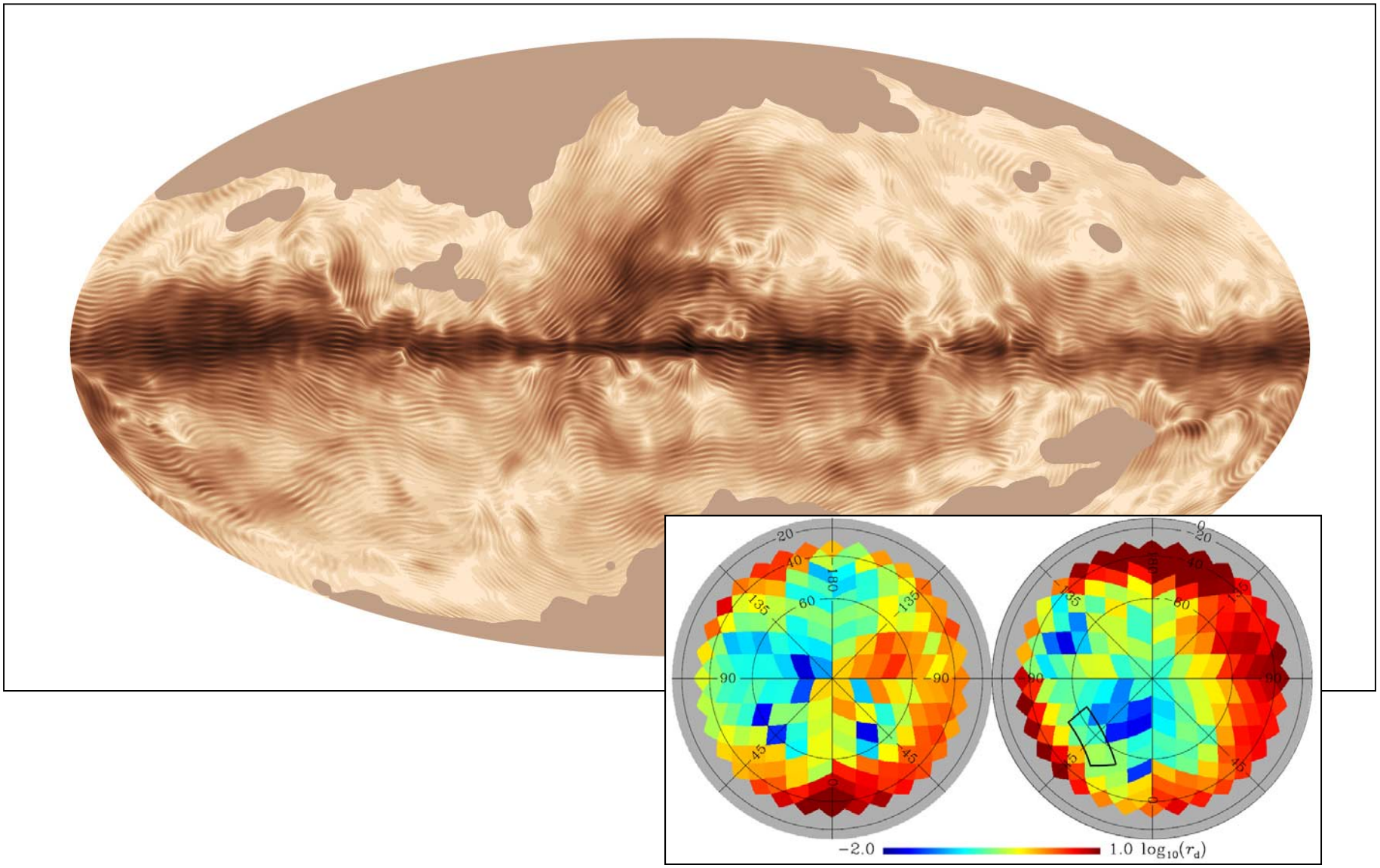

Target: primordial B-modes **and** gravitational lensing

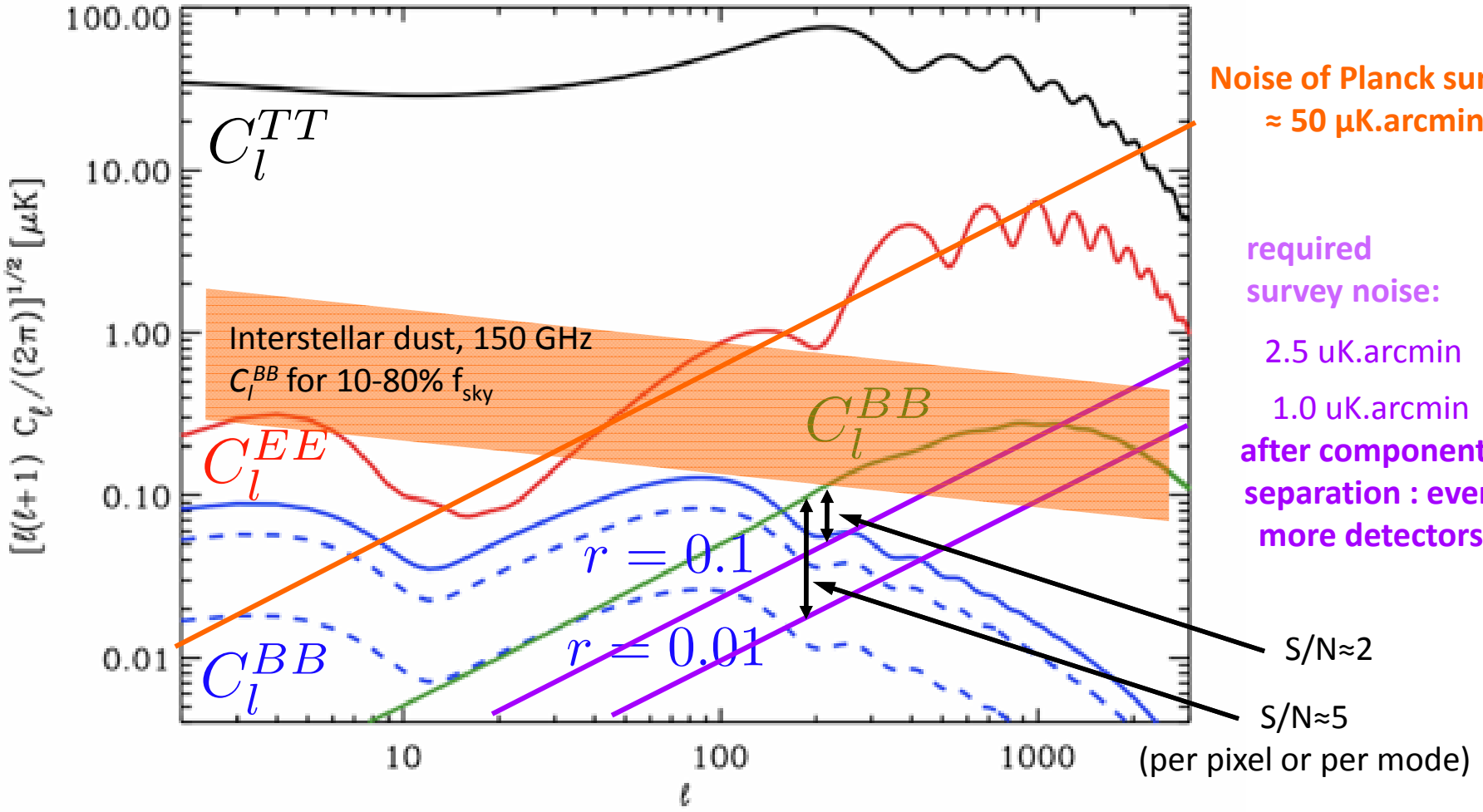

We **do need** a space-based survey

- Given the importance of polarized forgrounds, the required survey sensitivity has to be reached after the foregrounds separation process.
- To achieve this, we need
  - wide frequency coverage (70 to 600 GHz minimum)
  - a sufficient number of independent bands (order or 15)
  - absence of atmospheric fluctuations
- … i.e. we need a space based survey

Atmospheric fluctuations : quantum

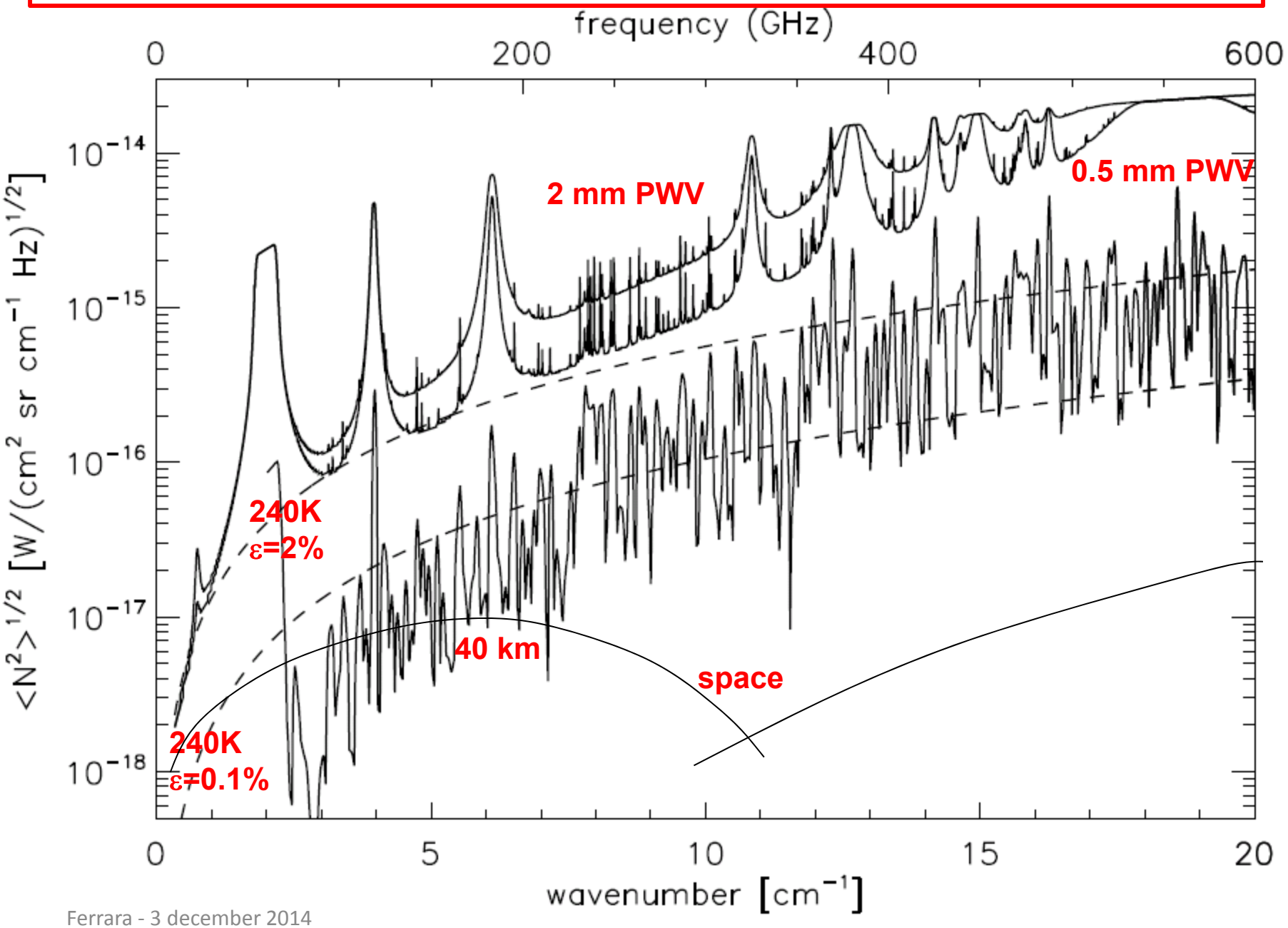

Atmospheric fluctuations : Turbulence

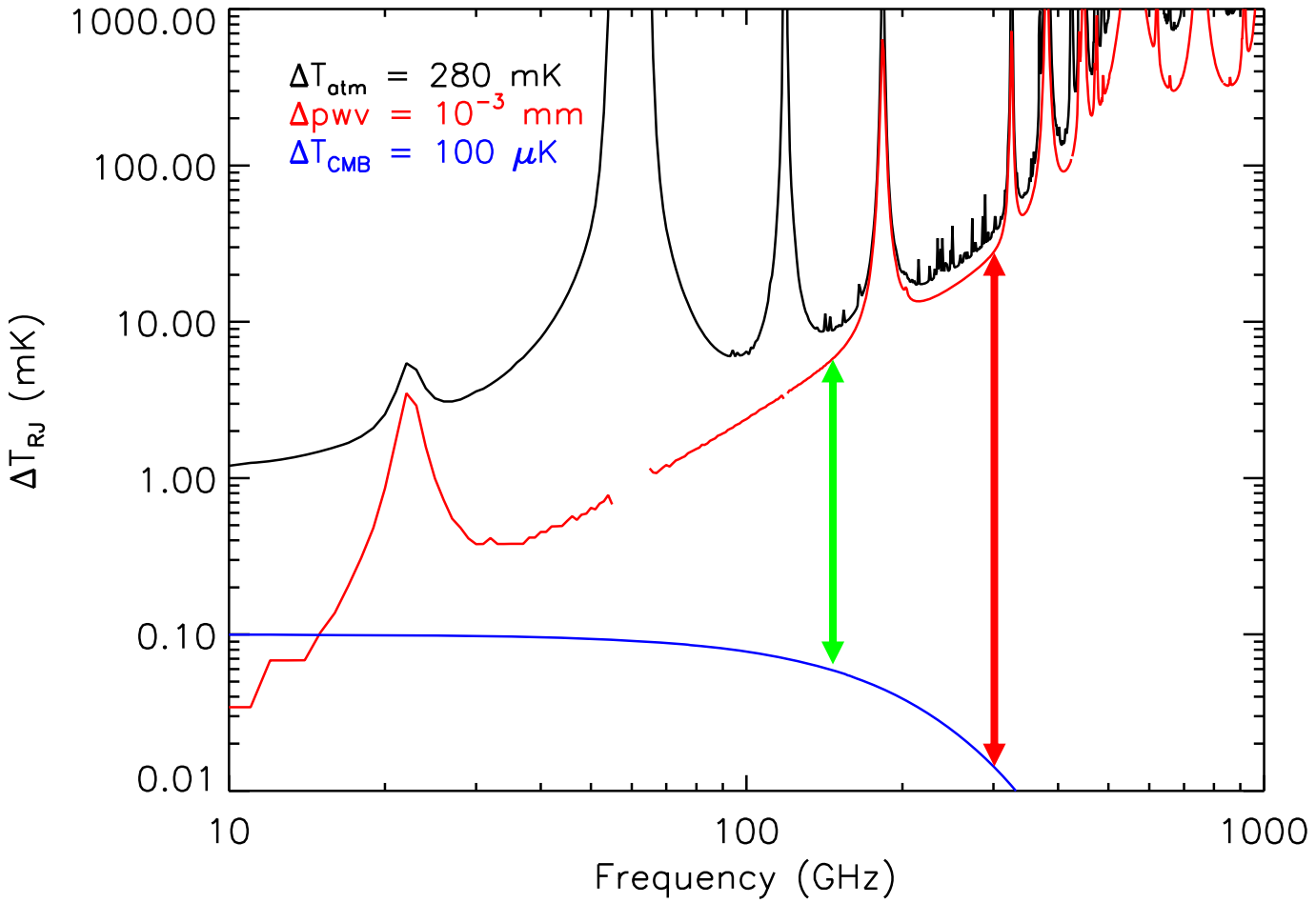

Extremely difficult to measure CMB fluctuations from the ground at f > 300 GHz, even in the best sites

Foreground complexity

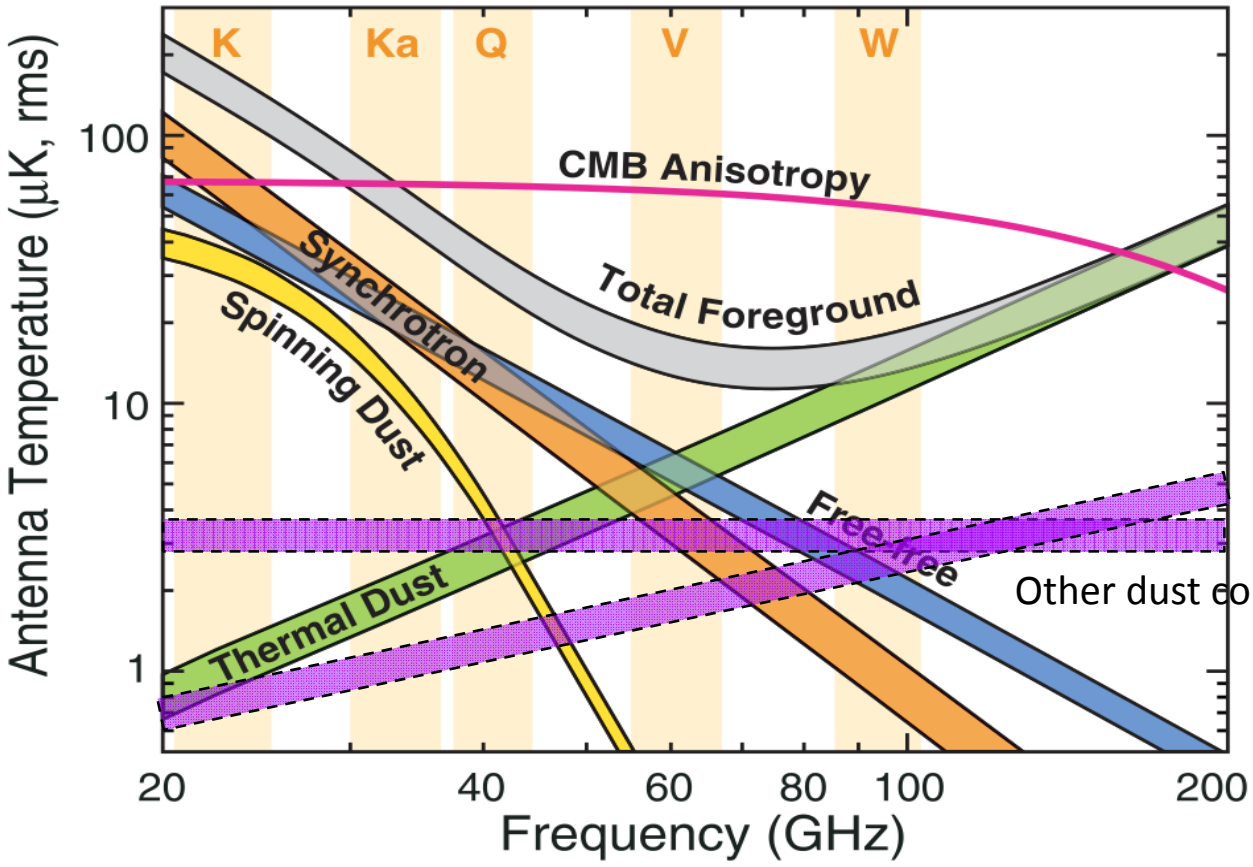

Other dust component ?

Bennett et al., ApJSS 208, 20 (2013)

We need more bands than components

Count components (or parameters)	I	P
CMB	1	1
Thermal SZ	2	0
2-component thermal dust	6	6
2-component synchrotron	4-6	4-6
Free-free	1-2	0 ?
Spinning dust	a few	?
CIB	many	0 ?
Zodiacal light	1-3	0 ?
Radio source background	a few	a few
Surprises	?	?
TOTAL	**15-20 +**	**11-13 +**

In cleaner regions of the sky, less parameters are needed, but this depends on the sensitivity of the survey.

ESA call for M4

- Mission in 2025
- Similar to previous M calls, BUT
  - Cost for ESA < 450 M€ (Δ=-150 M€)
  - TRL 5-6 in 2018 (start of implementation): in practice, rely on available technologies already at the time of the proposal
  - State clearly the share of responsibilities between ESA and the national agencies funded consortia (who provides what, who pays for what)
  - Requires a somewhat more defined letter of endorsement from the national agencies.
- Sept. 16th 2014, 12:00 CEST : letter of intent
- Jan. 15th 2015, 12:00 CEST : full proposal

Which polarization mission for M4 ?

- Sensitivity between 1.5 and 2.5 μK.arcmin ≈ 6000-2000 detectors
- Angular resolution for CMB between 4' and 6‘ (1m-1.5m class telescope)
- Enough frequency channels (15) for an efficient extraction of the CMB from the foregrounds
- Simplified, optimized CORE 2010 (see www.core-mission.org)
- Similar to Planck, with many more polarization sensitive detectors, and optimized scanning strategy